MULTIPLE SCATTERING AND LOCALIZATION OF LIGHT

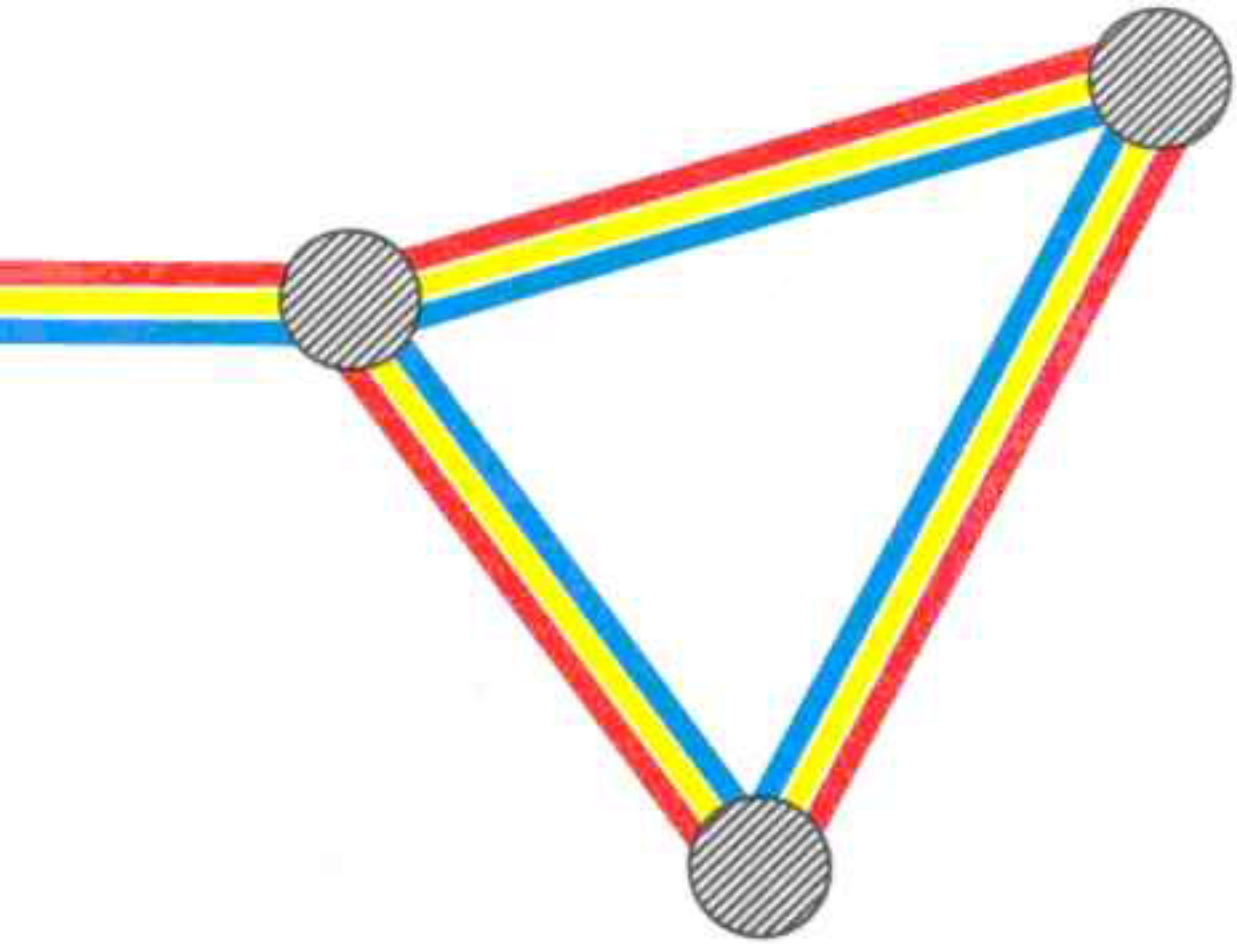

BART A.
VAN TIGGELEN

MULTIPLE SCATTERING AND LOCALIZATION OF LIGHT

ACADEMISCH PROEFSCHRIFT

ter verkrijging van de graad van doctor
aan de Universiteit van Amsterdam,
op gezag van de Rector Magnificus
prof. dr. P.W.M. de Meijer
in het openbaar te verdedigen in de Aula der Universiteit
(Oude Lutherse Kerk, ingang Singel 411, hoek Spui),
op dinsdag 29 september 1992 te 13:30 uur

door

BAREND ADRIANUS VAN TIGGELEN

geboren te Schoonhoven

promotor: prof. dr. A. Lagendijk
co-promotor: dr. A. Tip

overige leden:

prof. dr. D. Frenkel
prof. dr. H.C. van de Hulst
prof. dr. V. Icke
prof. dr. A.W. Kleyn
dr. Th.M. Nieuwenhuizen

This work was part of the research program of the "Stichting voor Fundamenteel Onderzoek der Materie" (FOM) and was made possible by financial support of the "Nederlandse Organisatie voor Wetenschappelijk Onderzoek" (NWO). It was carried out at the

FOM-Institute for Atomic and Molecular Physics
Kruislaan 407
1098 SJ Amsterdam
The Netherlands

Pride!
In the Name of Love

(U2, 1984)

Contents

Summary

This thesis reports on theoretical work concerning the propagation of light in the presence of a large number of small scatterers. By definition a "scatterer" is an object that influences light propagation somehow. To scatter visible light (wavelength 500 - 600 nanometer) one often makes use of dielectric particles immersed in a fluid, or paint-air pockets. Dielectric materials scatter light by means of refraction which, in turn, is caused by different speeds of light inside and outside the dielectric. Scattering of light can become very efficient if the particle size is of the order of the wavelength. In practice, the shape of the scatterers is hardly ever spherical but is more potato-like. In our theory we assume them to be spherical.

We speak about "multiple scattering" if we deal with more than one scatterer. In this thesis we study multiple scattering in the presence of "disorder". Disorder can be of any kind, but the one relevant for many light experiments is called "topological disorder". The scatterers are in that case randomly (for instance Poisson-) distributed in space. Experimentally one usually averages scattered light over many different realizations of the system. Another kind of disorder occurs if the dielectric constant of the scatterers or their size is randomized. This kind of disorder will be used in chapter 4.

One important condition for the occurrence of multiple scattering is energy conservation. In the presence of absorption all light is lost completely after a finite number of collisions, so that multiple scattering is suppressed considerably. To treat light scattering from a very large number of non-absorbing scatterers, we introduce point-scatterer models. These are the simplest objects that scatter light with conservation of energy, but do not exist in reality. Although more sophisticated models exist to describe light scattering from a single particle, point scatterers are very useful for multiple-scattering calculations (chapters 2 and 3).

In one way do point scatterers lack some relevant properties to describe multiple scattering. The "dwell time" of light inside pointlike objects is zero. A dwell time larger than zero corresponds to time-delay suffered by waves during scattering. This delay can become of the order of the average time between two successive collisions (the mean free time) near resonances, and is then not negligible at all. Resonances in dielectric scatterers show up if the wavelength of the light fits somehow with the shape and size of the scatterer. Delay in propagation results from a temporary formation of a standing wave inside each scatterer, and accumulates in multiple scattering. The dwell time will be discussed in chapter 1; the consequences for the speed of light v_E in the presence of multiple scattering have been worked out in chapter 3.

A number of reasons exist why multiple scattering is worth studying. Until recently it was believed that *interference* in multiple scattering will be averaged out automatically if some disorder is introduced. In the last 30 years people have realized that this is definitely not the case. Some examples have been identified that do not average out to zero, but should nevertheless be attributed to constructive interference in multiple scattering. One of them, "enhanced backscattering", has been observed in reflection

experiments. Interference contributions will be investigated in chapter 2.

If the medium containing the randomly distributed scatterers is sufficiently dense, it is known that light propagation becomes *diffusive*. In chapter 3 we emphasize that it is physically instructive to separate between *stationary* and *dynamic* properties of diffusive propagation. This is rather customary in electronics (the diffusing electrons giving rise to Ohmic resistance) where one usually distinguishes between AC and DC, but not in optics. In stationary, multiple scattering experiments one deals with a stationary flow of light through the scattering medium. In that case one measures length scales such as the mean free path ℓ. This is essentially the "step length" of the random walk with which a diffusion process can be associated. On the other hand, a dynamic experiment concerns the propagation of a short pulse that will be spread out by the diffusion process in the random medium. Such an experiment probes the diffusion constant D, consisting of both length and time scales. This is evident from the classical formula $D = \frac{1}{3} v_E \ell$.

In chapter 3 we have investigated the impact of interference on the mean free path. Contrary to the interference discussed in chapter 2, we now deal with interference *inside* the random medium. It was predicted by Anderson in 1958 in his Noble Prize paper that interference might ultimately lead to a *vanishing* of the diffusion constant (Anderson localization). We shall argue that it is in fact the mean free path ℓ that vanishes, making Anderson localization a stationary phenomenon. Localization means that the eigenstates in the medium are no longer "extended" (or "diffusive"), but have become "localized". We show that a small diffusion constant can have a dynamic origin as well, which is as interesting as Anderson localization. This happens when the velocity v_E is small, giving rise to a considerable renormalization of time scales. The eigenstates remain extended, but the diffusive transport suffers from "trapping" inside resonant particles or subsequent Bragg-reflection (in periodic systems).

The theory of Anderson localization was originally developed for electrons to give a satisfactory description of metal-insulator transitions. The insulator regime is associated with "localized" states, and the electric conductivity vanishes. Since the basic elements of the theory are "disorder" and "interference", the ideas apply to all sorts of waves, not just electrons. With respect to classical wave scattering (among which light scattering) nobody has ever observed Anderson localization unambiguously. It is still one of the major experimental challenges in this field.

The last chapter discusses light localization in one dimension. By "one dimension" we mean that only one dimension suffers from disorder; the remaining dimensions obey translational symmetry. We solve Maxwell's equations for a dielectric multilayer. Disorder is introduced by varying the dielectric constant of the layers according to some probability distribution. The interesting (actually mathematically rigorous) statement for one-dimensional systems is that all states are exponentially localized irrespective the strength of the disorder. This makes Anderson localization in one dimension very suitable for a thorough theoretical study. The results may be relevant for the manufacturing of optical filters or to enhance the effective critical angle of a dielectric multilayer.

In this thesis a serious attempt has been made to illustrate the beautiful similarities

between light and electrons. Many concepts of Schrödinger potential scattering apply to electromagnetic waves as well. However, the blind use of similarities can be misleading and gives sometimes erroneous results. From an optimistic point of view this indicates that we did not yet understand the similarity completely. For instance, it turns out in chapter 3 that the scattering of classical waves in dielectric materials is in some ways very similar to scattering of electrons from two-level systems, rather than from (one-level) potentials. Another example is the fact that the introduction of point scatterers for classical waves in three dimensions requires extra mathematical care. On the other hand, point scatterers for Schrödinger potential scattering in three dimensions can be introduced straightforwardly.

The theoretical research in chapters 2 and 3 was performed in close collaboration with experimental phycisists at the "Natuurkundig Laboratorium" of the University of Amsterdam. Some results of chapter 4 will be used in the near future as a starting point for the experimental realization of dielectric multilayers in both the X-ray and the visible regime of the spectrum.

Finally we draw attention to Appendix C, in which many symbols, used in this thesis, have been clarified.

Amsterdam, July 24, 1992.

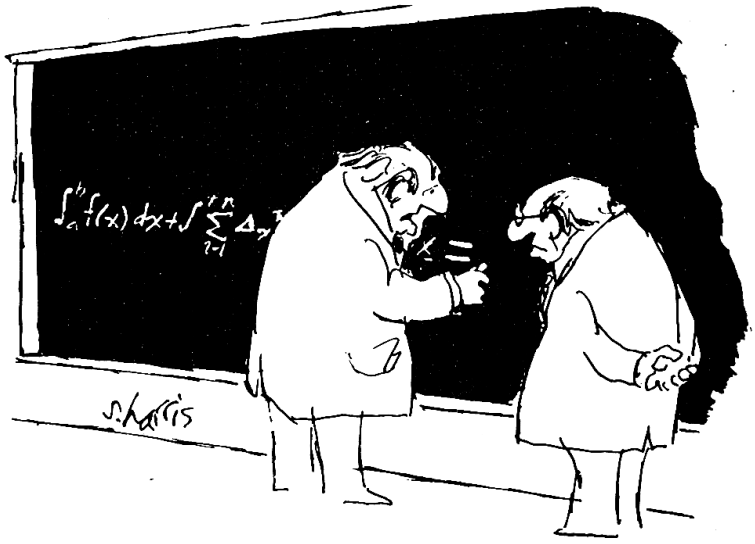

This is always the most difficult part .....

Chapter 1

Time-Dependent Scattering Theory

1.1 Introduction

This chapter deals with the time-dependent formulation of electromagnetic wave propagation in inhomogeneous media. The fundamental problem we want to tackle is how to obtain the distribution of electromagnetic energy at arbitrary times $t > 0$ given an initial distribution at $t = 0$. In this respect, the goal is not different from many other dynamical problems. The time-dependent treatments of the set of Maxwell equations, governing the propagation of light, and the Schrödinger wave equation, the dynamic equation for quantum mechanical waves, will turn out to be quite similar.

With the unification of the electric and magnetic force by Maxwell, roughly one century ago, the first quantitative theoretical description of light propagation was established. The theory can be summarized by four equations, written down in differential form,

$$\begin{array}{llll} \partial_t \mathbf{E} = \boldsymbol{\nabla} \times \mathbf{B} - \mathbf{J} & (a) & ; & \boldsymbol{\nabla} \cdot \mathbf{E} = \rho \quad (c) \\ \partial_t \mathbf{B} = -\boldsymbol{\nabla} \times \mathbf{E} & (b) & ; & \boldsymbol{\nabla} \cdot \mathbf{B} = 0 \quad (d)\,. \end{array} \tag{1.1}$$

In these equations $\mathbf{E}$ is the electric field, $\mathbf{B}$ the magnetic field, $\mathbf{J}$ is the charge current density and ρ the charge density.

It has become clear that Eqs. (1.1) contain the rigorous classical description of light propagation and obey the principle of Lorentz-invariance, that later emerged from the theory of special relativity. In order to describe the behavior of light in macroscopic media one must integrate Maxwell's equations over microscopic properties, thereby taking into account the interaction of light with individual atoms. This was first done by Lorentz. He demonstrated that Eqs. (1.1) take the form [1] [2],

$$\begin{array}{llll} \partial_t \mathbf{D} = \boldsymbol{\nabla} \times \mathbf{H} - \mathbf{J}_f & (a) & ; & \boldsymbol{\nabla} \cdot \mathbf{D} = \rho_f \quad (c) \\ \partial_t \mathbf{B} = -\boldsymbol{\nabla} \times \mathbf{E} & (b) & ; & \boldsymbol{\nabla} \cdot \mathbf{B} = 0 \quad (d)\,. \end{array} \tag{1.2}$$

where now $\mathbf{J}_f$ and ρ_f are to be understood as "free" charge current density and "free" charge density. The *dielectric displacement* $\mathbf{D}$ and the *magnetic flux* $\mathbf{H}$ are defined ac-

cording to

$$\mathbf{D} \equiv \mathbf{E} + \mathbf{P} \ , \ \mathbf{H} \equiv \mathbf{B} - \mathbf{M} \, , \tag{1.3}$$

in which $\mathbf{P}$ is the electric dipole density and $\mathbf{M}$ the magnetic dipole density. As a matter of fact the macroscopic Maxwell equations (1.2) were originally published by Maxwell, whereas the microscopic equations (1.1), supplemented by the first microscopic treatment of material properties, were later postulated by Lorentz. Hence, a Lorentz-covariant theory emerged from a non-covariant treatment of a non-covariant theory.

To find a closed set of equations, one must specify relations between the microscopic polarizations $\mathbf{P}$ and $\mathbf{M}$ and macroscopic fields. In fact, after Maxwell and had given the first impulse, this became a major challenge in condensed matter physics. Microscopic theory focusses upon the introduction of "linear response" quantities. A linear-response theory assumes that microscopic changes in the material properties are linear in the applied electromagnetic field. The most important linear-response quantities are the dielectric "constant" $\boldsymbol{\varepsilon}$, the magnetic permeability $\boldsymbol{\mu}$ and the electric conductivity $\boldsymbol{\sigma}$. These tensors are defined by

$$|\mathbf{D}_t\rangle = \boldsymbol{\varepsilon} \cdot |\mathbf{E}_t\rangle \ , \ |\mathbf{H}_t\rangle = \boldsymbol{\mu}^{-1} \cdot |\mathbf{B}_t\rangle \ , \ |\mathbf{J}_{f,\,t}\rangle = \boldsymbol{\sigma} \cdot |\mathbf{E}_t\rangle \, , \tag{1.4}$$

(we introduce the abstract Dirac notation $\langle \mathbf{r} | f_t \rangle = f(\mathbf{r}, t)$). More generally these so-called *constitutive equations* can be written as convolutions over time so as to describe memory effects properly. Using the abstract notation of Eqs. (1.4), convolutions in space can still be taken care of by letting the linear-response quantities functionally depend on the momentum operator $\mathbf{p}$. This possibility will not be considered here. Instead, we assume that these quantities are local operators, being functions of the position operator $\mathbf{r}$ only. Scattering particles will be characterized by local deviations of the tensors $\boldsymbol{\varepsilon}$, $\boldsymbol{\mu}$ and $\boldsymbol{\sigma}$ from their vacuum values, the dielectric constant in particular.

In this thesis we shall adopt Eqs. (1.4) as rigorous. We thus ignore both nonlinear response and time-dependence (c.q. frequency-dependence) of the material response. For low field intensities and away from microscopic resonances this is a very good approximation. We show in the next section that these simplifications allow for a rigorous time-evolution setting of the macroscopic Maxwell equations, in which the similarity to the Schrödinger equation becomes apparent.

Causality on a microscopic level puts constraints on the frequency-dependence of the dielectric "constant" and the conductivity. It prescribes that both quantities are real and imaginary part of the same analytic function of frequency [2], giving rise to the well known Kramers-Kronig relations. This is trivially true when both quantities are frequency-independent. Hence the ignorance of frequency-dependence does not violate microscopic causality.

A finite conductivity gives rise to absorption of electromagnetic energy, thus suppressing multiple scattering of light. In order to describe macroscopic light transport we will often assume that conducting properties of the scatterers can be ignored.

1.2 Hilbert Space Setting

Keeping in mind the Schrödinger equation,

$$i\partial_t|\psi_t\rangle = H|\psi_t\rangle\,, \tag{1.5}$$

where H is the energy operator or Hamiltonian playing the role of time-evolution generator, one seeks a similar dynamics applicable to light. The dynamics for light propagation was already obtained in the previous section. In what follows we assume that the dielectric constant $\boldsymbol{\varepsilon}$ and the conductivity $\boldsymbol{\mu}$ are real-valued, strictly positive, symmetric operators. We let $\boldsymbol{\Gamma} \equiv \boldsymbol{\varepsilon}^{-1/2}$, $\boldsymbol{\Lambda} \equiv \boldsymbol{\mu}^{-1/2}$, and define the state vector,

$$|\underline{\mathbf{F}}_t\rangle = \frac{1}{\sqrt{2}} \begin{pmatrix} \boldsymbol{\Gamma}^{-1} \cdot |\mathbf{E}_t\rangle \\ \boldsymbol{\Lambda} \cdot |\mathbf{B}_t\rangle \end{pmatrix}. \tag{1.6}$$

Eqs. (1.2) can be written in the form resembling the Schrödinger wave equation (1.5),

$$i\partial_t|\underline{\mathbf{F}}_t\rangle = \underline{\underline{\mathbf{K}}} \cdot |\underline{\mathbf{F}}_t\rangle\,, \tag{1.7}$$

in which the time-evolution generator is given by

$$\underline{\underline{\mathbf{K}}} = \begin{pmatrix} 0 & \boldsymbol{\Gamma} \cdot (\boldsymbol{\epsilon} \cdot \mathbf{p}) \cdot \boldsymbol{\Lambda} \\ -\boldsymbol{\Lambda} \cdot (\boldsymbol{\epsilon} \cdot \mathbf{p}) \cdot \boldsymbol{\Gamma} & 0 \end{pmatrix} - i \begin{pmatrix} \boldsymbol{\Gamma} \cdot \boldsymbol{\sigma} \cdot \boldsymbol{\Gamma} & 0 \\ 0 & 0 \end{pmatrix}. \tag{1.8}$$

A finite conductivity gives rise to dissipation, which is described by the second term. The Maxwell equations (1.2) (c), (d) give the additional requirement that

$$\begin{pmatrix} \mathbf{p} \cdot \boldsymbol{\Gamma}^{-1} & 0 \\ 0 & \mathbf{p} \cdot \boldsymbol{\Lambda}^{-1} \end{pmatrix} \cdot |\underline{\mathbf{F}}_t\rangle = -i \begin{pmatrix} \rho_f \\ 0 \end{pmatrix}. \tag{1.9}$$

We have introduced the momentum operator $\mathbf{p} = -i\boldsymbol{\nabla}$ and the Levi-Cévita tensor density $\boldsymbol{\epsilon}$ (not to be confused with the dielectric constant $\boldsymbol{\varepsilon}$). By definition, $(\boldsymbol{\epsilon} \cdot \mathbf{p})_{ij} = \sum_k \epsilon_{ijk} p_k$; ϵ_{ijk} is anti-symmetric in all indices with the convention that $\epsilon_{123} = 1$.

We restrict ourselves to the case that there are no free charges ($\rho_f = 0$) and no losses due to Ohmic dissipation ($\boldsymbol{\sigma} = 0$). It can be checked from Eqs. (1.2) that the total electromagnetic energy,

$$\begin{aligned} W(t) &= \frac{1}{2}\int d\mathbf{r}\ \Big[\mathbf{E}^*(\mathbf{r},t) \cdot \boldsymbol{\Gamma}^{-2}(\mathbf{r}) \cdot \mathbf{E}(\mathbf{r},t) + \mathbf{B}^*(\mathbf{r},t) \cdot \boldsymbol{\Lambda}^2(\mathbf{r}) \cdot \mathbf{B}(\mathbf{r},t)\Big] \\ &= \int d\mathbf{r}\ \|\underline{\mathbf{F}}(\mathbf{r},t)\|^2\,, \end{aligned} \tag{1.10}$$

is conserved in time. Here $\|\underline{\mathbf{F}}\|^2 \equiv \sum_{i=1}^6 |F_i|^2$ is the Euclidean norm in six dimensions. The above suggests an inner product associated with Maxwell's equations,

$$\langle \underline{\mathbf{f}}\,|\,\underline{\mathbf{g}}\rangle = \int d\mathbf{r}\ \underline{\mathbf{f}}(\mathbf{r})^* \cdot \underline{\mathbf{g}}(\mathbf{r})\,, \tag{1.11}$$

where $\underline{\mathbf{f}}(\mathbf{r})$ and $\underline{\mathbf{g}}(\mathbf{r})$ are six-dimensional vectorfields on $\mathbb{R}^3$. The associated Hilbert space is

$$\mathcal{K} := L^2\left(\mathbb{R}^3, d\mathbf{r}, \mathbb{C}^6\right) , \tag{1.12}$$

consisting of square-integrable six-dimensional vector fields on $\mathbb{R}^3$ equipped with the inner product in Eq. (1.11). With respect to this inner product, the time-evolution $\underline{\underline{\mathbf{K}}}$ is a symmetric operator. The free time evolution,

$$\underline{\underline{\mathbf{K}}}_0 = \begin{pmatrix} 0 & (\boldsymbol{\epsilon}\cdot\mathbf{p}) \\ -(\boldsymbol{\epsilon}\cdot\mathbf{p}) & 0 \end{pmatrix} , \tag{1.13}$$

can readily be shown to be self-adjoint, since it becomes a multiplication in Fourier-space. In the absence of free charges Eq. (1.9) takes the form,

$$\mathbf{p}\cdot\begin{pmatrix} \boldsymbol{\Gamma}^{-1} & 0 \\ 0 & \boldsymbol{\Lambda}^{-1} \end{pmatrix}\cdot|\underline{\mathbf{F}}_t\rangle = 0\,. \tag{1.14}$$

Since

$$\mathbf{p}\cdot\begin{pmatrix} \boldsymbol{\Gamma}^{-1} & 0 \\ 0 & \boldsymbol{\Lambda}^{-1} \end{pmatrix}\cdot\underline{\underline{\mathbf{K}}} = 0\,,$$

it follows that Eq. (1.14) is satisfied for all $t > 0$ provided it holds true at $t = 0$. Because Eq. (1.14) restricts the vector of state to the transverse subspace $\underline{\underline{\boldsymbol{\Pi}}}\mathcal{K}$ of $\mathcal{K}$ in which both $\mathbf{B}$ and $\mathbf{D}$ are transverse, it is thus established that transversality is conserved in time.

We observe that $\underline{\underline{\mathbf{K}}}$ has an eigenvalue zero (of infinite multiplicity) in the orthogonal complement of this subspace. This means that if the initial wave function has a longitudinal component, the latter does not evolve in time.

¿From the time-evolution generator one constructs another fundamental operator. The *resolvent* $\underline{\underline{\mathbf{R}}}(z)$ is defined as

$$\underline{\underline{\mathbf{R}}}(z) = -i\int_0^\infty dt\exp(izt)\,\exp(-i\underline{\underline{\mathbf{K}}}t) = \left(z - \underline{\underline{\mathbf{K}}}\right)^{-1} , \tag{1.15}$$

with z complex, $\mathrm{Im}\, z > 0$, and similarly for $\mathrm{Im}\, z < 0$. Upon introducing the projectors

$$\underline{\underline{\mathbf{P}}} = \begin{pmatrix} 1 & 0 \\ 0 & 0 \end{pmatrix} \text{ and } \underline{\underline{\mathbf{Q}}} = \begin{pmatrix} 0 & 0 \\ 0 & 1 \end{pmatrix}$$

we note that $\underline{\underline{\mathbf{P}}}\cdot\underline{\underline{\mathbf{K}}}\cdot\underline{\underline{\mathbf{P}}} = \underline{\underline{\mathbf{Q}}}\cdot\underline{\underline{\mathbf{K}}}\cdot\underline{\underline{\mathbf{Q}}} = 0$. The application of Feshbach's projection formula [3] results in

$$\begin{aligned}\underline{\underline{\mathbf{R}}}(z) = z^{-1}\underline{\underline{\mathbf{Q}}} \;\; &+ \;\; z\left[\underline{\underline{\mathbf{P}}} - z^{-1}\boldsymbol{\Lambda}\cdot(\boldsymbol{\epsilon}\cdot\mathbf{p})\cdot\boldsymbol{\Gamma}\cdot\begin{pmatrix} 0 & 0 \\ 1 & 0 \end{pmatrix}\right]\cdot \\ &\cdot \;\; \boldsymbol{\Gamma}^{-1}\cdot\mathbf{G}(z)\cdot\boldsymbol{\Gamma}^{-1}\cdot\left[\underline{\underline{\mathbf{P}}} + z^{-1}\boldsymbol{\Gamma}\cdot(\boldsymbol{\epsilon}\cdot\mathbf{p})\cdot\boldsymbol{\Lambda}\cdot\begin{pmatrix} 0 & 1 \\ 0 & 0 \end{pmatrix}\right] ,\end{aligned} \tag{1.16}$$

where $\mathbf{G}(z)$ is an operator working on three-dimensional vector fields,

$$\mathbf{G}(z) = \left[z^2\left(\boldsymbol{\varepsilon} + iz^{-1}\boldsymbol{\sigma}\right) + (\boldsymbol{\epsilon}\cdot\mathbf{p})\cdot\boldsymbol{\mu}^{-1}\cdot(\boldsymbol{\epsilon}\cdot\mathbf{p})\right]^{-1}. \tag{1.17}$$

From this formula it is clear that all interesting spectral properties of the resolvent are contained in the operator $\mathbf{G}(z)$. This operator is recognized as the "resolvent" of the Helmholtz equation, that can be obtained by a combination of the Maxwell equations (1.2),

$$\boldsymbol{\varepsilon}(\mathbf{r})\cdot\partial_t^2\mathbf{E} + \boldsymbol{\nabla}\times\boldsymbol{\mu}(\mathbf{r})^{-1}\cdot(\boldsymbol{\nabla}\times\mathbf{E}) = \boldsymbol{\sigma}(\mathbf{r})\cdot\partial_t\mathbf{E}\,. \tag{1.18}$$

The operator $\mathbf{m}^2(z) = \boldsymbol{\varepsilon} + iz^{-1}\boldsymbol{\sigma}$ is sometimes referred to as the *complex index of refraction* [4]. In the case we are dealing with a pure dielectric ($\boldsymbol{\mu} = 1$, $\boldsymbol{\sigma} = 0$) the operator $\mathbf{G}(z)$ reduces to

$$\mathbf{G}(z) = \left[z^2\boldsymbol{\varepsilon} - p^2\boldsymbol{\Delta}_{\mathbf{p}}\right]^{-1}, \tag{1.19}$$

with $\boldsymbol{\Delta}_{\mathbf{p}} = \mathbf{I} - \hat{\mathbf{p}}\hat{\mathbf{p}}$ the projection upon the transverse subspace of $\underline{\underline{\mathbf{K}}}_0$ in $\mathcal{K}$.

We turn to the eigenvalue problem of the free time evolution given in Eq. (1.13). Its solutions are usually referred to as "plane waves", but are here to be understood as six-dimensional vectors. Upon solving $\underline{\underline{\mathbf{K}}}_0|E\rangle = E|E\rangle$, we find the solutions,

$$|E\rangle = \begin{pmatrix} \mathbf{g} \\ \hat{\mathbf{k}}\times\mathbf{g} \end{pmatrix}|\mathbf{k}\rangle \quad (E\in\mathbb{R})\,.$$

Here $\mathbf{k} \equiv E\,\hat{\mathbf{k}}$; the direction of $\hat{\mathbf{k}}$ is arbitrary. By definition $|\hat{\mathbf{k}}| = 1$. Transversality requires $\mathbf{g}\perp\hat{\mathbf{k}}$. This allows two orthogonal choices for the polarization vector $\mathbf{g}$, which we shall denote by the index $j = \pm 1$. We define the set,

$$|j\hat{\mathbf{k}}, E\rangle = \frac{1}{\sqrt{2}}\begin{pmatrix} \mathbf{g}_j \\ \hat{\mathbf{k}}\times\mathbf{g}_j \end{pmatrix}|E\hat{\mathbf{k}}\rangle \quad (E\in\mathbb{R},\, j=\pm1, \hat{\mathbf{k}}\in 4\pi)\,. \tag{1.20}$$

With the convention that $|\mathbf{g}_j| = 1$ these eigenfunctions of $\underline{\underline{\mathbf{K}}}_0$ satisfy continuum normalization,

$$\langle j\hat{\mathbf{k}}, E|j'\hat{\mathbf{k}}', E'\rangle = (2\pi)^3\,\delta_{jj'}\delta(E-E')\delta(\hat{\mathbf{k}}-\hat{\mathbf{k}}')\,, \tag{1.21}$$

and form a *complete set* on the transverse subspace of $\underline{\underline{\mathbf{K}}}_0$ in $\mathcal{K}$: $\underline{\underline{\boldsymbol{\Pi}}}_0\mathcal{K}$,

$$\int \underline{\underline{\mathbf{E}}}_0(dE) \equiv \sum_{j\hat{\mathbf{k}}E} |j\hat{\mathbf{k}}, E\rangle\cdot\langle j\hat{\mathbf{k}}, E| = \underline{\underline{\boldsymbol{\Pi}}}_0\,. \tag{1.22}$$

The operator $\underline{\underline{\mathbf{K}}}_0$ has continuous spectrum along the whole real axis. This is a striking difference with the free time evolution $H_0 = p^2$ in the Schrödinger picture, which is obviously a positive operator. This is not unrelated to the different interpretation of

the electromagnetic wave function $|\underline{\mathbf{F}}_t\rangle$ when compared to the quantum-mechanical wave function $|\psi_t\rangle$. The concept of quantum mechanics associates with every observable a self-adjoint operator A. The inner product is then used to obtain the real-valued expectation $\langle\psi_t|A|\psi_t\rangle$ and is supposed to make predictions about an experiment. On the other hand, the electromagnetic wave function contains the electric and magnetic fields, which are observables themselves. Consequently, any physical wave function $\underline{\mathbf{F}}(\mathbf{r},t)$ should be real-valued. Indeed, if $\underline{\mathbf{F}}_E(\mathbf{r})\exp(iEt)$ is a solution of Maxwell's equations at eigenvalue E, one has sufficient freedom to choose $\underline{\mathbf{F}}_E(\mathbf{r}) = \underline{\mathbf{F}}_{-E}(\mathbf{r})^*$ so that

$$\underline{\mathbf{F}}(\mathbf{r},t) = \int_{-\infty}^{\infty} dE\, \underline{\mathbf{F}}_E(\mathbf{r})\exp(iEt) \tag{1.23}$$

is real-valued. In this respect, although square-integrable, not every wave function in $\mathcal{K}$ can be considered physical. It is also remarked that the eigenvalues of the time-evolution generator $\underline{\underline{\mathbf{K}}}$ do not coincide with the energy of the electromagnetic field. The field energy is given by the inner product in Eq. (1.11)!

1.3 Scattering of Light

We suppose again that $\boldsymbol{\sigma} = 0$ so that we have conservation of energy, and that the regions where $\boldsymbol{\varepsilon} = \boldsymbol{\varepsilon}(\mathbf{r})$, $\boldsymbol{\mu} = \boldsymbol{\mu}(\mathbf{r})$ deviate from their vacuum values are well-localized in space. It was indicated in the previous section that $\underline{\underline{\mathbf{K}}}_0$ and $\underline{\underline{\mathbf{K}}}$ have non-empty eigenspaces at the eigenvalue zero, corresponding to longitudinal components of the electromagnetic field that do not evolve in time. In a scattering situation one has to stay away from these subspaces. At $t \to -\infty$, the wave packet has not yet reached the region where $\boldsymbol{\varepsilon}(\mathbf{r})$ and $\boldsymbol{\mu}(\mathbf{r})$ deviate from their vacuum values and the propagation is governed by $\underline{\underline{\mathbf{K}}}_0$. Hence the initial state must be in the transverse subspace $\underline{\underline{\boldsymbol{\Pi}}}_0\mathcal{K}$ of $\underline{\underline{\mathbf{K}}}_0$ in $\mathcal{K}$, which has projector $\underline{\underline{\boldsymbol{\Pi}}}_0 = \boldsymbol{\Delta}_{\mathbf{p}}\underline{\underline{\mathbf{I}}}$. The transverse projector of $\underline{\underline{\mathbf{K}}}$ will be denoted by $\underline{\underline{\boldsymbol{\Pi}}}$. We expect that

$$|\underline{\mathbf{F}}_t\rangle = \exp(-i\underline{\underline{\mathbf{K}}}t)\cdot|\underline{\mathbf{F}}^0\rangle \overset{t\to\pm\infty}{\to} \exp(-i\underline{\underline{\mathbf{K}}}_0 t)\cdot|\underline{\mathbf{F}}_\pm\rangle\,, \tag{1.24}$$

where $|\underline{\mathbf{F}}_\pm\rangle \in \underline{\underline{\boldsymbol{\Pi}}}_0\mathcal{K}$ and $|\underline{\mathbf{F}}^0\rangle \in \underline{\underline{\boldsymbol{\Pi}}}\,\mathcal{K}$. This leads to the definition of the *Møller Wave Operators*,

$$\begin{aligned}\underline{\underline{\boldsymbol{\Omega}}}_\pm &= \text{s}-\lim_{t\to\pm\infty}\exp(i\underline{\underline{\mathbf{K}}}t)\cdot\exp(-i\underline{\underline{\mathbf{K}}}_0 t)\cdot\underline{\underline{\boldsymbol{\Pi}}}_0 \\ &= \text{s}-\lim_{t\to\pm\infty}\underline{\underline{\boldsymbol{\Pi}}}\cdot\exp(i\underline{\underline{\mathbf{K}}}t)\cdot\exp(-i\underline{\underline{\mathbf{K}}}_0 t)\,.\end{aligned} \tag{1.25}$$

This limit is to be understood as a strong limit [5], indicated by the "s". The question under which conditions of the interaction this limit exists is a major challenge in the mathematical formulation of scattering theory. As might be expected, the answer puts constraints on the precise nature of the interaction [6] [7] [8], its asymptotic form in particular.

It follows from the definition Eq. (1.25) that

$$\underline{\underline{\mathbf{\Omega}}}^{*}_{\pm} \cdot \underline{\underline{\mathbf{\Omega}}}_{\pm} = \underline{\underline{\mathbf{\Pi}}}_{0} \,. \tag{1.26}$$

Thus, provided they exist, the wave-operators are isometric in the transverse subspace $\underline{\underline{\mathbf{\Pi}}}_{0}\mathcal{K}$. From

$$\lim_{t\to\pm\infty} \exp(i\underline{\underline{\mathbf{K}}}t) \cdot \exp(-i\underline{\underline{\mathbf{K}}}_{0}(t+s)) \cdot \underline{\underline{\mathbf{\Pi}}}_{0} = \lim_{t\to\pm\infty} \exp(i\underline{\underline{\mathbf{K}}}(t-s)) \cdot \exp(-i\underline{\underline{\mathbf{K}}}_{0}t) \cdot \underline{\underline{\mathbf{\Pi}}}_{0} \,,$$

one obtains the useful relation,

$$\underline{\underline{\mathbf{K}}} \cdot \underline{\underline{\mathbf{\Omega}}}_{\pm} = \underline{\underline{\mathbf{\Omega}}}_{\pm} \cdot \underline{\underline{\mathbf{K}}}_{0} \,. \tag{1.27}$$

This identity indicates that $\underline{\underline{\mathbf{\Omega}}}_{\pm}|j\hat{\mathbf{k}}, E\rangle$ is an eigenfunction of $\underline{\underline{\mathbf{K}}}$, which has, by Eq. (1.26), continuum normalization. Since the set of plane waves $|j\hat{\mathbf{k}}, E\rangle$ is a complete set on $\underline{\underline{\mathbf{\Pi}}}_{0}\mathcal{K}$ we conclude that the $\underline{\underline{\mathbf{\Omega}}}_{\pm}$ have a range spanned by the continuum eigenfunctions of $\underline{\underline{\mathbf{K}}}$ only. In most cases of physical interest the ranges of both wave operators coincide and equal precisely the part of Hilbert space spanned by the absolute continuous eigenfunctions of the Hamiltonian. The wave operators are then said to be *complete* [6]. In the case of light one must make an additional restriction to the transverse subspace.

¿From now on we assume that the transverse Maxwell Hamiltonian possesses an absolute continuous spectrum only and that the wave operators are complete. One can check that

$$\underline{\underline{\mathbf{\Omega}}}_{\pm} \cdot \underline{\underline{\mathbf{\Omega}}}^{*}_{\pm} = \underline{\underline{\mathbf{\Pi}}} \,. \tag{1.28}$$

The *scattering operator* can be defined as

$$\underline{\underline{\mathbf{S}}} = \underline{\underline{\mathbf{\Omega}}}^{*}_{+} \cdot \underline{\underline{\mathbf{\Omega}}}_{-} \,. \tag{1.29}$$

The S-operator is constructed such that it maps the initial wave packet upon the asymptotic, scattered wave packet. By applying Eq. (1.27) twice we get $\underline{\underline{\mathbf{K}}}_{0} \cdot \underline{\underline{\mathbf{\Omega}}}^{*}_{+} \cdot \underline{\underline{\mathbf{\Omega}}}_{-} = \underline{\underline{\mathbf{\Omega}}}^{*}_{+} \cdot \underline{\underline{\mathbf{K}}} \cdot \underline{\underline{\mathbf{\Omega}}}_{-} = \underline{\underline{\mathbf{\Omega}}}^{*}_{+} \cdot \underline{\underline{\mathbf{\Omega}}}_{-} \cdot \underline{\underline{\mathbf{K}}}_{0}$. Hence,

$$\underline{\underline{\mathbf{S}}} \cdot \underline{\underline{\mathbf{K}}}_{0} = \underline{\underline{\mathbf{K}}}_{0} \cdot \underline{\underline{\mathbf{S}}} \,. \tag{1.30}$$

The S-operator is said to be *on the energy shell*. From the completeness of the wave operators, one obtains the unitarity of the S-operator,

$$\underline{\underline{\mathbf{S}}}^{*} \cdot \underline{\underline{\mathbf{S}}} = \underline{\underline{\mathbf{S}}} \cdot \underline{\underline{\mathbf{S}}}^{*} = \underline{\underline{\mathbf{\Pi}}}_{0} \,. \tag{1.31}$$

If the wave operators exist and are complete, the conventional scattering theory can be applied [6] [9] [10]. Writing $\underline{\underline{\mathbf{V}}} = \underline{\underline{\mathbf{K}}} - \underline{\underline{\mathbf{K}}}_{0}$ we can rewrite Eq. (1.25) as

$$\underline{\underline{\mathbf{\Omega}}}_{\pm} = \underline{\underline{\mathbf{\Pi}}}_{0} + i \lim_{\epsilon\downarrow 0} \int_{0}^{\pm\infty} dt \, \exp(\mp\epsilon t) \, \exp(i\underline{\underline{\mathbf{K}}}t) \cdot \underline{\underline{\mathbf{V}}} \cdot \exp(-i\underline{\underline{\mathbf{K}}}_{0}t) \cdot \underline{\underline{\mathbf{\Pi}}}_{0} \,.$$

Proceeding formally we have

$$\begin{aligned}\underline{\underline{\mathbf{V}}}\cdot\underline{\underline{\mathbf{\Omega}}}_{-} &= \underline{\underline{\mathbf{V}}}\cdot\underline{\underline{\mathbf{\Pi}}}_{0} + i\lim_{\epsilon\downarrow 0}\int_{0}^{-\infty} dt\,\exp(\epsilon\, t)\,\underline{\underline{\mathbf{V}}}\cdot\exp(i\underline{\underline{\mathbf{K}}}t)\cdot\underline{\underline{\mathbf{V}}}\cdot\int\exp(-iEt)\,\underline{\underline{\mathbf{E}}}_{0}(dE)\\ &= \lim_{\epsilon\downarrow 0}\int\underline{\underline{\mathbf{T}}}(E+i\epsilon)\cdot\underline{\underline{\mathbf{E}}}_{0}(dE)\,. \qquad (1.32)\end{aligned}$$

Here we invoked the spectral decomposition of $\underline{\underline{\mathbf{K}}}_{0}$,

$$\underline{\underline{\mathbf{K}}}_{0} = \int_{\mathbb{R}} E\,\underline{\underline{\mathbf{E}}}_{0}(dE)\,, \qquad (1.33)$$

where $\underline{\underline{\mathbf{E}}}_{0}(dE)$ was defined in Eq. (1.22), and performed the time integral. Furthermore we introduced the *T-operator* according to

$$\underline{\underline{\mathbf{T}}}(z) = \underline{\underline{\mathbf{V}}} + \underline{\underline{\mathbf{V}}}\cdot\Big[z-\underline{\underline{\mathbf{K}}}\Big]^{-1}\cdot\underline{\underline{\mathbf{V}}}. \qquad (1.34)$$

This clears the way to arrive at a convenient representation of the S-operator. Since

$$\begin{aligned}\underline{\underline{\mathbf{S}}} &= \underline{\underline{\mathbf{\Pi}}}_{0} - \underline{\underline{\mathbf{\Omega}}}^{*}_{+}\cdot\Big(\underline{\underline{\mathbf{\Omega}}}_{+} - \underline{\underline{\mathbf{\Omega}}}_{-}\Big) =\\ &= \underline{\underline{\mathbf{\Pi}}}_{0} - i\int_{-\infty}^{\infty} dt\,\exp(i\underline{\underline{\mathbf{K}}}_{0}t)\cdot\underline{\underline{\mathbf{V}}}\cdot\underline{\underline{\mathbf{\Omega}}}_{-}\cdot\exp(-i\underline{\underline{\mathbf{K}}}_{0}t)\cdot\underline{\underline{\mathbf{\Pi}}}_{0}\,,\end{aligned}$$

we find, using Eq. (1.32) that

$$\underline{\underline{\mathbf{S}}} = \underline{\underline{\mathbf{\Pi}}}_{0} - 2\pi i\,\underline{\underline{\boldsymbol{\mathcal{T}}}}, \qquad (1.35)$$

in which

$$\underline{\underline{\boldsymbol{\mathcal{T}}}} = \lim_{\epsilon\downarrow 0}\underline{\underline{\mathbf{\Pi}}}_{0}\cdot\int\delta(E-\underline{\underline{\mathbf{K}}}_{0})\cdot\underline{\underline{\mathbf{T}}}(E+i\epsilon)\cdot\underline{\underline{\mathbf{E}}}_{0}(dE)\,. \qquad (1.36)$$

The unitarity of $\underline{\underline{\mathbf{S}}}$ gives rise to the *Optical Theorem*,

$$\underline{\underline{\boldsymbol{\mathcal{T}}}}^{*}\cdot\underline{\underline{\boldsymbol{\mathcal{T}}}} = \frac{i}{2\pi}\left(\underline{\underline{\boldsymbol{\mathcal{T}}}} - \underline{\underline{\boldsymbol{\mathcal{T}}}}^{*}\right). \qquad (1.37)$$

By insertion of the complete set in Eq. (1.20) this can be worked out for the matrix elements $T_{j\mathbf{k}j'\mathbf{k}'}(E^{\pm})$ defined by

$$T_{j\mathbf{k}j'\mathbf{k}'}(E^{\pm}) \equiv 2E\,\langle j\hat{\mathbf{k}}, E|\,\underline{\underline{\mathbf{T}}}(E\pm i0)\,|j'\hat{\mathbf{k}}', E\rangle\,. \qquad (1.38)$$

We replaced the limit $\epsilon\downarrow 0$ by "$i0$". It is understood that $\mathbf{k} = E\hat{\mathbf{k}}$. This important scattering quantity is usually called the *T-matrix* or *scattering amplitude* and has (due to the factor E) the dimension of a length. In terms of the T-matrix the Optical Theorem reads,

$$\frac{2\pi i}{E}\Big[\,T_{n\mathbf{k}n''\mathbf{k}''}(E^{+}) - T_{n\mathbf{k}n''\mathbf{k}''}(E^{-})\,\Big] = \sum_{n'}\int\frac{d\hat{\mathbf{k}}'}{4\pi}\,T_{n\mathbf{k}n'\mathbf{k}'}(E^{-})\,T_{n'\mathbf{k}'n''\mathbf{k}''}(E^{+})\,. \qquad (1.39)$$

Specifically, choosing $\hat{\mathbf{k}} = \hat{\mathbf{k}}''$, $n = n''$, one obtains the form of the Optical Theorem as it can be found in most text books,

$$-\frac{1}{E}\,\mathrm{Im}\,T_{n\mathbf{k}n\mathbf{k}}(E^+) = \sum_{n'} \int d\mathbf{k}'\,\frac{1}{(4\pi)^2}\,|T_{n\mathbf{k}n'\mathbf{k}'}(E^+)|^2\,. \tag{1.40}$$

In the next section we show that the right-hand side is the total scattering cross-section. The left-hand side is called the *extinction* term and represents the amount of energy that is being removed from the coherent (incoming) beam. By energy conservation, the radiation loss at forward scattering must equal the amount of scattered energy. This is the message of Eq. (1.40). Different conventions show up in literature [4] [9] [11] [12] with respect to sign and normalization of the scattering amplitude. The conventions above result in the simplest "Feynman rules" for multiple scattering.

A straightforward evaluation of the scattering amplitude, using the explicit form of the eigenstates $|j\hat{\mathbf{k}}, E\rangle$ given in Eq. (1.20), as well as the Feshbach formula (1.16), yields a very convenient expression for the scattering amplitude, namely

$$T_{j\mathbf{k}j'\mathbf{k}'}(E^\pm) = \langle E\hat{\mathbf{k}}|\mathbf{g}_j^* \cdot \mathbf{T}(E \pm i0) \cdot \mathbf{g}_{j'}|E\hat{\mathbf{k}}'\rangle\,, \tag{1.41}$$

in which

$$\mathbf{T}(z) = \mathbf{\Phi} z^2 + \mathbf{\Phi} z^2 \cdot \left[z^2 - p^2\mathbf{\Delta_p} - \mathbf{\Phi} z^2\right]^{-1} \cdot \mathbf{\Phi} z^2\,. \tag{1.42}$$

We have assumed that $\boldsymbol{\mu} = 1$; $\mathbf{T}(z)$ is an operator working on *three*-dimensional vector fields. It has properties of a T-operator, corresponding to an *energy-dependent*, still complex, potential $V(z) = \mathbf{\Phi}\, z^2 = [1 - \boldsymbol{\varepsilon}(\mathbf{r})]z^2$ and complex energy z^2. Indeed it can be viewed as the T-matrix of the Helmholtz equation (1.18). The fact that light scattering strongly resembles ordinary potential scattering from an energy-dependent potential has far reaching consequences. These will be discussed in chapter 3.
The Eqs. (1.42) and (1.41) imply the useful symmetry relations,

$$T_{j\mathbf{k}j'\mathbf{k}'}(E^\pm) = T_{j'\mathbf{k}'j\mathbf{k}}(E^\mp)^* = T_{j\mathbf{k}j'\mathbf{k}'}(-E^\pm)^*\,. \tag{1.43}$$

In the definition of the T-matrix, Eq. (1.38), the T-operator has been sandwiched between two eigenfunctions at the same eigenvalue E, meaning that the T-matrix in Eq. (1.38) is defined *on-shell* only. By Eq. (1.30) the on-shell T-matrix is all that we need in the standard scattering situation that both initial wave packet and detector are infinitely separated from the region where the scattering takes place. Nevertheless, the T-operator itself has off-shell extensions. It is well known that such extensions play a role when the scattered wave is manipulated at finite distance from the region where the scattering takes place. In particular, this happens in multiple scattering. The total T-matrix (for clarity symbolized by a capital T) must again be on-shell, but t-matrices of the individual scatterers (indicated by a small t), are typically off-shell.

Moreover, to arrive at a multiple scattering formulation of macroscopic light transport (diffusion) one often considers an unbounded scattering medium. In an unbounded medium the wave packet is never asymptotically free, and neither the S-operator, nor the "energy shell" associated with it, exists.

1.4 Cross-sections

Having formulated the S-matrix we address the question how to calculate the cross-section of a scattering system. To this end we let the incoming wave packet approach a plane wave. Mathematically, this plane wave limit can be handled using kernels in Fourier space. Despite the fact that a plane wave has an infinite amount of energy and is therefore unphysical, the procedure yields a finite scattering cross-section that is supposed to describe an experiment.

Let the incoming state be $|\underline{\mathbf{F}}^0\rangle \in \underline{\underline{\mathbf{\Pi}}}_0\mathcal{K}$. Eventually, we take the limit of a plane wave propagating along the x_3-direction. By Eq. (1.35) we have

$$|\underline{\mathbf{F}}_t\rangle \stackrel{t\to\infty}{\to} \exp(-i\underline{\underline{\mathbf{K}}}_0 t)\cdot|\underline{\mathbf{F}}^0\rangle - 2\pi i\,\exp(-i\underline{\underline{\mathbf{K}}}_0 t)\cdot\underline{\underline{\boldsymbol{\mathcal{T}}}}\cdot|\underline{\mathbf{F}}^0\rangle\,. \tag{1.44}$$

The first part is the unperturbed incoming wave packet traversing the scattering region. The second part constitutes the scattered wave which we shall focus upon. The electromagnetic energy finally emerging in a volume-element $d\mathbf{k} = k^2 dk d\Omega$ in Fourier space as well as in the polarization channel j is by definition,

$$dW_j = (2\pi)^2\langle\underline{\mathbf{F}}^0|\,\underline{\underline{\boldsymbol{\mathcal{T}}}}^*\cdot\underline{\underline{\boldsymbol{\chi}}}_j(d\mathbf{k})\cdot\underline{\underline{\boldsymbol{\mathcal{T}}}}\,|\underline{\mathbf{F}}^0\rangle\,.$$

We have assumed that the incoming wave packet has no support in the element $d\mathbf{k}$. The associated intensity (energy density per solid angle per polarization channel) is found by insertion of the complete set in Eq. (1.20),

$$\frac{dW_j}{dkd\Omega}(\mathbf{k}) = \frac{(2\pi)^2}{(2\pi)^3}k^2\langle\underline{\mathbf{F}}^0|\,\underline{\underline{\boldsymbol{\mathcal{T}}}}^*\,|j\hat{\mathbf{k}},k\rangle\cdot\langle j\hat{\mathbf{k}},k|\,\underline{\underline{\boldsymbol{\mathcal{T}}}}\,|\underline{\mathbf{F}}^0\rangle\,.$$

Using the explicit form of $\underline{\underline{\boldsymbol{\mathcal{T}}}}$ in Eq. (1.36) this can be worked out to

$$\begin{aligned}\frac{dW_j}{dkd\Omega}(\mathbf{k}) &= \frac{1}{8\pi}\sum_{j'\mathbf{k}'}\sum_{j''\mathbf{k}''}\delta(k-k')\,\delta(k-k'')\\ &\times\; T_{j\mathbf{k}j''\mathbf{k}''}(k'^+)^*\,T_{j\mathbf{k}j'\mathbf{k}'}(k''^+)\,\langle j'\hat{\mathbf{k}}',k'|\underline{\mathbf{F}}^0\rangle\,\langle\underline{\mathbf{F}}^0|j''\hat{\mathbf{k}}'',k''\rangle\,.\end{aligned} \tag{1.45}$$

This can be further simplified for a polarized (no longer square-integrable) incoming wave packet with components along the x_3 direction only,

$$\langle j\hat{\mathbf{k}},k|\underline{\mathbf{F}}^0\rangle = (2\pi)^3\delta_{jm}\,\delta(k_1)\,\delta(k_2)\,\phi(k_3)\,. \tag{1.46}$$

With this choice we arrive at

$$\frac{dW_j}{dkd\Omega}(\mathbf{k}) = \frac{1}{8\pi}|T_{j\mathbf{k}\,m\,k\hat{\mathbf{e}}_3}(k^+)|^2\,|\phi(k)|^2\,. \tag{1.47}$$

The total amount of energy $d\Xi_j(k)$ that has been carried by the wave packet in Eq. (1.46) through a unit surface perpendicular to the x_3-axis is, in terms of the Poynting vector $\mathbf{S}(x_3) = \mathbf{E}^*\times\mathbf{H} = |\phi(x_3)|^2\hat{\mathbf{e}}_3$,

$$\frac{d\Xi_j}{dk}\,dk = \int_{-\infty}^{\infty}dt\,\mathbf{S}(t)\cdot\hat{\mathbf{e}}_3 = 2\pi\int_{dk}dk|\phi(k)|^2\,. \tag{1.48}$$

By definition, the *differential cross-section* $d\sigma/d\Omega$ is given by the ratio of Eqs. (1.48) and (1.47). This leads us to the desired result that

$$\frac{d\sigma}{d\Omega}(j\hat{\mathbf{k}} \to j'\hat{\mathbf{k}}', k) = \frac{1}{(4\pi)^2} \left| T_{j\mathbf{k}j'\mathbf{k}'}(k^+) \right|^2 . \tag{1.49}$$

1.5 Separable Interactions

It is well known from potential-scattering theory that the evaluation of a scattering amplitude becomes very easy if the interactions are separable. For N identical separable dielectric scatterers one starts with

$$\boldsymbol{\varepsilon} = 1 + 4\pi\boldsymbol{\alpha} \sum_{n=1}^{N} |\varphi_n\rangle\langle\varphi_n| . \tag{1.50}$$

Here $|\varphi_n\rangle = \exp(i\mathbf{p}\cdot\mathbf{r}_n)|\varphi\rangle$ is the scatterer translated from the origin to position $\mathbf{r}_n$; $\boldsymbol{\alpha}$ is a real-valued symmetric 3×3 matrix. We assume $\langle\varphi|\varphi\rangle < \infty$. From Eq. (1.42) we obtain

$$\mathbf{T}(z) = -4\pi z^2 \sum_{n,m}^{N} |\varphi_n\rangle\, \mathbf{D}^{-1}_{nm}(z)\, \langle\varphi_m| , \tag{1.51}$$

in which $\mathbf{D}(z) \in \mathbb{C}^{3,3} \otimes \mathbb{C}^{N,N}$ is given by

$$\mathbf{D}_{nm}(z) = \boldsymbol{\alpha}^{-1}\delta_{nm} + 4\pi z^2 \langle\varphi_n|\mathbf{G}^0(z)|\varphi_m\rangle . \tag{1.52}$$

The operator $\mathbf{G}^0(z)$ is the free resolvent of the Helmholtz equation as given in Eq. (1.19). We can identify the t-matrix of a single scatterer according to $t_{j\mathbf{k}j'\mathbf{k}'}(E^+) = \mathbf{g}_j^* \cdot \mathbf{t}(E^+) \cdot \mathbf{g}_{j'}$,

$$\mathbf{t}(E^+) = \frac{-4\pi E^2 |\varphi(E)|^2}{\boldsymbol{\alpha}^{-1} + 4\pi E^2 \langle\varphi|\mathbf{G}^0(E^+)|\varphi\rangle} . \tag{1.53}$$

With the definition of the "bare propagator" (Green's function),

$$\mathbf{G}^0_{nm}(E^+) = \frac{\langle\varphi_n|\mathbf{G}^0(E^+)|\varphi_m\rangle}{|\varphi(E)|^2} , \tag{1.54}$$

the scattering amplitude in Eq. (1.41) of N identical separable scatterers becomes,

$$T^{(N)}_{j\mathbf{k}j'\mathbf{k}'}(E^+) = \mathbf{g}_j^* \cdot \mathbf{t}(E^+) \cdot \sum_{n,m}^{N} \mathrm{e}^{i\mathbf{k}\cdot\mathbf{r}_n}\, \mathbf{D}^{-1}_{nm}(E^+)\, \mathrm{e}^{-i\mathbf{k}'\cdot\mathbf{r}_m} \cdot \mathbf{g}_{j'} , \tag{1.55}$$

in which now $\mathbf{D}_{nm}(E^+) = \delta_{nm} - (1-\delta_{nm})\, \mathbf{t}(E^+) \cdot \mathbf{G}^0_{nm}(E^+)$. The diagonalization of the matrix $\mathbf{D}$ corresponds physically to a summation over all possible light paths in the scattering medium. Such a diagonalization principle is a convenient property of separable interactions.

We discuss one specific and useful choice for $|\varphi\rangle$, to which we shall refer as the "pseudo-hard sphere model". One takes $\boldsymbol{\alpha}$ scalar and

$$\langle \mathbf{r}|\varphi\rangle = \frac{3\,\theta(a-r)}{4\pi a^3} \;\;;\;\; \langle \mathbf{k}|\varphi\rangle \equiv \varphi(ka) = 3\,\frac{j_1(ka)}{ka}\,. \tag{1.56}$$

Here $j_1(x)$ is the spherical Bessel function of the first kind of order 1. We find

$$t(E^+) = -\frac{4\pi}{E}\,\frac{x^3\varphi(x)^2}{\alpha^{-1} + H(x) - \frac{2}{3}ix^3\varphi(x)^2}\,. \tag{1.57}$$

We have introduced the "size parameter" $x = Ea$ and

$$H(x) = 3 + 3\,\frac{(x^2-1)\sin 2x + 2x\cos 2x}{x^3}\,. \tag{1.58}$$

It can be inferred that $0.441 < H(x) < 3.893$, so that the equation $\alpha^{-1} + H(x) = 0$ has solutions only for $-2.27 < \alpha < -0.267$. These solutions are physically relevant since they correspond to *resonances* in the scattering process. The value $\alpha = -1/3$ is special in the sense that the "unitarity limit" $t(E^+) = -6\pi i/E$ is reached in the high-frequency limit. The cross-section is in that case proportional to the square of the wavelength.

The Green's function $\mathbf{G}^0{}_{nm}(E^+)$ can be found by straightforward contour integration. With $|\mathbf{r}_n - \mathbf{r}_m| \equiv r_{nm}$ we obtain

$$\mathbf{G}^0{}_{nm}(E^+) = \frac{E}{4\pi}P_E(Er_{nm})\boldsymbol{\Delta}_{\mathbf{r}} + \frac{E}{4\pi}Q_E(Er_{nm})\hat{\mathbf{r}}\hat{\mathbf{r}}\,. \tag{1.59}$$

The orthogonal operators $\boldsymbol{\Delta}_{\mathbf{r}}$ and $\hat{\mathbf{r}}\hat{\mathbf{r}}$ project upon the subspaces perpendicular to and along the direction of $\mathbf{r}$, respectively. If $r_{nm} > 2a$, thus without overlap of the pseudo spheres, we find

$$P_E(y) = \frac{\mathrm{e}^{iy}}{y}\left(-1 + \frac{1}{iy} + \frac{1}{y^2}\right) \;\;;\;\; Q_E(y) = -2\frac{\mathrm{e}^{iy}}{y}\left(\frac{1}{iy} + \frac{1}{y^2}\right)\,. \tag{1.60}$$

On the other hand if $r_{nm} < 2a$,

$$\begin{aligned}
-\frac{1}{3}x^3Q_E(y) &= \frac{1}{2}\left[H(x) - 1 - \frac{2}{3}ix^3\varphi(x)^2\right][s(y) + s''(y)] + 1 \\
&+ \frac{3}{2x^3}\left[(x^2+1)\,[(c(y) + c''(y)] - \frac{x^2y}{2} - \frac{y}{4} + \frac{y^3}{24}\right], \\
-\frac{1}{3}x^3P_E(y) &= \frac{1}{2}\left[H(x) - 1 - \frac{2}{3}ix^3\varphi(x)^2\right][s(y) - s''(y)] + 1 \\
&+ \frac{3}{2x^3}\left[(x^2+1)\,[(c(y) - c''(y)] - \frac{x^2y}{2} - \frac{3y}{8} + \frac{y^3}{24}\right].
\end{aligned} \tag{1.61}$$

Here, again $x = Ea$ and $s(y) = \sin y/y$, $c(y) = (1-\cos y)/y$. It can be checked that Eq. (1.60) equals the free Green's function of the Helmholtz equation $\langle \mathbf{r}_n|\mathbf{G}^0(E^+)|\mathbf{r}_m\rangle$. The pseudo-hard sphere thus sees its non-overlapping neighbors as if they were point scatterers [13].

1.6 Point Scatterers

To obtain a transparent model for multiple scattering, one searches for the simplest scatterer that mimics the relevant physics. One automatically thinks of a point scatterer although, for electrons, some other simple models are known [14]. In this section we shall discuss some mathematical problems associated with point scatterers for light.

We have seen that separable interactions have the convenient property that the scattering amplitude of N scatterers is found by a simple diagonalization of an $N \times N$ matrix. Separable interactions correspond to a dielectric constant of the form $\langle \mathbf{r}|\boldsymbol{\varepsilon}|\mathbf{r}'\rangle = f(\mathbf{r})f(\mathbf{r}')$. If we do not want to take spatial correlation effects into account, it must be of the *local* form $f(\mathbf{r})\delta(\mathbf{r}-\mathbf{r}')$.

The only interaction that satisfies both the convenient property of separability and the physical constraint of locality is the point interaction. A single point scatterer located in the origin is represented by

$$\boldsymbol{\varepsilon} = 1 + 4\pi\boldsymbol{\alpha}\,|\mathbf{0}\rangle\langle\mathbf{0}|\,. \tag{1.62}$$

We assume the "polarizability" $\boldsymbol{\alpha}$ to be a real-valued symmetric 3×3 matrix. By definition $\langle \mathbf{r}|\mathbf{0}\rangle = \delta(\mathbf{r})$. However, insertion into Eq. (1.53) gives a problem, since we end up with a strongly divergent integral in the denominator,

$$\mathbf{t}(z) = -4\pi\left[\frac{\boldsymbol{\alpha}^{-1}}{z^2} + 4\pi\sum_{\mathbf{p}}\left(\frac{\hat{\mathbf{p}}\hat{\mathbf{p}}}{z^2} + \frac{\boldsymbol{\Delta}_{\mathbf{p}}}{z^2-p^2}\right)\right]^{-1}\,, \tag{1.63}$$

and we conclude that the above point scatterer does not scatter. The longitudinal part gives the strongest divergence, but can be renormalized into the coupling constant $\boldsymbol{\alpha}$ since both terms have the same z-dependence. For Schrödinger potential scattering in three dimensions, it is the divergence of the second part of the integral above, the only part present then, that can and should be renormalized. Such a procedure yields the *Fermi interaction* [15] [16],

$$t(E^+) = \frac{-4\pi}{\alpha^{-1} - i\sqrt{E}}\,, \tag{1.64}$$

in which $E = k^2$ is the energy. Disappointingly, this procedure cannot be repeated for the transverse part in Eq. (1.63). Obviously, an energy-dependent "scattering length" $\boldsymbol{\alpha}z^2$ can be identified, being related to the earlier notion of "energy-dependent potential" in section 1.3. The transverse divergence is, unlike the longitudinal divergence, energy-independent, and to renormalize it one is forced to let $\boldsymbol{\alpha}$ depend on energy. This is inconsistent with assumptions made already in section 1.1, and we must conclude that the singularity of the point interaction in Eq. (1.62) is not renormalizable. To this end we consider the following collection of "generalized" point scatterers,

$$\boldsymbol{\varepsilon} = 1 + 4\pi\boldsymbol{\alpha}\sum_n \mathrm{e}^{i\mathbf{p}\cdot\mathbf{r}_n}\mathcal{L}^*\,|\mathbf{0}\rangle\,\langle\mathbf{0}|\,\mathcal{L}\,\mathrm{e}^{-i\mathbf{p}\cdot\mathbf{r}_n}\,, \tag{1.65}$$

where $\mathcal{L}$ is a real-valued operator to be specified later, but let us agree to normalize it adjoint to $\mathcal{L}^*|\mathbf{0}\rangle = |\mathbf{0}\rangle$. To obtain a scattering amplitude different from zero we require

$$\begin{aligned} \mathbf{A}_{nm}(z) &\equiv 4\pi z^2 \langle \mathbf{0}| \, \mathcal{L} \, \mathrm{e}^{i\mathbf{p}\cdot\mathbf{r}_{nm}} \, \mathbf{G}^0(z) \, |\mathbf{0}\rangle \\ &= 4\pi z^2 \sum_{\mathbf{p}} \mathcal{L}(\mathbf{p}) \, \mathrm{e}^{i\mathbf{p}\cdot\mathbf{r}_{nm}} \left(\frac{\hat{\mathbf{p}}\hat{\mathbf{p}}}{z^2} + \frac{\mathbf{\Delta}_{\mathbf{p}}}{z^2 - p^2} \right) < \infty \, . \end{aligned} \tag{1.66}$$

We must choose $\mathcal{L}(\mathbf{p})$ such that the diagonal part, $n = m$ exists as a finite integral. By no means is this choice unique, but one that does the job is

$$\mathcal{L}_{\mathrm{Wu}}(\mathbf{p}) = \frac{2}{3} \mathbf{p} \cdot \partial_{\mathbf{p}} + \frac{1}{3} (\mathbf{p} \cdot \partial_{\mathbf{p}})^2 \, . \tag{1.67}$$

It can be checked that $\mathcal{L}^*|\mathbf{0}\rangle = |\mathbf{0}\rangle$. Since $\mathbf{p} \cdot \partial_{\mathbf{p}} = p \, \partial_p$ this operator effectively projects the divergent longitudinal part away. The choice $\mathcal{L}_{\mathrm{Wu}}$ in Eq. (1.65) will be called the *Wu model* hereafter. A coordinate-space representation of the model was proposed by Grossmann & Wu [17] and Wu [18]. An alternative derivation of the Wu model was presented in Ref. [19]. It follows after calculation that

$$\mathbf{A}_{nn}(z) = \frac{32}{9\pi} z^4 \int_0^\infty dp \, \frac{p^4}{(z^2 - p^2)^3} \, \mathbf{I} = -\frac{2}{3} i z^3 \mathrm{sign}(\mathrm{Im}\, z) \, \mathbf{I} \, ,$$

so that we obtain for the one-particle t-matrix, similar to Eq. (1.53),

$$\mathbf{t}(E^+) = \frac{-4\pi E^2}{\boldsymbol{\alpha}^{-1} - \frac{2}{3} i E^3} \, . \tag{1.68}$$

This t-matrix has the E^2-behavior at low frequencies reminiscent of dielectric scattering, and satisfies the Optical Theorem Eq. (1.40). In this respect the Wu model can be considered as a very convenient starting point for calculations on multiple scattering. For scalar α the corresponding cross-section has the "$\frac{3}{4}(1 + \cos^2\theta)$" phase-function known for Rayleigh scatterers. Hence this interaction is also being referred to as "Rayleigh Point Scatterer". Causality arguments [20] put constraints on the sign of α. We will come back to this in section 3.4.4.

One major shortcoming of the Wu model is the fact that the resonance is located at infinite frequency. The question is which modification of this model gives a resonance at finite frequency. Indeed by taking

$$\mathcal{L} = (1 + \beta \, \partial_p) \, \mathcal{L}_{\mathrm{Wu}} \, , \tag{1.69}$$

with $\beta \in \mathbb{R}$, Eq. (1.68) is replaced by

$$t(E^+) = \frac{-4\pi E^2}{\alpha^{-1} - \frac{80}{27\pi} \beta E^2 - \frac{2}{3} i E^3} \, , \tag{1.70}$$

and is, for $\alpha\beta > 0$, at resonance near $E^2 = E_0^2 \approx 1/\alpha\beta$. For simplicity we have taken $\boldsymbol{\alpha}$ scalar. An alternative treatment (put forward by Nieuwenhuizen [21]) regularizes the momentum integral of Eq. (1.63) according to

$$\sum_{\mathbf{p}} \frac{1}{z^2 - p^2} = \sum_{\mathbf{p}} \left(\frac{1}{z^2 - p^2} + \frac{1}{p^2} \right) - \sum_{\mathbf{p}} \frac{1}{p^2} \,. \tag{1.71}$$

The second (energy-independent) divergent integral is regularized to $\beta > 0$ and is naturally interpreted as the inverse extent $1/r_0$ of the scatterer. This reproduces Eq. (1.70) and strongly suggests that $\beta > 0$ if Eq. (1.70) is to represent a simplistic model for a true (finite size) scatterer. Identifying $\alpha \sim (\varepsilon - 1) r_0^3$ [22] locates the resonance at $\sqrt{\varepsilon - 1}\, E_0 r_0 \sim 1$.

The t-matrix (1.70) also emerges from the semi-classical treatment of light scattering from a harmonic oscillator with eigenfrequency E_0 [11] [23]. In that case β^{-1} is associated with the classical electron radius. We can conclude that this semi-classical t-matrix can be considered as a formal solution of Maxwell's equations.

The off-diagonal elements of the matrix $\mathbf{A}$ represent spherical waves from scatterer n to m. We write for $n \neq m$,

$$\frac{1}{4\pi z^2} \mathbf{A}_{nm}(z) = \langle \mathbf{0} | \, \mathcal{L} \, \mathrm{e}^{i\mathbf{p}\cdot\mathbf{r}_{nm}} \mathbf{G}^0(z) \, | \mathbf{0} \rangle = \langle \mathbf{0} | \, \mathrm{e}^{i\mathbf{p}\cdot\mathbf{r}_{nm}} \mathbf{G}^0(z) \, | \mathbf{0} \rangle = \mathbf{G}^0_{nm}(z) \,, \tag{1.72}$$

where $\mathbf{G}^0_{nm}(z)$ was already defined in Eqs. (1.59) and (1.60). We have made use of the identity $\langle \mathbf{0} | \mathcal{L} | f \rangle = \langle \mathbf{0} | f \rangle$, provided the latter inner product exists and $\mathcal{L}^* | \mathbf{0} \rangle = | \mathbf{0} \rangle$. This is formally true if $r_{nm} \neq 0$.

The usual procedure to come to an elegant and general description of point scatterers is by removing the origin from the domain of the free time evolution generator. One proceeds by looking for all self-adjoint extensions of the yet symmetric operator. These can, quite generally, be formulated using Krein's formula [15]. In this sense, a point scatterer is naturally interpreted as a boundary condition imposed on one single point of the domain of the free time-evolution.

In the Schrödinger case in more than three dimensions [17], as well as in the Maxwell situation, this strategy breaks down. The only self-adjoint extension thus found is again the free time evolution. We encounter a case of *essential self-adjointness*. For the Schrödinger equation in three dimensions [15] on the other hand, this procedure gives the Fermi model (1.64).

Recently, the above recipe was generalized for the cases where the usual methods failed. It was realized that divergences of the kind discussed in Eq. (1.63) can be dealt with by a renormalization procedure of the inner product, at the price of giving up its positive-definiteness. The enlarged vector space, equipped with such an inner product, is called a *Pontryagin space* and is a direct sum of two Hilbert spaces of which one is of finite dimensionality and contains the states with negative metric. The use of a Pontryagin space, suggested by Grossmann & Wu [17], was first taken up by Van Diejen and Tip [24] [25] for the Schrödinger equation in more than three dimensions. The outcome of the Pontryagin space setting is an S-matrix that is unitary in the "physical" subspace of

positive metric. In particular, the unphysical poles (poles in the physical sheets) of the models (1.68) and (1.70) can be taken care of. Later, the procedure was repeated for the Maxwell situation [22] [26]. Among the set of point interactions, the Wu model, as well as the finite-resonance modification show up as special cases.

1.7 Dwell Times

In the preceding sections we have discussed a time-dependent theory for light propagation. This theory turned out to be quite similar to the time-dependent treatment of the Schrödinger equation, although some conceptual but fundamental differences emerged. In this section we apply the time-dependent theory to find an answer to the question "How long does light spend in a dielectric scatterer?". This time is usually called the *dwell time*.

We will argue in chapter 3 that the concept of dwell time in a dielectric scatterer is of fundamental importance to the issue of multiple scattering. This is in sharp contrast with the common belief that only the total amount of scattering of the individual scatterers is the conclusive single-scatterer property relevant for multiple scattering.

Given a region B in coordinate space with projector χ_B, and an electromagnetic wave function $|\underline{\mathbf{F}}_t\rangle$, the dimensionless quantity

$$\frac{W_B(t)}{W(t)} = \frac{\langle \underline{\mathbf{F}}_t | \, \chi_B \, | \underline{\mathbf{F}}_t \rangle}{\langle \underline{\mathbf{F}}_t | \underline{\mathbf{F}}_t \rangle} \,, \tag{1.73}$$

is the relative amount of energy in region B at time t. We expect that $W_B(t) \to 0$ for $t \to \pm\infty$, because the wave packet has either not yet reached, or already left the region B. By energy conservation, the denominator in Eq. (1.73) does not depend on time. We can define a dwell time as

$$\tau_B = \int_{-\infty}^{\infty} dt \, \frac{W_B(t)}{W} \,. \tag{1.74}$$

A more sophisticated approach allows for a definition of "dwell time" provided initial and final wave packet satisfy some imposed constraints. These constraints can be formulated abstractly by projection operators $\underline{\underline{\mathbf{P}}}_i$, respectively $\underline{\underline{\mathbf{P}}}_f$, for the incoming, respectively outgoing wave, projecting upon subspaces of $\mathcal{K}$ with the requested properties. One can think of a specific solid angle, which we want the final or incoming packet to be in. In one dimension one can project upon either the reflection or transmission channel.

By virtue of the S-matrix, the asymptotic solution of the scattering set-up, satisfying our constraints for both $t \to \pm\infty$ is

$$|\underline{\mathbf{F}}_{t\to\infty}(i \to f)\rangle = \exp(-i\underline{\underline{\mathbf{K}}}_0 t) \cdot \underline{\underline{\mathbf{P}}}_f \cdot \underline{\underline{\mathbf{S}}} \cdot \underline{\underline{\mathbf{P}}}_i |\underline{\mathbf{F}}^0\rangle \,.$$

Thus at finite times,

$$\begin{aligned} |\underline{\mathbf{F}}_t(i \to f)\rangle &= \lim_{t'\to\infty} \exp(-i\underline{\underline{\mathbf{K}}}(t-t')) \cdot \exp(-i\underline{\underline{\mathbf{K}}}_0 t') \cdot \underline{\underline{\mathbf{P}}}_f \cdot \underline{\underline{\mathbf{S}}} \cdot \underline{\underline{\mathbf{P}}}_i |\underline{\mathbf{F}}^0\rangle \\ &= \underline{\underline{\mathbf{\Omega}}}_+ \cdot \exp(-i\underline{\underline{\mathbf{K}}}_0 t) \cdot \underline{\underline{\mathbf{S}}}_{fi} |\underline{\mathbf{F}}^0\rangle \,, \end{aligned}$$

where Eq. (1.25) has been inserted for the wave operator. For brevity we let $\underline{\underline{\mathbf{S}}}_{fi} = \underline{\underline{\mathbf{P}}}_f \cdot \underline{\underline{\mathbf{S}}} \cdot \underline{\underline{\mathbf{P}}}_i$. The *conditional dwell time* can now be defined according to

$$\tau_B(i \to f) \equiv \frac{D_B(i \to f)}{W(i \to f)} = \int_{-\infty}^{\infty} dt \, \frac{W_B(t, i \to f)}{W(i \to f)} \,, \tag{1.75}$$

in which,

$$\begin{aligned} W_B(t, i \to f) &= \langle \underline{\mathbf{F}}_t(i \to f) \,|\, \chi_B \,|\, \underline{\mathbf{F}}_t(i \to f) \rangle \\ &= \langle \underline{\mathbf{F}}^0 | \, \underline{\underline{\mathbf{S}}}^*_{if} \cdot \exp(i \underline{\underline{\mathbf{K}}}_0 t) \cdot \underline{\underline{\mathbf{\Omega}}}^*_+ \, \chi_B \, \underline{\underline{\mathbf{\Omega}}}_+ \cdot \exp(-i \underline{\underline{\mathbf{K}}}_0 t) \cdot \underline{\underline{\mathbf{S}}}_{fi} \, | \underline{\mathbf{F}}^0 \rangle \,, \\ W(i \to f) &= \langle \underline{\mathbf{F}}^0 | \, \underline{\underline{\mathbf{S}}}^*_{if} \cdot \underline{\underline{\mathbf{S}}}_{fi} \, | \underline{\mathbf{F}}^0 \rangle \,. \end{aligned} \tag{1.76}$$

We can work out this expression by insertion of the complete set (1.20). The numerator becomes

$$\begin{aligned} D_B(i \to f) = \int_{-\infty}^{\infty} dt \sum_{n\hat{\mathbf{k}}E} \sum_{n'\hat{\mathbf{k}}'E'} \mathrm{e}^{i(E-E')t} \; \times \\ \langle \underline{\mathbf{F}}^0 | \, \underline{\underline{\mathbf{S}}}^*_{if} | n\hat{\mathbf{k}}, E \rangle \, \langle n\hat{\mathbf{k}}, E | \, \underline{\underline{\mathbf{\Omega}}}^*_+ \chi_B \, \underline{\underline{\mathbf{\Omega}}}_+ \, | n'\hat{\mathbf{k}}', E' \rangle \, \langle n'\hat{\mathbf{k}}', E' | \, \underline{\underline{\mathbf{S}}}_{fi} \, | \underline{\mathbf{F}}^0 \rangle \,. \end{aligned} \tag{1.77}$$

The time integral can be performed and gives a factor $2\pi\delta(E - E')$; $\underline{\underline{\mathbf{\Omega}}}_+ | n\hat{\mathbf{k}}, E \rangle$ is a continuum eigenfunction of $\underline{\underline{\mathbf{K}}}$ and is, like in potential scattering theory [9], referred to as a *distorted incoming plane wave*. We shall denote it by $|\varphi^-_{n\hat{\mathbf{k}}}(E)\rangle$, and use the abbreviation

$$\langle \varphi^-_{n\hat{\mathbf{k}}}(E) | \, \chi_B \, | \varphi^-_{n'\hat{\mathbf{k}}'}(E) \rangle = W_{n\hat{\mathbf{k}}n'\hat{\mathbf{k}}'}(B, E) \,. \tag{1.78}$$

From the definition of the S-matrix in Eq. (1.35) one obtains

$$\langle n\hat{\mathbf{k}}, E | \, \underline{\underline{\mathbf{S}}}_{fi} \, | n'\hat{\mathbf{k}}', E' \rangle = \chi_f(n\hat{\mathbf{k}}) \, \chi_i(n'\hat{\mathbf{k}}') \, \delta(E - E') \, \left[\delta_{nn'} \delta(\hat{\mathbf{k}} - \hat{\mathbf{k}}') - \frac{\pi i}{E} \, T_{n\mathbf{k}n'\mathbf{k}'}(E^+) \right] .$$

Eq. (1.77) becomes

$$\begin{aligned} \frac{dD_B}{dE}(i \to f) &= 2\pi \sum_{n\hat{\mathbf{k}}} \sum_{n'\hat{\mathbf{k}}'} \chi_i(n\hat{\mathbf{k}}) \, \chi_f(n'\hat{\mathbf{k}}') \, W_{n\hat{\mathbf{k}}n'\hat{\mathbf{k}}'}(B, E) \; \times \\ &\times \; \left[I^0_E(n'\hat{\mathbf{k}}') - i \, I_E(n'\hat{\mathbf{k}}') \right]^* \left[I^0_E(n\hat{\mathbf{k}}) - i \, I_E(n\hat{\mathbf{k}}) \right] , \end{aligned} \tag{1.79}$$

where we defined $I^0_E(n\hat{\mathbf{k}}) = \langle n\hat{\mathbf{k}}, E | \underline{\mathbf{F}}^0 \rangle$, and introduced the scattered amplitude in the channel $n\hat{\mathbf{k}}$ as

$$I_E(n\hat{\mathbf{k}}) = \frac{\pi}{E} \sum_{n''\hat{\mathbf{k}}''} T_{n\mathbf{k}n''\mathbf{k}''}(E^+) \; I^0_E(n''\hat{\mathbf{k}}'') \,. \tag{1.80}$$

For simplicity we supposed that $|\underline{\mathbf{F}}^0\rangle \in \underline{\underline{\mathbf{P}}}_i \mathcal{K}$. Eq. (1.76) can now be written as

$$\frac{dW}{dE}(i \to f) = \sum_{n\hat{\mathbf{k}}} \left[|I^0_E(n\hat{\mathbf{k}})|^2 \, + |I_E(n\hat{\mathbf{k}})|^2 + 2 \, \mathrm{Im} \left(I^0_E(n\hat{\mathbf{k}})^* \, I_E(n\hat{\mathbf{k}}) \right) \right] . \tag{1.81}$$

This is recognized as a sum of the coherent wave, a scattered part, and an interference between them. Both in Eq. (1.79) and in Eq. (1.81) we have assumed that the initial wave packet has support in a small frequency range dE only. As the S-operator is on the energy-shell, the asymptotic, scattered wave has the same support. One obtains the solution for a non-monochromatic wave packet by a simple integration over frequencies E.

By combination of Eqs. (1.79) and (1.81) the conditional dwell time can be found. Starting from these general equations we can proceed by taking $\chi_i(n\hat{\mathbf{k}}) = \delta_{ni}\theta(\hat{\mathbf{k}} \in d\Omega_i)$ and $\chi_f(n\hat{\mathbf{k}}) = \delta_{nj}\theta(\hat{\mathbf{k}} \in d\Omega_f)$. By definition, the *coherent channel* is the channel in which the coherent wave is present: $d\Omega_i = d\Omega_f$, $j = i$. A *scattering channel* is a channel in which there is no contribution from the coherent wave: $d\Omega_i \cap d\Omega_f = \emptyset$ or $j \neq i$. We get

$$\frac{d\tau_B}{d\Omega_i}(i\hat{\mathbf{p}} \to i\hat{\mathbf{p}}, p) = \frac{d\tau_B}{d\Omega_f}(j\hat{\mathbf{p}}' \to i\hat{\mathbf{p}}, p) = \left(\frac{p}{2\pi}\right)^2 W_{i\hat{\mathbf{p}}i\hat{\mathbf{p}}}(B, p)\,. \tag{1.82}$$

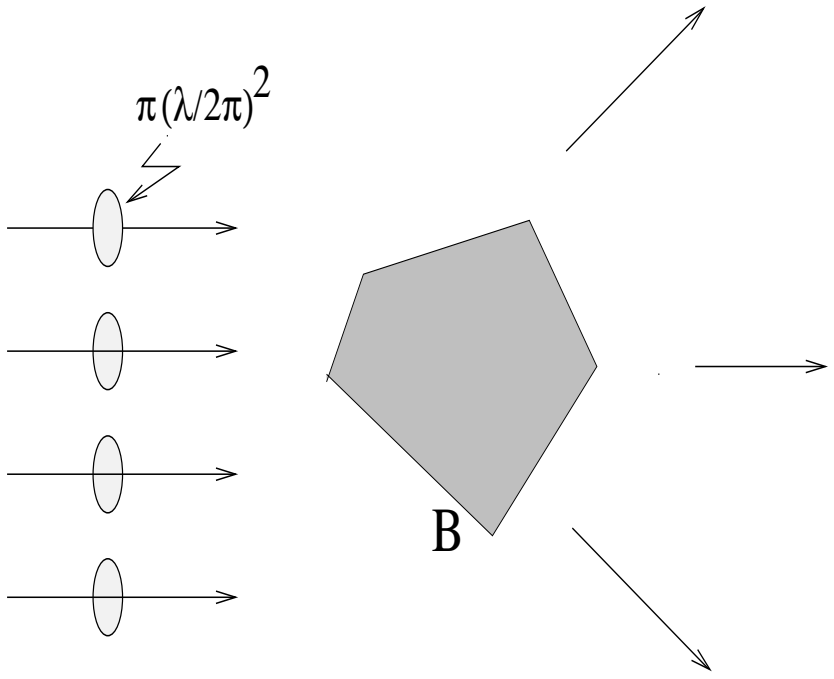

Figure 1.1: *The ray picture, see text for explanation.*

We come to a remarkable property of the monochromatic limit: the conditional dwell time in a specific channel depends only on the orientation of this channel with respect to the dielectric barrier B. The history, that is the channel through which the wave packet came in originally, is completely forgotten! Indeed, if the barrier has sufficient symmetry, all channels, including the coherent channel, have the same conditional dwell time. This is no longer true beyond the monochromatic limit.

In the absence of symmetry, a dwell time averaged over outgoing channels can be

obtained from

$$\frac{\tau_B(p)}{4\pi} \equiv \left(\frac{p}{2\pi}\right)^2 \langle W_{j\hat{\mathbf{p}}j\hat{\mathbf{p}}}(B,p)\rangle_{j\hat{\mathbf{p}}} \equiv \frac{V_B}{\lambda^2}\, W(B,p)\,. \tag{1.83}$$

We introduced the wavelength $\lambda = 2\pi/p$, and the volume V_B of the region B. $W(B,p)$ is identified as an averaged, normalized electromagnetic energy density of the region B (in a stationary situation).

Having found the (average) dwell time per scattering channel we discuss the *charging time*. When the scattering region B is large compared to the wavelength λ, one can use the *ray concept* to visualize the scattering process. In this picture, shown in Fig. 1.1, an incoming plane wave is considered as a collection of channels, called rays, which have typical size $\lambda/2\pi$. If $\sigma(p)$ is the total scattering cross-section, the number of "open" input channels is estimated as $\sigma(p)/\pi(\lambda/2\pi)^2 = 4\pi\sigma(p)/\lambda^2$. The average dwell time per open channel is called the charging time. By Eq. (1.83),

$$\tau_B^c(p) = \frac{V_B W(B,p)}{\sigma(p)}\,. \tag{1.84}$$

In chapter 3, this time will turn out to be of fundamental importance for the time-dependent properties of multiple scattering of light. Since Eq. (1.84) corrects for the two-dimensional degeneracy of the incoming wave, the charging time rather than Eq. (1.83) is expected to give an estimate of the time spent by the light in the region B, or alternatively, the time needed to "charge" the dielectric particle to energy $W(B,p)$.

The degeneracy problem can be handled more rigorously for rotationally symmetric scatterers. In that case a partial wave analysis becomes feasible, and a subsequent projection of the scattered wave upon the subspace with specified rotational quantum numbers can be performed. It is known [4] that for high frequencies such a partial wave treatment goes over into the ray concept mentioned above.

To calculate $W(B,p)$ the eigenvalue problem has to be solved. For the *Mie sphere* ($\boldsymbol{\varepsilon}(\mathbf{r}) = m^2$ inside a sphere with radius r_0 and 1 outside), this solution can be found in almost any text book on light scattering. The corresponding energy density for a Mie sphere was calculated recently by Bott [27]. The dwell time for a partial wave with principal quantum number n is, similar to Eq. (1.83),

$$\tau_B^n(p) = \frac{4\pi}{\lambda^2} V_B W^n(B,p)\,, \qquad n = 1,\, 2,\, \cdots, \tag{1.85}$$

and does not depend on the $(2n+1)$ magnetic quantum numbers. The s-wave ($n = 0$) is absent for rotationally symmetric light scatterers because of the intrinsic spin 1 of the electromagnetic field. The average energy density $W^n(B,p)$ is conveniently written in the form,

$$\begin{aligned} W^n(B,p) &= \frac{3}{4}\frac{m}{x^3} \lim_{m_i \to 0} \left(\frac{\mathrm{Re}\, a_n - |a_n|^2}{m_i} + \frac{\mathrm{Re}\, b_n - |b_n|^2}{m_i} \right) \\ &+ \frac{3}{4}\frac{m}{x^3} \left(|d_n|^2 - |c_n|^2 \right) \psi_n(mx)\psi_n'(mx)\,. \end{aligned} \tag{1.86}$$

Here $x = pr_0$ is the size parameter, $\psi_n(x) \equiv x j_n(x)$; a_n and b_n are the standard (Van de Hulst) coefficients for the Mie sphere [4]. Apart from some conventions in sign and normalization (see chapter 3), a_n respectively b_n can be considered as true on-shell t-matrices of the Mie sphere in the corresponding angular momentum subspace of the TM, respectively TE modes [28]. As such they satisfy (in the absence of absorption) an Optical Theorem of the kind discussed in Eq. (1.40). The parameters c_n and d_n instead, characterize the electromagnetic field *inside* the sphere. In Eq. (1.86) we have introduced a small absorption $m_i \equiv \mathrm{Im}\, m > 0$. The influence of small dissipation near resonances on the scattering cross-section was discussed in Ref. [29].

In Fig. 1.2 we evaluated this expression for an index of refraction $m = 2.73$ as well as for an index $m = 0.75$. The horizontal axis is labeled with the parameter $(n + 1/2)\,\lambda/2\pi$, which is recognized as the "impact parameter" in the ray picture [4] (section 12.31) and is inversely proportional to the frequency. The pronounced peaks for $m > 1$ correspond to *shape resonances* in which case the wave is trapped inside the Mie sphere, and a standing wave is built up. The dwell time can exceed the "free time" r_0/c_0 by even two orders of magnitude. Most strong peaks arise for impact parameters $(n + 1/2)\,\lambda/2\pi > r_0$. This means that they are geometrically forbidden, in the sense that these impact parameters are not expected to be captured by the sphere.

To conclude this section we draw attention to the very convenient relation between absorption and dwell time, apparent from Eq. (1.86). Such a relation can be expected in general since the longer the wave spends in the dielectric, the more it will suffer from the presence of absorption. Summing Bott's result over all partial waves yields,

$$W(B,p) = \frac{3}{8}\frac{m}{x} \lim_{m_i \to 0} \frac{Q_{\mathrm{abs}}}{m_i} + \mathrm{rest}\,, \tag{1.87}$$

where Q_{abs} is the Quality factor for absorption, and is the absorption cross-section normalized to πr_0^2. The rest term is known explicitly, but turns out to be negligible near resonances. A similar formula has been derived by Ishimaru [30]: Eq. (2-21). Accordingly, from Eq. (1.84) we obtain for the charging time,

$$\tau_B^c(p) \approx \frac{m}{p} \lim_{m_i \to 0} \frac{1-a}{2m_i}\,. \tag{1.88}$$

We introduced the *albedo* a of the scatterer, $a = 1 - Q_{\mathrm{abs}}/Q_E$. Without absorption ($m_i = 0$) we expect, by the Optical Theorem (1.40), that $a = 1$.

Eq. (1.88) can be understood heuristically. The wave amplitude ψ in the dielectric barrier is expected to be of the form $\psi(s,t) \sim \exp(imps - it)$ where s is some hypothetical coordinate along the path of the wave in the scatterer. If the *path length* in the barrier is denoted by L, we arrive at the formal expression $a = |\psi(L,t)|^2 = \exp(-2m_i L p)$ for the albedo. As a matter of fact, for $m_i \downarrow 0$, this formula can serve as *definition* for the path length in a homogeneous scatterer without absorption. Since the velocity in the dielectric is $1/m$, the time spent by the wave in the barrier is given by $\tau = Lm$. This reproduces Eq. (1.88).

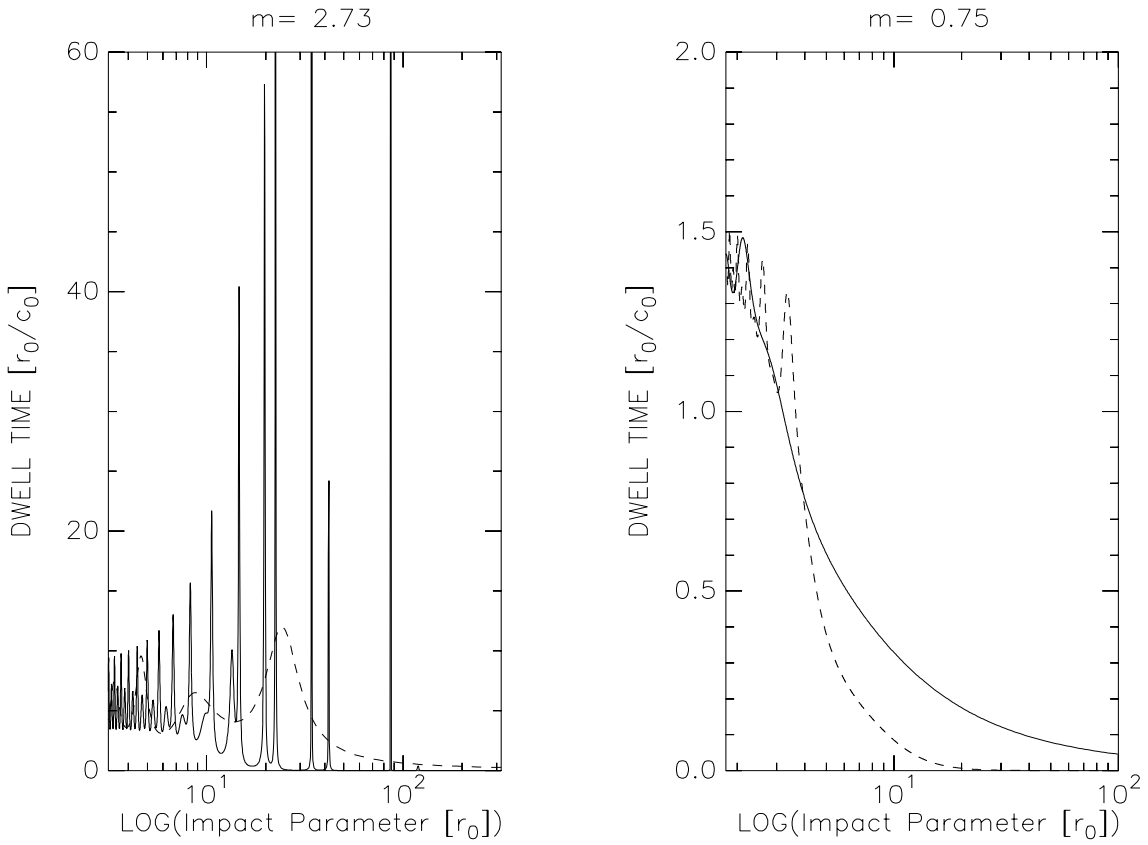

Figure 1.2: *Conditional dwell time for different partial waves. The dashed line corresponds to the partial wave $n = 2$, the bold line to $n = 10$. The critical impact parameter $b_{\rm crit}$ is the one beyond which the rays come in beyond the critical angle.*

A similar, but *exact* formula can be derived for Schrödinger potential scattering (Appendix A). The rest term in Eq. (1.87) is a manifestation of the so-called "logarithmic derivative", causing different boundary conditions for the TE and TM modes in the sphere. This term is absent in potential scattering. The set of electric (TM) modes, characterized by the coefficients a_n, is influenced by this term.

Chapter 2

Reflection and Transmission of Multiply Scattered Light

2.1 Interference in Multiple Scattering

In this chapter we shall be concerned with the propagation of light in three-dimensional slabs, containing randomly positioned scatterers. The study of multiply scattered light in dense media has a long history that probably finds its roots in the description of light transport through stellar atmospheres and interstellar clouds. The basic assumption on which most treatises rely is the neglect of all interference, hoping that it will be averaged out in the presence of disorder anyway. In this introduction we focus upon a variety of multiple-scattering phenomena that can be expected in either transmission or reflection of light from a three-dimensional random medium. For clarity, they have been summarized in Table I.

It was realized by Watson [31], De Wolf [32], Barabanenkov [33] and others, that the interference of two *time-reversed* light paths is always constructive, provided one would look exactly at backscattering (Fig. 2.1), outside the scattering medium. This phenomenon, now known as *enhanced backscattering*, is expected to be of exactly the same numerical value as the (standard) incoherent background. Both the incoherent and enhanced-backscattering contribution are present beyond the first order of scattering, on a one-to-one basis. One thus expects an enhancement factor slightly less than 2.0. In fact, from the well-documented treatment of the incoherent component [34] [35] from a semi-infinite slab one knows that the relative amount of single-scattering to the total incoherent background equals 12 % for isotropic scalar scatterers, and 17 % for Rayleigh scatterers [35] (table 43). If one ignores all other contributions to the backscattered intensity, one would obtain values of 1.87 and 1.83 respectively for the enhancement factor.

The phenomenon of enhanced backscattering is observable in the backscattering direction only. The next question is to what extent in angle around the direction of backscattering this interference effect survives. The length scale determining interference properties is the wavelength λ of light. On the other hand, the length scale relevant for multiple

scattering is the *mean free path* ℓ. Somehow, the (usually very small) ratio λ/ℓ must determine the significance of an interference phenomenon involving multiple scattering. In the treatment of multiply scattered (sometimes confusingly called incoherent) light ℓ plays the role of "step length" of the random walk with which the transport of light can be associated. The parameter ℓ can satisfactorily be envisaged as the average length scale over which the unscattered (or "coherent") wave exists before it disappears due to extinction. In a simple random-walk picture the endpoints of a light path involving N orders of scattering are roughly $\sqrt{N}\ell$ separated (more sophisticated models for multiple scattering still allow for a random-walk interpretation, but interference causes different mean free paths for extinction and diffusion). Standard arguments show that the width of the enhanced-backscattering cone is essentially $\Delta\theta \sim \lambda/(2\pi\ell\sqrt{N})$ radians.

In a random walk picture, the direction of propagation will be reset after one mean free path, but this does apparently *not* hold for the phase. Without any explicit phase-breaking processes, the phase-coherence remains intact beyond many orders of scattering. This is characteristic for *elastic* scattering. In this context, the common terminology "incoherent" does certainly not honor the multiply scattered light. From now on, the word "incoherent" will be used only for contributions in reflection and transmission that interfere with themselves.

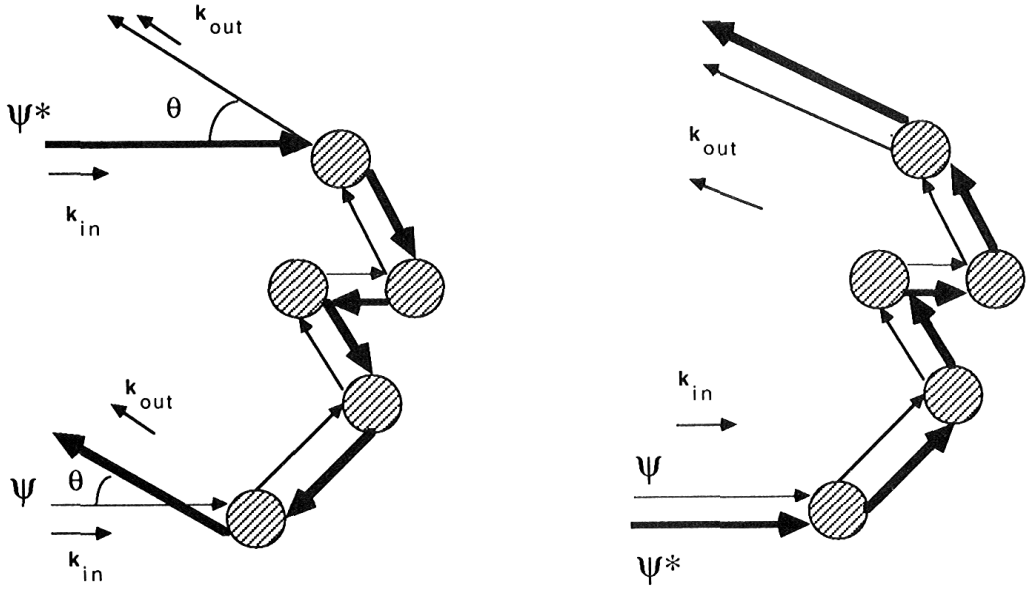

Figure 2.1: *The interference effect responsible for "Enhanced Backscattering". There is constructive interference at exact backscattering ($\theta = 0$). The figure on the right is the corresponding incoherent contribution.*

Thus both height and width of the "enhanced backscattering" from a slab can be understood qualitatively. The phenomenon was observed in 1985 by several groups [36] [37] [38]. An exact numerical solution for scalar waves in slabs of arbitrary optical depth was presented by Van der Mark *et al.* [39] [40]. The scalar-wave approximation is very often

used to study the copolarized component of multiply scattered, linearly polarized light, as well as the helicity-preserving channel of circularly polarized light. To our surprise a *diffusion approximation* turned out to be very successful in describing the enhanced-backscattering phenomenon. In the diffusion approximation one replaces an exact transport equation by a diffusion equation with appropriate boundary conditions. Such an approximation effectively replaces the light transport on arbitrary length scales by the random-walk picture mentioned earlier. One anticipates this picture to break down at length scales smaller than a few mean free paths, where low orders of scattering start to dominate and the transport becomes ballistic. Nevertheless, from a pragmatic point of view, the diffusion theory is of such a high accuracy and simplicity that it has advantages over rigorous, analytical, but complicated solutions for the enhanced backscattering [41]. In section 2.5 we shall indicate why the diffusion approximation is so accurate for scalar isotropic point scatterers.

An important reason why the diffusion approximation is *not* satisfactory is related to the *vector nature* of light. A diffusion approximation for vector waves [42] [43] does not predict all polarization features properly, because these effects are mainly caused by low orders of scattering. Low orders have a tendency to remember the direction of polarization of the incoming (linearly polarized) light. High orders of scattering, on the other hand, completely scramble the incoming polarization vector.

DIAGRAM	SECTION	EXPERIMENT	OBSERVED
single scattering	2.4	enhancement factor < 2	yes
ladder series	3.3.1 3.4	Boltzmann diffusion $D^B = v_E \ell^B/3$	yes
	3.1.4	$1/L$ transmission	yes
most-crossed series	2.5	enhanced backscattering $\Delta\theta \sim \lambda/\ell$	yes
	3.3.2	Anderson localization $D = 0$	no
	3.5	$1/L^2$ transmission	yes?
two-scatterer most-crossed	2.5	wings of enhanced backscattering $\sim 1/\theta$	yes?
	2.4	enhanced backscattering in cross-polarized channel	yes
incoherent loops	2.6	enhancement factor $\ll 2$	no?
two-scatterer forward-crossed	2.4	broad enhanced forward scattering	no
high-order forward-crossed	2.6	enhanced forward scattering $\Delta\theta \sim \lambda/\ell$	no
	3.3.2	enhanced diffusion	no

Table I. Intensity diagrams together with their experimental significance and current status. See text for discussion.

The observed polarization effects can be classified into three categories [44]. Firstly, if the incident wave is 100 % linearly polarized, the incoherent backscattered light turns out to be still partially (27 %) polarized.

The second effect, probably the one of most fundamental importance, involves the enhanced backscattering in the *cross-polarized* channel, perpendicular to the polarization of the incoming light. Only for double scattering does the incoherent contribution equal its time-reversed counterpart in backscattering. For higher orders this is no longer true, and one estimates an enhancement factor of only 1.12 in the cross-polarized channel [45]. Surprisingly, this value also emerges from the diffusion approximation [43].

The third polarization effect amounts to the spatial anisotropy of the "cone". Experimentally, the contours of equal backscattering intensity turn out to be ellipsoidal rather than circular. This can be understood in terms of the preferential direction imposed by the incoming polarization vector [44].

A general quantitative treatment of the vector nature of light in multiple scattering is very complicated. For reasons mentioned above, a vector approach beyond the diffusion approximation is more desired than an exact solution for scalar waves, for which this approximation is quite adequate. Alternatively, one can hope that a diffusion approximation in combination with an explicit treatment of the lowest orders of scattering reveals the most important effects caused by the vector nature. In this chapter it will be demonstrated that a calculation of the single and double scattering alone already gives a fair account of the qualitative importance of the polarization effects.

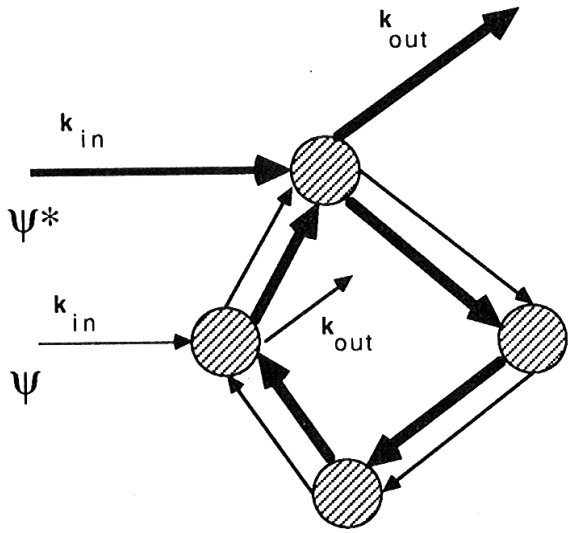

Figure 2.2: *Enhanced Forward Scattering: it consists of the interference of two loops visiting the same particles, in the same order, but ending and starting at at different members.*

An interesting question that will also be addressed is which other scattering contributions in either reflection or transmission survive in the presence of disorder. A possible candidate is the constructive interference of two identical light paths, starting and ending

at the same scatterer (*incoherent loops*). The usual incoherent treatment of multiply scattered light [35] does not take into account the fact that waves can visit the same scatterer more than once. The existence of loops generates small corrections to the incoherent background of the reflected or transmitted signal, and is not an interference effect like enhanced backscattering. It has been suggested in the literature that loops might account for reported low enhancement-backscattering factors [39], too much below 2.0 to be attributed to single-scattering alone. An alternative explanation refers to an insufficient experimental resolving power for the narrow contributions of high orders of scattering in the cone. At present, a conclusive answer has not yet been given. The alternative explanation involves a (rather uninteresting) technical detail, the first one would be a unique (!) experimental verification of recurrent wave propagation.

The question arises whether an interference effect can be associated with loops, just like the enhanced backscattering is the interference counterpart of the non-recurrent incoherent light. The answer is yes and the phenomenon is shown in Fig. 2.2. It involves the interference of two loops starting and ending at different scatterers, and visiting the same scatterers in either the same or the reversed order. These loops interfere constructively in the *forward* direction, regardless of the exact position of the scatterers. We have called it *enhanced forward scattering*. The importance of this (as yet unobserved) phenomenon will also be discussed in the present chapter.

The concept of "enhanced backscattering" has become a well-documented topic in physics. The cone has been studied in two-dimensional disordered [40] [46] media. An external magnetic field breaks the time-reversal symmetry by means of Faraday-rotation of the polarization vector [42], giving rise to a lowering of the enhancement factor. In addition, the wavelength dependence of the backscattering cone $\Delta\theta \sim \lambda/\ell$ has been discussed [47] in the context of a "terrestrial" redshift originally put forward by Wolf [48]. The principle of enhanced backscattering is also known to be relevant for rough surface scattering where some other interesting interference effects, such as *Enhanced Transmission* and *Enhanced Refraction* have been reported [49]. A fingerprint of enhanced backscattering can also be found in the phase function of a rough (dust) particle, which seems to provide an explanation for the *Opposition Effect*. This terminology refers to the observed increase of luminosity of some planets within 10° at opposition [50]. The reversal of polarization, with which this phenomenon is known to be accompanied by, can also be accounted for satisfactorily.

Time-of-Flight measurements of the cone have been performed in order to resolve different orders of scattering [51] [52]. A new dynamical technique has been employed, called *Diffusing Wave Spectroscopy* [53] [54] [55], making use of the extreme phase-sensitivity of multiple scattering to trace microscopically small movements of the scatterers. This method has successfully been applied to study the velocity-autocorrelation function in the presence of Brownian motion. In this way the existence of "long-time tails" [56] of this correlation function have been confirmed experimentally [57].

The study of the cone in the presence of amplification by each scatterer will be investigated in the near future [58], making use of the concept of stimulated emission, familiar

from laser physics. The response of *multiply scattered* light in the presence of stimulated emission is one of the future challenges in the study of multiple light scattering. Since long light paths will be favored, while retaining coherency, this study might reveal new effects.

The most important consequence, however, of the very existence of enhanced backscattering was immediately realized. Enhanced backscattering is an interference of time-reversed waves *outside* the scattering medium. On the other hand, *inside* the medium where the transport takes place, the same interference gives rise to an enhanced probability of return of the wave function to the origin. In case of diffusive transport this will result in a *lowering* of the diffusion constant. The link with *Anderson Localization* was first established by Götze [59] and Vollhardt & Wölfe [60]. Anderson localization, named after its discoverer P.W. Anderson in 1958 [61], is the phenomenon that a wave becomes localized in the presence of disorder, giving rise to a vanishing of diffusion. It was originally discussed in the context of electron transport. A lowering of diffusion is in that case recognized as a decrease of the electron conductivity. The theory predicts a continuous phase transition from a metallic (conducting) to an insulator regime [60]. As a result, the phenomenon of enhanced backscattering is sometimes recognized as *the* precursor of Anderson localization. Hence the name *Weak Localization* that has sometimes been given to it. Anderson localization will be discussed more thoroughly in chapter 3.

2.2 Scattering from a Slab

The scattering of light from slabs containing randomly positioned scatterers is a well-documented topic. We will not make any attempt to give a complete review of such studies. Different, complementary approaches have been given been given in the books of Ishimaru [30], Chandrasekhar [34], Van de Hulst [35], and Frisch [62]. In the present section we will discuss some definitions and methods that serve as input and context of the rest of this chapter.

The scattering situation is pictured in Fig. 2.3. For mathematical convenience the slab is taken infinite in extent in two dimensions, and is supposed to contain randomly distributed, identical scatterers of which the physical size is negligible with respect to the thickness of the slab. Given an incoming wave, with well-defined frequency, phase and angle of incidence, one can discriminate between "coherent" and "incoherent" scattering from the slab. The first one consists of (Fresnel) reflection from the front interface and refraction through the slab. If the slab is optically thick (many times thicker than one mean free path), the refraction is expected to be exponentially small by either absorption or scattering out of the forward direction (together referred to as *extinction*). The incoherent scattering, on the other hand, is caused by multiple scattering in the slab. As was pointed out in the previous section, multiple scattering can still give rise to interference, which is in our terminology classified as neither coherent nor incoherent.

To calculate the scattered intensity let us first consider a slab of finite extent in all directions. The differential cross-section for a finite number of scatterers was obtained

in section 1.4, and has the dimension of m^2/radians. When the slab becomes larger in transverse directions, this cross-section is expected to become proportional to the front surface A of the slab. The dimensionless *bistatic coefficient*, defined as [30]

$$\gamma(\mu_i,\mu_s) \equiv \lim_{N,A\to\infty} \frac{4\pi}{A\,\mu_i} \left\langle \frac{d\sigma}{d\Omega}^{(N)}(\hat{\mathbf{k}}_i \to \hat{\mathbf{k}}_s) \right\rangle = \lim_{N,A\to\infty} \frac{1}{4\pi A\mu_i} \left\langle |T^{(N)}_{\mathbf{k}_i\mathbf{k}_s}(k^+)|^2 \right\rangle , \qquad (2.1)$$

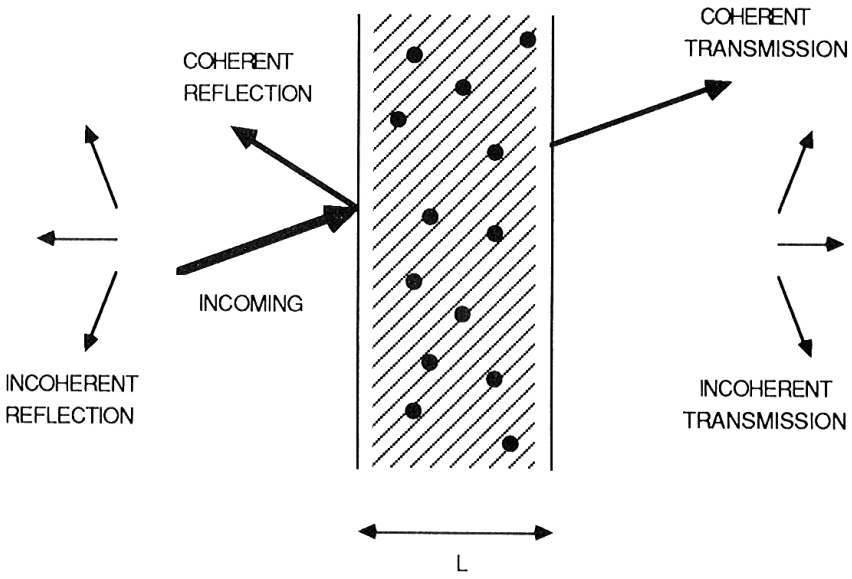

Figure 2.3: *The slab set-up. Shown are the coherent contribution (zero order) and the incoherent multiply scattered light. Interference contributions such as enhanced backscattering are not shown.*

is a very convenient quantity characterizing the scattered intensity. We use the conventional notation $\cos\theta_{i,s} \equiv \mu_{i,s}$. Apart from a factor $4\mu_s$ the bistatic coefficient coincides with the emerging intensity $R(\mu_i,\mu_s), T(\mu_i,\mu_s)$ used in the extensive tables of Van de Hulst [35]. In the above, polarization effects can be dealt with at the cost of extra bookkeeping. It is understood that the limit $N, A \to \infty$ is being performed at constant number density n, according to $N = nAL$. Such a limit is known as a *Thermodynamic Limit*. The brackets $\langle \cdots \rangle$ denote an ensemble-averaging over all possible realizations. For identical, symmetric scatterers this involves the averaging over all positions of the scatterers only, and an averaging over orientations does not need to be performed.

Since the bistatic coefficient describes the scattering from an infinite number of scatterers, it is clear that no rigorous solutions can be obtained. The first simplification without losing too much physics is the adoption of *point scatterers*. It was demonstrated in section 1.6 that the scattering from N such scatterers can be taken care of by a diagonalization of an $N \times N$ complex matrix.

Standard multiple scattering theory ignores a lot of contributions to the scattered intensity. To estimate the significance of other contributions we have calculated the bistatic

coefficient by solving *ab initio* the multiple scattering from N scalar point scatterers at resonance (i.e. $\sigma = \lambda^2/\pi$) located in a slab geometry choosing $\ell = 15.9\,\lambda$, $k\ell = 100$. Using the *bulk* value for the mean free path $\ell = 1/n\sigma$, we have taken a fixed optical thickness $\tau = L/\ell = 1$ and a front surface $A = N\sigma/\tau$, thereby increasing N. The results are shown in Fig. 2.4. A geometrical average has been performed over a thousand realizations, which turns out to be sufficient to eliminate realization-dependent fluctuations in intensity (speckles). The contribution of "single scattering" is $\gamma_s = \tau = 1$ independent of angle. This is also more or less the incoherent bistatic coefficient at backscattering predicted by Milne theory [35] for this optical depth. The N-particle bistatic coefficient of the incoherent background does not converge as N becomes larger, but is certainly much larger than the prediction of Milne theory. This strongly suggests that Milne theory underestimates multiple scattering near the boundaries. We might anticipate convergence of the thermodynamic limit when $N \geq 800$. In that case the front surface covers more than one mean free path. A calculation for such a large number of scatterers is very time-consuming, even on a supercomputer. A similar numerical experiment can be done for a sphere geometry, for which a Milne theory was recently obtained [63].

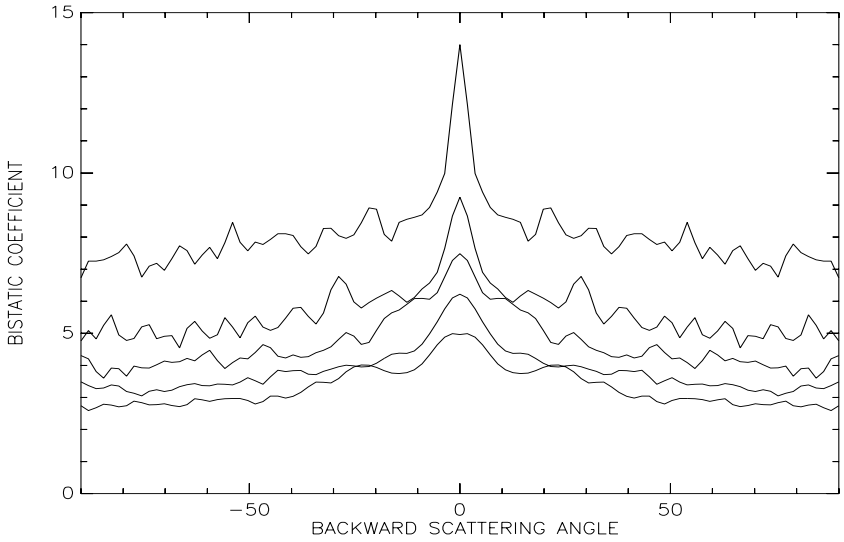

Figure 2.4: *Exact numerical solution of N scalar resonating point scatterers in a slab geometry with unity optical depth. N is given by* 50, 100, 200, 300, 500 *(upwards). On the y-axis the bistatic coefficient. The calculation for $N = 500$ was performed on the Cray Y-MP machine at SARA (with thanks to Frans Vitalis).*

The figure confirms the existence of enhanced backscattering. When correcting for single-scattering, the enhancement factor turns out to be very close to 2.0, which is exactly what one would expect (for low densities). Because the transverse size of the slab is still less than one mean free path, the width is still determined by the transverse size of the slab, and is not proportional to the "bulk theory prediction": $\lambda/2\pi\ell$.

2.3 Averaging Techniques

The usual approach to deal with multiple scattering in the presence of an infinite number of scatterers involves a perturbative treatment which we shall now discuss briefly. The main advantage of such a treatment is that one can discriminate between different scattering events, thus hopefully being able to decide whether or not certain contributions are relevant. One must arrive, according to Eq. (2.1), at a general expression for the averaged square of the T-operator in the thermodynamic limit. Let us first consider the T-operator itself. For brevity, we shall ignore polarization. In terms of this operator, the full Green's function is given by

$$G(z) = G_0(z) + G_0(z)\, T(z)\, G_0(z) = G_0(z) + G_0(z)\, V(z)\, G(z)\,. \tag{2.2}$$

Here $G_0(z) = [z^2 - p^2]^{-1}$ is the bare Green's function, corresponding to the free scalar wave equation, and $V(z) = [1 - \varepsilon]z^2$ is the "energy-dependent potential" relevant for the scalar wave equation. *By definition*, the ensemble-averaged Green's function is written as

$$\langle G(z)\rangle = G_0(z) + G_0(z)\, \Sigma(z)\ \langle G(z)\rangle\ . \tag{2.3}$$

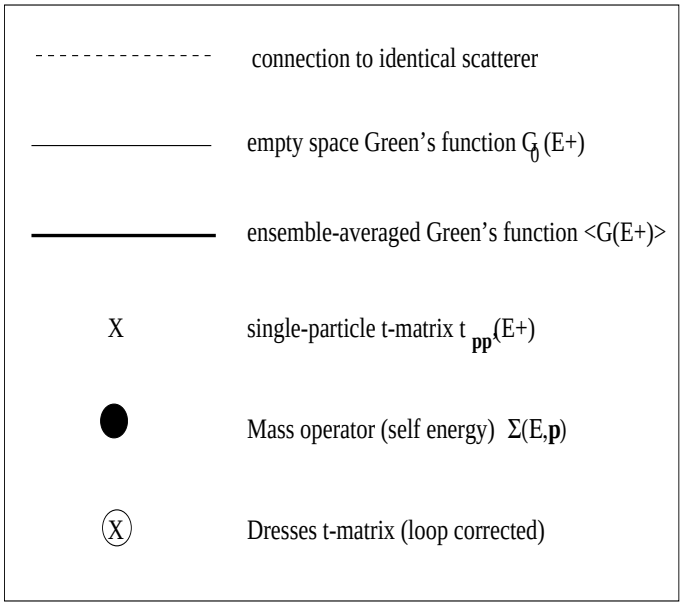

Figure 2.5: *The Feynman rules used in this thesis.*

This equation is known as the *Dyson Equation*. It introduces the *Mass Operator* or *Self-energy* $\Sigma(z)$, names acquired by its role in quantum field theory. The elegant way to deal with the averaging procedure, so as to arrive at a microscopic expression for $\Sigma(z)$, is the (Zwanzig) projection method [64]. Indeed, since "averaging twice equals averaging once" the ensemble averaging can be looked upon as a projection operation in a suitable vector space [65]. Similar methods have successfully been employed in the theory of scattering

from systems with internal degrees of freedom [3] [10], where one projects upon the elastic scattering channel (usually the ground state).

In principal, the averaged Green's function as well as the average T-operator are known as soon as we have obtained the mass operator. In general, this mass operator depends functionally on the t-operators of the individual scatterers, being linked together with bare Green's functions describing the propagation of the spherical waves from one scatterer to another. Formula (1.55) is a special but transparent demonstration of this so-called Fadeev picture. It is therefore convenient to introduce a diagrammatic approach for multiple scattering. The "Feynman" conventions have been summarized in Fig. 2.5.

The irreducible nature is a crucial property of the operator $\Sigma(z)$. Irreducibility means that any diagram that can be associated with this mass operator, cannot be separated into individual diagrams. Such a "cooking recipe" is well known from linked-cluster expansions [69] in statistical mechanics in connection with virial approximations to the equation of state. The irreducible nature makes it possible to write down at least the first and second order contributions in the density (Fig. 2.6).

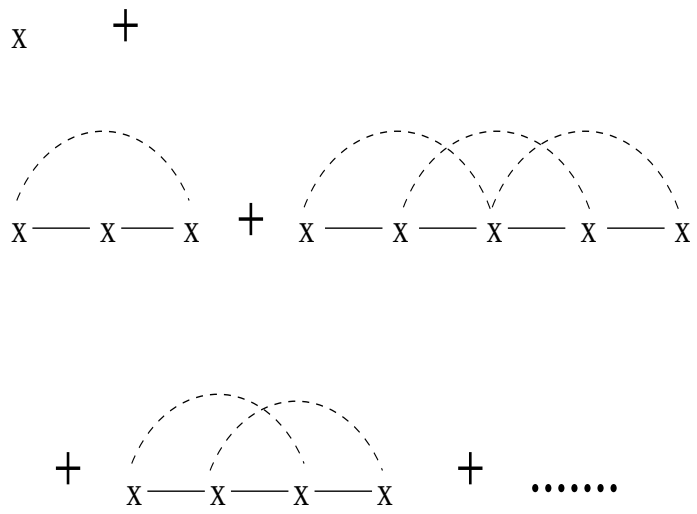

Figure 2.6: *The first and second order contributions in density of the mass operator.*

In the presence of full translational symmetry of the averaged scattering medium, the Dyson equation can readily be solved in momentum space. Writing

$$\langle \mathbf{p}| \, \Sigma(z) \, |\mathbf{p}'\rangle = (2\pi)^3 \delta(\mathbf{p} - \mathbf{p}') \, \Sigma(z, \mathbf{p}) \,, \tag{2.4}$$

with a similar expression for the Green's function, we arrive at

$$\langle G(z, \mathbf{p}) \rangle = \frac{1}{z^2 - p^2 - \Sigma(z, \mathbf{p})} \,. \tag{2.5}$$

The lowest order in density of $\Sigma(z, \mathbf{p})$ is easily obtained using the diagrammatic conven-

tions. We find

$$\begin{aligned}\Sigma^{(1)}(z,\mathbf{p},\mathbf{p}') &= \int \frac{d\mathbf{r}_1}{V}\cdots\int \frac{d\mathbf{r}_N}{V}\sum_{j=1}^{N} \mathrm{e}^{i\mathbf{p}\cdot\mathbf{r}_j}\, t_{\mathbf{p}\mathbf{p}'}(z)\, \mathrm{e}^{-i\mathbf{p}'\cdot\mathbf{r}_j} \\ &= (2\pi)^3 n\, t_{\mathbf{p}\mathbf{p}}(z)\,\delta(\mathbf{p}-\mathbf{p}')\,.\end{aligned}$$

Thus we obtain the result,

$$\Sigma^{(1)}(z,\mathbf{p}) = n\, t_{\mathbf{p}\mathbf{p}}(z)\,. \tag{2.6}$$

This approximation goes under the name of *independent scattering* and is widely used. Higher orders in density in Σ correspond to repeated scattering from clusters of particles and will be discussed in chapter 3. For rotationally symmetric scatterers, $t_{\mathbf{p}\mathbf{p}}(z)$ is independent of the direction of $\mathbf{p}$. For asymmetric scatterers an additional average over the orientation of the scatterer must be performed. This restores rotational symmetry.

According to results obtained in chapter 1, we must evaluate the mass operator at energy (frequency) $z = E + i0 \equiv E^+$. We note that the t-matrix element $t_{\mathbf{p}\mathbf{p}}(E^+)$ is not *on-shell*, since $p \neq E$. The existence of an energy shell heavily relies on the fact that the scattered wave is asymptotically free. This is definitely not true in a infinite scattering medium.

The poles of the Green's function in Eq. (2.5) correspond to collective excitations of the system, and are found by solving the implicit *complex dispersion law* [66],

$$E^2 - p^2 - \Sigma(E^+, p) = 0\,. \tag{2.7}$$

The solution $p(E)$ in the upper sheet is written as

$$p(E) \equiv m(E)E + \frac{i}{2\ell_e(E)}\,. \tag{2.8}$$

We have assumed that the averaged medium is rotationally invariant.

The fact that $-E\,\mathrm{Im}\,\Sigma(E^+,p) > 0$ is a manifestation of the fluctuation-dissipation theorem [67]. Hence we can choose $m > 0$ and $\ell > 0$. The quantities $m(E)$ and $\ell_e(E)$ are called the *average index of refraction* and the *extinction mean free path* respectively. ¿From the independent scattering approximation (2.6) one finds in lowest order of the density,

$$\begin{aligned} m^2(E) &= 1 - n\,E^{-2}\,\mathrm{Re}\,t_{\mathbf{p}\mathbf{p}}(E^+,\,\mathbf{p}=E\hat{\mathbf{p}})\,, \\ 1/\ell_e(E) &= -n\,E^{-1}\,\mathrm{Im}\,t_{\mathbf{p}\mathbf{p}}(E^+,\,\mathbf{p}=E\hat{\mathbf{p}}) = n\,\sigma(E) \equiv 1/\ell_s(E)\,. \end{aligned} \tag{2.9}$$

The parameter ℓ_s is the *scattering mean free path* and equals, by the Optical Theorem (1.40), the extinction mean free path in the absence of absorption. By contour integration we can find the Green's function in coordinate space,

$$\Big\langle G(E^+,\mathbf{r})\Big\rangle = -\frac{1}{4\pi r}\mathrm{e}^{ip(E)\,r}\,. \tag{2.10}$$

The light "intensity" is given by the square of the Green's function. The *Irreducible Vertex* $U(z_1, z_2)$ can be defined similar to the mass operator,

$$\begin{aligned}\langle G(z_1) \otimes G^*(z_2)\rangle &= \langle G(z_1)\rangle \otimes \langle G^*(z_2)\rangle \\ &+ \langle G(z_1)\rangle \otimes \langle G^*(z_2)\rangle \; U(z_1, z_2) \; \langle G(z_1) \otimes G^*(z_2)\rangle \; . \end{aligned} \tag{2.11}$$

This equation is usually referred to as the *Bethe-Salpeter Equation*. The super operator $U(z_1, z_2)$ can again be checked to be irreducible [62] [64]. On one hand, iteration yields

$$\begin{aligned}\langle G(z_1) \otimes G^*(z_2)\rangle &= \langle G(z_1)\rangle \otimes \langle G^*(z_2)\rangle \\ &+ \langle G(z_1)\rangle \otimes \langle G^*(z_2)\rangle \; R(z_1, z_2) \; \langle G(z_1)\rangle \otimes \langle G^*(z_2)\rangle \; , \end{aligned} \tag{2.12}$$

where we have introduced the *Reducible Vertex* satisfying

$$R(z_1, z_2) = U(z_1, z_2) + U(z_1, z_2) \; \langle G(z_1)\rangle \otimes \langle G^*(z_2)\rangle \; R(z_1, z_2) \, . \tag{2.13}$$

On the other hand, using Eq. (2.2), we deduce that

$$\begin{aligned}&\langle G(z_1) \otimes G^*(z_2)\rangle = \langle G(z_1)\rangle \otimes \langle G^*(z_2)\rangle \; + \\ &+ G_0(z_1) \otimes G_0^*(z_2) \, [\, \langle T(z_1) \otimes T^*(z_2)\rangle - \langle T(z_1)\rangle \otimes \langle T(z_2)^*\rangle \,] \, G_0(z_1) \otimes G_0^*(z_2). \end{aligned} \tag{2.14}$$

Comparing to Eq. (2.12) we identify

$$\begin{aligned}G_0(z_1) \otimes G_0^*(z_2) \; [\, \langle T(z_1) \otimes T^*(z_2)\rangle - \langle T(z_1)\rangle \otimes \langle T(z_2)^*\rangle \,] \, G_0(z_1) \otimes G_0^*(z_2) = \\ = \langle G(z_1)\rangle \otimes \langle G^*(z_2)\rangle \; R(z_1, z_2) \; \langle G(z_1)\rangle \otimes \langle G^*(z_2)\rangle \, . \end{aligned} \tag{2.15}$$

The first term in Eq. (2.14) will be referred to as the *coherent* wave. It is attenuated by multiple scattering, but will nevertheless be classified as "zero order". The second term contains the true multiple scattering phenomena. Denoting the solution of the scalar wave equation by $\psi(\mathbf{r})$, one obtains for the multiply scattered "intensity",

$$\begin{aligned}\left\langle |\psi(\mathbf{r})|^2 \right\rangle = \int\int\int\int d\mathbf{x}_1 \, d\mathbf{x}_2 \, d\mathbf{x}_3 \, d\mathbf{x}_4 \; \times \\ \langle G(\mathbf{r}, \mathbf{x}_1)\rangle \, \langle G^*(\mathbf{r}, \mathbf{x}_2)\rangle \, R(\mathbf{x}_1, \mathbf{x}_2, \mathbf{x}_3, \mathbf{x}_4) \, \langle \psi_{\rm inc}(\mathbf{x}_3)\rangle \, \langle \psi_{\rm inc}^*(\mathbf{x}_4)\rangle \, . \end{aligned} \tag{2.16}$$

We have omitted the frequency index. In a steady-state situation all components are evaluated at the same frequency E. $\psi_{\rm inc}(\mathbf{r})$ is the incoming wave. Eq. (2.16) can be considered as an *equation of radiative transfer* but is still too general to be of any practical use. The bistatic coefficient corresponds to $\mathbf{r}$ either taken far beyond the slab (transmission) or far in front of the slab (reflection). Obviously, we must first solve the Dyson equation to obtain the average Green's function. This has been done for the translationally symmetric case in Eq. (2.10). The solution of the Dyson equation in the absence of full translational symmetry is non-trivial, even if such a symmetry is broken for one dimension only, as is the case for a slab or spherical geometry. We shall deal with the presence of the slab

boundaries under the assumption that they are ideal interfaces between bulk and vacuum. We write for reflection,

$$\langle G(\mathbf{r},\mathbf{x})\rangle = -\frac{1}{4\pi r}\mathrm{e}^{i|E|r}\,\mathrm{e}^{-i\mathbf{K_s}\cdot\mathbf{x}}\,, \tag{2.17}$$

and for transmission,

$$\langle G(\mathbf{r},\mathbf{x})\rangle = -\frac{1}{4\pi r}\mathrm{e}^{i|E|r}\,\mathrm{e}^{-i\mathbf{K_s}\cdot(L\hat{\mathbf{z}}-\mathbf{x})}\,. \tag{2.18}$$

For $\mathbf{r}$ and $\mathbf{x}$ in the slab we adopt the form given in Eq. (2.10). The complex vector $\mathbf{K}_s$ satisfies, by definition, $K_s^2 = p(E)^2$, $p(E)$ being the complex wave number in the bulk defined in Eq. (2.9). Furthermore, the transverse component of the momentum must be continuous. This fixes $\mathbf{K}_s$ completely. In low order of the density one finds

$$\mathbf{K}_s = \mathbf{k}_s + i\frac{\hat{\mathbf{z}}}{2\ell_e\mu_s}\,. \tag{2.19}$$

Since the averaged differential cross-section is $r^2\langle|\psi(\mathbf{r})|^2\rangle$, we get for the bistatic coefficient in the direction μ_s in front of the slab,

$$\begin{aligned}\gamma_R(\mu_i,\mu_s) = \frac{1}{4\pi A\mu_i}\int\int\int\int_{\mathrm{slab}} d\mathbf{x}_1\,d\mathbf{x}_2\,d\mathbf{x}_3\,d\mathbf{x}_4 \\ \mathrm{e}^{-(\tau_1+\tau_2)/2\mu_s}\,\mathrm{e}^{i\mathbf{k}_s\cdot\mathbf{x}_{12}}R(\mathbf{x}_1,\mathbf{x}_2,\mathbf{x}_3,\mathbf{x}_4)\,\mathrm{e}^{-(\tau_3+\tau_4)/2\mu_i}\mathrm{e}^{i\mathbf{k}_i\cdot\mathbf{x}_{34}}\,,\end{aligned} \tag{2.20}$$

and behind the slab,

$$\begin{aligned}\gamma_T(\mu_i,\mu_s) = \frac{\mathrm{e}^{-\tau/\mu_s}}{4\pi A\mu_i}\int\int\int\int_{\mathrm{slab}} d\mathbf{x}_1\,d\mathbf{x}_2\,d\mathbf{x}_3\,d\mathbf{x}_4 \\ \mathrm{e}^{(\tau_1+\tau_2)/2\mu_s}\,\mathrm{e}^{i\mathbf{k}_s\cdot\mathbf{x}_{12}}R(\mathbf{x}_1,\mathbf{x}_2,\mathbf{x}_3,\mathbf{x}_4)\,\mathrm{e}^{-(\tau_3+\tau_4)/2\mu_i}\mathrm{e}^{i\mathbf{k}_i\cdot\mathbf{x}_{34}}\,,\end{aligned} \tag{2.21}$$

Here $\tau_i = z_i/\ell_e$ and $\tau = L/\ell_e$ is the optical depth of the slab. The reducible vertex can in principle be found by solving Eq. (2.13). Solving this equation with the lowest order in density $U^{(1)} \equiv s$ substituted for the irreducible vertex U ignores all repeated scattering from one particle. The diagram s itself describes incoherent scattering from one scatterer ("single scattering"), but as part of the irreducible vertex it is used as "building block" for arbitrary orders of incoherent scattering. The latter are associated with the so-called *ladder diagrams* and are part of the reducible vertex. For isotropic point scatterers one infers that

$$\begin{aligned}s(\mathbf{r}_1,\mathbf{r}_2,\mathbf{r}_3,\mathbf{r}_4) &= n\sum_{\{\mathbf{p}_i\}} t_{\mathbf{p}_1\mathbf{p}_3}(E^+)\,t_{\mathbf{p}_2\mathbf{p}_4}(E^-) \\ &\times\ (2\pi)^3\,\delta(\mathbf{p}_1-\mathbf{p}_2-\mathbf{p}_3+\mathbf{p}_4)\,\mathrm{e}^{i\mathbf{p}_1\cdot\mathbf{r}_1-i\mathbf{p}_2\cdot\mathbf{r}_2-i\mathbf{p}_3\cdot\mathbf{r}_3+i\mathbf{p}_4\cdot\mathbf{r}_4} \\ &= \frac{4\pi}{\ell_s(E)}\delta(\mathbf{r}_{14})\,\delta(\mathbf{r}_{24})\,\delta(\mathbf{r}_{34})\,.\end{aligned} \tag{2.22}$$

Writing for the ladder diagrams [69],

$$L(\mathbf{r}_1,\mathbf{r}_2,\mathbf{r}_3,\mathbf{r}_4) = s(\mathbf{r}_1,\mathbf{r}_2,\mathbf{r}_3,\mathbf{r}_4) + \ell_s^{-2} F(\mathbf{r}_1,\mathbf{r}_3)\,\delta(\mathbf{r}_{12})\,\delta(\mathbf{r}_{34})\,, \tag{2.23}$$

one obtains a simple integral equation for $F(\mathbf{r}_i,\mathbf{r}_j)$,

$$F(\mathbf{r}_1,\mathbf{r}_3) = A(\mathbf{r}_{13}) + (4\pi\ell_s)^{-1}\int_{\text{slab}} d\mathbf{r}_0\, A(\mathbf{r}_{10})\, F(\mathbf{r}_0,\mathbf{r}_1)\,, \tag{2.24}$$

where $A(\mathbf{x}) = x^{-2}\exp(-x/\ell_e)$. Using the translational symmetry of the slab in the transverse direction, one can, from Eq. (2.24), recover the Milne-problem [35].

It is instructive to solve the ladder equation (2.24) in an infinite system instead of a slab. Without absorption ($\ell_e = \ell_s$) we find for the Fourier transform $F(q)$ of $F(\mathbf{r}_i,\mathbf{r}_j) = F(|\mathbf{r}_i - \mathbf{r}_j|)$,

$$F(q) = \frac{(\arctan q\,\ell_s)/q\,\ell_s}{1-(\arctan q\,\ell_s)/q\,\ell_s}\,. \tag{2.25}$$

The diffusion approximation corresponds to approximating $F(q)$ by $3/q^2\ell_s^2$. This is exact for long light paths only ($q \to 0$).

So far we have discussed stationary transport properties (incoming plane wave), and only diagonal components ($z_1 = z_2 = E + i0$) of the Bethe-Salpeter equation were needed. It will be emphasized in chapter 3 that correlations between *different frequencies* correspond to fundamentally different *dynamical* experiments.

The theoretical description of intensity fluctuations (speckles) involves the averaging of *four* Green's functions. These again, reveal new interesting information about the random medium, in particular for parts of $\langle G_1 G_2 G_3 G_4\rangle$ for which the averaging cannot be replaced by a multiplication of averaged squares of Green's functions. This is the case for universal fluctuations (see Ref. [68] for a simple description). They will not be discussed in this thesis.

2.4 Recurrent Scattering from Two Particles

We proceed with the calculation of low-order scattering events which can, using the point scattering models discussed in chapter 1, be calculated analytically.

Why is this investigation important? One of the major experimental challenges is the preparation of a strongly scattering sample. To this end one requires efficient scatterers packed sufficiently closely together. Except for the possible onset of Anderson localization, other effects may also start contributing to the multiply scattered intensity. In this section we discuss effects induced by multiple scattering from two scatterers.

Let us first discuss contributions that renormalize single scattering. For the Rayleigh point scatterer in Eq. (1.68) the two-scatterer intensity *loops*, shown diagrammatically in Fig. 2.7, contribute to the bistatic coefficient at exact backscattering,

$$\gamma_{\mathcal{L}2} = \frac{n^2|t|^6}{4\pi A}\int\int_{\text{slab}} d\mathbf{x}_1\, d\mathbf{x}_2\, |\mathcal{L}(\mathbf{x}_{12})|^2\, \mathrm{e}^{-2\tau_1}\,, \tag{2.26}$$

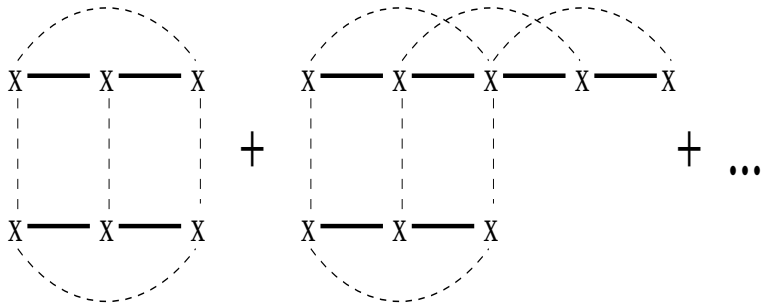

Figure 2.7: *Two-particle intensity loops: high orders correspond to high orders of recurrent scattering.*

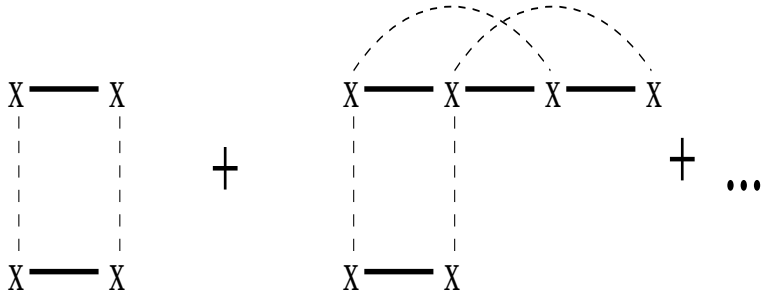

Figure 2.8: *Two-particle ladder diagrams.*

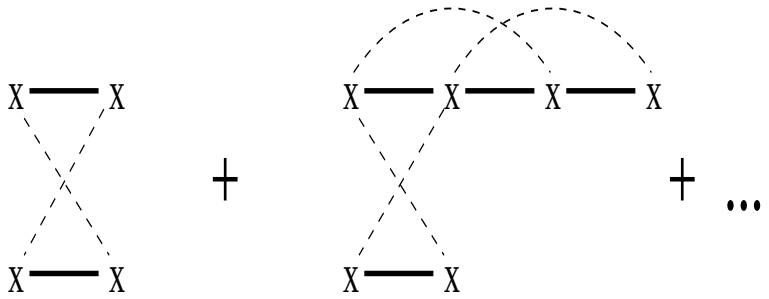

Figure 2.9: *Two-particle most-crossed diagrams.*

where the loop kernel is

$$\mathcal{L}(\mathbf{x}) = \mathbf{g} \cdot \mathbf{G}^2(\mathbf{x}) \cdot \left[1 - t^2 \mathbf{G}^2(\mathbf{x})\right]^{-1} \cdot \mathbf{g}' \,, \tag{2.27}$$

A is again the illuminated surface of the slab; t is the scattering amplitude of a single scatterer given in Eq. (1.68) with scalar α; $\mathbf{g}$ and $\mathbf{g}'$ are the polarization vectors of the incoming and outgoing light. We have chosen the z-axis normal to the slab, along the direction of the incoming wave; $\mathbf{G}(\mathbf{x})$ is the vector analogue of the averaged Green's function defined in Eq. (2.10), and is discussed in detail in section 3.3.3 of the next chapter. The bare vector Green's function has been defined in Eq. (1.59).

The bistatic coefficient is still a function of the slab thickness, the density of the scatterers, and their t-matrix t. To get some physical insight, suppose that $k\ell_e \gg 1$. As the kernel falls off rapidly with distance, $|\mathcal{L}(x)|^2 \sim \exp(-2x/\ell_e)/x^4$, we shall rely on the "infinite space approximation" and integrate the position of the second scatterer over all of space. A convenient quantity describing the amount of disorder is the dimensionless parameter

$$\eta \equiv \frac{4\pi n}{E^3} \,. \tag{2.28}$$

In terms of this parameter we find that

$$\gamma_{\mathcal{L}2} = \frac{3}{4}\,\eta\,|s|^4 \left[1 - \mathrm{e}^{-2\tau}\right] \mathcal{G}(s, \mathbf{g}\cdot\mathbf{g}') \,. \tag{2.29}$$

We defined

$$\begin{aligned} \mathcal{G}(s,X) &= X^2 \int_0^\infty dy\, y^2 \left[|T-1|^2 + \frac{2}{15}|R-T|^2 + \frac{2}{3}\mathrm{Re}\,(T-1)(R-T)^*\right] \\ &+ \frac{1}{15}\int_0^\infty dy\, y^2 |R-T|^2 \,. \end{aligned}$$

We have introduced the dimensionless quantities $s \equiv E\,t(E)/4\pi$, the optical depth of the slab τ, and

$$T = \frac{1}{1 - s^2 P^2} \;,\; R = \frac{1}{1 - s^2 Q^2}. \tag{2.30}$$

P and Q are defined in Eq. (1.60) and represent the transverse and longitudinal part of the vector Green's function. Eq. (2.29) can be solved numerically for any allowed value s. At resonance ($s = i$) we get

$$\gamma_{\mathcal{L}2} = \eta \left[1.41 + 6.52\,(\mathbf{g}\cdot\mathbf{g}')^2\right] \left[1 - \mathrm{e}^{-2\tau}\right] . \tag{2.31}$$

This is to be taken as an upper limit for the contribution of these loops at backscattering, and can be compared to the single-scattering bistatic coefficient,

$$\gamma_{\mathrm{s}} = \frac{3}{4}\,(\mathbf{g}\cdot\mathbf{g}')^2 \left[1 - \mathrm{e}^{-2\tau}\right] . \tag{2.32}$$

For $\eta \approx 0.1$, the contribution of these loops is thus comparable to single scattering and has, in addition, a cross-polarized component. It is seen that they scale with a first power of the density. As we shall see in section 2.6, this is not true for loops involving more than two scatterers. Because two-particle loops renormalize single scattering considerably, they can be responsible for a change in the enhanced-backscattering factor in weak localization experiments.

We proceed by considering corrections to double scattering. The total two-scatterer ladder sum is illustrated in Fig. 2.8. The first diagram in this series represents the usual incoherent scattering from two particles. In the backward direction we have

$$\gamma_{L2} = \frac{n^2|t|^4}{4\pi A} \int\int_{\text{slab}} d\mathbf{x}_1\, d\mathbf{x}_2\, |L(\mathbf{x}_{12})|^2\, \mathrm{e}^{-\tau_1-\tau_2}\,, \tag{2.33}$$

where the ladder-kernel is

$$L(\mathbf{x}) = \mathbf{g}\cdot\mathbf{G}(\mathbf{x})\cdot\left[1-t^2\mathbf{G}^2(\mathbf{x})\right]^{-1}\cdot\mathbf{g}'\,.$$

It is interesting to note that, because of the singular nature of the vector Green's function, the incoherent ladder (first diagram of Fig. 2.8) suffers from an UV singularity. Only by summing the whole geometric series, thus taking into account all orders of repeated scattering, can this singularity be taken care of. Proper scaling with $k\ell_e$ gives the ladder-kernel in the "far-field" approximation ($x \gg \lambda$),

$$|L_\infty(\mathbf{x})|^2 = \frac{1}{x^2}\mathrm{e}^{-x/\ell_e}\,\left(\mathbf{g}\cdot\boldsymbol{\Delta}_{\mathbf{x}}\cdot\mathbf{g}'\right)^2\,, \tag{2.34}$$

which does not suffer from the singularity mentioned above. The bistatic coefficient becomes, in the copolarized ($\mathbf{g}\parallel\mathbf{g}'$) and cross-polarized ($\mathbf{g}\perp\mathbf{g}'$) channel,

$$\begin{aligned}\lim_{k\ell_e\to\infty}\begin{pmatrix}\gamma_{L(2)}(\text{copol})\\ \gamma_{L(2)}(\text{cross})\end{pmatrix} = & \\ \frac{9}{8}\left[1-\mathrm{e}^{-2\tau}\right] \;\times\; & \int_0^1 \frac{dc}{1+c}\left[c^2\begin{pmatrix}1\\0\end{pmatrix}+(1-c^2)^2\begin{pmatrix}3/8\\1/8\end{pmatrix}\right]\left[1-\mathrm{e}^{-(1+c)\tau}\right] \\ \xrightarrow{\tau>1} \;& \frac{9}{8}\begin{pmatrix}\log 2-\frac{11}{32}\\ \frac{5}{96}\end{pmatrix} = \begin{pmatrix}0.3930\\0.0586\end{pmatrix}\,.\end{aligned} \tag{2.35}$$

The copolarized value compares well to the incoherent double scattering for isotropic point scatterers $\frac{1}{2}\log 2 = 0.3466$ [35] (page 553). Whereas the single scattering in Eq. (2.32) is 100 % polarized, the two-scatterer contribution at backscattering has a polarization degree of

$$\frac{\gamma(\text{copol})-\gamma(\text{cross})}{\gamma(\text{copol})+\gamma(\text{cross})} = 74\,\%\,. \tag{2.36}$$

The total incoherent bistatic coefficient for Rayleigh scatterers, summed for both polarization channels, equals 4.588 at backscattering [35] (table 54). We deduce that single and

double scattering events *alone* are responsible for a polarization degree equal to 23.7 % in the backscattered signal. This is not far different from the value $\pm 27\,\%$ found in Ref. [45] by numerical simulation, confirming that the partial polarization of the backscattered signal is due to the very low orders of scattering.

Near-field corrections to incoherent double scattering can be found by subtracting Eq. (2.34) from Eq. (2.33). Writing $\gamma_{L2} = \gamma_{L2}(\text{far field}) + \Delta\gamma_{L2}$ we find in the limit of weak disorder $k\ell_e \gg 1$,

$$\Delta\gamma_{L2} = \Delta\gamma(\text{trans.}) + \Delta\gamma(\text{long.}) + \Delta\gamma(\text{trans./long.})\,,$$

where

$$\begin{aligned}
\Delta\gamma(\text{trans.}) &= \frac{3}{4}\,\eta\,|s|^2 \begin{pmatrix} 8/15 \\ 1/15 \end{pmatrix} \int_0^\infty dy\, y^2 \left(|PT|^2 - \frac{1}{y^2} \right), \\
\Delta\gamma(\text{long.}) &= \frac{3}{4}\,\eta\,|s|^2 \begin{pmatrix} 1/5 \\ 1/15 \end{pmatrix} \int_0^\infty dy\, y^2 |QR|^2\,, \\
\Delta\gamma(\text{trans./long.}) &= \frac{3}{4}\,\eta\,|s|^2 \begin{pmatrix} 2/15 \\ -1/15 \end{pmatrix} \int_0^\infty dy\, y^2\, 2\,\mathrm{Re}\,(QRP^*T^*)\,. \qquad (2.37)
\end{aligned}$$

Again, the upper number of the column vector applies in the copolarized channel and the lower number in the cross-polarized channel. The integrals can be evaluated numerically for any one-scatterer t-matrix. Setting this t-matrix to resonance ($s = i$) we get

$$\Delta\gamma_{L2} = \begin{pmatrix} -1.36 \\ +0.19 \end{pmatrix} \eta\,. \qquad (2.38)$$

The time-reversed variants of the two-scatterer ladders (Fig. 2.9) give the lowest order contribution to the backward cone. Assuming again $k\ell_e \to \infty$ we deduce, as a function of the backscattering angle θ,

$$\gamma_{C2}(\theta) = \frac{n^2|t|^4}{4\pi A} \int\int_{\text{slab}} d\mathbf{x}_1\, d\mathbf{x}_2\, |L_\infty(\mathbf{x}_{12})|^2\, \mathrm{e}^{-s(\theta)(\tau_1+\tau_2)/2} \cos \mathbf{b}\cdot\mathbf{x}_{12}\,, \qquad (2.39)$$

with $\mathbf{b} \equiv \mathbf{k} + \mathbf{k}'$ and $s(\theta) \equiv 1 + 1/\mu_s$. In the next section this equation is further analyzed in the regime where it is of experimental importance, namely in the wings: $\theta > 1/k\ell$.

Corrections to the cone induced by the near-field between two scatterers can be found as follows,

$$\Delta\gamma_{C2}(\theta) = \frac{3}{2}\,\frac{\eta\,|s|^2}{s(\theta)} \int \frac{d\mathbf{y}}{4\pi} \left[|L(\mathbf{y})|^2 - |L_\infty(\mathbf{y})|^2 \right] \cos \mathbf{b}\cdot\mathbf{y}\,. \qquad (2.40)$$

Contrary to Eq. (2.39) we do not need extinction-factors to ensure convergence of this integral. Physically this means that the angular width of this correction is by no means equal to the typical $1/k\ell$ predicted by the most-crossed diagrams in the far-field approximation. Whereas the latter account for a large narrow cone, the diagrams in Eq. (2.40)

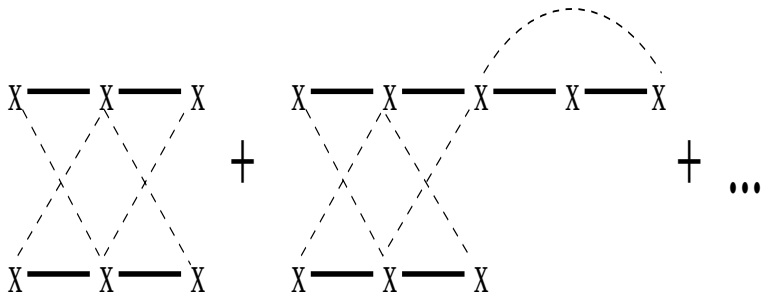

Figure 2.10: *The full diagrammatic representation of the Enhanced Forward Scattering from two scatterers.*

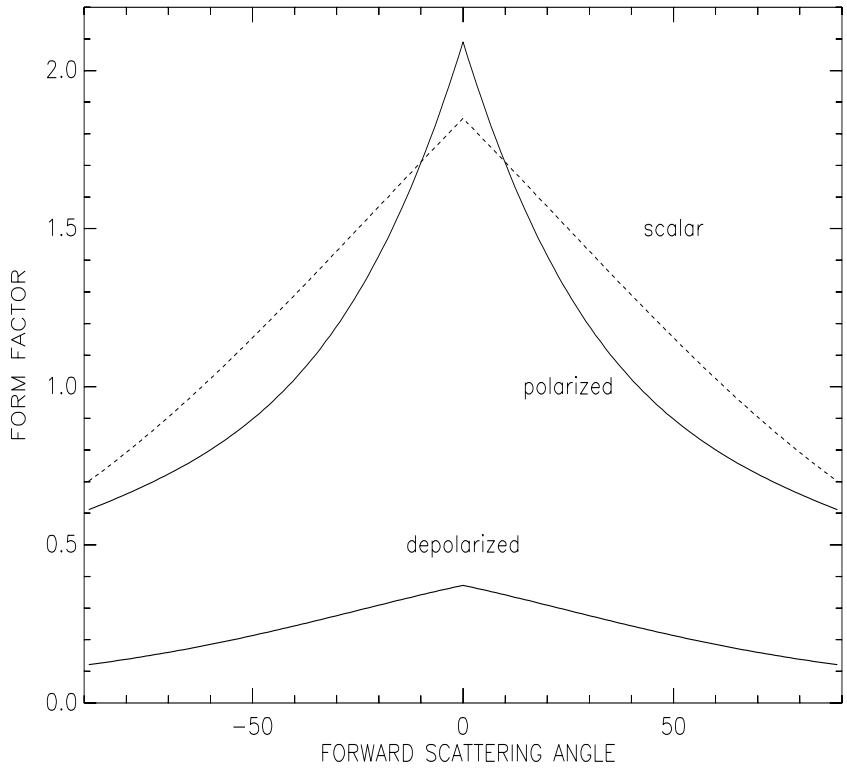

Figure 2.11: *The structure factor of the vector forward cone, as well as a scalar calculation. The cusp near $\theta = 0$ is an artifact of the "infinite-space approximation".*

yield a small broad cone, and can better be classified as a density-correction to the *background*. We emphasize that the range of the near field is essentially the wavelength λ, so that an interference effect involving this near field induces a typical width of $\lambda/\lambda = 1$ radians. In this sense, although this near-field correction obeys the one-to-one mapping of ladders and most-crossed diagrams, it nevertheless influences the enhanced-backscattering factor! In the copolarized channel this factor is *increased* by the near field (for Rayleigh scatterers).

The last two-scatterer intensity diagrams we will discuss are shown in Fig. 2.10. It is easy to see that these diagrams give rise to constructive interference in the *forward* direction. Moreover, their value at forward scattering is equal to the loop-background. The bistatic coefficient behind the slab is, in the "infinite space approximation", as a function of the forward scattering angle θ,

$$\gamma_{\mathcal{F}2}(\theta) = \frac{2}{3}\eta\,|s|^4\,\left[\frac{\mathrm{e}^{-\tau} - \mathrm{e}^{-\tau/\mu_s}}{1/\mu_s - 1}\right]\int \frac{d\mathbf{y}}{4\pi}|\mathcal{F}(\mathbf{y})|^2\cos\mathbf{f}\cdot\mathbf{y}\,, \tag{2.41}$$

with

$$\mathcal{F}(\mathbf{y}) = (T-1)\,\mathbf{g}\cdot\mathbf{g}' + (R-T)(\mathbf{g}\cdot\hat{\mathbf{y}})(\mathbf{g}'\cdot\hat{\mathbf{y}})\,, \tag{2.42}$$

and $\mathbf{f} = \mathbf{k} - \mathbf{k}'$. Because the integral exists for any θ without damping the Green's function, the angular width of this forward cone is *not* given by the "extinction-limited" value $1/k\ell$, but is much broader and is mainly determined by the τ-dependent front factor. The broadness will complicate verification of enhanced forward scattering in transmission experiments. The form factor in Eq. (2.41) of enhanced forward scattering is shown in Fig. 2.11. The individual scatterers are set to resonance.

2.5 Wings of Enhanced Backscattering

We would like to find the angular scaling behavior of the wings of enhanced backscattering, by definition, the regime where $\theta > 1/k\ell$. These wings are determined by the very low orders of scattering. We adopt conservative scattering with $\langle\cos\theta\rangle = 0$ so that $\ell_s = \ell_e = \ell$. The simplest description involves the scalar backscattering from a semi-infinite slab. The two-scatterer cone is given by the bistatic coefficient,

$$\gamma_{C2}\,(\theta) = \frac{1}{s(\theta)k\ell}\int_{\text{slab}}\frac{d\mathbf{y}}{4\pi}\,\frac{1}{y^2}\,\mathrm{e}^{-(y+y_z s(\theta))/k\ell}\,\cos\mathbf{b}\cdot\mathbf{y}\,, \tag{2.43}$$

with $\mathbf{b} = k^{-1}\,(\mathbf{k} + \mathbf{k}')$, $b = 2\sin(\theta/2)$. This integral can be solved numerically. To get more physical insight, suppose that $k\ell \gg 1$. In the wings we have, by definition, $b > 1/k\ell$ and the bistatic coefficient simplifies to

$$\gamma_{C2}\,[\theta > 1/k\ell] = \frac{1}{s(\theta)k\ell}\int_0^\infty dy\,\frac{\sin by}{by} = \frac{1}{s(\theta)k\ell}\,\frac{\pi}{2}\,b(\theta)^{-1}\,. \tag{2.44}$$

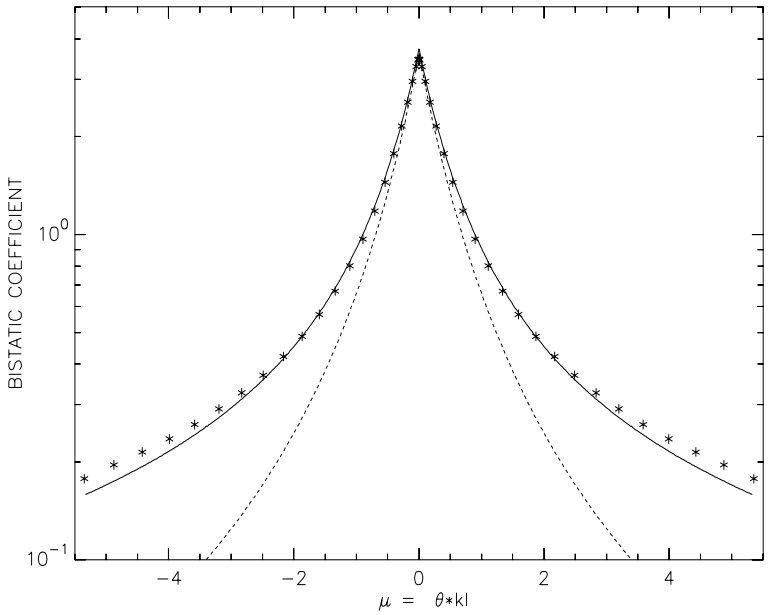

Figure 2.12: *Exact numerical solution of the scalar EB cone (△) for isotropic point scatterers in a slab with $\tau = 70$ (kindly provided by Martin van der Mark), as well as the diffusion approximation with the explicit inclusion of double scattering. Dashed: conventional diffusion approximation.*

Defining $\mu \equiv \theta\, k\ell$, we find the following scaling behavior,

$$\gamma_{C2}\,[\theta > 1/k\ell] \to \frac{\pi}{4}\mu^{-1}\,. \tag{2.45}$$

This can be contrasted to results obtained on the basis of a diffusion approximation [36] [39],

$$\gamma_{C(\mathrm{diff})}\,[\theta > 1/k\ell] \to \frac{3}{2}\,\mu^{-2}\,. \tag{2.46}$$

This μ^{-2} decay is an erroneous result of the diffusion approximation. An earlier variant of this approximation [70] makes the wings even proportional to $\exp(-\mu^2)$. What goes wrong when applying the diffusion approximation? In the diffusion approximation, one replaces the (Fourier transform of the) ladder kernel $F(q)$ in Eq. (2.25) by its hydrodynamic ($q \to 0$) limit $3/q^2\ell^2$. To our surprise, we observe that this approximation holds for large q as well, provided we drop the lowest order (the two-scatterer contribution) in the geometric series (2.25), corresponding to double scattering. Then

$$F^{(2)}(q) \equiv \frac{(\arctan q\,\ell)^2/(q\ell)^2}{1-(\arctan q\,\ell)/(q\,\ell)} \begin{cases} \overset{q\to\infty}{\to} 2.47\,(q\,\ell)^{-2} \\ \overset{q\to 0}{\to} 3.00\,(q\,\ell)^{-2} \end{cases} \approx \alpha^{-1}(q\,\ell)^{-2}\,. \tag{2.47}$$

This is the reason that the diffusion approximation works so well for point scatterers [39]. An inspection shows that the variable q can be mapped upon the backscattering angle

θ. Eq. (2.47) is thus consistent with Eq. (2.46). The absence of double scattering in Eq. (2.47) explains the difference between Eqs. (2.45) and (2.46). Moreover, it suggests that the diffusion approximation can be improved considerably by a simple addition of the double-scattering contribution. The "effective" diffusion constant for orders of scattering larger than two, proportional to the front factor $0.333 < \alpha < 0.405$, can be estimated by fitting the diffusion approximation *plus* explicitly first and second order of scattering to the total exact incoherent bistatic coefficient for an optical thick slab. The diffusion approximation yields $\gamma_R(\text{diff}) = \alpha^{-1}(z_0 + 1/2)$ whereas $\gamma_R(\text{exact}) = 4.228$ for the bistatic coefficient at reflection. We obtain $\alpha = 0.3579$. A similar procedure for the incoherent transmission beyond the slab fits the exact asymptotic result [35] (page 82), $\gamma_T(\text{exact}) = 8.4553/(\tau + 2z_0)$ to the diffusive result [40] $\gamma_T(\text{diff}) = \alpha^{-1}(z_0 + 1)^2/(\tau + 2z_0)$, giving $\alpha = 0.3460$. Here $z_0 = 0.7104 \cdot \cdot$ is the extrapolation length for conservative isotropic point scatterers that emerges from a fit of the diffusion approximation to the standard Milne problem [35] [71]. In Fig. 2.12 we have demonstrated the exact numerical solution, the usual diffusion approximation, and the sum of double scattering *and* higher orders adopting $\alpha = 0.3579$.

We conclude on the basis of a scalar treatment that the θ^{-1} scaling in the wings of the cone follows rigorously from the double-scattering contribution. A θ^{-1} behavior was also reported in Ref. [72], though under completely different assumptions.

Because the wings are described by double scattering only, one can hope to describe the impact of the vector nature of light on the wings. The wings of the Rayleigh vector cone can be evaluated using Eq. (2.39),

$$\begin{aligned} \gamma_{C2}\left[\theta > 1/k\ell\right] &= \frac{9}{4}\frac{1}{s(\theta)k\ell}\int \frac{d\mathbf{y}}{4\pi}\,\frac{\cos\mathbf{b}\cdot\mathbf{y}}{y^2}\,\times \\ &\times \left[(\mathbf{g}\cdot\mathbf{g}')^2 + (\mathbf{g}\cdot\hat{\mathbf{y}})^2(\mathbf{g}'\cdot\hat{\mathbf{y}})^2 - 2(\mathbf{g}\cdot\mathbf{g}')(\mathbf{g}\cdot\hat{\mathbf{y}})(\mathbf{g}'\cdot\hat{\mathbf{y}})\right]. \end{aligned} \quad (2.48)$$

The angular integral is

$$\begin{aligned} &(\mathbf{g}\cdot\mathbf{g}')^2\, j_0(by) + \left[1 + 2(\mathbf{g}\cdot\mathbf{g}')^2\right]\frac{j_2(by)}{(by)^2} + \left(\mathbf{g}\cdot\hat{\mathbf{b}}\right)^2\left(\mathbf{g}'\cdot\hat{\mathbf{b}}\right)^2 j_4(by) \\ &\quad - \left[\left(\hat{\mathbf{b}}\cdot\mathbf{g}\right)^2 + \left(\hat{\mathbf{b}}\cdot\mathbf{g}'\right)^2 + 4(\mathbf{g}\cdot\mathbf{g}')\left(\mathbf{g}\cdot\hat{\mathbf{b}}\right)\left(\mathbf{g}'\cdot\hat{\mathbf{b}}\right)\right]\frac{j_3(by)}{by} \\ &\quad -2(\mathbf{g}\cdot\mathbf{g}')^2\,\frac{j_1(by)}{by} + 2(\mathbf{g}\cdot\mathbf{g}')\left(\mathbf{g}\cdot\hat{\mathbf{b}}\right)\left(\mathbf{g}'\cdot\hat{\mathbf{b}}\right) j_2(by), \end{aligned}$$

where j_m is the spherical Bessel function of the first kind of order m, and $\hat{\mathbf{b}} \equiv \mathbf{b}/b$. Using the standard integral [73],

$$\int_0^\infty dx\,\frac{j_n(x)}{x^m} = \frac{\sqrt{\pi}}{2}\,2^{-m}\,\frac{\Gamma\left(\frac{1}{2} + \frac{1}{2}(n-m)\right)}{\Gamma\left(1 + \frac{1}{2}(n+m)\right)}, \quad (2.49)$$

the wings become equal to

$$\gamma_{C2}\left[\theta > 1/k\ell\right] = \frac{9}{4}\frac{1}{s(\theta)k\ell}\frac{\pi}{b}\,\mathcal{W}\left(\mathbf{g}, \mathbf{g}', \hat{\mathbf{b}}\right), \quad (2.50)$$

where

$$\begin{aligned}\mathcal{W}\left(\mathbf{g},\mathbf{g}',\hat{\mathbf{b}}\right) &= \frac{1}{8}\left(\mathbf{g}\cdot\mathbf{g}'\right)^2+\frac{1}{16}+\frac{3}{16}\left(\hat{\mathbf{b}}\cdot\mathbf{g}\right)^2\left(\hat{\mathbf{b}}\cdot\mathbf{g}'\right)^2 \\ &- \frac{1}{16}\left[\left(\hat{\mathbf{b}}\cdot\mathbf{g}\right)^2+\left(\hat{\mathbf{b}}\cdot\mathbf{g}'\right)^2\right]+\frac{1}{4}\left(\mathbf{g}\cdot\mathbf{g}'\right)\left(\hat{\mathbf{b}}\cdot\mathbf{g}\right)\left(\hat{\mathbf{b}}\cdot\mathbf{g}'\right). \qquad (2.51)\end{aligned}$$

The complex nature of the function $\mathcal{W}$ clearly illustrates the anisotropy of the vector cone. The vector $\hat{\mathbf{b}}$ is given by $\hat{\mathbf{b}}=\sin\frac{\theta}{2}\,\hat{\mathbf{z}}+\cos\frac{\theta}{2}\,\hat{\mathbf{R}}$ where $\hat{\mathbf{z}}$ is normal to the slab, and $\hat{\mathbf{R}}$ parallel. We set $\hat{\mathbf{R}}=\cos\phi\,\hat{\mathbf{x}}+\sin\phi\,\hat{\mathbf{y}}$ and define the direction of the incoming polarization $\mathbf{g}=\hat{\mathbf{y}}$. To calculate the anisotropy of the wings, we distinguish [44] two cases:

$$\begin{aligned}&\text{case I}: && \phi=0 \text{ or } \phi=\pi\,,\\ &\text{case II}: && \phi=-\pi/2 \text{ or } \phi=\pi/2\,. \qquad (2.52)\end{aligned}$$

Suppose that $\theta\equiv\mu/k\ell\ll 1$. Then $\hat{\mathbf{b}}=\hat{\mathbf{R}}$ and it follows for the wings in the copolarized channel ($\mathbf{g}\parallel\mathbf{g}'$) that

$$\gamma_{C2}(\text{copol}) = \frac{9\pi}{128}\left(3+5\,\sin^2\phi\right)\,\mu^{-1}\,. \qquad (2.53)$$

The copolarized wings for case I compare well to the scalar result in Eq. (2.45). Both for the scalar case and the copolarized Rayleigh case we recover the μ^{-1} scaling. For the cross-polarized channel ($\mathbf{g}\perp\mathbf{g}'$) we find

$$\gamma_{C2}(\text{cross}) = \frac{27\pi}{512}\,\sin^2 2\phi\;\;\mu^{-1}\,. \qquad (2.54)$$

For both the cases I and II, Eq. (2.54) vanishes, and we need higher orders in $1/k\ell$. Through an additional expansion of the extinction factors in the bistatic coefficient of the backscattering cone it follows,

$$\gamma_{C2}(\text{cross, case I \& II}) = \frac{21}{64}\,\mu^{-2}\,. \qquad (2.55)$$

This $1/\mu^2$ scaling in the cross-polarized channel is a new (fourth) polarization effect that has not yet been reported experimentally. A μ^{-2} decay was also found by Stephen and Cwilich [43] on the basis of the diffusion approximation, though for *both* channels. As has been demonstrated in Eq. (2.47) for scalar waves, this is due to a neglect of the two-scatterer contribution. In the cross-polarized channel the wings are in principle given by the sum of the diffusive part found by Stephen and Cwilich and the two-scatterer contribution in Eqs. (2.54) and (2.55).

¿From Eq. (2.53) we infer that the wings of case II in the copolarized channel are (for Rayleigh scatterers) larger in magnitude than for case I, in agreement with Ref. [44]. More precisely the intensities compare as I : II = 3 : 8. The cross-polarized wings are the same for both case I and II, and are narrower. For fixed θ they reach a maximum

at $\phi = \pi/4, -\pi/4$, thus exactly in between the directions of both polarization vectors. Then, copol : cross = 22 : 3.

We can generalize Eq. (2.50) for the case of circularly polarized light in which case the polarization vectors become complex-valued. If the incoming and outgoing waves have the same helicities (pres) we set, at backscattering ($\mathbf{k}' = -\mathbf{k}$),

$$\mathbf{g} = \mathbf{g}'^{*} = \frac{1}{2}\sqrt{2}\,(\hat{\mathbf{x}} + i\,\hat{\mathbf{y}})\ , \tag{2.56}$$

and for opposite (opp) helicity,

$$\mathbf{g} = \mathbf{g}' = \frac{1}{2}\sqrt{2}\,(\hat{\mathbf{x}} + i\,\hat{\mathbf{y}})\ . \tag{2.57}$$

Since $|\mathbf{g}\cdot\hat{\mathbf{b}}|^2 = |\mathbf{g}'\cdot\hat{\mathbf{b}}|^2 = \frac{1}{2}$ independent of ϕ, and using the complex equivalent of Eq. (2.51), we find for the circularly-polarized wings,

$$\gamma_{C2}(\text{opp}) = \frac{171\pi}{512}\,\mu^{-1} \quad ; \quad \gamma_{C2}(\text{pres}) = \frac{27\pi}{512}\,\mu^{-1}\,, \tag{2.58}$$

with a ratio of 19 : 3. Both helicity channels exhibit the θ^{-1} scaling, and are *independent* of ϕ. The absence of anisotropic effects makes the wings very similar to the scalar wings in Eq. (2.45). The similarity of enhanced backscattering of scalar waves and vector waves in the helicity-preserving channel was noticed by MacKintosh and John [42], again on the basis of the diffusion approximation.

2.6 Loops in High Orders of Scattering

In this section we calculate the contribution of some closed light paths involving many scatterers. For three reasons it is meaningful to have an estimate for the contribution of such light paths to reflection and transmission.

Firstly, the standard theory of (diffusive) multiple scattering in dense random media ignores the fact that waves might visit the same region more than once ("recurrent random walk"). The question is beyond which strength of the disorder this assumption is no longer justified.

Secondly, there is some (very weak) experimental evidence that closed light paths can be held responsible for low enhancement factors in enhanced backscattering [39]. Closed light paths involving two scatterers were calculated in the previous section with the conclusion that they may indeed be as relevant as single scattering.

Finally, closed light paths generate an interference effect as well. We call this "enhanced forward scattering". We show in this section that contrary to this phenomenon involving only two scatterers, enhanced forward scattering for orders beyond three is very interesting.

The total incoherent ladder sum for conservative scalar isotropic point scatterers is characterized by the ladder kernel $F(\mathbf{x}_1, \mathbf{x}_2)$ that satisfies Eq. (2.24), with $\ell_e = \ell_s = \ell$. We define

$$F^{(j+1)}(\mathbf{x}_1, \mathbf{x}_2) = (4\pi\ell)^{-1} \int_{\text{slab}} d\mathbf{x}_0 \, A(\mathbf{x}_{10}) \, F^{(j)}(\mathbf{x}_0, \mathbf{x}_2) \,, \tag{2.59}$$

and $F^{(1)} \equiv F$. In the backward direction, the contribution of the loops involving three scattering events or more (Fig. 2.13) to the bistatic coefficient is given by

$$\begin{aligned} \gamma_{\mathcal{L}\geq 3} &= 2 \, \frac{n \, |t|^4}{4\pi A} \int \cdots \int d\mathbf{x}_0 \, \cdots d\mathbf{x}_4 \, \langle G(\mathbf{x}_{01}) \rangle \, \langle G^*(\mathbf{x}_{02}) \rangle \, \ell^{-2} F(\mathbf{x}_1, \mathbf{x}_3) \\ &\qquad \times \delta(\mathbf{x}_1 - \mathbf{x}_2) \, \delta(\mathbf{x}_3 - \mathbf{x}_4) \, \langle G(\mathbf{x}_{30}) \rangle \, \langle G^*(\mathbf{x}_{40}) \rangle \, \mathrm{e}^{-2\tau_0} \\ &= \frac{2|t|^2}{A\ell^3} \int \int \int d\mathbf{x}_0 \, d\mathbf{x}_1 \, d\mathbf{x}_3 \, | \, \langle G(\mathbf{x}_{01}) \rangle \, |^2 \, F(\mathbf{x}_1, \mathbf{x}_3) | \, \langle G(\mathbf{x}_{30}) \rangle \, |^2 \, \mathrm{e}^{-2\tau_0} \,. \end{aligned}$$

An extra factor of 2 enters because the loops with inner most-crossed diagrams equal the loops with inner ladders. It follows, using Eq. (2.59),

$$\gamma_{\mathcal{L}\geq 3} = 2 \, \frac{|s|^2}{(k\ell)^2} \int_0^\tau d\tau_0 \, F^{(3)}(\tau_0, \tau_0) \, \mathrm{e}^{-2\tau_0} \,. \tag{2.60}$$

It is readily seen in Fourier space, using the translationally invariant expression for F in Eq. (2.25), that both $F^{(2)}(\tau_0, \tau_0)$ and $F^{(3)}(\tau_0, \tau_0)$ are infinite: low-order loops suffer from an UV-singularity. In fact, the singularity of $F^{(3)}$ is logarithmic. This problem will be dealt with later. For orders of scattering beyond three the loops add to

$$\gamma_{\mathcal{L}\geq 4} = 2 \, \frac{|s|^2}{(k\ell)^2} \int_0^\tau d\tau_0 \, F^{(4)}(\tau_0, \tau_0) \, \mathrm{e}^{-2\tau_0} \,. \tag{2.61}$$

Before we evaluate this expression in a finite slab, we observe that the significance of these loops with respect to the (non-recurrent) incoherent contribution is determined by the dimensionless variable

$$\nu \equiv \eta \, |s|^3 = \frac{|s|}{k\ell} \,. \tag{2.62}$$

This parameter is proportional to the "average number of scatterers per optical volume".

The kernel F is translationally invariant *along* the slab but not perpendicular to it. To account for this we use the method of images [39] [42]: for any optical depth the diffusion propagator is assumed to be given by

$$F^{(j)}\left(\tau_{1,2}, \mathbf{x}_{12}^{\parallel}\right) = \sum_{m=-\infty}^{\infty} F_{TS}^{(j)}\left(\tau_1 - \tau_2 + m\beta, \mathbf{x}_{12}^{\parallel}\right) - F_{TS}^{(j)}\left(\tau_1 + \tau_2 + m\beta + 2z_0, \mathbf{x}_{12}^{\parallel}\right) . \tag{2.63}$$

where $\beta = 2\,(\tau + 2z_0)$. F_{TS} is the translationally symmetric diffusion operator defined in Eq. (2.25). Substitution of Eq. (2.63) and applying Poisson's summation rule,

$$\frac{1}{2\pi} \sum_{m=-\infty}^{\infty} \mathrm{e}^{imx} = \sum_{j=-\infty}^{\infty} \delta\,(x - 2\pi j) \;, \tag{2.64}$$

Eq. (2.61) can be written as

$$\gamma_{\mathcal{L}\geq 4} = \frac{4\nu^2}{\beta} \sum_{j=-\infty}^{\infty} K_R(\tau, y_j) \int \frac{d^2\mathbf{y}^{\parallel}}{4\pi} \mathcal{F}(\mathbf{y}^{\parallel}, y_j)\,, \tag{2.65}$$

where

$$K_R(\tau, y) = 1 - \mathrm{e}^{-2\tau} - \frac{[1 - \mathrm{e}^{-2\tau}\mathrm{e}^{2i\tau y}]\,\mathrm{e}^{2iz_0 y}}{1 - iy}\,.$$

We introduced the dimensionless variable $\mathbf{y} = \mathbf{q}\,\ell$. We have set $y_j = (2\pi/\beta)\ j$ and

$$\mathcal{F}(y) = \frac{(\arctan y/y)^4}{1 - (\arctan y)/y}\,.$$

For a semi-infinite slab the sum over j reduces to an integral,

$$\lim_{\tau\to\infty} \gamma_{\mathcal{L}\geq 4} = \frac{2\nu^2}{\pi} \int \frac{d^3\mathbf{y}}{4\pi} \mathcal{F}(y) \left[1 - \frac{\mathrm{e}^{2iz_0 y_z}}{1 - iy_z}\right] = 2.6028\,\nu^2\,. \tag{2.66}$$

In the forward direction the same formula (2.65) applies but now

$$K_T(\tau, y) = 2\tau\mathrm{e}^{-\tau} \left[1 - \mathrm{e}^{i\beta y}\,\frac{\sin \tau y}{\tau y}\right]\,.$$

The expressions (2.65) were evaluated numerically for a finite slab, both for reflection (R) and transmission (T). The outcome is demonstrated in Fig. 2.14. Analytical fits are

$$\gamma_{\mathcal{L}\geq 4}(\mathrm{R}) \approx 2.60\,\nu^2 \left(1 - \mathrm{e}^{-1.25\tau}\right) \quad ; \quad \gamma_{\mathcal{L}n\geq 4}(\mathrm{T}) \approx 3.79\,\nu^2\,\tau\,\mathrm{e}^{-0.85\tau}\,. \tag{2.67}$$

Judging from these expressions, it follows that these loops have a penetration depth larger than ℓ. Contrary to the two-scatterer loops in Eq. (2.31) they can thus not be considered as renormalized single scattering.

As mentioned before the incoherent loops involving three scatterers suffer from a logarithmic UV-divergence. Physically this indicates that some relevant mechanism has been overlooked so far at very small length scales. Similar problems showed up in the description of loops involving two scatterers and the inclusion of *repeated scattering* between two scatterers turned out to renormalize the divergence. Mathematically, the propagator from one scatterer to another can be replaced by the whole geometric series according to

$$\langle G(\mathbf{x})\rangle \to \frac{\langle G(\mathbf{x})\rangle}{1 - t^2\,\langle G(\mathbf{x})\rangle^2}\,. \tag{2.68}$$

This procedure renormalizes the Green's function on scales $x^2 < |t|^2/(4\pi)^2 = \sigma/4\pi$ in which case *the optical volumes of the scatterers overlap.* Such an overlap causes a substantial decrease of the collective scattering efficiency and will be addressed thoroughly

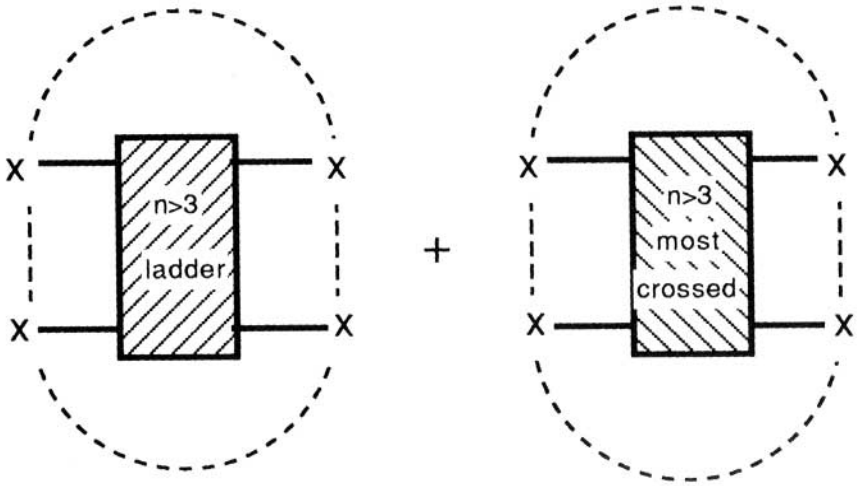

Figure 2.13: *Incoherent or diffusive loops with* 4 *scattering events or more.*

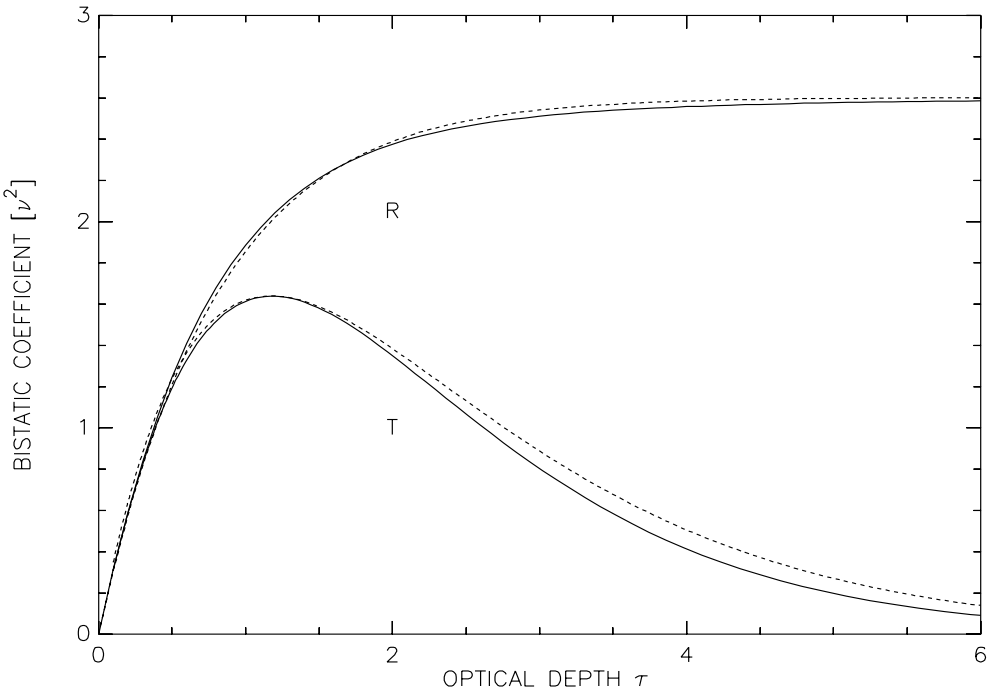

Figure 2.14: *The bistatic coefficient* γ *for reflection and transmission generated by the upper light paths, in units of* ν^2*. The dashed lines are the analytical fits discussed in the text.*

in section 3.3.3 of the next chapter. We note here that it provides an *upper cut-off* for integrals in Fourier space of order $q_c \approx 4\pi/|t| = 1/(\nu\,\ell)$, even for point scatterers which do not have a cut-off associated with the physical size. With this cut-off we estimate the contribution of the loops involving three scatterers to be, using Eq. (2.60),

$$\gamma_{\mathcal{L}3} \approx Z_3(\nu)\,\nu^2\left(1-\mathrm{e}^{-2\tau}\right)\,, \tag{2.69}$$

in which

$$Z_3(\nu) = \frac{2}{\pi}\int_{y<1/\nu}\frac{d\mathbf{y}}{4\pi}\left(\frac{\arctan y}{y}\right)^3 \sim -\left(\frac{\pi}{2}\right)^2\log\nu\,. \tag{2.70}$$

These loops thus give rise to a *non-analytic* density dependence of the incoherently scattered light.

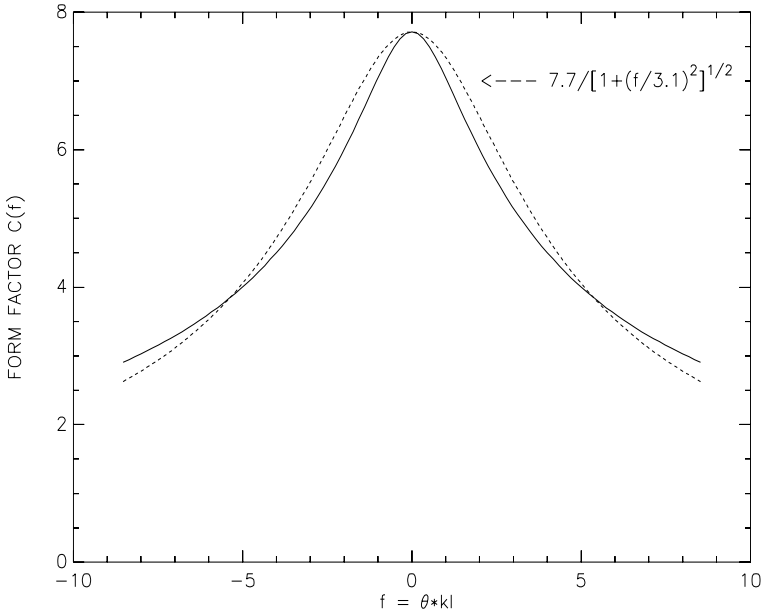

Figure 2.15: *The form factor $C(f)$ defined in Eq. (2.72) for the forward cone caused by constructive interference of* 2 *diffusive loops. The dashed line is a simple fit with same FWHM.*

The loops involving three or more scatterers have an interference equivalent as well, but because of the complex irreducible nature of these high order forward-crossed diagrams, it was not possible to get an expression for them using the method of images. In order to find out whether or not these diagrams are responsible for a narrow forward cone, we will again rely on the "infinite space approximation". It is easily demonstrated that the enhanced forward scattering caused by three events has a logarithmic form factor and is therefore not interesting as an interference effect. In the limit $k\ell \gg 1$ we obtain for the bistatic coefficient of the cone involving 4 scatterers and more,

$$\begin{aligned} \gamma_{\mathcal{F}\geq 4}(\theta) &\approx 2\,\frac{n^2\,|t|^6}{4\pi A}\,\mathrm{e}^{-\tau}\int_{\mathrm{slab}} d\mathbf{x}_0 \int_{\mathbb{R}^3} d\mathbf{x}_{10} \int_{\mathbb{R}^3} d\mathbf{x}_{20} \\ &\times \;|\,\langle G(\mathbf{x}_{01})\rangle\,|^2\,\ell^{-2} F_{TS}^{(2)}(\mathbf{x}_{12})\,|\,\langle G(\mathbf{x}_{20})\rangle\,|^2 \mathrm{e}^{i(\mathbf{k}-\mathbf{k}')\cdot\mathbf{x}_{10}}\,. \end{aligned} \tag{2.71}$$

The integral over $\mathbf{x}_0$ is equal to AL. We get

$$\gamma_{\mathcal{F}\geq 4}(\theta) \approx \nu^2\tau \mathrm{e}^{-\tau}\, C(\mathbf{f}) \equiv \nu^2\tau \mathrm{e}^{-\tau}\,\frac{4}{\pi}\int \frac{d\mathbf{y}}{4\pi}\,\frac{A(|\mathbf{y}+\mathbf{f}|)A^3(y)}{1-A(y)}\,. \tag{2.72}$$

We defined $A(y) = (\arctan y)/y$ and $\mathbf{f} = \ell\,(\mathbf{k}-\mathbf{k}')$. Eq. (2.72) is an estimate because long loops suffer severely from the finiteness of the slab, but at forward scattering ($f = 0$), the exact numerical value is given by Eq. (2.67). We infer a forward cone (Fig. 2.15) with angular width $\Delta\theta \approx 3/k\ell$. Whereas enhanced backscattering is a diffusion process with long light paths involving N scattering events being responsible for a small backscattering angle $\Delta\theta \approx 1/k\ell\sqrt{N}$, the physical picture for enhanced forward scattering is a recurrent random walk. The endpoints of the two interfering loops are roughly one step length ℓ apart, giving $\Delta\theta \approx 1/k\ell$, independent of the length of the loops. This fact makes enhanced forward scattering less pronounced than enhanced backscattering.

Due to the scaling with the square of the number density of the scatterers, as well as the exponential optical depth dependence of the bistatic coefficient, it will be very difficult to detect this enhanced forward scattering. It may be argued that this cone is also present in the cross-polarized channel for which detection is much easier. In this channel we expect no contribution from the attenuated incoming wave, nor from single scattering. Detection of this forward cone would be a unique direct verification of the very existence of recurrent light paths. Unfortunately, attempts in our group to measure the enhanced forward scattering in the cross-polarized channel were unsuccessful up to now.

In some localization experiments in our group, the packing fraction is 36 %, corresponding to $\eta = 0.81$. If the scattering efficiency $|s|$ is assumed to be 0.7 (which would correspond to $k\ell_s \approx 2.5$) we find $\nu \approx 0.3$. Enhanced forward scattering must therefore in principle be observable.

Chapter 3

Diffusion and Localization in Three Dimensions

3.1 Transport in Multiple Scattering

In this chapter we discuss light transport in *unbounded* random media. The absence of boundaries of the scattering medium simplifies the theory enormously. The reason is that an averaging procedure for the positions of the scatterers over all of space (often according to a Poisson distribution) generates translational symmetry. The simple diagonal form of the averaged *amplitude* Green's function in Eq. (2.5) is an example of such a simplification.

To describe propagation of *energy* (= amplitude $\times$ amplitude), one must deal with the average square of the Green's function, which is certainly not simply the square of the averaged amplitude Green's function. In multiple scattering theory the latter has a meaning, and represents the so-called *coherent beam*. This beam suffers from extinction, because its energy is used for scattering or other mechanisms (absorption).

One of the most important issues in multiple scattering theory is the formulation of an *equation of continuity*, describing the conservation of energy (or in case of electrons, probability). *Before* averaging, thus for a given realization of the random medium, such an equation can be derived using the equation of motion (the wave equation), provided of course that the scatterers do not absorb energy. It must hold *after* averaging as well, simply because the averaging procedure is a linear operation. Since we have chosen for a separate treatment of the averaged amplitude and the averaged scattered intensity, an energy balance may be destroyed once we start approximating both in some way. Since the averaged amplitude suffers from extinction (described mathematically by a complex-valued self-energy) in favor of the scattered intensity (represented by the irreducible vertex), the requirement of energy or particle conservation must somehow relate the mass-operator to the irreducible vertex defined in section 2.3. This so-called *Ward Identity* will be discussed in this chapter.

3.1.1 Classical Particles

It was already pointed out in section 2.1 of the previous chapter that the process by which light transport takes place on macroscopic scales is diffusion. Let us first briefly discuss what can be expected for classical particles, and treat the influence of the wave nature later. The simplest continuous diffusion process that one can imagine is a stochastic model for a classical particle with velocity v. The step length between two successive "collisions" is supposed to be given by a distribution $P(\Delta)$. After one collision the particle is scattered elastically in a direction prescribed by another distribution $\sigma(v, \theta)$ which is readily interpreted as the "differential cross-section". Random walk arguments show that the displacement vector $\mathbf{x}_t$ of the classical particle at time t satisfies

$$\left\langle \frac{\mathbf{x}_t^2}{t} \right\rangle \stackrel{t\to\infty}{\to} 6\, D(v)\,. \tag{3.1}$$

This equation can be considered as one of the definitions of the *diffusion coefficient* $D(v)$, not only for this model. For our stochastic process we find that

$$D(v) = \frac{1}{3}\, v\, \ell_s\, \frac{\langle \Delta^2 \rangle + \langle \cos\theta \rangle\, (2\langle \Delta \rangle^2 - \langle \Delta^2 \rangle)}{2\,(1 - \langle \cos\theta \rangle)\, \langle \Delta \rangle^2}\,. \tag{3.2}$$

Here $\langle \cos\theta \rangle$ is the average of the cosine of the scattering angle, taken over the differential cross-section $\sigma(\theta)$. The average step length $\langle \Delta \rangle \equiv \ell_s$ is the scattering mean free path.

We did not yet specify the step length distribution $P(\Delta)$. We can try to take advantage of this freedom to find a simple model for multiple wave scattering. The amplitude Green's function in Eq. (2.10) suggests the step length distribution for waves to be of the form $P(\Delta) \sim \exp(-\Delta/\ell_s)/\Delta^2$. This specific distribution obeys $2\langle \Delta \rangle^2 = \langle \Delta^2 \rangle = 2\ell_s^2$. We arrive at

$$D(v) = \frac{1}{3}\, v\, \frac{\ell_s}{1 - \langle \cos\theta \rangle} \equiv \frac{1}{3}\, v\, \ell\,. \tag{3.3}$$

The characteristic length ℓ is referred to as the *transport mean free path*, and is the length over which the memory of the direction of the particle velocity remains appreciable. Identifying $\ell_s = 1/n\sigma$ (with σ the total cross-section) maps this simple stochastic model onto the dilute classical Lorentz gas with n scatterers per unit volume.

We can ask whether diffusive behavior, $\mathbf{x}_t^2 \sim t$, still occurs if the classical particle is replaced by a wave. One can think of either a quantum particle, with De Broglie wavelength $\lambda = h/mv$, or a classical wave such as sound or light. To be more specific, what is going to change in the above diffusion picture due to interference between the scattered waves? In particular, the impact of the wave nature on both velocity v and transport mean free path ℓ is interesting. The velocity v is no longer fixed when the different scattered waves interfere, and both physical quantities provide information about the random medium. They deserve equal attention, not just their product in the form of the diffusion coefficient.

3.1.2 Quantum Transport

What do we know about quantum particles such as electrons? Direct experimental studies on interference effects in multiple electron-impurity scattering are very difficult to carry out because of problems in preparing a "one channel in - one channel out" scattering set-up, as well as the persisting, phase-destroying influence of electron-electron and electron-phonon scattering. One important physical quantity that is intimately related to the diffusive transport of electrons *and* is also easily accessible by an experiment, is the electric conductivity $\sigma(E)$. The Einstein relation,

$$\sigma(E) = e^2\, N(E)\, D(E)\,, \tag{3.4}$$

relates the conductivity to the diffusion coefficient of the electrons. Here $N(E)$ is the density of states (DOS) per unit volume at energy E, and e is the elementary charge. By the exclusion principle, only electrons at the Fermi-level $E_F = \hbar^2 k_F^2/2m_e$ contribute to the electric conductivity at zero temperature so that Eq. (3.4) is evaluated at energy E_F.

The appearance of a diffusion constant in Eq. (3.4) suggests a diffusive picture to be applicable for a quantum particle. Indeed, a quantum mechanical treatment of (single-) electron-impurity scattering in three dimensions confirms this picture in lowest order of the impurity density [69] [74], in which case again Eq. (3.3) emerges for the diffusion constant. The velocity is in that case the Fermi-velocity $\hbar k_F/m_e$. It depends weakly on the impurity density and is mainly determined by the electron density. The lowest order in impurity or density is usually referred to as the *Boltzmann limit*. Accordingly, Eq. (3.3) is called the *Boltzmann diffusion constant* $D^B(E)$.

The next question is whether a classical picture still coincides with the quantum picture beyond the Boltzmann limit. It is apparent from Eq. (3.3) that if the scattering is predominantly in the backward direction ($\langle\cos\theta\rangle < 0$), the transport mean free path becomes smaller than the scattering mean free path. It was already remarked in chapter 2 that in *multiple* scattering, interference effects favor backscattering directions. The same interference effects can be expected to give rise to *negative* corrections to the transport mean free path c.q. diffusion coefficient. A naive, but transparent treatment yields for the reduction of the diffusion coefficient [75]

$$D \approx D^B \left(1 - \frac{3}{(k\ell_s)^2}\right)\,. \tag{3.5}$$

Here k is the wavenumber of the electron. A more accurate derivation of this formula will be presented later in this chapter. We infer that the diffusion coefficient is drastically lowered if $k\ell_s$ becomes sufficiently small. Extrapolating Eq. (3.5) to large densities, it follows that for $k\ell_s = \sqrt{3} \approx 1$ the diffusion coefficient vanishes with a critical exponent equal to unity. The disorder-induced vanishing of diffusion in an infinite system is called *Anderson localization*. The ideas were first introduced by P.W. Anderson in 1958 in his pioneering, "often quoted but hardly ever read" Noble Prize paper [61].

It seems that interference effects are in principle capable of breaking down a diffusion picture for electrons completely. The energy at which this happens is commonly referred

to as the *mobility edge*. The criterion $k\ell_s \approx 1$ is the *Ioffe-Regel Criterion*. This criterion was originally put forward in 1960 by Ioffe and Regel [76] [77] who argued that $k\ell_s$ must necessarily be greater than unity (in fact 2π in the paper of Ioffe and Regel) since a mean free path less than a wavelength is no longer compatible with the idea of a travelling wave. If $k\ell_s < 1$ they anticipated an Ohmic picture for the electron transport in a metal to break down. This led Mott (see Ref. [78] for a complete review) to the introduction of a *minimum diffusivity* defined by substituting $k\ell_s = m_e v_F \ell_s/\hbar \approx 1$ into the Boltzmann diffusion coefficient. This yields the universal constant $D_{\mathrm{mott}} = \hbar/3m_e = 3.85{\cdot}10^{-5}\, m^2 s^{-1}$. Eq. (3.5) suggests that interference contributions violate this Mott minimum, and possibly lead to a catastrophe in the diffusive transport.

What happens exactly if $k\ell_s \leq 1$? Microscopic theory [60] [79] predicts the onset of an exponentially localized state as first suggested by Anderson [61]. In particular, the critical exponents on both sides of the mobility edge turn out to be unity. These predictions are consistent with the scaling theory of localization [80]. This theory describes the appearance of localization in a *finite* system, featuring the *dimensionless conductance* $g \sim \sigma L^{2-d}$ as the fundamental parameter in a random medium of size L in any dimension d. The most important prediction of the scaling theory of localization is that for $d \leq 2$ one expects *always*, that is for ("almost") any energy and arbitrary degree of disorder, Anderson localization. This means that interference completely destroys a random-walk picture for an electron in one and two dimensions.

Localization of waves in one dimension can be treated rigorously using transfer matrices [81] and one does not need the scaling theory. The onset of localization in two dimensions is still subject to discussion and even some models have been published that, contrary to the prediction of the scaling theory, do not have localized states [82]. The scaling theory of localization predicts (sometimes astronomically) large localization lengths under realistic conditions of disorder. If the system is smaller than this length, localization corrections show up as corrections to a quasi two-dimensional diffusion constant and there is no true localized behavior. In this chapter we will not be concerned with localization in dimensions other than three. Chapter 4 discusses some results in one dimension.

3.1.3 Localization of Light

The ideas behind Anderson localization were originally developed for electron waves. The important elements are "disorder" and "interference", together with the observation that the first does not eliminate the second. As such, any kind of wave in some random medium must in principle be subject to localization, and thus also light. Phycisists realized this only 20 years ago, which is surprising because the wave nature of light has been established longer than the wave nature of electrons!

The similarity between the classical wave equations and the Schrödinger equation substantially simplifies the inclusion of interference in multiple scattering of classical waves. Many concepts of electron transport theory have been taken over to describe propagation of light in random media with the usual recipe that the Fermi wavelength is replaced by

the wavelength of light. Well known examples are the formulations of criteria for strong localization for classical waves such as the above-mentioned Ioffe-Regel criterion and the more general Thouless criterion [83]. The Thouless criterion was put forward in close connection with the scaling theory of localization. Another crucial example is the application of conservation laws, expressed by means of Ward identities. Such identities were originally developed for electron-impurity scattering and were then simply supposed to be valid for the scattering of light from randomly distributed dielectric particles. Concerning the validity of Ward identities we shall argue that they turn out to be considerably different for light scattering. With respect to the Thouless criterion we will see in the last section that great care is needed when applying it to localization of light rather than electrons. There are several reasons why multiple light scattering is different from and thus *complementary* to multiple electron scattering, which we shall now discuss.

Electron-electron interactions are known to be able to induce a localized state as well, with the same critical exponents [84]. In order to discriminate this kind of localization from the disorder-driven Anderson localization, it is called *Mott-Hubbard Localization*. Since "photon-photon" interactions are absent on the level of Maxwell's equations, a Mott transition can safely be ruled out for light localization.

Secondly, in the case of electron-impurity scattering one always deals with phase-destroying effects which prohibit interference effects on a large scale, possibly preventing the onset of Anderson localization. In the case of light, however, one has sufficient control over the influence of inelastic effects to stay in the *mesoscopic regime*, where the phase-breaking length scale exceeds the physical size of the random medium. This has only recently become possible for electrons, an achievement that stimulated the progress of mesoscopic condensed matter physics enormously.

Contrary to multiple electron scattering, the role of absorption is very important in multiple light scattering. Electrons lose at most the phase memory, but their number is conserved under normal conditions. Consequently (and fortunately!), the electron conductivity does not decay exponentially with the size of the Ohmic conductor in the presence of phase-destroying processes. As a matter of fact, the resetting of the electron phase after each inelastic collision automatically performs an averaging procedure [74].

Diffusive light on the other hand, disappears completely after one *absorption length* L_a, defined in terms of the *absorption mean free path* $\ell_a = \ell_e/(1-a)$ (with a the albedo)

$$L_a^2 = \frac{1}{3}\ell\,\ell_a\,. \tag{3.6}$$

As a result, the incoherent transmission ("photon conductivity") of a slab will decay exponentially beyond one absorption length. Although the albedo a is very close to unity in the best optical experiments ($a \approx 0.9999$) the length L_a is short enough to influence the propagation of light in thick slabs.

The absorption of light is not necessarily a disadvantage. By itself, the interplay between absorption and localization is very interesting to study. Both can be the origin of an exponentially small transmission coefficient. In the conventional theory of localization,

applied to light, all interference effects are restricted to a volume L_a^d [85] [86]. The outcome is an anomalous absorption length,

$$L_a^3 \sim \ell_s^2 \, \ell_a \,, \tag{3.7}$$

rather than the length in Eq. (3.6). At present, the impact of absorption on localization of classical waves is still controversial.

A property that makes light scattering *fundamentally* different from electron-impurity scattering was already mentioned in section 1.3, and involves the presence of an energy-dependent potential,

$$V(\mathbf{r}, E) = [1 - \varepsilon(\mathbf{r})] \, E^2 \,, \tag{3.8}$$

where ε is the dielectric constant. We will show in this chapter that this property has a dramatic impact on the microscopic formulation of the velocity that enters the diffusion constant in Eq. (3.3). Our theory demonstrates that, already in the Boltzmann approximation, this velocity can become an order of magnitude (!) less than the phase velocity, defined in terms of the averaged index of refraction given by Eq. (2.9). The rather smooth phase-velocity was always believed to be the speed relevant for diffusion. This is of vital importance for the interpretation of localization experiments: a small velocity as well as a short mean free path can be the origin of a small diffusion constant.

If the speed v is low one might, on the basis of measurements on the diffusion constant alone, erroneously deduce a short mean free path, and in turn, the nearness of a mobility edge. Time-resolved experiments (probing the broadening of a narrow pulse in time) yield an independent estimate of this velocity, and should be carried out in order to verify such a spectacular possibility. Indeed, in optical experiments in our group [87] (performed at the University of Amsterdam), and conceivably others [88], the observed small diffusion constants turn out to be consistent with a Boltzmann picture involving very low speeds of light.

For which energies do we expect Anderson localization of classical waves? (In this thesis we use both the terminology "frequency" and "energy" to refer to the variable E for classical waves). To answer this question, we suppose that the Ioffe-Regel criterion $k(E)\ell(E) \sim 1$ is the criterion for Anderson localization, and substitute the lowest order in density for both the average wavenumber k and the scattering mean free path ℓ_s at frequency E. Then $E/n\sigma(E) \sim 1$ at the mobility edge.

For low frequencies (corresponding to wavelengths much larger than the particle) the potential vanishes as E^2. Consequently, the cross-section behaves as E^4 at low energies, a phenomenon called Rayleigh scattering. This well known sensitive energy dependence of the cross-section favors the scattering of small wavelengths over long ones and is responsible for the sky being blue and the sun being red. The Rayleigh behavior gives $E/n\sigma(E) \sim 1/E^3 \to \infty$. We conclude that localization is absent at low frequencies.

At very high frequencies one enters the geometrical optics regime where light waves can be treated as 'rays". The ultimate limit $E \to \infty$ yields a non-vanishing total cross-section which equals *twice* the geometrical area of the particle (the extinction paradox,

which is not a paradox if one recalls that half the scattered light actually emerges within a very narrow diffraction cone). At high frequencies one finds $E/n\sigma(E) \sim E \to \infty$, and no localization seems possible.

Thus, if one wants to observe localization of light in three dimensions, one must tune to intermediate frequencies, with the wavelength more or less comparable to the size of the dielectric scatterers. This is exactly the regime of resonant scattering. Since the cross-section is large at resonances, the mean free path is expected to be small. Using resonant scatterers one can thus hope for a localization window where $k\ell_s \leq 1$ [89]. The existence of such a window has indeed been predicted, and the localization lengths have been calculated [90] [91] . The conclusion was that it must in principle be possible to observe Anderson localization of light.

The optimistic calculations are based upon extrapolation of results obtained in the low-disorder limit, and there is considerable suspicion that such an extrapolation might not be justified. In particular, we made use of the familiar "independent-scattering" expression for the mean free path $\ell_s = 1/n\sigma$, although more sophisticated "effective medium approaches" have been published [92]. When developing a theory for densely packed resonant scatterers, the following complications immediately appear:

- The "excluded volume" of the scatterers prevents them from being distributed independently (= "Poisson statistics").
- The possibility that a wave visits one particular scatterer more than once (*dependent scattering*) can no longer be ignored.
- A scattered wave leaving one particle will not yet have reached its asymptotic limit when undergoing a subsequent collision: *off-shell* contributions of the scattering amplitude play a part.
- Other mechanisms than light scattering carry the energy in between the particles.

In this chapter we shall use a point-scatterer model to investigate the importance of the second and third issue. We develop a sophisticated model to find the Ioffe-Regel parameter $k\ell_s$ as a function of the density of the scatterers. Since point scatterers do not have an "excluded volume" the first complication is absent here. It can certainly be relevant in an experiment and some workers have tried to include this effect on a Boltzmann level [54].

In this thesis we will not deal with alternative mechanisms for light transport. For the case of resonant atoms, the resonance dipole-dipole interaction is known to become important when the Ioffe-Regel criterion is obeyed [93], and gives rise to the fourth-mentioned complication. This dipole-dipole coupling is absent in dielectric scattering.

The main conclusion of our calculations is that dependent-scattering corrections have a strong tendency to decrease the *collective* scattering efficiency, thereby giving rise to a shift of the mobility edge to higher densities.

3.1.4 Light versus Electrons

In the preceding section we enumerated some specific properties of light localization. In comparing the theory for multiple light scattering and electron-impurity scattering we encounter a number of other differences.

The polarization of light enters in most cases as extra bookkeeping, and forbids the occurrence of spin 0 (s-wave) in the electromagnetic field. As a matter of fact, the intrinsic spin is what makes light special among other classical waves such as acoustic waves or capillary waves.

The linear dispersion law $E^2 = p^2\,c^2$, with E the frequency, introduces some minor modifications of the single-electron theory (where the energy is given by $E = p^2/2m_e$) applied to light.

The presence of an energy-dependent potential in the classical wave equations gives rise to some fundamental differences between classical waves and Schrödinger waves, of which some have already been discussed. ¿From a theoretical point of view it can be remarked that for classical waves, the well known Born Approximation applies at *low* energies rather than large energies $E \gg |V|$. For large energies the Born approximation describes potential scattering. In case of light scattering from dielectric particles, this last limit can be achieved only if the dielectric constant $\varepsilon(\mathbf{r})$ is near unity, since $V(E) = [1-\varepsilon(\mathbf{r})]E^2$ at "energy" E^2. In optics this is the regime of Rayleigh-Gans scattering [4] (chapter 11).

In the second part of this chapter we discuss the impact of an energy-dependent potential on the speed of light in multiple scattering. It will turn out that neither our theory nor any other physical principle provides a *lower* limit to the diffusive velocity of light. Hence, the notion of a "Mott minimum" for the diffusion constant, mentioned earlier in the context of electron diffusion, is even absent in the Boltzmann limit for light, without invoking localization concepts in multiple scattering.

Alternatively, one might ask which consequences the *absence* of an energy-dependent potential has for multiple scattering of electrons? An inspection of the literature on electron-impurity [69] and electron-phonon scattering [94] shows that the (Boltzmann) electron conductivity is given by

$$\sigma_B = \frac{n_e e^2 \tau}{m_e}\,, \tag{3.9}$$

where n_e is the electron density, τ the mean free time and m_e the *bare* electron mass. It can be argued that, due to interaction with phonons or impurities, this mass suffers from the so-called "mass enhancement". A careful study however, reveals that the same mass-enhancement factors enter into the mean free time τ, and all these factors cancel [94] [69] (page 659)! It turns out that this cancellation is not a coincidence as some text books make us believe, but is due to a very general conservation law (Ward identity) for energy-independent, local potentials.

The absence of an energy-dependent electron-impurity potential has far reaching consequences for the predicted energies at which Anderson localization sets in. At very low energies neither the impurity potential nor the scattering cross-section go to zero,

and the Ioffe-Regel criterion can (probably) be satisfied. Because the strong resonances reminiscent of light scattering from dielectrics are absent in electron-impurity scattering (again because the potential does not depend on energy), the only spectral region where Anderson localization of electrons can be expected is at low energy.

¿From a principal experimental point of view, electrons and light are not so different. In both cases there are two kinds of experiments: Stationary measurement probe length scales, dynamic measurements, on the other hand, probe time scales. Concerning electrons, we argue that the dc electron conductivity is a stationary quantity (justifying its appearance in stationary theories like the scaling theory of localization). The measurement of a dc Ohmic resistance must thus be categorized as a stationary experiment.

The classical counterpart is the time-integrated (=dc) incoherent transmission coefficient T of a slab with thickness L,

$$T(L) = \int_{-\infty}^{\infty} dt\, T(L,t) \sim \frac{\ell}{L}\,. \tag{3.10}$$

The transport mean free path ℓ is a length scale and is, as such, allowed to be part of a steady-state quantity. In a dynamic multiple light scattering experiment, on the other hand, one probes the whole distribution $T(L,t)$. Since *now* time-scales are involved, the velocity v_E (or the diffusion constant $D = v_E\ell/3$) of the multiply scattered light must come in as well. The diffusion constant can thus only be obtained from a dynamic measurement. The time-dependent transmission coefficient $T(L,t)$ is the classical counterpart of the AC electron conductivity.

3.1.5 Observation of Anderson Localization

How can we deduce the existence of Anderson localization from an experiment? Has Anderson localization ever been observed? The complication with regard to the first question is that an experiment is always performed in a finite sample. "Theoretical" Anderson localization ($D = 0$) on the other hand, is a prediction for an infinite system. The first question should thus be reformulated as: "What remains of Anderson localization in a finite system?"

The scaling theory of localization [80] is an attempt to answer this question. As such, it must still be considered as the most important contribution in our field. In a finite medium, the energy or probability in a "localized" state always leaks away through the boundaries. According to the scaling theory of localization this leaking can be represented by a *scale-dependent* transport mean free path $\ell(L) \sim \ell_s^2/L$. Likewise, the incoherent transmission is expected to behave as $T \sim \ell_s^2/L^2$ rather then $T \sim \ell_s/L$ if the transport would have been diffusive. The existence of anomalous absorption, Eq. (3.7), is another prediction of this theory.

Since it has recently become possible to manufacture three-dimensional dielectric crystals with a true gap [95], one is speculating about the observation of localization in such crystals subject to small disorder. Calculations by John [96] [97] show that the wavenumber in the Ioffe-Regel criterion is replaced by the crystal momentum, which vanishes at

the Brillouin-zone boundary making $k_{\rm crys}\ell_s < 1$. Thus localization might be achieved with relative ease near a (pseudo-) gap of such a crystal. This is consistent with the general belief that localization is easiest in regions with a low density of states. Since the bare group velocity of the crystal vanishes near the gaps (Van Hove singularities) one must again be very careful in attributing localization to small diffusion constants [98].

Up to now, nobody has observed Anderson localization for classical waves in three dimensions unambiguously. The only serious claim is due to Genack [99] who reports a $1/L^2$ behavior of the incoherent transmission coefficient, but no other groups have confirmed this experiment as of yet. Some others have misunderstood the concept of Anderson localization [100]. With regard to localization of light in dielectric crystals no experiments have been performed so far, and one is still in the process of optimizing the bandstructures.

What about Anderson localization of electrons? After all, the ideas of Anderson localization were developed to model metal-insulator transitions. Theoretically, one expects Anderson localization at small energies, more precisely at the bottom of the conduction band. Metal-insulator transitions are widely observed. The problem is however, that one cannot associate such a transition unambiguously either with Anderson or Mott localization [101]. The latter is caused by electron-electron interactions. Both the standard theory for Anderson localization and Mott localization predict a critical exponent of unity for both the conductivity in the extended regime and the dielectric constant in the localized regime. Thus even for electrons Anderson localization is still speculative. Yet more complicated to explain is the claim of a critical exponent 1/2 for the metal-insulator transition in uncompensated Si:P [102] [103].

Another important physical phenomenon for which the ideas of electron localization seem to be relevant is the *Quantum Hall Effect*. The observed plateaus in the Hall conductivity of a two-dimensional electron gas imposed by a sufficiently strong perpendicular magnetic field can be associated with extended states near the quantized cyclotron orbits (Landau-levels). Further away from these levels the wave-function becomes localized. This implies that these states do not contribute to the longitudinal conductivity of the electrons. A calculation demonstrates the existence of a plateau in the Hall conductivity [104] if the Fermi-level is situated in a localized regime. At first sight, the existence of extended states seems to be in disagreement with the scaling theory of localization which predicts all states to be localized. The states become "quasi-extended" as soon as the predicted exponential decay of the wave-function exceeds some phase-destroying length (possibly caused by spin-orbit coupling). The scaling theory of localization predicts localization to be the least pronounced in spectral regions where the density of states is highest. Thus one anticipates the quasi-extended states to occur right in the middle of the Landau levels. The work of Wei *et al.* [105] demonstrates that a one-parameter scaling theory of localization is in beautiful agreement with measurements on the scaling behavior in between the plateaus.

3.2 Boltzmann Equation for Classical Waves

This section is devoted to the derivation of a Boltzmann equation for scalar classical waves. This equation is of fundamental importance for the description of diffusion and localization of waves. Elements of this derivation can be found in the papers by Vollhardt and Wölfe [60] (which concerns electrons), Kirkpatrick [106] (acoustic waves) and Zhang and Sheng [107] (classical scalar waves).

For Schrödinger potential scattering, Liouville methods can be employed to arrive at this transport equation [59]. One thus finds a dynamic equation for the averaged density operator in terms of an as yet abstract collision operator J. The eigenvalue zero of this operator guarantees energy or probability conservation. In the following we choose for another approach which finally gives the collision operator in terms of the self-energy $\Sigma(z)$ and irreducible vertex $U(z_1, z_2)$ defined in section 2.3.
Given an unbounded, as yet unaveraged random medium, we study the quantity

$$P(\mathbf{r}', \mathbf{r}, t) \equiv |G(\mathbf{r}', \mathbf{r}, t)|^2 \,. \tag{3.11}$$

Integrated with a source at time $t = 0$ at position $\mathbf{r}'$ this quantity gives the "intensity" $|\psi(\mathbf{r}, t)|^2$ at later times t at position $\mathbf{r}$. The initial value problem can be handled through a Laplace transformation,

$$P(\mathbf{r}', \mathbf{r}|\omega) = \int_0^\infty dt\, \mathrm{e}^{i(\omega+i0)t}\, P(\mathbf{r}', \mathbf{r}, t) \,. \tag{3.12}$$

By decomposing the Green's function into frequency modes,

$$G(\mathbf{r}, \mathbf{r}', t) = \int_{-\infty}^{+\infty} \frac{dE}{2\pi}\, \mathrm{e}^{iEt}\, G(E|\mathbf{r}', \mathbf{r}) \,, \tag{3.13}$$

we can check that, with $E^\pm = E \pm \omega/2 \pm i0$,

$$P(\mathbf{r}', \mathbf{r}|\omega) = \int_{-\infty}^{+\infty} \frac{dE}{2\pi}\, G(E^+|\mathbf{r}', \mathbf{r})\, G(E^-|\mathbf{r}, \mathbf{r}') \,. \tag{3.14}$$

An averaging over ensembles restores translational symmetry, so that $\langle P(\mathbf{r}, \mathbf{r}'|\omega)\rangle = \langle P(\mathbf{r} - \mathbf{r}'|\omega)\rangle$. We construct

$$P_E(\omega\, \mathbf{q}) = \int d\mathbf{r} \left\langle G(E^+|\mathbf{r})\, G(E^-|-\mathbf{r})\right\rangle \mathrm{e}^{i\mathbf{q}\cdot\mathbf{r}} = \sum_{\mathbf{p}} \left\langle G(E^+, \mathbf{p}^+)\, G(E^-, \mathbf{p}^-)\right\rangle \,, \tag{3.15}$$

where $\mathbf{p}^\pm = \mathbf{p} \pm \mathbf{q}/2$. With the identification of

$$\Phi_{E\mathbf{p}}(\omega\, \mathbf{q}) \equiv \left\langle G(E^+, \mathbf{p}^+)\, G(E^-, \mathbf{p}^-)\right\rangle \,, \tag{3.16}$$

we have obtained a physical quantity which directly translates to $\langle P(\mathbf{r}, t)\rangle$ according to

$$\int_0^\infty dt\, \mathrm{e}^{i(\omega+i0)t} \int d\mathbf{r}\, \mathrm{e}^{i\mathbf{q}\cdot\mathbf{r}}\, \langle P(\mathbf{r}, t)\rangle = \int_{-\infty}^{+\infty} \frac{dE}{2\pi} \sum_{\mathbf{p}} \Phi_{E\mathbf{p}}(\omega\, \mathbf{q}) \,. \tag{3.17}$$

We shall therefore focus our attention on this quantity. We observe that E and $\mathbf{p}$ label "internal" oscillations of the wave packet in time, respectively space, over which should be integrated in the end. The "external" parameters ω and $\mathbf{q}$, on the other hand, give the space-time behavior of the quantity that we are interested in. In particular, the long-time behavior is determined by the limit $\omega \to 0$, whereas the asymptotic space distribution is governed by the solution near $\mathbf{q} = 0$. This so-called *Kubo limit* [67] is the regime of *macroscopic* transport that will be considered in this chapter.

Since $P(\mathbf{r}, t)$ will remain bounded as $t \to +\infty$, it is obvious from Eq. (3.17) that $\Phi_{E\mathbf{p}}(\omega\, \mathbf{q})$ is likely to have a *complex continuation* in the sheet $\mathrm{Im}\,\omega > 0$. This property is not always obvious from approximate solutions for this transport quantity.

A reader might already have noticed that all transport arguments so far (see Eqs. (3.11) and (2.16) in particular), treat the quantity $|\psi(\mathbf{r}, t)|^2$ as if it were the energy density. In the case of electrons this is certainly the appropriate transport quantity to look at, but all text books tell us that "$\varepsilon(\mathbf{r})(\partial_t \psi)^2 + (\boldsymbol{\nabla}\psi)^2$" is the true energy density for scalar classical scattering. We demonstrate in section 3.4.1 that this notion influences *dynamic* ($\omega \neq 0$) aspects of light propagation and not steady-state properties.

We can work out Eq. (3.16) by using the Bethe-Salpeter equation (2.11). The result is

$$\Phi_{E\mathbf{p}}(\omega\, \mathbf{q}) = \Big\langle G(E^+, \mathbf{p}^+) \Big\rangle \Big\langle G(E^-, \mathbf{p}^-) \Big\rangle \left[1 + \sum_{\mathbf{p}'} U_{\mathbf{p}\mathbf{p}'}(\omega\, \mathbf{q}|E)\, \Phi_{E\mathbf{p}}(\omega\, \mathbf{q}) \right] . \tag{3.18}$$

We have used the translational symmetry of the amplitude Green's functions. By momentum conservation, the irreducible vertex (see Fig. 3.1) has the representation

$$\begin{aligned} \Big[\langle \mathbf{p}^+| \otimes \langle \mathbf{p}^-| \Big]\, U(E^+, E^-)\, \Big[|\mathbf{p}'^+\rangle \otimes |\mathbf{p}''^-\rangle \Big] \\ = (2\pi)^3\, \delta(\mathbf{p}^+ - \mathbf{p}^- - \mathbf{p}'^+ + \mathbf{p}''^-)\, U_{\mathbf{p}\mathbf{p}'}(\omega\, \mathbf{q}|E)\,. \end{aligned} \tag{3.19}$$

Using the solution of the Dyson Equation (2.5) one can verify that

$$\Big\langle G(E^+, \mathbf{p}^+) \Big\rangle \Big\langle G(E^-, \mathbf{p}^-) \Big\rangle = \frac{\Delta G(E\, \mathbf{p}|\omega\, \mathbf{q})}{-2E\omega + 2\mathbf{q}\cdot\mathbf{p} + \Sigma(E^+, \mathbf{p}^+) - \Sigma(E^-, \mathbf{p}^-)}\,, \tag{3.20}$$

where $\Delta G = \langle G(E^+, \mathbf{p}^+)\rangle - \langle G(E^-, \mathbf{p}^-)\rangle$. Insertion Eq. (3.20) into Eq. (3.18) gives the equation,

$$\begin{aligned} \left[iE\omega - i\mathbf{q}\cdot\mathbf{p} + \frac{1}{2i}\Sigma(E^+, \mathbf{p}^+) - \frac{1}{2i}\Sigma(E^-, \mathbf{p}^-) \right] \Phi_{E\mathbf{p}}(\omega\, \mathbf{q}) \\ = -\frac{i}{2}\Delta G(E\, \mathbf{p}|\omega\, \mathbf{q}) \left[1 + \sum_{\mathbf{p}'} U_{\mathbf{p}\mathbf{p}'}(\omega\, \mathbf{q}|E)\, \Phi_{E\mathbf{p}'}(\omega\, \mathbf{q}) \right] . \end{aligned} \tag{3.21}$$

This *Generalized Boltzmann Equation* takes all time and spatial correlations into account. By using the explicit form of the Green's function in Eq. (2.5) we have already adopted a linear dispersion law, $E^2 \sim p^2$, specific for free classical waves, rather than $E \sim p^2$.

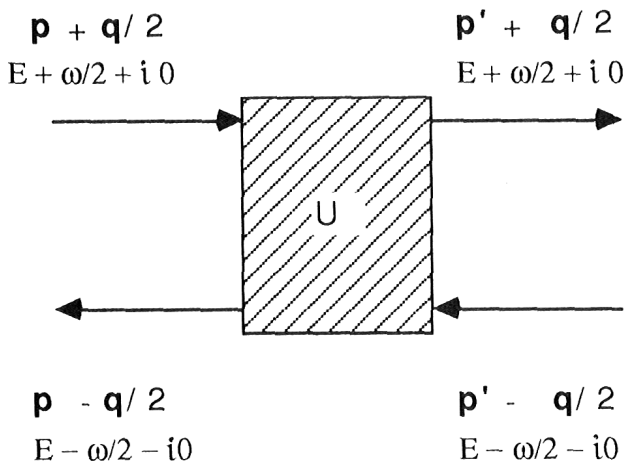

Figure 3.1: *The irreducible vertex* $U_{\mathbf{pp}'}(\omega\,\mathbf{q}|E)$.

Without proof we will state here a very fundamental conservation law,

$$-\mathrm{Im}\,\Sigma(E^+,\mathbf{p}) = \frac{1}{2E}\sum_{\mathbf{p}'} S(E,\mathbf{p}')\,U_{\mathbf{pp}'}(E)\,. \tag{3.22}$$

This identity is called a *Ward Identity*. It is valid for Schrödinger potential scattering and the proof can be found in the book of Mahan [69] (page 617) and in the paper of Vollhardt and Wölfe [60]. In section 3.4.2 we prove that this Ward-identity must also hold for scalar classical waves. Although the proof is rather technical, the message of Eq. (3.22) is simply energy-conservation. As such, the Ward Identity can be looked upon as a "generalized Optical Theorem". We introduced the *spectral function*,

$$S(E,\mathbf{p}) \equiv \lim_{\omega\,\mathbf{q}\to 0} iE\,\Delta G(E\,\mathbf{p}|\omega\,\mathbf{q}) = \frac{-2E\,\mathrm{Im}\,\Sigma(E^+,\mathbf{p})}{|E^2 - p^2 - \Sigma(E^+,\mathbf{p})|^2}\,. \tag{3.23}$$

This distribution is known to count the number of states with energy E and momentum $\mathbf{p}$ per unit volume [108]. Since $-E\,\mathrm{Im}\,\Sigma(E^+,\mathbf{p}) \geq 0$ both for negative and positive frequencies E, we observe that $S(E,\mathbf{p})$ is indeed positive-definite. In Appendix B a useful sum rule is derived for this quantity. For future reference we introduce

$$2\pi N(E) \equiv \sum_{\mathbf{p}} S(E,\mathbf{p})\,, \tag{3.24}$$

representing the density of states per unit volume at frequency E [108].

The rest of this chapter is organized as follows. Section 3.3 deals with *stationary* properties of the transport equation ($\omega = 0$, $\mathbf{q} \neq 0$). We will make an attempt to obtain the scattering and transport mean free path beyond the conventional Boltzmann approximation. In section 3.4 we discuss *dynamic* properties ($\omega \neq 0$, $\mathbf{q} \neq 0$), on a Boltzmann level only. This involves a calculation of the speed of light relevant for diffusive transport.

3.3 Stationary Properties: Mean Free Path

Stationary properties are characterized by the solution of the Boltzmann Equation (3.21) for $\omega = 0$, $\mathbf{q} \neq 0$. We anticipate that this limit can be taken provided that we are not in the localized regime. In the extended regime the limit signifies a stationary flow of energy on scales $1/q$ through the averaged medium. In the localized regime the total energy is "localized" on a sufficiently large scale $1/q > \xi$ (the localization length) and the limit $\omega \to 0$ (= time-integral), $0 < q < 1/\xi$ must diverge [109]. In what follows we assume that we are in the extended (diffusive) regime.

We will apply the weak localization theory, as developed by Götze [59] and Vollhardt and Wölfe [60], to a model of point scatterers in a scalar wave equation with inclusion of "dependent scattering". Existing theory predicts the occurrence of localization for this model, provided that both the density and the cross-section of the individual scatterers are sufficiently large. We will show, however, that the resonances of the individual scatterers play a major role in the magnitude of dependent scattering. Intuitively, one might say that, because the optical size of a resonating scatterer is larger than its physical size, the overlap of the optical volumes occurs at lower density than the one at which the scatterers start to touch physically. This will lead to a drastic reduction of the *collective* amount of scattering, which determines after all the onset of localization.

The theory that we present includes off-shell contributions in the scattering amplitude. In the presence of disorder the wave travels a finite distance, roughly equal to the scattering mean free path, before it scatters again. Most theories of multiple scattering take this finite mean free path into account, but do not appreciate the side effect that, in successive scattering, the wave does not yet satisfy the dispersion law. According to the uncertainty principle ($\Delta\mathbf{p} \cdot \Delta\mathbf{x} \sim 1$) the uncertainty in momentum is inversely proportional to the scattering mean free path. In the low-density (Boltzmann) limit the neglect of this finite width is consistent with energy conservation, and does not give problems. Beyond the Boltzmann limit, however, the neglect of this uncertainty makes it necessary to introduce an (ad hoc) momentum cut-off in the weak-localization correction of the diffusion coefficient [92] [106] [107].
For $\omega = 0$ the generalized Boltzmann equation takes the form

$$\Big[i\,\mathbf{q}\cdot\mathbf{p} - \mathrm{Im}\,\Sigma(E^+,p)\Big]\,\Phi_{E\mathbf{p}}(\mathbf{q}) = \frac{S(E,\mathbf{p})}{2E}\left[1 + \sum_{\mathbf{p}'} U_{\mathbf{p}\mathbf{p}'}(E)\,\Phi_{E\mathbf{p}'}(\mathbf{q})\right], \qquad (3.25)$$

where we have invoked the spectral function Eq. (3.23). The solution of the generalized Boltzmann equation is expanded as

$$E^2\Phi_{E\mathbf{p}}(\mathbf{q}) = \frac{S(E,p)}{2\pi\,N(E)}\left[P_E(\mathbf{q}) - \frac{E}{p}\,\frac{3\,\hat{\mathbf{p}}\cdot\mathbf{J}_E(\mathbf{q})}{v_p\,v_E} + \cdots\right], \qquad (3.26)$$

where the moments,

$$P_E(\mathbf{q}) \;\equiv\; E^2\sum_{\mathbf{p}}\Phi_{E\mathbf{p}}(\mathbf{q})\,,$$

$$\mathbf{J}_E(\mathbf{q}) \equiv -v_E E^2 \sum_{\mathbf{p}} \hat{\mathbf{p}}\, \Phi_{E\mathbf{p}}(\mathbf{q})\,, \tag{3.27}$$

represent "density" and "current" at frequency E. The latter has been given in terms of a, yet unspecified, speed of light v_E which is *by definition* the ratio of $\mathbf{J}_E$ and P_E. The minus sign in the current originates from our conventions with respect to the Fourier and Laplace Transforms (appendix C). We have defined the *phase velocity*,

$$v_p(E) = \left\langle \frac{E}{p} \right\rangle = \frac{\sum_{\mathbf{p}} S(E,p)\, E/p}{\sum_{\mathbf{p}} S(E,p)}\,, \tag{3.28}$$

We observe that the spectral function decays as $1/p^4$ for large momentum p so that not all moments of Eq. (3.25) exist. We proceed by multiplying Eq. (3.25) with $\mathbf{p}/p^2$ and summing over $\mathbf{p}$. In the limit $\mathbf{q} \to 0$ a constitutive relation between $\mathbf{J}_E$ and P_E is found. The proportionality factor is associated with the *diffusion coefficient* at frequency E,

$$i\,\mathbf{q}\, P_E(\mathbf{q}) = D(E)^{-1}\, \mathbf{J}_E(\mathbf{q})\,. \tag{3.29}$$

In the absence of absorption, this definition for D can be shown to agree with a definition of the kind (3.1). The *transport mean free path* in turn, is defined via the relation $D = v_E \ell/3$. This yields

$$\frac{1}{\ell(E)} = \frac{\sum_{\mathbf{p}\mathbf{p}'} S(E,p)\, U_{\mathbf{p}\mathbf{p}'}(E)\, S(E,p')\, (1/p^2 - \hat{\mathbf{p}}\hat{\mathbf{p}}'/pp')}{2\sum_{\mathbf{p}} S(E,p) E/p}\,, \tag{3.30}$$

and the transport velocity drops out, as expected. This is consistent with the idea that v_E is of no importance in steady-state situations, and ℓ (a length scale) is the relevant observable, determining for instance the incoherent transmission $T \sim \ell/L$ and the width of enhanced backscattering $\Delta\theta \sim \lambda/\ell$.

The expression for the transport mean free path, Eq. (3.30), is valid in all orders of the density. A calculation requires full knowledge of both the self-energy $\Sigma(E,p)$ and the irreducible vertex $U_{\mathbf{p}\mathbf{p}'}(E)$. Such a knowledge is not at hand, and one must look for suitable approximations.

If the $\hat{\mathbf{p}}\hat{\mathbf{p}}'$-term would not have been part of Eq. (3.30), one applies the Ward identity (3.22), and arrives at the conclusion that $\ell \approx \ell_s$. The scattering mean free path is a property of the self-energy only. For this amplitude property very sophisticated calculations are available, of which one can be found in this chapter. Apparently, the second term in the expression (3.30) makes the transport mean free path very difficult (if not impossible) to calculate. Fortunately, it also generates very interesting phenomena such as Anderson localization.

We remark that Eq. (3.30) ignores some partial derivatives with respect to $\mathbf{p}$ of both the self-energy and the irreducible vertex which generate contributions proportional to $\mathbf{q}$ as well, and in principle influence the diffusion constant. Higher order irreducible tensors in Eq. (3.26) do not contribute to D.

3.3.1 Boltzmann Limit: Equation of Radiative Transfer

The Boltzmann result for the mean free path,

$$\ell^B = \frac{\ell_s}{1 - a\langle\cos\theta\rangle}\,, \tag{3.31}$$

with a the single-scatterer albedo, is recovered if we use "on-shell" contributions in the spectral distribution,

$$S^B(E,p) = \pi\delta(|E|/v_p(E) - p)\,, \tag{3.32}$$

and approximate Σ and U by their lowest order in density as already given in Eqs. (2.6) and (2.22), thereby neglecting all interference. Since the spectral function is a delta function, all momenta entering the generalized Boltzmann equation have magnitude $|E|/v_p$. Consequently, we can define the *specific intensity* $I_E(\mathbf{q},\hat{\mathbf{p}})$ [30] at frequency E in direction $\hat{\mathbf{p}}$ according to

$$E^2\Phi_{E\mathbf{p}}(\mathbf{q}) \equiv \pi\delta(|E|/v_p - p)\, I_E(\mathbf{q},\hat{\mathbf{p}})\,. \tag{3.33}$$

Eq. (3.25) now takes the form of an ordinary, stationary Boltzmann equation,

$$\left(i\,\mathbf{q}\cdot\hat{\mathbf{p}} + \frac{1}{\ell_e}\right) I_E(\mathbf{q},\hat{\mathbf{p}}) = \frac{1}{2} + n\int d\hat{\mathbf{p}}'\,\frac{d\sigma}{d\Omega}(\hat{\mathbf{p}}'\to\hat{\mathbf{p}})\, I_E(\mathbf{q},\hat{\mathbf{p}}')\,. \tag{3.34}$$

We have inserted the extinction mean free path $-\mathrm{Im}\,\Sigma^{(1)}(E^+)/E = 1/\ell_e$ and the scattering part $U^{(1)}_{\mathbf{pp}'}(E) = n\,d\sigma/d\Omega \equiv h_E(\mu,\mu')/\ell_s$ with ℓ_s the scattering mean free path and $h_E(\mu,\mu')$ the normalized phase function of the scatterers [35]. The phase function is supposed to be solely dependent on the cosine of the scattering angles μ and μ'. Transforming the variable $\mathbf{q}$ back to real space yields the *Equation of Radiative Transfer* [31] [34] . By adopting translational symmetry for two transverse directions ($\mathbf{q}_{||} = 0$) it takes the form,

$$\mu\,\frac{dI_E(\tau,\mu)}{d\tau} = -I_E(\tau,\mu) + J_E(\tau,\mu)\,. \tag{3.35}$$

The optical depth is $\tau = z/\ell_e$ and the "source function" has been defined as

$$J_E(\tau,\mu) = \frac{a}{2}\int_{-1}^{1} d\mu'\, h_E(\mu',\mu)\, I_E(\tau,\mu')\,. \tag{3.36}$$

We conclude that the equation of transfer can, in lowest order of the scatterer density, be derived from the generalized Boltzmann equation. This gives the equation of radiative transfer a microscopic base. Crucial is the fact that the spectral function is a delta-function. At present, the formulation of an equation of radiative transfer is not evident if the spectral function obtains a finite width. Beyond the Boltzmann approximation a finite width must be included in order to satisfy energy conservation.

3.3.2 Beyond Boltzmann: Localization of Light

In order to evaluate Eq. (3.25) for a large density of the scatterers we must make assumptions concerning the vertex $U_{\mathbf{pp}'}(E)$ and the mass operator $\Sigma(E^+, p)$. We assert that $\Sigma(E^+, p)$ is independent of the momentum variable p. This will be proven later to be an accurate result in all densities when using point interactions. Upon solving the complex dispersion law (2.7) one obtains

$$\begin{aligned} k^2(E) - \frac{1}{4\,\ell_s(E)^2} &= E^2 - \mathrm{Re}\,\Sigma(E^+)\,, \\ \frac{k(E)}{\ell_s(E)} &= -\mathrm{Im}\,\Sigma(E^+)\,. \end{aligned} \tag{3.37}$$

We define a dimensionless Ioffe-Regel type parameter $\gamma(E) = k(E)\ell_s(E)$. The regime $\gamma \leq 1/2$ corresponds to $E^2 - \mathrm{Re}\,\Sigma(E^+) < 0$ and there is no longer a well-defined momentum shell. This is the domain of evanescent-wave propagation. This value for γ is very close to the predicted location of the mobility edge according to the Ioffe-Regel criterion $\gamma \approx 1$, so that any self-consistent localization theory must take the finite width of this shell into account if it is to be consistent in the first place.

As was already pointed out in Eq. (3.5), the existence of enhanced backscattering can be expected to lower the diffusion constant. To investigate this we add to the irreducible vertex the summation of the most-crossed diagrams. In the diffusion approximation we adopt, for conservative isotropic scatterers,

$$U^{(\mathrm{mc})}_{\mathbf{pp}'}(E) = \frac{4\pi}{\ell_s(E)}\,\frac{3}{\ell_s \ell^B(E)\,(\mathbf{p}+\mathbf{p}')^2}\,. \tag{3.38}$$

This form can be ascertained from a time-inversion operation on the (incoherent) ladder summation (2.47), which interchanges some of the incoming and outgoing momenta [110]. The Boltzmann transport mean free path was obtained in Eq. (3.31). If we neglect all other *angle-dependent* contributions to the irreducible vertex we find, after some algebraic rearranging, using Eqs. (3.22) and (3.37),

$$\frac{1}{\ell} = \frac{G(\gamma)}{\ell_s} - \frac{1}{\ell^B}\,\frac{3\,H(\gamma)}{\gamma^2}\int\!\!\int \frac{d\mathbf{x}}{4\pi}\frac{d\mathbf{y}}{4\pi}\,\frac{f_\gamma(x)\,f_\gamma(y)}{(\mathbf{x}+\mathbf{y})^2}\,\frac{\hat{\mathbf{x}}\hat{\mathbf{y}}}{xy}\,, \tag{3.39}$$

where we have dropped the energy label. Furthermore,

$$G(\gamma) \equiv \left(1 + \frac{1}{4\gamma^2}\right)\left(\frac{1}{2} + \frac{\arctan(\gamma - 1/4\gamma)}{\pi}\right) \tag{3.40}$$

is, for $\gamma > 1/2$, a smooth function of order unity. This implies that any difference between scattering and transport mean free path must be attributed to angle-dependent terms in the irreducible vertex. This statement is evidently true in the Boltzmann limit (3.31). Additionally,

$$H(\gamma) \equiv \frac{\gamma}{G(\gamma)}\left(1 + \frac{1}{4\gamma^2}\right) \quad , \quad f_\gamma(x) \equiv \frac{2}{\pi}\frac{1}{(x^2 - \gamma + 1/4\gamma)^2 + 1}\,. \tag{3.41}$$

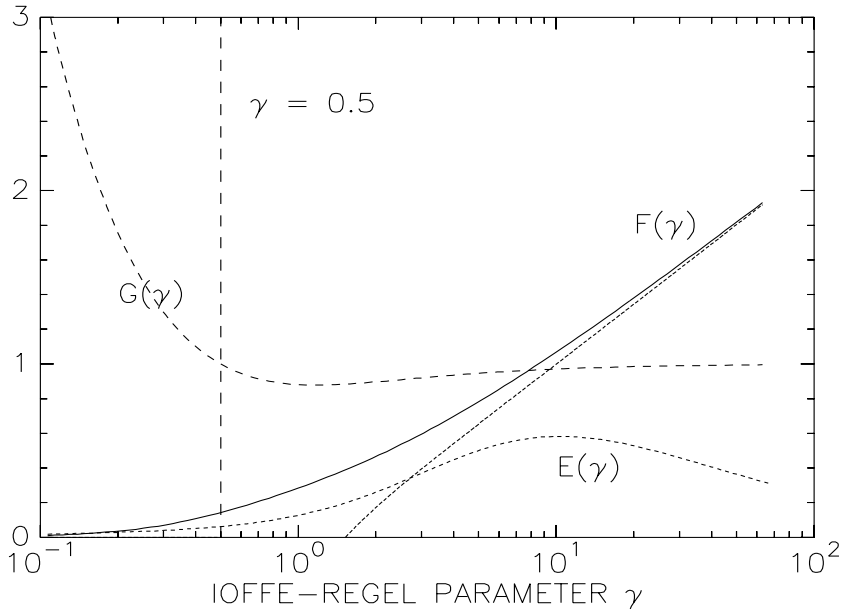

Figure 3.2: *The functions $F(\gamma)$, $G(\gamma)$ and $E(\gamma)$. F describes the "cut-off" in localization theory, E the importance of enhanced forward scattering and G the ratio of scattering and transport mean free path without consdidering the corrections from angular anisotropy . The vertical line at $\gamma = 1/2$ signifies the domain of evanescent-wave propagation.*

According to the localization theory of Vollhardt and Wölfe [60], the Boltzmann transport mean free path must be replaced self-consistently by the exact mean free path. This makes sense since the Boltzmann transport mean free path in Eq. (3.38) refers to a diffusive transport which is subject to the same interference. Solving for ℓ we obtain

$$\ell = \frac{\ell_s}{G(\gamma)} \left[1 - \frac{3}{\gamma^2} F(\gamma)\right] . \tag{3.42}$$

The second term between brackets represents the change in mean free path caused by the most-crossed diagrams. The integral over angles in Eq. (3.39) can actually be performed analytically. The function $F(\gamma)$ is given by

$$F(\gamma) = H(\gamma) \int_0^\infty \int_0^\infty dx\, dy\, f_\gamma(x)\, f_\gamma(y) \left[\frac{x^2+y^2}{4xy} \log\left|\frac{x+y}{x-y}\right| - \frac{1}{2}\right] . \tag{3.43}$$

We can compare this result to an alternative (less rigorous) approach which constitutes of taking for the most-crossed diagrams,

$$U^{(\mathrm{mc})}_{\mathbf{p}\mathbf{p}'}(E) \to \frac{1}{\ell_s^2}\, \delta(\mathbf{p}+\mathbf{p}') \int_{q<q_0} d\mathbf{q}\, \frac{3}{\ell^B\, q^2} , \tag{3.44}$$

to which we shall refer as the "cut-off procedure" [75] [90] [106] and locates the incoming and outgoing momenta of the enhanced backscattering on a momentum shell. With this

choice the transport mean free path becomes

$$\ell = \ell_s \left[1 - \frac{3}{\gamma^2}\frac{q_0 \ell_s}{\pi}\right] . \tag{3.45}$$

Some controversy existed in literature concerning what to take for the cut-off q_0. It was argued by Condat and Kirkpatrick [90] that q_0 must be inversely proportional to the Boltzmann transport mean free path. If this were true this cut-off would also be subject to the self-consistent renormalization of Vollhardt and Wölfe. This procedure turns out to destroy the existence of a mobility edge! Fortunately, our theory shows that no cut-off is needed. If one insists on sticking to a cut-off, our work shows that it must be inversely proportional to the *scattering mean free path*, with $F(\gamma)$ the factor of proportionality. For low density this factor equals $(\log 2\gamma - 1)/2$, and is also displayed in Fig. 3.2. The finite spectral width thus makes the cut-off proportional to π/ℓ_s, an *amplitude* property, rather than π/ℓ^B, a property of the *intensity* Green's function. This proves that no self-consistent renormalization procedure should be applied to this cut-off, notwithstanding the fact that $\ell_s = \ell^B$ for our isotropic model.
Eq. (3.42) locates the mobility edge ($\ell = 0$) at

$$\gamma_c = 0.972 , \tag{3.46}$$

a result valid for isotropic point scatterers. This is close to the criterion ($\gamma_c = 0.844$) found by Zdetsis *et al.* [111] on the basis of a "potential well analogy". Formula (3.42) has the convenient property that it provides a transport length scale once a solution for the amplitude Green's function is at hand. A diagrammatic calculation of the latter is obtained in the next section.

In section 2.6 we reported an additional angle-dependent multiple scattering event, namely enhanced forward scattering. Since the associated diagrams are irreducible, they must be part of the vertex $U_{\mathbf{pp'}}(E)$. We demonstrate that these contributions do not have dramatic consequences for the diffusion constant. Using Eq. (2.72) we write for the forward-crossed diagrams,

$$U^{(\mathrm{fc})}_{\mathbf{pp'}}(E) = \frac{4\pi\nu^2}{\ell_s} C\left[\ell_s(\mathbf{p} - \mathbf{p'})\right] . \tag{3.47}$$

where we use, for simplicity, the analytical fit in Fig. 2.15 for the form factor $C(\mathbf{f})$. The variable ν was defined in Eq. (2.62) and is proportional to the number of scatterers per optical volume. After scaling the momenta with $\sqrt{k/\ell_s}$ we obtain

$$\ell = \frac{\ell_s}{G(\gamma) - E(\gamma)\nu^2} , \tag{3.48}$$

in which

$$E(\gamma) = \frac{H(\gamma)}{\gamma} \int\int \frac{d\mathbf{x}}{4\pi}\frac{d\mathbf{y}}{4\pi} f_\gamma(x)\, f_\gamma(y)\, C\left[\sqrt{\gamma}(\mathbf{x} - \mathbf{y})\right] \frac{\hat{\mathbf{x}}\hat{\mathbf{y}}}{xy} . \tag{3.49}$$

This function has been plotted in Fig. 3.2. As expected, the enhanced forward scattering *enhances* the transport mean free path. In Eq. (3.48) we did not incorporate enhanced backscattering, nor did we renormalize the transport mean free path self-consistently. Such a procedure becomes necessary near a singularity of Eq. (3.48). In the proximity of the mobility edge we find $E(1) = 0.12$. The calculations of the next section indicate that $\eta = 0.81$ and $|s| \approx 0.86$ correspond to a realistic condition under which localization might be achieved. We find a negligible enhancement factor of 1.03 for the diffusion constant. The very existence of enhanced forward scattering demonstrates, however, that contributions other than "most-crossed" diagrams cannot be ruled out beforehand.

3.3.3 Calculation of the Self-Energy

In this section we deal with dependent-scattering effects in the amplitude Green's function and show that the use of point scatterers allows for a sophisticated estimate of all dependent scattering. Density corrections to the scattering mean free path were studied by Bringi *et al.* [112], who applied the elegant Waterman formalism [12] [113] and invoked the excluded volumes of the scattering particles. For the actual calculation they had to rely on a "Quasi Crystalline Approximation" which, in fact, neglects repeated scattering between scatterers.

We present a calculation scheme for the calculation of the self-energy for point scatterers. The solution of the Dyson equation for scalar waves was already given in Eq. (2.5). To investigate the influence of the vector nature we also study vector Rayleigh scatterers. The straightforward generalization of the Dyson equation to the Green's function of the Helmholtz equation (1.17) is

$$\mathbf{G}(z, \mathbf{p}) = \frac{1}{z^2 - p^2 \boldsymbol{\Delta}_{\mathbf{p}} - \boldsymbol{\Sigma}(z, \mathbf{p})}\,, \tag{3.50}$$

where $\boldsymbol{\Delta}_{\mathbf{p}} \equiv \mathbf{I} - \hat{\mathbf{p}}\hat{\mathbf{p}}$ is the transverse projection matrix. The self-energy $\boldsymbol{\Sigma}(z, \mathbf{p})$ is now a 3×3 complex matrix. The usual "independent-scattering" approximation consists of taking the lowest order in density in the self-energy, which is proportional to the single-scatterer t-matrix. In this low-density limit, the imaginary part of the self-energy directly relates to the scattering mean free path,

$$\frac{1}{\ell_0} = -n\,\frac{\operatorname{Im} t(E^+)}{E} = \begin{cases} n\,|t|^2/4\pi & \text{(scalar)} \\ n\,|t|^2/6\pi & \text{(vector)} \end{cases} \equiv n\,\sigma_s(E)\,. \tag{3.51}$$

The second equality applies for conservative scatterers and follows from an application of the Optical Theorem to the Rayleigh point scatterer, Eq. (1.68), and the isotropic point scatterer.

All dependent-scattering corrections in the self-energy in second order of the density were shown in Fig. 2.6. For the *scalar* point interaction they sum up to

$$\Sigma^{(2)}(p) = n^2 t^3 \int d\mathbf{x}\,\frac{G_0^2(x)}{1 - t^2 G_0^2(x)} + n^2 t^4 \int d\mathbf{x}\,\frac{G_0^3(x)}{1 - t^2 G_0^2(x)}\,\mathrm{e}^{i\mathbf{p}\cdot\mathbf{x}}\,. \tag{3.52}$$

Here G_0 is the bare scalar Green's function and t the scalar equivalent of Eq. (1.68),

$$t(E^+) = \frac{-4\pi E^2}{1/\alpha - iE^3}\,. \tag{3.53}$$

The parameter α determines the scattering efficiency of a single scatterer.

The first term in Eq. (3.52) represents the set of diagrams with the same scatterer at both sides (loops) and gives a dependent-scattering correction to the one-scatterer t-matrix, the second term the set with different scatterers at both sides and is, for point scatterers, the first contribution that depends on the momentum variable p. The first order, $n^2t^4G_0^3\exp(i\mathbf{p}\cdot\mathbf{x})$, is subject to an ultra-violet (UV) singularity that is automatically renormalized by adding the total geometric series. We shall evaluate this p-dependent contribution on-shell, $p = |E|$. A check afterwards will demonstrate that the computed self-energy is indeed insensitive to the momentum p.

We propose the following (selfconsistent) calculation scheme: first we replace every t-matrix by its loop-corrected value, and second we replace every Green's function by its averaged equivalent according to the Dyson Equation Eq. (2.5). Of course we must be careful not to double-count diagrams. This yields the following set of coupled equations:

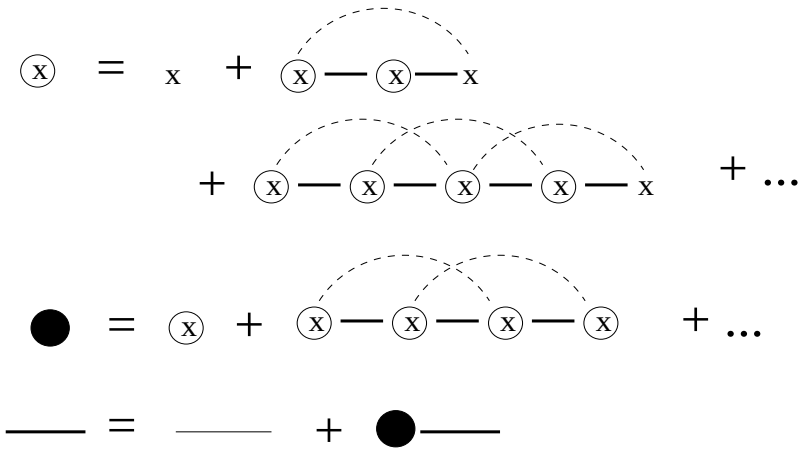

(3.54)

and was solved using a Newton-Raphson method. Eq. (3.54) can be considered as an extrapolation of the exact "two-body problem" towards high densities, rather than an extrapolation of the exact "one-body" problem (= independent scattering). The scattering quantities of interest, the average index of refraction $m(E) = k(E)/E$ and the scattering mean free path $\ell_s(E)$ follow from the complex dispersion law (3.37). The result for the scalar point scatterers is shown in Fig. 3.3 as a function of the parameter $\eta \equiv 4\pi n/E^3$. We have set the individual point scatterers to resonance ($\alpha = \infty$).

Before we discuss the results let us first investigate the Rayleigh point scatterer. By inserting the vector Green's function into the diagrams of Fig. 2.6, it turns out that the self-energy splits up into an isotropic (i) and a longitudinal (ℓ) part:

$$\mathbf{\Sigma}(\mathbf{p}) = nt\,\mathbf{I} + \Sigma_i^{(2)}(p)\,\mathbf{I} + \Sigma_\ell(p)\,\hat{\mathbf{p}}\hat{\mathbf{p}}\,, \tag{3.55}$$

$$\begin{aligned}
\Sigma_i^{(2)}(p) &= n^2t^3\int d\mathbf{x}\left[\frac{2}{3}\,\frac{P^2}{1-t^2P^2}+\frac{1}{3}\,\frac{Q^2}{1-t^2Q^2}\right]+\\
&+ n^2t^4\int d\mathbf{x}\left[\left(j_0(px)-\frac{j_1(px)}{px}\right)\frac{P^3}{1-t^2P^2}+\frac{j_1(px)}{px}\,\frac{Q^3}{1-t^2Q^2}\right],\\
\Sigma_\ell(p) &= n^2t^4\int d\mathbf{x}\, j_2(px)\left[\frac{P^3}{1-t^2P^2}-\frac{Q^3}{1-t^2Q^2}\right], \qquad (3.56)
\end{aligned}$$

where t is given in Eq. (1.68) with scalar α. Using this self-energy, the Green's function becomes

$$\mathbf{G}(\mathbf{p}) = \frac{1}{E^2-\Sigma_i(p)-p^2\boldsymbol{\Delta}_\mathbf{p}} + \frac{\Sigma_\ell(p)}{E^2-\Sigma_i(p)}\;\frac{\hat{\mathbf{p}}\hat{\mathbf{p}}}{E^2-\Sigma_i(p)-\Sigma_\ell(p)}\,, \qquad (3.57)$$

where $\Sigma_i(p)\equiv n\,t+\Sigma_i^{(2)}(p)$. The p-dependent contribution $\Sigma_i^{(2)}(p)$ is supposed to be weakly dependent on p and is finite for both small and large values of p. This assertion will be checked afterwards. It will therefore be evaluated "on-shell": $p=|E|$. Transforming to coordinate space yields the following averaged Green's function,

$$\mathbf{G}(\mathbf{x}) = \mathbf{G}_0(E\to z,\mathbf{x}) + \frac{1}{z^2}\sum_\mathbf{p}\frac{\Sigma_\ell(p)}{z^2-\Sigma_\ell(p)}\,\hat{\mathbf{p}}\hat{\mathbf{p}}\;\mathrm{e}^{i\mathbf{p}\cdot\mathbf{x}}\,. \qquad (3.58)$$

We defined $z^2\equiv E^2-\Sigma_i(p=E)$. Two comments are in order here.

Firstly, the x^{-3} singularity of the vector Green's function does not give UV problems in the self-energy because the full series is summed. In fact the problems occur when $t\to 0$. In that case the integrands of Eq. (3.57) have a pole at $E\,x_r\approx(Et/4\pi)^{1/3}$ approaching the real axis. Physically this pole reflects a standing wave between two scatterers. If we fit the t-matrix to a small Mie sphere with radius r_0 and dielectric constant $\varepsilon>1$ then $t\approx(4\pi/E)\,(Er_0)^3\,(\varepsilon-1)/(\varepsilon+2)$ so that $x_r<r_0$. This resonance is therefore not expected in a scattering event involving two identical small Mie spheres.

Secondly, the two-scatterer renormalization not only gives a damped wave vector, like in the scalar case, but also generates an extra term in the averaged Green's function. Replacing the Green's functions in Eq. (3.56) by their averaged counterparts, according to Eq. (3.54), demonstrates that the extra term in Eq. (3.58) represents an exponentially damped longitudinal mode with decay length $\ell_s/3$. In fact, our self-consistent procedure is essential for this conclusion. For simplicity we have dropped this term in the Green's function in the numerical calculations.

We now discuss the outcome of the calculations. The results for the scattering mean free path and the average index of refraction are shown in Fig. 3.3, again for resonating scatterers. We infer that the scalar and vector calculations behave qualitatively the same and the influence of the vector nature is rather small. Striking is the fact that resonating scatterers seem to obey $k\ell_s=\gamma>1$ for *any* amount of disorder, and no localization seems possible. This contradicts the intuitive feeling that localization is easiest to reach using strongly scattering particles. In fact what happens is that the optical volumes of

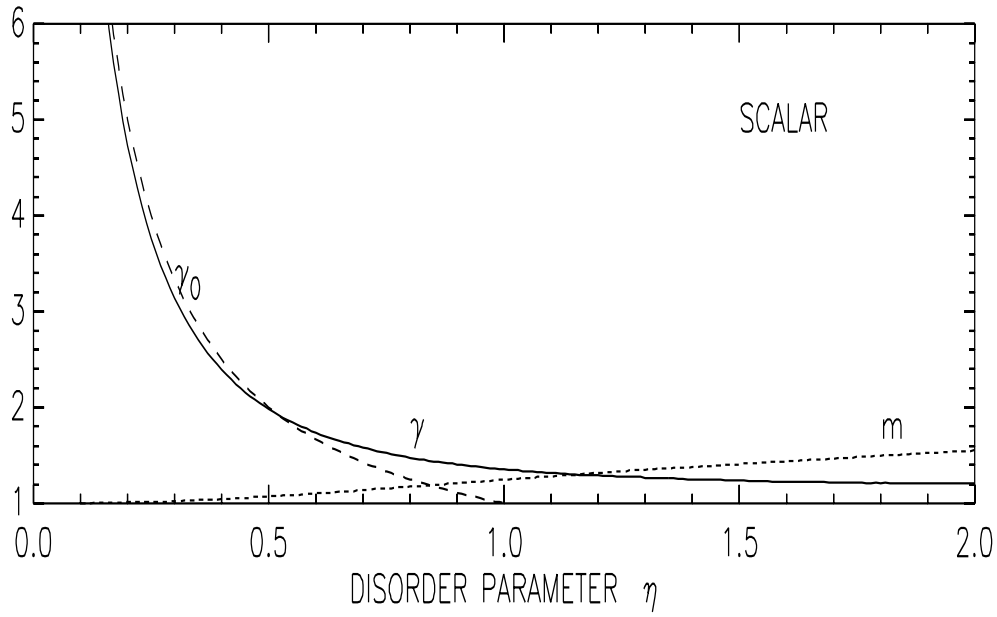

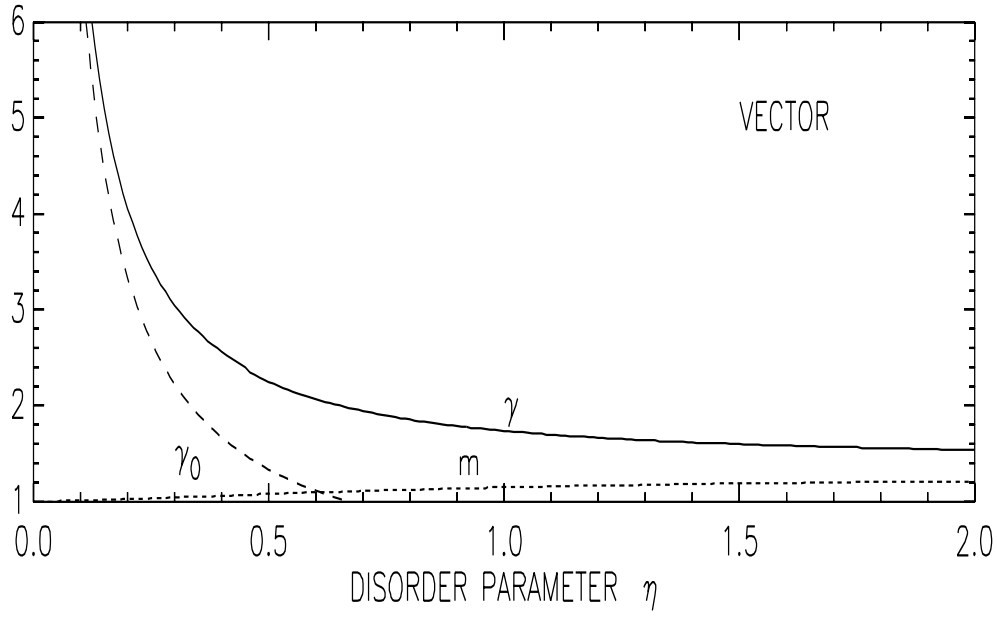

Figure 3.3: *The Ioffe-Regel type parameter $\gamma = k\ell_s$, and the average index of refraction m against disorder η; γ_0 is the independent scattering result, calculated from Eq. (3.51). The individual scatterers are set to resonance.*

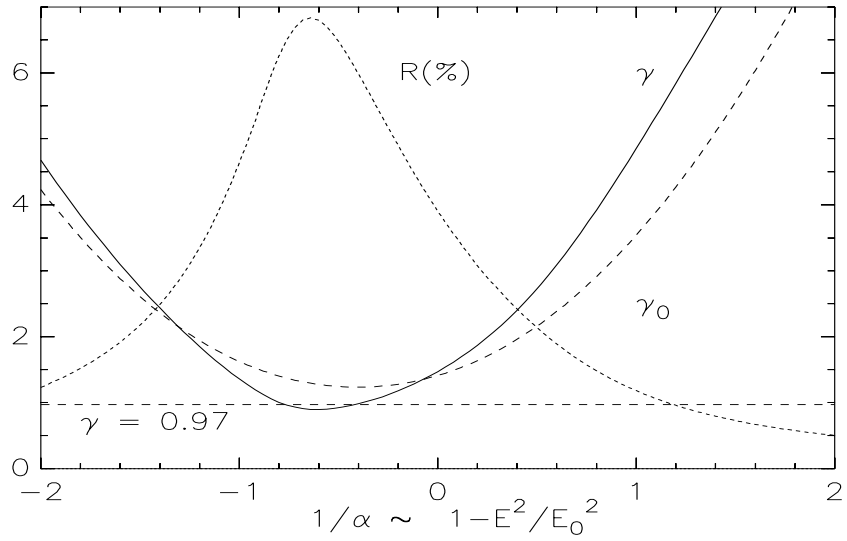

Figure 3.4: *The Ioffe-Regel type parameter γ and the Fresnel Reflection coefficient R for fixed density $\eta = 0.81$ in the neighborhood of a resonance (at E_0). The horizontal dashed line denotes the Ioffe-Regel criterion. Localization sets when $\alpha(E) < 0$.*

the scatterers start to overlap. In that case it can be deduced that the collective cross-section is smaller than the sum of the individual cross-sections. For resonating scatterers the optical radius is roughly equal to the wavelength λ, so that overlap occurs once $n\,\lambda^3 \sim 1/\gamma > 1$. This proves that in the regime of localization the overlap of optical volumes must be considerable. Our results are in disagreement with the work of Sornette and Souillard [89]. They maximized the amount of scattering, but did not distinguish between *individual* and *collective* scattering.

Off-resonance, a second expansion parameter determines the significance of dependent scattering, namely $s = E\,t/4\pi$. On-resonance we have $|s| = 1$, off-resonance $|s| < 1$. If $|s|$ becomes much less than unity, dependent scattering is strongly suppressed and the independent-scattering approximation becomes better.

On the basis of causality it will be argued in section 3.4.2 that $\alpha > 0$ for the above point models. In view of the modified version (1.70) of the Wu model, one can identify $1/\alpha \sim E_0^2 - E^2$ going from positive to negative near the resonance at E_0. The energy dependence of α restores causality [23]. In Fig. 3.4 we have solved our self-consistent equation (3.54) near E_0, for an experimentally realistic density $\eta = 0.81$. We find that the prospects for the occurrence of strong localization of light are better off-resonance. A small localization window is present in the right flank of the resonance, where $\alpha(E) < 0$. This calculation illustrates that not only the absolute value of the parameter s mentioned above is important off-resonance, but also its complex phase.

Using the solution of the self-consistent equation (3.54) it is possible to compute the self-energies in Eq. (3.56) for any momentum p. The self-energies are plotted in Fig. 3.5 for various amounts of disorder. We conclude that evaluating $\Sigma_i(p)$ on the energy shell does not introduce large inaccuracies. For the "longitudinal" self-energy $\Sigma_\ell(p)$ the

approximation is bad but this contribution has been ignored anyway.

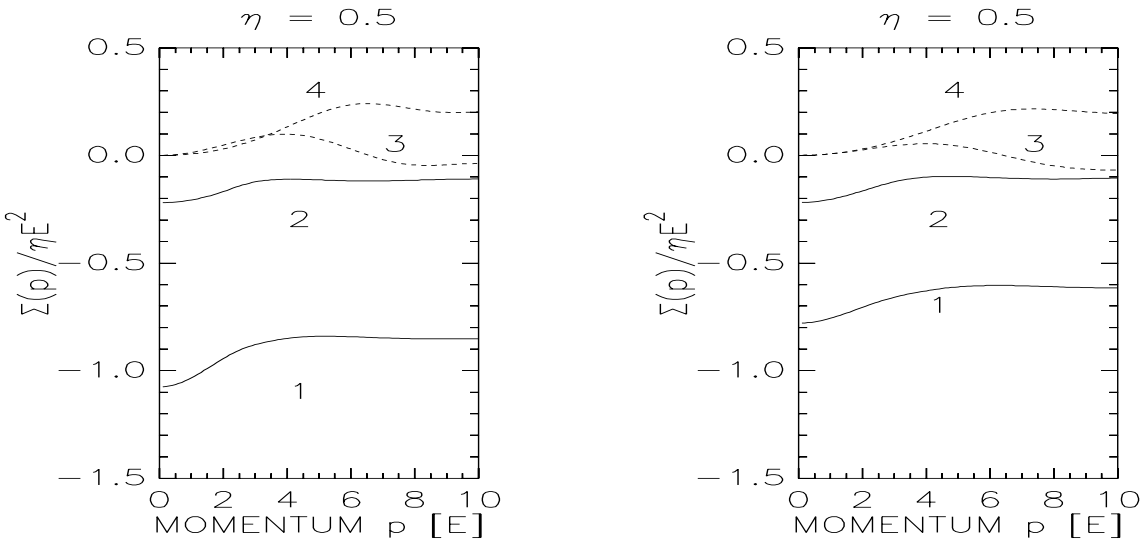

Figure 3.5: *The vector self-energies for fixed energy as a function of momentum. (1)* $\mathrm{Im}\,\Sigma_i(E,p)$*, (2)* $\mathrm{Re}\,\Sigma_i(E,p)$*, (3)* $\mathrm{Im}\,\Sigma_\ell(E,p)$*, (4)* $\mathrm{Re}\,\Sigma_\ell(E,p)$*.*

Our self-consistent calculation incorporates dependent scattering from two point scatterers exactly. The change in the scattering mean free path in lowest order of the density is found from Eq. (3.37),

$$\frac{\ell_s}{\ell_0} = 1 - \left[\frac{1}{2}\frac{\mathrm{Re}\,\Sigma^{(1)}(E)}{E^2} + \frac{\mathrm{Im}\,\Sigma^{(2)}(E)}{\mathrm{Im}\,\Sigma^{(1)}(E)}\right] + \mathcal{O}(\eta^2)\,. \tag{3.59}$$

The correction is still a function of the one-scatterer t-matrix, and can be calculated easily from Eq. (3.52) for scalar point scatterers, and from Eq. (3.56) for Rayleigh point scatterers. The parameter determining the importance of the correction in Eq. (3.59) is essentially nt^3 and is recognized as the "number of scatterers per optical volume". For the special case that the point scatterers are on resonance we find that

$$\frac{\ell_s}{\ell_0} = \begin{cases} 1 - 0.375\,\eta & \text{(scalar)} \\ 1 + 0.472\,\eta & \text{(vector)}\,. \end{cases} \tag{3.60}$$

The different behavior of the scattering mean free path for Rayleigh vector scatterers and isotropic scalar scatterers at low density can also be seen from Fig. 3.3.

3.3.4 Internal Reflection

We briefly discuss one application of the theory of the previous section. Having the complex wavenumber z available from the computer program we have estimated the importance of "internal reflection" [114] [115] [116]. The Fresnel reflection coefficient,

$$R(E) = \left|\frac{z(E)-1}{z(E)+1}\right|^2\,, \tag{3.61}$$

determines how much energy is being reflected coherently on an ideal interface separating bulk and vacuum. A value $R > 0$ indicates that any light in the sample will stay longer in the sample because it is reflected back into the medium. This trapping favors large path lengths and can be accounted for by a lowering of the effective transport mean free path.

The result for $R(E)$ is shown in Fig. 3.4. The energy sensitivity of the complex wavenumber $z(E)$ near the resonance certainly makes the internal reflection an interesting effect that cannot be ignored. This so-called *Selective Reflection* was already studied in another context (atomic resonances) in Refs. [117] and [118], where the parameter η exceeds 10. This regime of very close packing could not be studied with our method. On the other hand, dipole-dipole coupling between the atoms may be an important transport mechanism [93] there, and is absent in our models. In experiments involving dielectric particles rather than atoms, $\eta \leq 3/x^3$ is at most of order unity.

Formula (3.61) applies for normal incidence, but all angles of incidence are represented in a multiple-scattering situation. Large angles suffer more from internal reflection, so that this formula seriously underestimates the role of internal reflection. An angle-averaged reflectivity of 50 % is not unrealistic for large densities of the scatterers. Eq. (3.61) predicts $R \lesssim 10\,\%$. A forthcoming paper by Nieuwenhuizen and Luck will deal with the skin-layer in diffusive media.

3.3.5 Electron Localization and Dependent Scattering

The method (3.54) can serve to model localization of spinless low-energy electrons with scattering length α. To this end we use the Fermi t-matrix (1.64). The corresponding interaction has a bound state at energy $-1/\alpha^2$ for $\alpha < 0$.

Fig. 3.6 displays the Ioffe-Regel parameter as a function of energy. It is demonstrated that localization sets in for sufficiently low energy. Dependent scattering pushes the mobility edge towards larger energies than expected on the basis of the independent scattering approximation, which is mainly due to a shift of the energy threshold. We applied Eq. (3.42) to calculate the transport mean free path of the electrons. Below $\gamma = 1/2$ (indicated by a horizontal bar) only evanescent waves are present.

The standard argument for electron-impurity scattering is that $\gamma \to 0$ at low energies so that Anderson localization sets in no matter what the exact criterion is. By letting $\alpha > 0$ one infers from Eq. (3.37) that $\gamma \geq 1/2$ in the independent-scattering approximation, not being far below the criterion (3.46). Thus, Anderson localization of electrons at low energies (in the presence of topological disorder) seems to be less trivial than often suggested in literature. A rigorous mathematical proof exists for the onset of electron localization at low energies [119], but it applies for a lattice with diagonal disorder ("the standard Anderson Tight-binding model"). As a matter of fact it is still the *only-existing* proof for localization in three dimensions.

We remark that the "enhanced-forward-scattering" contribution in Eq. (3.48) to the mean free path does not vanish in the case of low-energy electron-impurity scattering. At low energies $\nu \to 4\pi n|\alpha|^3$ is proportional to the "average number per cubic scatter-

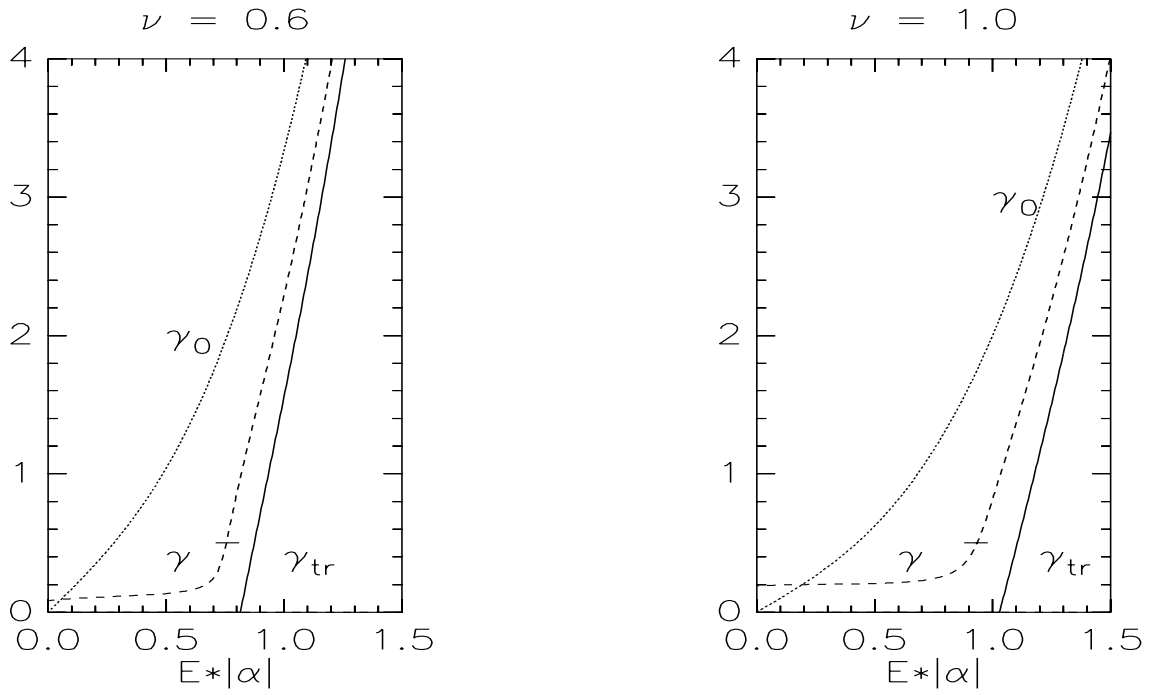

Figure 3.6: *Scattering and transport mean free path for spinless low-energy electrons. The horizontal bar indicates* $\gamma = 1/2$*. Energies for which* $\gamma < 1/2$ *have no propagating solutions. We have taken* $\alpha < 0$*.*

ing length". For the value $\nu \geq 3$ might this contribution become important, possibly destroying the mobility edge.

3.4 Dynamic Properties: Transport Velocity

We proceed with the definition and the calculation of the transport velocity of multiply scattered light. This involves the solution of a *dynamic* Boltzmann equation ($\omega \neq 0$ and $\mathbf{q} \neq 0$). The outcome will be worked out for scatterers for which the scattering properties are known explicitly, so that the calculation of this speed can be carried out exactly, either numerically or analytically. The generalized Boltzmann equation (3.21) is valid for scalar waves, so that we should be able to obtain an *exact* solution for such waves, at least in lowest order of the density. The relevant generalization for vector scatterers (among which the Mie sphere) will also be considered.

In the second part of this section we compare some heuristic approaches to rigorous results. At present, it is already obvious that some of these approaches, originally put forward by Meint van Albada and Martin van der Mark, give essentially the *exact* solution. To our surprise, the rigorous expression for the transport velocity turned out to coincide numerically with estimates based upon "charging of the scatterers" and absorption. The work of Bott *et al.* [27], discussed in section 1.7, already unifies both heuristic approaches satisfactorily.

We emphasize that all the theoretical work reported in this section was initiated by the wish to understand a persistent discrepancy between different experiments in our group. In the search for Anderson localization of light, it seemed beneficial to tune to resonances in the scattering cross-section, in combination with a large density of the dielectric particles, thereby minimizing the elastic mean free path. Following this road, small diffusion constants were reported [88], and were attributed to very short transport mean free paths and thus to the nearness of a mobility edge. They were also found in our experiments [87], which involved the multiple scattering of light of wavelength $\lambda = 633\,nm$ from TiO_2 particles with an average radius $r_0 = 110\,nm$, an index of refraction $m = 2.73$, and a volume fraction of 36 %. We measured a diffusion constant $D = 11.7\,m^2 s^{-1}$. This is very near the "Mott minimum" $D = c_0\,\lambda/6\pi = 10\,m^2 s^{-1}$, and we could have speculated about the nearness of localization.

An accurate comparison between *time-resolved* and *steady-state* measurements however, demonstrated that the low diffusion constants were not at all consistent with short transport mean free paths ($\ell = 0.57 \pm 0.05\,\mu m$, thus $k\ell \approx 5.6$) as should be the case near the mobility edge. There was no other way out than assigning an extremely small value to the speed of the diffusing light, $v_E = 5 \pm 1 \cdot 10^7\,ms^{-1} = 0.17 \pm 0.03\,c_0$. This was recently verified by independent measurements on the frequency-dependent intensity-intensity correlation function [120]. Up to now, no theory could account for such small speeds in elastic multiple scattering from dielectric particles. The phase velocity, either found from volume fraction arguments, or obtained from more sophisticated coherent potential methods, has frequently been used for the velocity entering the diffusion constant of classical waves. The volume-averaged index of refraction in our random medium is $\langle\varepsilon\rangle = 3.31$, corresponding to an effective-medium value for the phase velocity $v_p = 0.55\,c_0$. This is still a factor of three more than the experimental outcome. An exact low-disorder calculation

of the phase velocity [91] (see Eq. (3.64)) yields the even higher value of $0.76\,c_0$.

Theoretically, the concept of an "energy" velocity, different from both phase and group velocity is not new and was already introduced by Brillouin [121] and Loudon [23] [122]. Because both phase and group velocity, the latter in particular, were seen to become anomalous (larger than c_0) near the internal resonances of a semi-classical oscillator, the above authors wondered whether a velocity exists that satisfies the causality demand of being less than the vacuum speed of light. A velocity defined in terms of an average energy current divided by an average energy density, turns out to obey causality indeed. The authors concluded that the large amount of energy that is being stored in the scatterers themselves (thus not subject to propagation) near internal resonances, largely (!) compensates for the anomalous behavior of the group velocity. The result is that this energy velocity becomes very small near the resonant eigenfrequencies of the oscillator.

Although we were strongly inspired by this approach, there were some reasons why it was not directly applicable to dielectric scatterers. The most important reason is that the treatment is essentially phenomenological. The lowering of the energy speed of light was not directly written down in terms of microscopic properties of the scatterers, such as the S-matrix.

Secondly, the work of Brillouin and Loudon dealt with scatterers having internal degrees of freedom: the resonances are of the *Feshbach type* [10]. In the scattering from dielectrics the resonances are *shape resonances* in which case a standing wave (with velocity zero) is generated inside the scatterer. In that case internal degrees of freedom are absent.

The third reason why it was not at all evident that this energy velocity was relevant for our experimental discrepancy, was that the authors constructed this velocity *only* to prove that there was no violation of causality. They did not point out that this velocity is a fundamental observable physical quantity that describes the propagation of the diffusing light. As such it must enter into the diffusion constant of light!

Finally, from the theoretical side, a cancellation theorem valid for multiple electron-impurity scattering was known. If applied straightforwardly to classical wave scattering, this so-called Ward-Takahashi identity demonstrates unambiguously that the speed in the diffusion coefficient is essentially the phase velocity [90]. Any velocity different from the phase velocity would thus violate this very fundamental theorem.

Concerning the difference between internal and shape resonances, it soon became clear that both cases were not so different after all. The internal resonances show up as singularities of an *optical*, energy-dependent potential [10]. It was already pointed out that the scattering of light can be viewed as potential scattering from an energy-dependent potential. Near a resonance, either shape or Feshbach resonance, the t-matrices are indistinguishable. Guided by the principle that "the same equations have the same solutions" we had great confidence that the decrease of the energy speed discussed by Loudon and Brillouin had been overlooked so far in the treatment of dielectric scattering.

3.4.1 Microscopic Derivation of Transport Velocity

We present a microscopic derivation of the transport speed of light. The generalized Boltzmann equation will be solved in lowest order of the density (the Boltzmann approximation). In this approximation, sometimes also referred to as "first-order smoothing" [62], the mass-operator and irreducible vertex are expressed in terms of the bare t-matrices of the individual particles. In addition, the spectral function is completely on-shell and was found in section 3.3.1. Contrary to section 3.3.1 we now include dynamic effects.

Next a careful expansion of the mass operator and the vertex into the variable ω is made. These terms are collected together with the dynamic ω-term already present in the Boltzmann equation (3.21). We have

$$\begin{aligned}
\Sigma^1(E^\pm \pm \omega/2, \mathbf{p}^\pm) &= n\, t_{\mathbf{p}(\pm)\mathbf{p}(\pm)}(E^\pm \pm \omega/2) \\
&= n\, t_{\mathbf{pp}}(E^\pm) \pm n\, \frac{\omega}{2}\, \frac{\partial t_{\mathbf{pp}}(E^\pm)}{\partial E} + \mathcal{O}(\omega^2, \mathbf{q})\,, \\
U^1_{\mathbf{pp}'}(\omega\, \mathbf{q}|E) &= n\, t_{\mathbf{p}(+)\mathbf{p}'(+)}(E^+ + \omega/2)\, t_{\mathbf{p}'(-)\mathbf{p}(-)}(E^- - \omega/2) \\
&= n\, |t_{\mathbf{pp}'}(E^+)|^2 \left(1 + i\omega \frac{\partial \phi_{\mathbf{pp}'}(E)}{\partial E}\right) + \mathcal{O}(\omega^2, \mathbf{q})\,. \qquad (3.62)
\end{aligned}$$

Here $\phi_{\mathbf{pp}'}(E)$ denotes the phase shift according to $t_{\mathbf{pp}'}(E^+) \equiv |t_{\mathbf{pp}'}| \exp(i\phi_{\mathbf{pp}'})$. Furthermore $E^\pm = E \pm i0$ and $\mathbf{p}^\pm = \mathbf{p} \pm \mathbf{q}/2$. A similar expansion, involving partial derivatives with respect to p, can be employed in terms of the variable $\mathbf{q}$. These extra terms will later be argued to vanish rigorously. The spectral function is written as

$$S^1(E, p) = 2\pi |E| \delta\left(E^2/v_p^2 - p^2\right)\,, \qquad (3.63)$$

where the phase-velocity v_p is given by [91]

$$\frac{1}{v_p(E)} = \sqrt{1 - n\, \frac{\mathrm{Re}\, t_{\mathbf{pp}}(E^+)}{E^2}}\,. \qquad (3.64)$$

It is understood that $p = |E|$. Using the "density" and "current" defined in Eq. (3.27), the Boltzmann equation can be integrated over all momenta $\mathbf{p}$ to give

$$i\,\omega \left[1 + n\, \delta^1(E)\right] P_E(\omega\, \mathbf{q}) + \frac{i\, \mathbf{q} \cdot \mathbf{J}_E(\omega\, \mathbf{q})}{v_E\, v_p} = -\pi N(E) \qquad (\omega \to 0)\,, \qquad (3.65)$$

in terms of the yet unspecified velocity v_E. We abbreviated

$$\delta^1(E) \equiv -\frac{\partial \mathrm{Re}\, t_{\mathbf{pp}}(E^+)}{\partial (E^2)} + \int d\Omega\, \frac{d\sigma}{d\Omega}\, \frac{\partial \phi(\Omega, E)}{\partial E}\,, \qquad (3.66)$$

where $d\sigma/d\Omega = |t_{\mathbf{pp}'}(E^+)|^2/(4\pi)^2$ is the differential cross-section, and again $p = |E|$ after the partial derivatives with respect to E have been performed. In deriving Eq. (3.65) we made use of the optical theorem,

$$-\frac{1}{E}\, \mathrm{Im}\, t_{\mathbf{pp}}(E^+) = \int d\Omega\, \frac{d\sigma}{d\Omega}(E)\,, \qquad (3.67)$$

cancelling some terms in Eq. (3.65) on the basis of energy conservation. This identity is in fact the low-density limit of the Ward identity (3.22). If we want Eq. (3.65) to be an *equation of continuity*,

$$\partial_t P_E(\mathbf{r},t) + \boldsymbol{\nabla}\cdot\mathbf{J}_E(\mathbf{r},t) \sim \delta(\mathbf{r})\,\delta(t)\,, \tag{3.68}$$

Fourier-transformed with respect to position (with conjugate variable $\mathbf{q}$) and Laplace-transformed with respect to time (conjugate variable ω), it follows that

$$\frac{1}{v_E(E)} = v_p(E)\left[1 + n\,\delta^1(E) + \cdots\right]. \tag{3.69}$$

Let us comment on the results obtained so far. Eq. (3.65) seems to suggest that not P_E but rather

$$P_E^*(\omega\,\mathbf{q}) \equiv \left[1 + n\,\delta^1(E)\right] P_E(\omega\,\mathbf{q}) \tag{3.70}$$

represents the true energy density for our problem. Accordingly, to satisfy Eq. (3.68), the current must be

$$J_E^*(\omega\,\mathbf{q}) = -\frac{E^2}{v_p(E)}\sum_{\mathbf{p}}\hat{\mathbf{p}}\,\Phi_{E\mathbf{p}}(\omega\,\mathbf{q})\,. \tag{3.71}$$

Concerning the formulation of the diffusion constant and the transport velocity in section 3.3, this does not offer new insights because these transport properties depend only on the ratio $J_E/P_E = J_E^*/P_E^* = v_E$. However, the definitions above relate better to the ones *before* averaging. For the scalar wave equation [123],

$$\begin{aligned} P^*(\mathbf{r},t) &= \frac{1}{2}\,\varepsilon(\mathbf{r})|\partial_t\psi|^2 + \frac{1}{2}|\boldsymbol{\nabla}\psi|^2 \\ &\qquad \stackrel{SVEA}{\to} E^2|\psi_E|^2\,(1 + \text{corrections inside scatterers})\,, \\ \mathbf{J}^*(\mathbf{r},t) &= -\mathrm{Re}\,(\partial_t\psi)(\boldsymbol{\nabla}\psi)^* \stackrel{SVEA}{\to} -\frac{E^2}{v_p(\mathbf{r})}\hat{\mathbf{p}}\,|\psi_E|^2\,. \end{aligned} \tag{3.72}$$

The abbreviation "SVEA" stands for the *Slowly Varying Envelope Approximation* [124],

$$\psi(\mathbf{r},t) = \psi_E(\mathbf{r},t)\,\mathrm{e}^{iEt}\,,$$

under the assumption that the exponent oscillates much more rapidly than the "envelope" $\psi_E(\mathbf{r},t)$. As a matter of fact our limit $\omega \to 0$ describes this approximation in reciprocal space. The above demonstrates that $\delta^1 \neq 0$ for classical waves, and moreover, implies that this quantity is related to the energy density *inside* the dielectric particles and thus, as was pointed out in section 1.7, to the "charging time". Note that if δ^1 would vanish, just like for electrons, the velocity entering the diffusion constant would equal c_0^2/v_p and not v_p. The facts that $\delta^1 = 0$ and $v_E = v_p$ are thus not compatible, contrary to what was "believed" so far [90].

Without the second (collision) term of Eq. (3.66) the transport velocity would be equal to the *group velocity*,

$$v_g(E) \equiv \frac{dE}{dk} = \frac{k(E)}{E}\left(\frac{dk^2}{dE^2}\right)^{-1} = \frac{1}{v_p(E)}\left(1 - \frac{d\,\mathrm{Re}\,\Sigma(E^+)}{d(E^2)} + \frac{d}{d(E^2)}\frac{1}{4\,\ell_s^2}\right)^{-1}, \quad (3.73)$$

with $k(E)$ the renormalized wave vector defined in Eq. (3.37). The term $1/4\ell_s^2$ is second order in density and is therefore often ignored. The group velocity is known to lose its meaning near scattering resonances [121], and may even become negative. Text books usually get around this problem by stating that the resonantly enhanced extinction (most confusingly referred to as "absorption" by Loudon [122]) makes a discussion of transport properties irrelevant. Inspection of our formula (3.69) demonstrates that the true energy velocity takes into account the energy carried by the *elastically* scattered wave in *all* directions. We will show that this collision contribution largely compensates for the anomalous behavior of the group velocity. The group velocity in a random medium has a physical significance only if the attenuated coherent wave is measured [125].

Often a group velocity enters into the diffusion constant [98], but then it is entirely the result of an effective mass approximation. The effective mass is a property of the (dispersion law of the) underlying crystal and does *not* contain information on impurities! As a matter of fact, the group velocity of a crystal maps upon the *bare* speed of light (c_0) in our theory. Therefore we prefer the terminologies *group velocity* and *velocity enhancement* to distinguish "bare" velocities from "dressed" ones.

By letting $\mathbf{q} = 0$ in the equation of continuity we obtain the sum rule,

$$\int_{-\infty}^{\infty} \frac{dE}{2\pi}\, P_E^*(\omega, \mathbf{q}=0) = \frac{1}{-2i\omega}\int_{-\infty}^{\infty} dE\, N(E)\,. \quad (3.74)$$

Translated back to times and coordinates, Eq. (3.74) expresses the fact that the integral of $P_E^*(\mathbf{r}, t)$ does not depend on time. This justifies the statement that P_E^* is the true energy density, and not P_E. The integral in Eq. (3.74) gives the total number of states per unit volume, which is positive but infinite.

3.4.2 Ward-Takahashi Identity Revised

Since $|\psi(\mathbf{r}, t)|^2$ is a conserved quantity for Schrödinger dynamics (describing for instance electron-impurity scattering), the corrections in Eq. (3.72) are not expected for potential scattering. The absence of these corrections is expressed by a rigorous identity, the *Ward-Takahashi identity*,

$$\Sigma(E^+ + \omega/2, \mathbf{p}^+) - \Sigma(E^- - \omega/2, \mathbf{p}^-) = \sum_{\mathbf{p}'} \Delta G(E\,\mathbf{p}|\omega\,\mathbf{q})\; U_{\mathbf{p}\mathbf{p}'}(\mathbf{q}\,\omega|E)\,, \quad (3.75)$$

valid for electron-impurity scattering [60] [69] [126]. This is a generalization of the Ward identity in Eq. (3.22). In particular it cancels all dynamic corrections in the equation of

continuity so that $\delta(E) = 0$ in all orders of the density. One very fundamental consequence is the absence of the so-called "mass-enhancement" factor in some crucial transport coefficients such as the dc-conductivity [94]. As a result, the velocity in the quantum diffusion constant is the Fermi-velocity $\hbar k_F/m_e$, being the quantum analogue of the classical wave velocity c_0^2/v_p.

A close examination of the proof of the Ward-Takahashi identity [69] demonstrates its validity for non-interacting, local and energy-independent potentials. Indeed, it is known that mass-enhancement factors do enter the equation of continuity once many-particle interactions become important. Examples are Fermi liquids [84] [127], as well as moderately dense gases [128] [129], where these correlation effects successfully produce the second virial constant.

What remains of this identity in the case of scalar wave scattering? Inspection of the scalar wave equation,

$$\left[\varepsilon(\mathbf{r})\,\partial_t^2 - \boldsymbol{\nabla}^2\right]\psi(\mathbf{r},t) = 0\,, \tag{3.76}$$

illustrates that, in view of the Schrödinger equation, and after application of the above-mentioned SVEA, a *local* but *energy-dependent* "potential" can be identified via $V(\mathbf{r},E) = [1-\varepsilon(\mathbf{r})]\,E^2$. Thus $V(E+\omega) \neq V(E-\omega)$. An equality here is essential for the Ward-Takahashi identity (3.75) to be valid. This is true if $\omega = 0$, i.e. as long as *stationary* properties are discussed. Since the scalar wave equation is mapped upon the Schrödinger equation *only* for $\omega = 0$, we can conclude that the Ward-Takahashi identity must apply for classical waves only when $\omega = 0$. The validity of Eq. (3.75) for $\mathbf{q} \neq 0$ proves that spatial vertex corrections cancel in the equation of continuity for scalar waves satisfying Eq. (3.76).

The question what changes matrix-element formulations of conservation laws when dealing with the vector nature of light is not easy to answer. Looking at the Helmholtz equation for the electric field, it turns out that this equation has more resemblance to the "other" scalar wave equation,

$$\left[\partial_t^2 - \boldsymbol{\nabla}\cdot\frac{1}{\varepsilon(\mathbf{r})}\boldsymbol{\nabla}\right]\psi(\mathbf{r},t) = 0\,. \tag{3.77}$$

In view of Eq. (3.76), this equation suffers from the so-called "logarithmic derivative" $(\boldsymbol{\nabla}\log\varepsilon)\cdot\boldsymbol{\nabla}$ which can be envisaged as a non-local ("velocity dependent") potential. In most cases, the dielectric constant is piecewise constant and this term gives rise to different boundary conditions. Nevertheless, the convenient analogy of Eq. (3.76) to the Schrödinger equation is lost.

The non-local extra term in Eq. (3.77) will cause a violation of the "$\mathbf{q} \neq 0$" Ward-Takahashi identity (3.75) for waves obeying Eq. (3.77). This extra complication shows up in the calculation of the transport velocity for vector waves, which have properties of both kinds of scalar waves. Using an ("Wigner") approximation we can avoid this problem. In the next two sections we argue that the energy dependence of the potential

is the crucial effect. The energy-dependence of the potential is inherently present in the Maxwell's equations (see Eq. (1.42)), not only in scalar wave equations.

We remark again that a Ward identity signifies the presence of a conserved quantity. For waves satisfying Eq. (3.76) the (averaged) conserved quantity is given in Eq. (3.72). On the average, both terms in Eq. (3.72) represent an equal amount of energy, so that $\langle P_E^* \rangle \sim \langle \varepsilon \times |\psi_E|^2 \rangle$. An incorrect treatment of $\langle P_E^* \rangle$ results in an incorrect Ward identity and vice-versa. Both ε and $|\psi_E|^2$ are realization-dependent but one might argue that $\langle P_E^* \rangle \sim \langle \varepsilon \rangle \times \langle |\psi_E|^2 \rangle$. Such a procedure would make the phase velocity coincide *exactly* with the transport velocity. The *erroneous* Ward-Takahashi identity that decouples the averaging procedure was published by Barabanenkov [130]. The exact solution that we will give in Eq. (3.82) as well as the SVEA in Eq. (3.72) proves that fluctuations in the dielectric constant are strongly correlated with the intensity inside the scatterers. Near resonances the intensity inside a scatterer can be orders of magnitude larger than the space-averaged intensity $\langle |\psi_E|^2 \rangle$.

3.4.3 Transport Velocity of Scalar Waves

The present section is devoted to the calculation of the dynamic vertex correction $\delta^1(E)$ for scalar waves satisfying Eq. (3.76), determining the transport velocity v_E into first order of the density. Before going over to the actual computation, let us first consider alternative, perhaps more convenient, representations for δ^1. The definition in Eq. (3.66) involves partial derivatives with respect to the energy, at constant momentum. As such it does not seem to be of any numerical use since text books provide the *on-shell* t-matrix only.

To resolve this problem we can make the observation that partial derivatives with respect to momentum are usually very small, especially near resonances of scattering where the E-dependence is expected to be large. Besides, as pointed out in the previous section, a cancellation theorem applies for such derivatives, also for classical waves. This leads us to replace the partial derivatives with respect to E by *total* derivatives,

$$\delta^1(E) \approx \delta^W(E) \equiv -\frac{d}{d(E^2)} \mathrm{Re}\, t_{\mathbf{pp}}(E^+) + \int d\Omega \, \frac{d\sigma}{d\Omega} \, \frac{d\phi(\Omega)}{dE} \,, \tag{3.78}$$

where $\mathbf{p} = E\hat{\mathbf{p}}$. The right-hand side of this equation turns out to be the three-dimensional formulation of the *Wigner phase-delay time* [20] [131], as will become more clear later. The delay of all channels is hereby taken into account, the first term representing the coherent wave, the second all scattering channels. For a point scatterer there is no p-dependence in the t-matrix and Eq. (3.78) must be rigorous.

For scalar waves, obeying the scalar wave equation (3.76) we can follow the following *rigorous* procedure. Using the concept of an "energy-dependent" potential,

$$V(\mathbf{r}, E) = [1 - \varepsilon(\mathbf{r})] \; E^2 \equiv g(\mathbf{r}) \, V_0(E^2) \,, \tag{3.79}$$

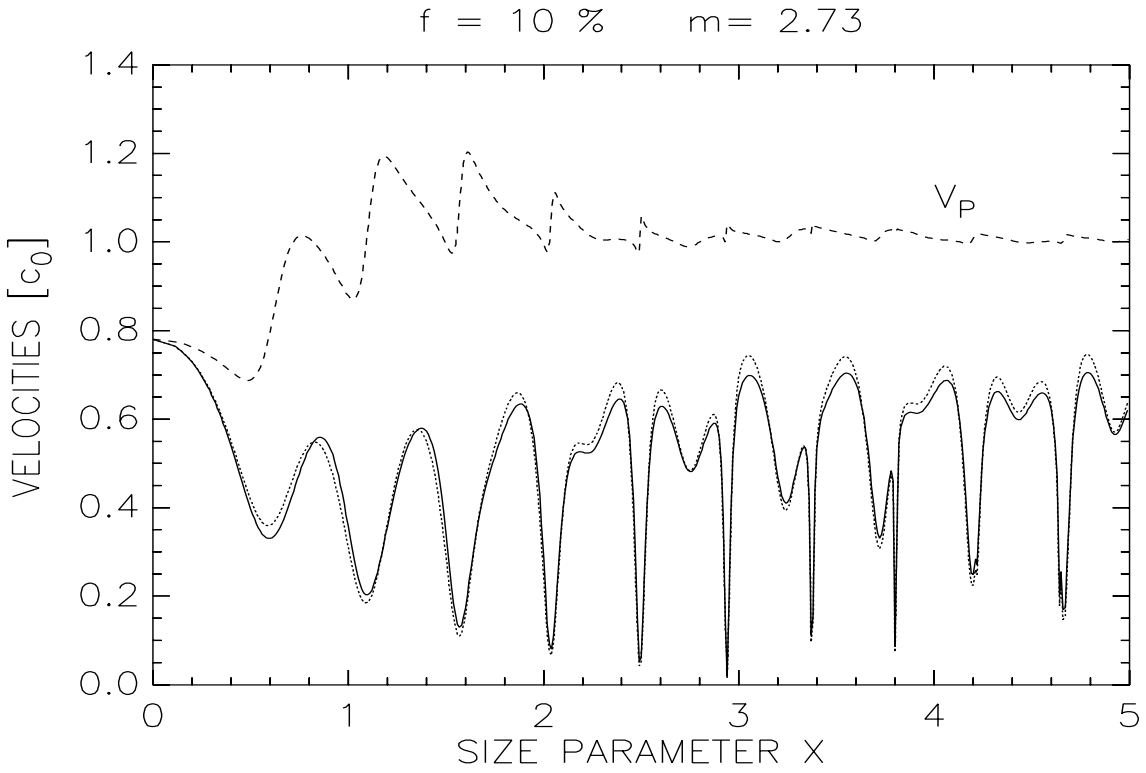

Figure 3.7: *Transport velocity v_E (bold), phase velocity v_p (dashed dotted) as well as the Wigner approximation for v_E (dotted), for scalar Mie spheres with index of refraction* 2.73 *and packing* 10 %.

we can apply the identity,

$$\frac{\partial}{\partial(E^2)}\Big)_{\mathbf{p},\mathbf{p}'} = \frac{\partial}{\partial(E^2)}\Big)_{\mathbf{p},\mathbf{p}',V_0} + \frac{dV_0}{d(E^2)}\,\frac{d}{dV_0}\,, \tag{3.80}$$

to evaluate expression for δ^1. By the Ward-Takahashi identity for energy-*in*dependent potential scattering, all partial derivatives with respect to E^2 at constant potential and momentum cancel (!) in the expression for δ^1. We arrive at

$$\delta^1(E) = \left[-\frac{d}{dV_0}\mathrm{Re}\,t_{\mathbf{pp}}(E^+) + 2E\int d\Omega\,\frac{d\sigma}{d\Omega}\,\frac{d\phi(\Omega)}{dV_0}\right] \times \frac{dV_0}{d(E^2)}\,. \tag{3.81}$$

The vertex correction δ^1 is thus *inherently* a property of the on-shell t-matrix. This is in agreement with the physical intuition that observable quantities should be expressed by properties of the on-shell t-matrix of the individual scatterers, at least in lowest order of the density in which case the scattered wave is given enough room to reach its asymptotic limit before undergoing a subsequent collision. This is not clear from the original formula (3.66).

It turns out that the expression (3.81) can be put into an even more convenient form. The details have been worked out in appendix A. We have

$$\delta^1(E) = -\frac{dV_0}{d(E^2)} \, \langle \psi^+_{\mathbf{k}} | \, g \, | \psi^+_{\mathbf{k}} \rangle = \int d\mathbf{r} \, |\psi^+_{\mathbf{k}}(\mathbf{r})|^2 \, [\varepsilon(\mathbf{r}) - 1] \, , \tag{3.82}$$

where $|\psi^+_{\mathbf{k}}\rangle$ is the "normalized outgoing plane wave" at momentum $\mathbf{k}$, $k = |E|$. Alternatively,

$$\delta^1(E) = E \, \frac{dV_0}{d(E^2)} \, \frac{d\,\sigma_{\rm abs}(E)}{d(\mathrm{Im}\, V_0)} \, . \tag{3.83}$$

Here $\sigma_{\rm abs}$ is the absorption cross-section, which vanishes for $\mathrm{Im}\, V_0 = 0$. We have allowed for a small imaginary part of the potential according to $V_0 \to V_0 + i \, \mathrm{Im}\, V_0$.

¿From Eq. (3.82) it is clear that δ^1 is determined by properties *inside* the dielectric. Particularly, it represents the (negative) potential energy inside the scatterer in a steady-state situation. This is in qualitative agreement with results obtained near Eq. (3.72). It is inferred that $\delta^1 > 0$ if the "potential" is *attractive* corresponding to $\varepsilon(\mathbf{r}) > 1$. In that case incoming waves are captured by the scattering obstacle, leading to the formation of a standing wave. The time needed to "charge" the scatterer to the binding energy in Eq. (3.82) can be held responsible for the slowing down of the macroscopic energy transport.

The representation for δ^1 in Eq. (3.83) is very convenient for numerical purposes. The equivalence of absorption arguments to the energy density in the scatterer was already found in section 1.7. It was pointed out that an equation of the kind of (3.83) might serve as a definition for the path length in the scatterer. This path length thus emerges in the transport velocity and can become orders of magnitude larger than the physical size of the scatterer.

We will now work out the rigorous expression for scalar waves for a special case: the scalar Mie sphere. One must solve the eigenvalue problem of the scalar wave equation with the $\varepsilon(\mathbf{r})$ of a usual Mie sphere. Writing $g(\mathbf{r}) = \theta(r_0 - r)$ and $V_0(E) = (1 - m^2)E^2$ we obtain, using L'Hôspital's formula,

$$\delta^1(E) = V_m \, \times \, \frac{3}{8} \, \frac{m^2 - 1}{m \, x} \, \lim_{m_i \to 0} \frac{Q_{\rm abs}}{m_i} \, . \tag{3.84}$$

The volume $V_m = 4\pi r_0^3/3$ of the sphere can be collected together with the density n in favor of the packing fraction $f = nV_m$. Furthermore $x = Er_0$ is the size parameter and $Q_{\rm abs}$ the quality factor for absorption. In Eq. (3.84) we have assumed that the dielectric constant of the sphere is positive so that $\varepsilon = (m + im_i)^2$. If negative, which is true for perfect *metallic* spheres, we must write $\varepsilon = (i\,m + m_r)^2$ where now m_r goes to zero. Eq. (3.84) can easily be evaluated numerically. The t-matrix is, using our conventions,

$$t_{\mathbf{p}\mathbf{p}'}(E^+) = -\frac{4\pi i}{E} \sum_{n=0}^{\infty} (2n+1) \, P_n(\cos\theta) \, b^*_n(x) \, , \tag{3.85}$$

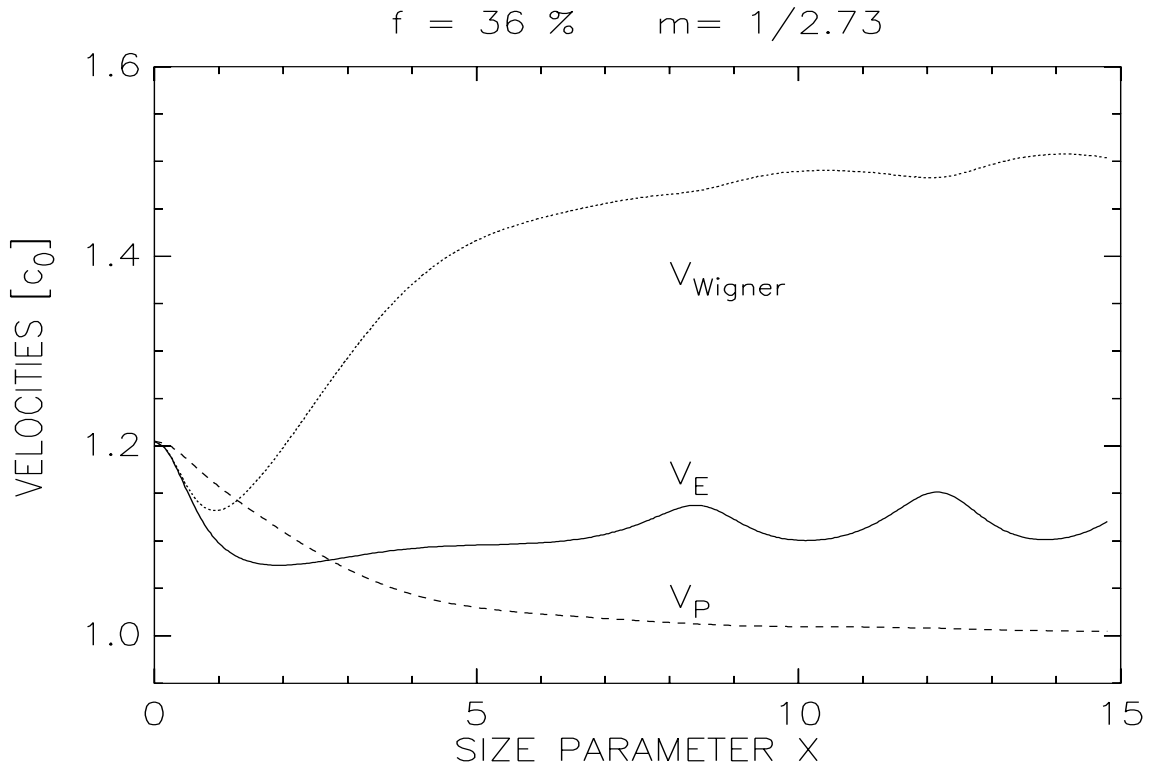

Figure 3.8: *As in Fig. 3.7 but now* $m = 1/2.73$ *and* $f = 36\,\%$.

corresponding to an absorption Q-factor,

$$Q_{\rm abs}(x) = \frac{4}{x^2} \sum_{n=0}^{\infty} (2n+1) \left(\mathrm{Re}\, b_n - |b_n|^2 \right) . \tag{3.86}$$

In these equations, the variable b_n (with complex phase $-\beta_n$) is the (standard) Van de Hulst coefficient for the TE mode of the vector Mie sphere. Because the formula (3.84) is an exact solution, it makes sense to compare it to the approximation made in Eq. (3.78). Using the orthogonality of the different partial waves this expression can be worked out to

$$\delta^W(E) = V_m \times \left(\frac{3}{2x^2} \sum_{n=0}^{\infty} (2n+1) \frac{d\beta_n}{dx} - \frac{1}{2} C(x) \right) . \tag{3.87}$$

Here

$$C(x) = \frac{3}{x^3} \sum_{n=0}^{\infty} (2n+1)\, \mathrm{Im}\, b_n \, . \tag{3.88}$$

In terms of this variable the phase velocity is given by

$$v_p(E) = \frac{1}{\sqrt{1 + f\, C(x)}} \, . \tag{3.89}$$

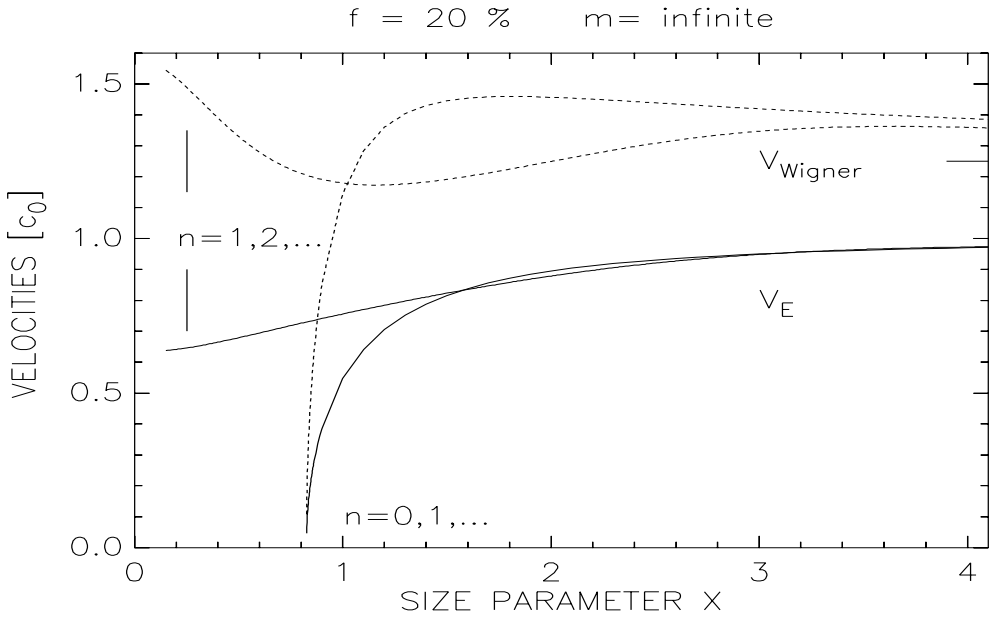

Figure 3.9: *The transport velocity v_E (bold) for a medium filled with scalar ideal reflectors ($m = \infty$) with volume fraction $f = 20\,\%$. The calculation is done with and without the s-wave ($n = 0$).*

For a more explicit derivation of these results we refer to the treatment of the vector Mie sphere in the next section, for which the calculation is analogous. The results are shown in Fig. 3.7. We infer that both approaches give essentially the same result, which justifies the inclusion of some partial derivatives with respect to p in Eq. (3.78). In Fig. 3.8 we took $\varepsilon < 1$ and the potential is repulsive. Because now strong resonance behavior is absent, the results do differ. The exact solution is larger than c_0. This is not a violation of causality because the average-medium value for the speed of light is larger than c_0 as well. The exact solution is seen to be less than or equal to (at small frequencies) this average-medium value.

Finally we have calculated the transport velocity for the scalar ideal reflector, corresponding to the t-matrix in Eq. (3.85) with $m = \infty$. Since there is no energy in the sphere, we get $\delta^1 = 0$ so that

$$v_E = \frac{1}{v_p} \qquad (m = \infty)\,, \tag{3.90}$$

in units of c_0. This model is shown in Fig. 3.9. Contrary to the phase velocity and the Wigner velocity, the transport velocity remains below the vacuum speed of light c_0 so that causality is obeyed. For large frequencies, the Wigner approximation approaches the "causality limit" for the phase-shift [20]: $1/(1-f) = 1.25$.

We performed the computation with and without inclusion of the s-wave. If the s-wave is incorporated, there is a cut-off frequency at which the transport velocity vanishes (with critical exponent 1/2) and the phase velocity diverges. Excluding the s-wave gives the

model a Rayleigh limit at low frequencies so that this cut-off is absent. As such, the scalar reflector without s-wave relates better to the scattering of *light* from an ideal reflector [4].

3.4.4 Transport Velocity for Simplified Models

The expression for the transport velocity, in particular the one for δ^1, was derived for scalar waves, but suggests a straightforward inclusion of polarization. In that case we must sum the second term in Eq. (3.66) over all possible polarization states of the scattered wave, and evaluate the first term, since it represents the coherent wave, for equal polarization of the incoming and outgoing wave.

Let us treat a scattering situation for which phenomenological formulations of the transport velocity exist in literature. We begin with the t-matrix

$$t_{\mathbf{pp}'}(E^+) = \frac{-4\pi E^2}{1/\alpha - \beta\, E^2 - \frac{2}{3} i E^3}\ \mathbf{g}_{\rm in}\cdot\mathbf{g}_{\rm out}\,. \tag{3.91}$$

This t-matrix emerged in Eq. (1.70) as a generalization of the Wu model, but is also the result of a semi-classical treatment of light scattering of an harmonic oscillator [23] [122]. In that case $1/\alpha\beta = E_0^2 > 0$ represents the resonant eigenfrequency, and $1/\beta = r_e > 0$ is the classical electron radius; $\mathbf{g}_{in}$ and $\mathbf{g}_{out}$ are the normalized polarization vectors of incoming and outgoing wave. Since the model in Eq. (3.91) is essentially point-like, the "Wigner" approximation discussed in the previous section is exact. It can readily be verified that

$$\sum_{\mathbf{g}_{\rm out}} \int \frac{d\Omega}{4\pi}\ \left(\mathbf{g}_{\rm in}\cdot\mathbf{g}_{\rm out}\right)^2 = \frac{2}{3}\,. \tag{3.92}$$

We introduce the phase angle ρ according to

$$t_{\mathbf{pp}'}(E^+) = -(6\pi/E)\sin\rho\, e^{i\rho}\ \mathbf{g}_{\rm in}\cdot\mathbf{g}_{\rm out}\,, \tag{3.93}$$

with $\tan\rho = \frac{2}{3}E^3/(1/\alpha - \beta E^2)$. Upon direct differentiation

$$\delta^1(E) = \frac{3\pi}{E^2}\frac{d\rho}{dE} + \frac{3\pi}{2E^3}\sin 2\rho\,. \tag{3.94}$$

Neglecting higher orders in density in the phase velocity, yields the final result,

$$\frac{1}{v_E} = 1 + 2\pi n\ \frac{1/\alpha + \beta\, E^2}{(1/\alpha - \beta\, E^2)^2 + (\frac{2}{3}E^3)^2} + \mathcal{O}(n^2)\,. \tag{3.95}$$

This speed is seen to be strictly less than unity, provided that $\beta \geq 0$ and $\alpha \geq 0$. The positivity of β was anticipated in section 1.6. The values for the semi-classical oscillator satisfy these requirements. The group velocity v_g equals in the same approximation,

$$\frac{1}{v_g} = 1 + 2\pi n\ \frac{(1/\alpha - \beta E^2)^2(1/\alpha + \beta E^2) + (\frac{2}{3}E^3)^2(3\beta E^2 - 5/\alpha)}{\left[(1/\alpha - \beta E^2)^2 + (\frac{2}{3}E^3)^2\right]^2}\,, \tag{3.96}$$

and becomes strongly anomalous near the resonance at $E = E_0$. Inspection of Eq. (3.95) proves that the transport velocity sharply drops in the neighborhood of a resonance. This drop is essentially determined by the product of density, total cross-section and lifetime of the resonance. We have plotted phase, group and transport velocity in Fig. 3.10. Sufficiently far from the resonance, all velocities coincide. The two singularities in the group velocity are characteristic for an S-shaped dispersion law [132].

The result obtained by Loudon [23], as well as Brillouin [121], is in complete agreement with Eq. (3.95). This is not self-evident for their model differs from ours. The t-matrix in Eq. (3.91) is the result of a coupling of the radiation field to and a subsequent integration over *internal* degrees of freedom (excited states) which then become internal (Feshbach) resonances. On the other hand, Eq. (3.81) was derived without inclusion of any internal degree of freedom. Nevertheless, from the appearance of the on-shell t-matrix alone one cannot distinguish between both kinds of resonances. This is consistent with the fact that an application of our formula to their t-matrix yields the same result as an explicit treatment of these internal degrees of freedom. Mathematically, the decrease of the transport velocity in the presence of internal resonances can be attributed to a singular energy-dependent "optical" [10] potential $V_0(E)$ so that the factor dV_0/dE in Eq. (3.81) becomes large. In the case of shape resonances in dielectric scattering, there is an energy-dependent potential indeed, but the derivatives with respect to V_0 are the ones that generate the decrease of the transport velocity.

Letting $\beta = 0$ in the t-matrix above we recover the Wu point model derived in Eq. (1.68). We can establish that

$$\frac{1}{v_E} = \frac{1}{v_p} = \sqrt{1 + \frac{4\pi n/\alpha}{1/\alpha^2 + (\frac{2}{3}E^3)^2}}\,. \tag{3.97}$$

This result is a beautiful demonstration of the conjecture that transport and phase velocity coincide away from resonances. In view of Eq. (3.97), the variable $1 + 4\pi\, n\, \alpha$ can be interpreted as the average dielectric constant of the random medium. This conclusion also emerges from a fit of the Wu model to the dielectric sphere at low frequencies [26]. Eq. (3.97) has been plotted in Fig. 3.11 for an "average dielectric constant" of 5.

Among the set of point interactions in Eq. (3.91), the choice $\alpha = \infty$, $\beta > 0$ satisfies $\delta^1(E) = 0$. The corresponding t-matrix is sometimes used to model the interaction of light with an antenna [18]. We find that $v_E = 1/v_p < 1$. Because the E^2-behavior at low frequencies is absent, this model has a cut-off frequency $E_c \approx \sqrt{4\pi n/\beta}$ at which the phase velocity diverges and the energy velocity vanishes. Below E_c no energy transport is possible. This model bears a strong resemblance to the metallic sphere in Fig. 3.9.

3.4.5 Transport Velocity for Mie Scatterers

Due to the occurrence of the non-local "logarithmic derivative" in the Helmholtz equation, the approximation of replacing partial derivatives with respect to energy by total derivatives must still be preferred over the original (only for scalar waves rigorous) expression.

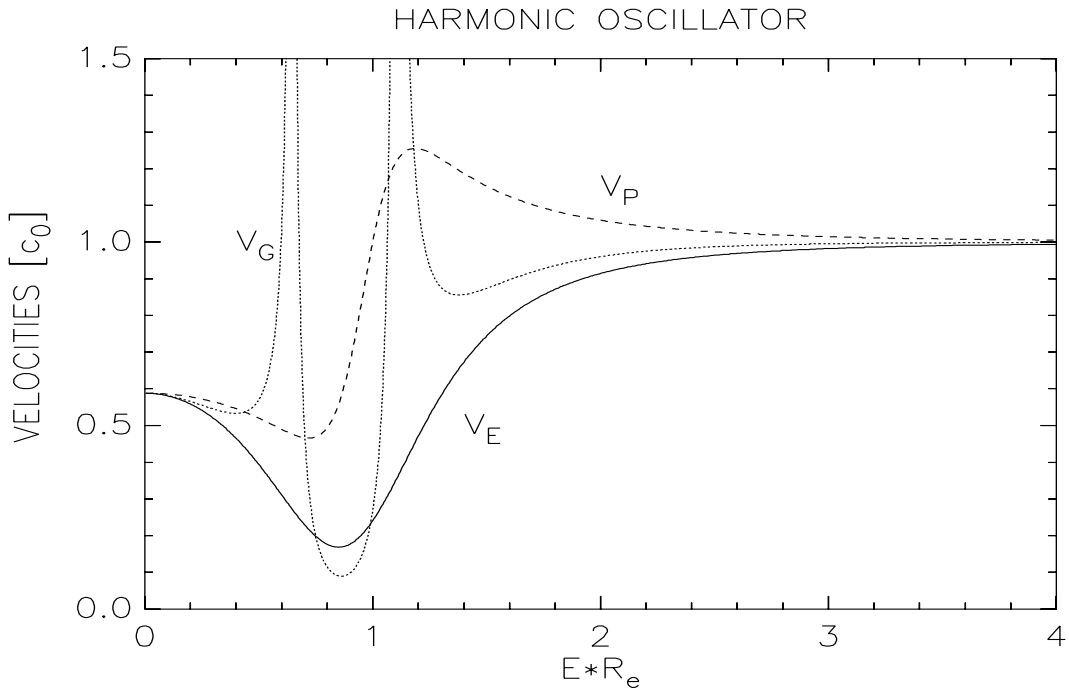

Figure 3.10: *Transport velocity $v_E = v_{\text{Wigner}}$, group velocity v_g and phase velocity v_p for the semi-classical model with $2\pi n r_e^3 = 0.7$ and $E_0 = 1/r_e$.*

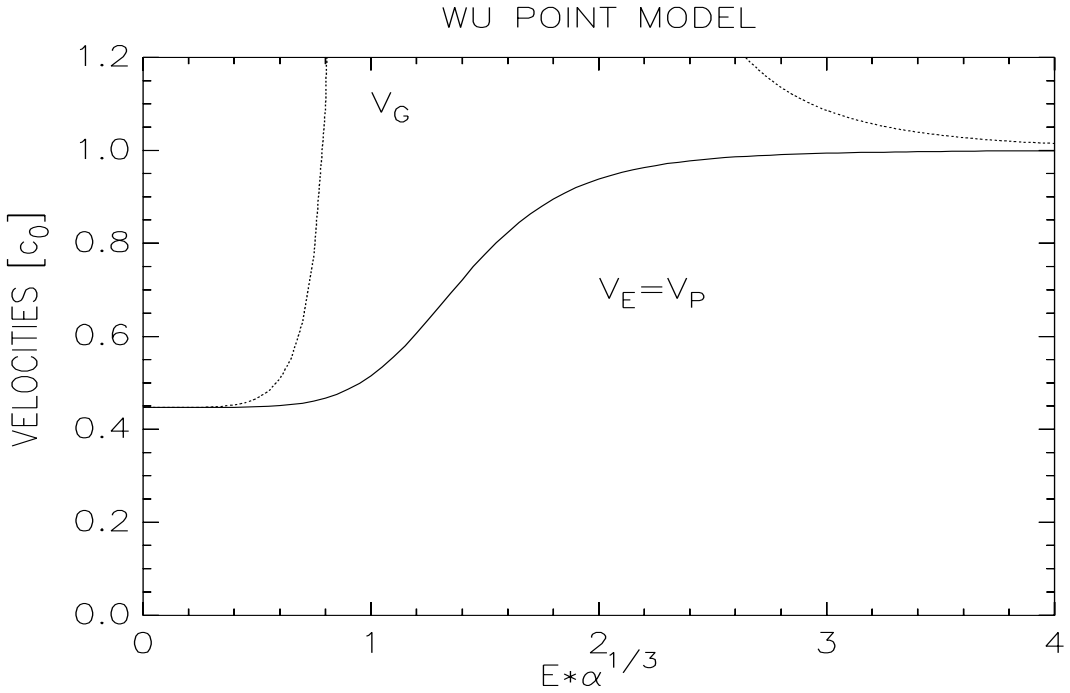

Figure 3.11: *Transport velocity $v_E = v_p = v_{\text{Wigner}}$ for a medium filled with Rayleigh point scatterers. The "average dielectric constant" is 5. Dashed: part of anomalous group velocity v_g.*

We will later see that the for scalar waves rigorous expressions (3.82) and (3.83) remain valid to high accuracy for vector waves. The impact of the logarithmic derivative is large at low energies, which is precisely one regime where Eq. (3.78) can be demonstrated to be exact.

We evaluate Eq. (3.81) for spherical dielectric (Mie) scatterers with radius r_0 and real-valued index of refraction m. The on-shell t-matrix, in terms of the copolarized and cross-polarized channels, is given by [4]

$$\mathbf{t_{pp'}}(E^+) = -\frac{4\pi i}{E}\begin{pmatrix} S_2^*(\theta)\cos\varphi & 0 \\ 0 & S_1^*(\theta)\sin\varphi \end{pmatrix}, \tag{3.98}$$

where

$$\begin{aligned} S_1(\theta) &= \sum_{n=1}^{\infty}\frac{2n+1}{n(n+1)}\left[a_n(x)\pi_n(\cos\theta)+b_n(x)\tau_n(\cos\theta)\right], \\ S_2(\theta) &= \sum_{n=1}^{\infty}\frac{2n+1}{n(n+1)}\left[b_n(x)\pi_n(\cos\theta)+a_n(x)\tau_n(\cos\theta)\right]. \end{aligned} \tag{3.99}$$

Here $x = Er_0$ is the size parameter; π_n and τ_n are vector harmonics. The phase shift ϕ_i of a particular channel is given by the phase of the corresponding $S_i(\theta)$. The orthogonality relations [9] (page 43) are

$$\langle \pi_l\pi_n + \tau_l\tau_n\rangle = \delta_{nl}\frac{l^2(l+1)^2}{2l+1} \quad , \quad \langle \pi_l\tau_n + \tau_l\pi_n\rangle = 0\,, \tag{3.100}$$

and it follows that the second term in Eq. (3.78), the collision contribution, can be worked out to

$$\frac{4\pi}{E^2}\sum_i\int\frac{d\Omega(\theta,\varphi)}{4\pi}\left|S_i(\theta)\right|^2\frac{\partial\phi_i(x,\theta)}{\partial x}\cos^2\varphi = \frac{2\pi}{E^2}\sum_{n=1}^{\infty}(2n+1)\left[|a_n|^2\frac{d\alpha_n}{dx}+|b_n|^2\frac{d\beta_n}{dx}\right].$$

The phases $\alpha_n(x)$ and $\beta_n(x)$ of the different partial waves are defined according to

$$a_n(x) \equiv \frac{1}{2}\left[1-\mathrm{e}^{-2i\alpha_n(x)}\right],\ b_n(x) \equiv \frac{1}{2}\left[1-\mathrm{e}^{-2i\beta_n(x)}\right]. \tag{3.101}$$

In the forward direction $\theta = 0$ it can be shown that $S_1 = S_2$. Direct differentiation yields

$$-\frac{1}{2E^2}\frac{d\left(E\,\mathrm{Re}\,t_{\mathbf{pp}}\right)}{dE} = \frac{\pi}{E^2}\sum_{n=1}^{\infty}(2n+1)\left[\cos 2\alpha_n\frac{d\alpha_n}{dx}+\cos 2\beta_n\frac{d\beta_n}{dx}\right].$$

Insertion of both parts into the expression for v_E gives the final answer,

$$v_E = \frac{1}{v_p}\left[1+\frac{3}{4}\frac{f}{x^2}\sum_{n=1}^{\infty}(2n+1)\left(\frac{d\alpha_n}{dx}+\frac{d\beta_n}{dx}\right)-\frac{1}{2}f\,C(x)\right]^{-1}. \tag{3.102}$$

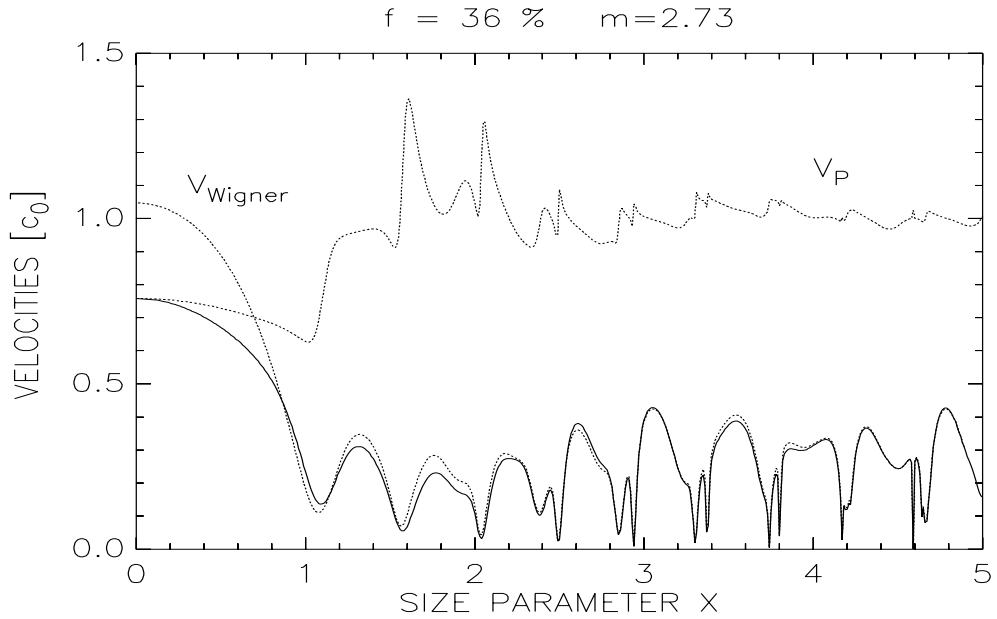

Figure 3.12: *Transport velocity (bold) in the Wigner approximation, the heuristic velocity v_W based upon charging (dotted) and phase velocity v_p for vector Mie spheres with index $m = 2.73$ and packing fraction 36 %.*

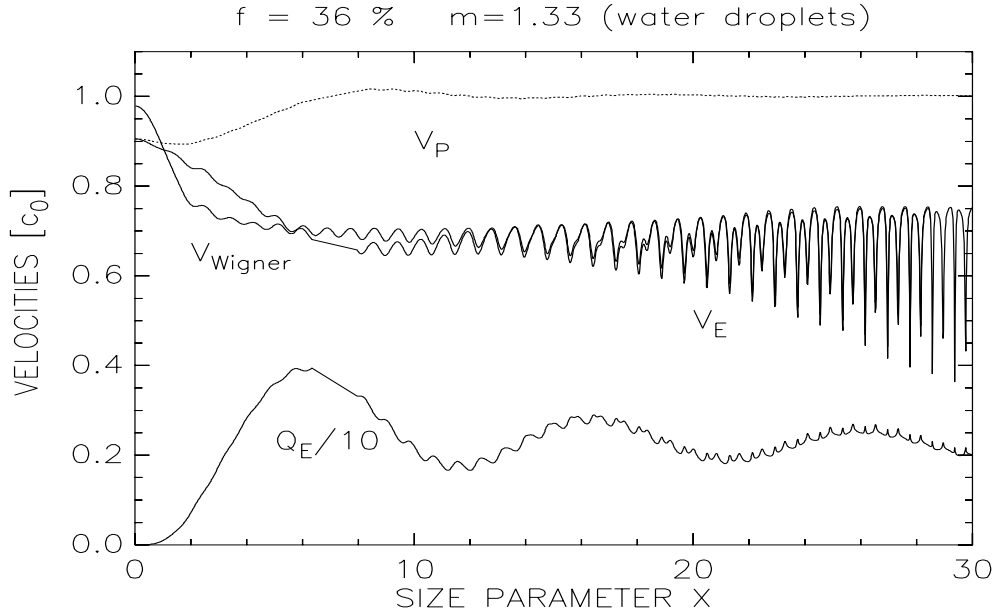

Figure 3.13: *As above but now for "rain drops": $m = 1.33$. The extinction curve has also been plotted.*

We defined the packing fraction $f = \frac{4}{3}\pi n r_0^3$ and, as in Eq. (3.88),

$$C(x) \equiv \frac{3}{2x^3} \sum_{n=1}^{\infty} (2n+1) \left(\operatorname{Im} a_n + \operatorname{Im} b_n \right) . \tag{3.103}$$

In terms of this parameter, the phase velocity is given by Eq. (3.89). Fig. 3.12 shows the numerical evaluation of Eq. (3.102) for Mie scatterers with index of refraction $m = 2.73$, and packing $f = 36\,\%$, relevant for some of our experiments. There is a strong suspicion that a volume fraction of 36 % is no longer consistent with the applied Boltzmann approximation, but at the moment it is the best that we can do.

The transport velocity differs considerably from the phase velocity throughout the spectrum. The reason is that the spectrum is dominated by electric and magnetic multipole resonances and their overtones. Only sufficiently far away from resonances do we expect all velocities to coincide. In fact this holds for the Rayleigh limit $x \to 0$. ¿From the electric dipole contribution we find that

$$\frac{1}{v_E} = \frac{1}{v_p} = \frac{1}{v_g} = \sqrt{1 + 3f\,\frac{m^2-1}{m^2+2}} \qquad (x \to 0) . \tag{3.104}$$

We recover the Lorentz-Lorenz formula for the "effective index of refraction". This is the rigorous low-frequency limit for Mie spheres, in all orders of the density. In Fig. 3.13 we show the transport velocity for an index of refraction $m = 1.33$ which applies to water at optical frequencies. Fig. 3.14 displays the contribution of two individual partial waves, whose resonant structures approximately coincide in the spectrum.

3.4.6 Heuristic Approaches

In this section we indicate the relation between the transport speed and the formation of standing waves inside the scatterer, responsible for the considerable delay of the scattering near resonances. To this end let us reconsider the semi-classical model of Eq. (3.91). We argue that, in this case, the decrease of the transport velocity can be understood in terms of *spontaneous emission*. Semi-classically, the linear scattering of light from an harmonic oscillator or two-level system, can be viewed as a single-photon excitation followed by a subsequent spontaneous decay. The delay caused by the scattering process is expressed by the inverse Einstein spontaneous emission coefficient A, and should be taken into account in the transport of photons. The average time between two scattering events is the *scattering* mean free time $\tau_s = 1/n\sigma$. We obtain for the transport velocity,

$$\frac{v_E}{v_p} \approx \frac{\tau_s}{\tau_s + 1/A} . \tag{3.105}$$

The uncertainty relation relates the energy width of the cross-section to the Einstein coefficient according to (see Eq. (4.91) of Ref. [23]) $A = \frac{2}{3}E^2 r_e$. Eq. (3.105) can be proven to coincide exactly with the microscopic outcome Eq. (3.95) with $\beta = 1/r_e$ and $1/\alpha = E_0^2$.

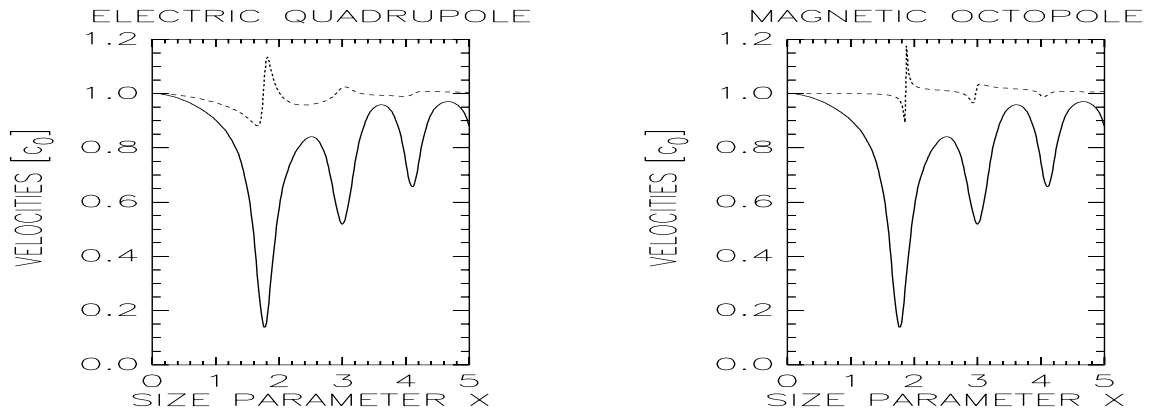

Figure 3.14: *Contribution of electric (TM) quadrupole (a_2) and magnetic (TE) octopole (b_3) to v_E for Mie spheres with $m = 3.0$ and packing 36 %. The resonances of a_n and b_{n+1} coincide in the limit $m \to \infty$.*

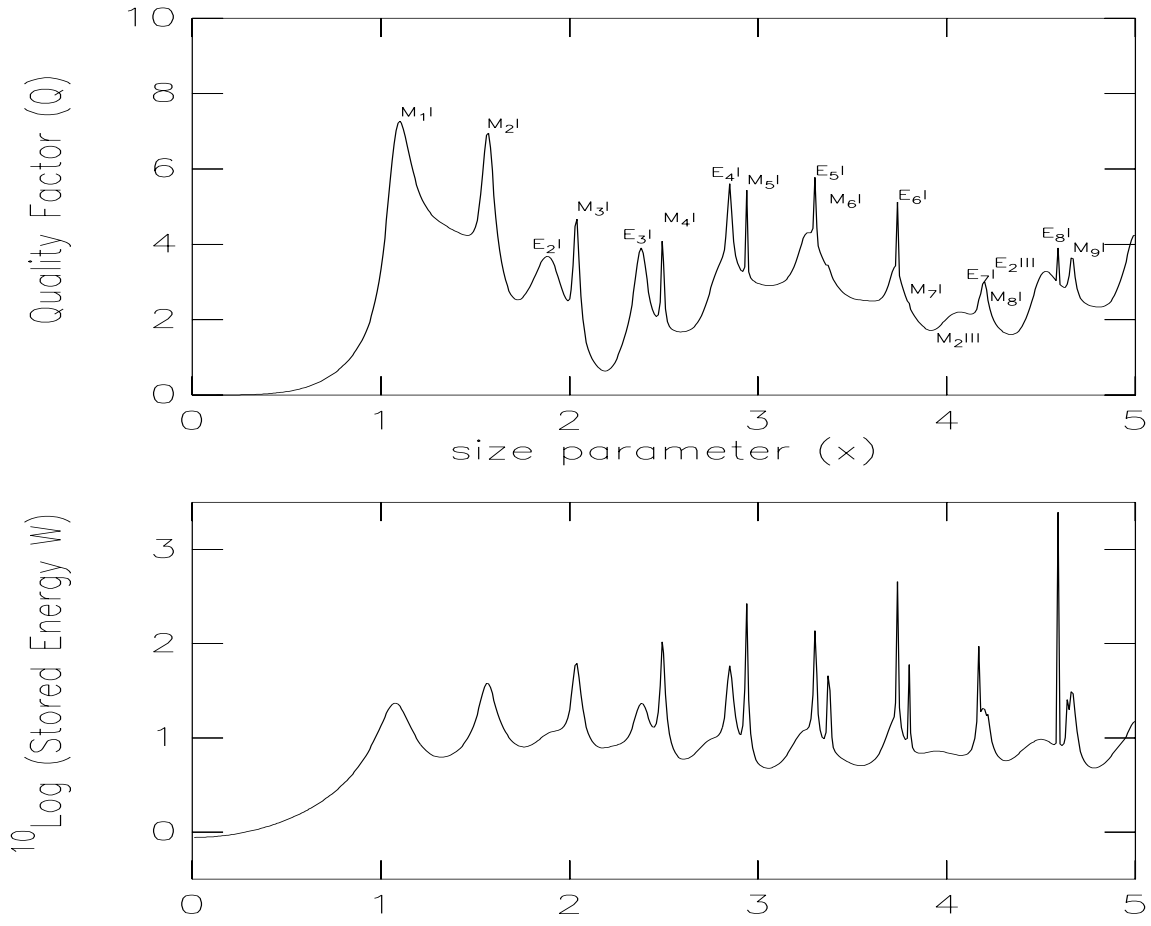

Figure 3.15: *The energy density W and the extinction curve Q_E for a single Mie sphere with index of refraction $m = 2.73$. The electric and magnetic resonances have been identified. See Table II for some numerical values.*

A similar heuristic procedure can be followed for the Mie scatterer [133]. The time τ_W needed for the incoming plane wave with flux $S = \Xi_0$ ($c_0 = 1$) to "charge" the volume V_m of the dielectric particle to energy $\int dV\, \Xi \equiv W\, V_m\, \Xi_0$ is $\tau_W = V_m \Xi_0 (W-1)/\sigma S$. Here $\Xi_0\,, \Xi$ denote the electromagnetic energy density of the vacuum and scatterer in a steady-state situation. Again using $\tau_s = 1/n\sigma$ we estimate that

$$\frac{v_W}{v_p} = \frac{1}{1+\tau_W/\tau_s} = \frac{1}{1+f\,(W-1)}\,. \tag{3.106}$$

x	x^∞	resonance	Q_E	$W-1$	$3mQ_{\rm abs}/8m_ix$	δ^W/V_m	L_a/r_0
1.100	1.15	M1I	7.275	20.82	23.21	24.14	1.558
1.565	1.65	M2I,E1I	6.979	37.15	40.50	43.61	2.834
2.035	2.11	M3I,E2I	4.788	63.16	68.85	73.38	7.023
2.380	2.60	E3I (M1II)	3.907	22.38	22.26	25.04	2.783
2.495	2.60	M4I	4.583	123.2	134.0	141.0	14.28
2.850	3.00	E4I (M2II)	5.612	57.25	55.89	62.75	4.864
2.940	3.00	M5I	5.438	265.3	286.7	299.7	25.75
3.300	3.43	E5I (M3II)	5.782	135.6	132.0	146.0	11.15
3.375	3.43	M6I	5.005	565.9	607.7	631.2	59.30
3.740	3.85	E6I (M4II)	5.118	455.7	444.2	480.2	42.39
3.800	3.85	M7I	2.430	59.00	63.56	65.04	12.77
3.940	3.99	M2III,E1III	1.748	6.240	7.199	6.412	2.011
4.170	4.28	E7I	2.534	92.69	91.93	100.2	17.72
4.195	4.29	M5II	3.018	19.81	21.12	20.80	3.418
4.225	4.28	M8I	2.412	80.53	86.11	90.56	17.44
4.495	4.51	E2III,M3III	3.314	8.617	9.482	8.910	1.397
4.590	4.70	E8I	3.909	2473	2424	2554	302.9
4.640	4.75	M6II	2.937	24.33	26.22	27.14	4.360
4.665	4.70	M9I	3.750	31.84	33.55	33.65	4.370
5.000	5.01	E3III,M4III	4.230	14.01	14.71	14.73	1.700

Table II. *Numerical evaluation of the energy density W in the sphere, the absorption Q-factor for vanishing m_i and the dynamic vertex correction δ^1 in the Wigner-time approximation. We considered resonant size parameters x of a $m = 2.73$ Mie sphere. The ground tone of the magnetic (electric) multipole resonance of order n is indicated by MnI (EnI), the overtones are given by higher Roman numbers; $E(n-1)$ coincides approximately with Mn. The last column gives an estimate of the path length of the wave in the dielectric barrier, on the basis of the absorption arguments in section 1.7. The parameter x^∞ is the size parameter at which free vibration of the sphere is expected in the limit $m \to \infty$. These are adapted from table 10 of Ref. [4].*

This velocity is expected to give a good estimate provided the energy is well confined within the sphere, which is the case if $m \gg 1\,,\, x \gg 1$. A large value for W corresponds to

the formation of a standing wave inside the scatterer. The exact solution for scalar waves Eq. (3.82) makes it clear that this heuristic approach must be very near the exact solution for vector waves. This is confirmed in Fig. 3.12 where v_W is displayed as well. Fig. 3.15 shows the energy density for Mie spheres with an index of refraction $m = 2.73$. Note the extremely strong resonance near the size parameter $x \approx 4.6$. The energy density inside the Mie sphere is roughly 2500 times the energy density of the vacuum. For a packing fraction of 36 % this would imply a transport velocity $v_E \approx c_0/800$!

The delay that occurs in resonant scattering can also be estimated by allowing small absorption. This was already indicated in section 1.7. It turned out that the "charging time" can be expressed by means of the absorption cross-section according to Eq. (1.88). In analogy with Eq. (3.105), a transport velocity can be introduced,

$$\frac{v_a}{v_p} = \frac{\tau_s}{\tau_s + \tau_c} \,. \tag{3.107}$$

Again, the outcome is surprisingly close to the exact result for scalar waves, Eq. (3.83). This was not at all clear at the time that we started to investigate the transport velocity. It is very satisfactory that heuristic approaches lead to an essentially exact solution.

The link between small absorption and energy density in the sphere was established by Bott *et al.* [27] for the Mie sphere, by means of Eq. (1.87). It is pointed out in appendix A that such a relation is a manifestation of a general identity, Eq. (A.10), for potential scattering applied to classical waves. This explains why the heuristic approaches are much more accurate than was expected beforehand.

Table II shows some numerical results for $m = 2.73$ spheres, near different scattering resonances. The parameter x^∞ is the size parameter at which a "free vibration" of the sphere is expected in the limit $m \to \infty$ [28]. The inaccuracy of the parameters $W - 1$, δ^W and $3mQ_{\rm abs}/8m_i x$ is at most 10 %. For larger index m we found even better agreement.

3.4.7 Wigner Phase-Delay Time

We come back to the Wigner (phase-) delay time in Eq. (3.78). The rigorous expression for scalar waves indicates that the energy velocity suffers from corrections that translate to properties of the radiation field *inside* the scatterers. As a result, the decrease of the transport velocity is attributed to an enormous *dwell time* of the waves inside the scatterer. On the other hand, it is known from the literature [134] [135] that the *Wigner phase-delay time* is expressed in terms of the energy (or probability) density over *whole* space. For Schrödinger dynamics, this exact (Jauch) formula reads

$$-\frac{d}{dE}\mathrm{Re}\, t_{\mathbf{pp}}(E^+) + 2p \int d\Omega \, \frac{d\sigma}{d\Omega} \, \frac{d\phi(\Omega)}{dE} = \int d\mathbf{r} \, \left[|\psi_E^+(\mathbf{r})|^2 - 1 \right] \,. \tag{3.108}$$

It is understood that $E = p^2$; ψ_E^+ is the eigenfunction at energy E. In this expression we have already performed a plane-wave limit. Both left and right-hand sides of Eq. (3.108) allow for a more sophisticated operator formulation [135]. The subtraction of the "free

plane wave" $|\exp(i\mathbf{p}\cdot\mathbf{x})|^2 = 1$ guarantees the right-hand side to exist. In one dimension, the left-hand side equals $d\phi/dE$, with ϕ the phase shift of the transmission coefficient.

Using the theory of the previous sections we prove that Eq. (3.108) holds for scalar waves as well, *provided* one uses the inner product associated with scalar waves. With now $E^2 = p^2$ we prove that

$$-\frac{d}{d(E^2)}\mathrm{Re}\, t_{\mathbf{pp}}(E^+) + \int d\Omega \frac{d\sigma}{d\Omega}\frac{d\phi(\Omega)}{dE} = \int d\mathbf{r}\left[\frac{\varepsilon(\mathbf{r})}{2}|\psi_E^+(\mathbf{r})|^2 + \frac{1}{2E^2}|\boldsymbol{\nabla}\psi_E^+(\mathbf{r})|^2 - 1\right]. \tag{3.109}$$

Proof.
For brevity, we sketch the proof. By mapping the scalar wave equation onto Schrödinger dynamics, one identifies an "energy" E^2 and an energy-dependent potential $[1-\varepsilon(\mathbf{r})]E^2$. We have shown in Eq. (3.82) that the latter generates an extra term in the left-hand side of Eq. (3.108) (see also Appendix A). Adding the same term to the right-hand side of Eq. (3.108) yields the desired result. In addition, it must be realized that the terms $|\boldsymbol{\nabla}\psi_E^+|^2$ and $\varepsilon E^2|\psi_E^+|^2$ represent an equal amount of energy. □

We discuss the difference between the dwell time and phase-delay time. The dwell time is the time that a wave spends inside the scatterer. Mathematically, it is given by the derivative of the phase-shift with respect to potential (see Appendix A). On the other hand, by Eq. (3.109), the phase-delay time is the delay that the wave suffers both inside *and* outside the scatterer. It is given by the derivative of the same phase shift with respect to energy (or frequency), rather than potential. Classically, delay can only occur inside the scattering region, but for waves this is no longer true.

Nevertheless, near resonances of scattering, the delay inside the scatterer is so large that we can neglect any additional delay outside. Hence the dwell time and the phase-delay time become essentially equal time scales. This is exactly why the "Wigner" approximation in Eq. (3.78) works so well near resonances: it replaces the dwell time of the waves in the dielectric particle by the Wigner phase-delay time.

3.5 Thouless Criterion for Light

Knowledge of the conditions under which Anderson localization sets in is of extreme importance, even if it were only for its experimental significance. One seeks a general, but nevertheless very practical criterion, hopefully derivable from first principles. The Ioffe-Regel (IR) criterion, putting the wavelength equal to the mean free path, $\lambda \approx \ell$, later revised by Mott to $\lambda/2\pi \approx \ell$, was the first attempt to predict the location of the mobility edge in three dimensions. The IR criterion predicts the localization of low-energy electrons and can serve to estimate the desired density of scatterers near scattering resonances [89] [90]. Diagrammatic theories [60] as well as non-linear σ models [136] [97] gave this criterion a microscopic foundation, and can be used to generalize the IR criterion to, for instance, other dimensions, or anomalous spectral behavior [92] [98], but a "first-principle" interpretation is still lacking.

The Thouless criterion [83], developed in close connection with the scaling theory of localization [80], can be considered as one of the most important breakthroughs in the description of localization. Not only does this theory provide clear and verifiable predictions concerning the appearance of localization in finite media of arbitrary dimension and the value of critical exponents, it also introduces a fundamental parameter known as "dimensionless conductance", $g = \sigma L^{d-2}$. Here σ is the dc electrical conductivity, and L is a typical size of the d-dimensional random medium. A simple analysis, with application of the Einstein relation (3.4) relating diffusion constant, density of states and conductivity, demonstrates the equivalence of this parameter to the Thouless parameter defined by

$$g(L) = \frac{\Delta E(L)}{\delta E(L)}\,, \tag{3.110}$$

with $\Delta E(L) \sim D/L^2$ the uncertainty in energy due to the finite traversal time of the (diffusive) transport in the medium, and $\delta E(L)$ the average level spacing. The criterion

$$g(L) = g_c \approx 1\,, \tag{3.111}$$

is known as the *Thouless criterion* for localization.

The Thouless parameter in Eq. (3.110) is proportional to the diffusion constant and thus, when applied to classical waves, to the transport speed. The enormous decrease of this speed near scattering resonances thus lowers this parameter by an order of magnitude. A straightforward application of the Thouless criterion would locate the mobility edge at much smaller disorders than expected, for instance, on the basis of the Ioffe-Regel criterion, which was seen in Eq. (3.46) not to be any different for classical waves. This is physically unacceptable. The decrease of the transport speed of light is a renormalization of time scales, and does not enhance the correlation of the scattering medium. It merely takes longer to accomplish a certain correlation length, which is determined by the transport mean free path only, and not by the diffusion constant as a whole.

To incorporate these ideas we propose a Thouless parameter in terms of *length scales* only,

$$\hat{g}(L) = \frac{\Delta p(L)}{\delta p(L)}\,. \tag{3.112}$$

Here $\Delta p(L)$ is the uncertainty in momentum and is determined by the path length distribution between two points in coordinate space, a distance L apart. The modified Thouless criterion becomes

$$\hat{g}(L) = g_c \approx 1\,. \tag{3.113}$$

We shall refer to this criterion as the *Tauros Criterion* for localization [137]. We will show that the use of this modified criterion is in agreement with previous work and does introduce neither the transport nor the group velocity in a localization criterion.

Before we evaluate Eq. (3.112) for a specific situation we emphasize the equivalence of the Tauros parameter $\hat{g}(L)$ to the original Thouless parameter $g(L)$, if electron-impurity scattering is considered. Since dynamic vertex-corrections are absent in the diffusion constant as well as in the density of states per energy interval dE, the velocities entering numerator and denominator of Eq. (3.110) quantities coincide, and equal the Fermi-velocity evaluated at the Fermi-surface, without mass-enhancement corrections. Thus Eq. (3.110) is equivalent to Eq. (3.112) for elastic electron-impurity scattering. Since the scaling theory is a theory about length scales, it seems to us that a Thouless parameter formulated in terms of length scales, as indicated by Eq. (3.112), is a natural consequence of the scaling theory of localization, notwithstanding the fact that there is a one-to-one correspondence of time and length scales in situations for which the Thouless criterion was developed originally. A dynamical scaling theory was recently presented [138], but did not yet incorporate our dynamic vertex corrections.

We will now evaluate the Tauros criterion (3.113) for classical waves. For a diffusion process with step length ℓ the *path length distribution* is given by [36] [42] [54]

$$P(s) = \frac{3}{(4\pi s\ell)^{3/2}} \exp\left(-\frac{3L^2}{4s\ell}\right) , \tag{3.114}$$

and has a maximum at $s_m = L^2/2\ell$. The uncertainty in momentum is thus estimated to be $\Delta p(L) \approx 1/s_m = 2\ell/L^2$. The level spacing between momentum states is defined as $\delta p(L) = dp/dN$, in which dN denotes the total number of states with momentum between p and $p + dp$. Since the scalar spectral function $S(E, p)$ in Eq. (3.23), counts the number of states per unit volume with momentum $\mathbf{p}$ and energy E, it follows that

$$\frac{dn}{dp} \equiv 2 \sum_{\mathbf{p}'} \int_{-\infty}^{\infty} \frac{dE}{2\pi}\, \delta(p - p')\, S(E, p') = \frac{p^2\, \langle c^2 \rangle}{\pi^2} . \tag{3.115}$$

The prefactor 2 comes from the spin degeneracy, specific for light, and is here put in by hand. The second equality follows from a sum rule derived in appendix B and applies for a non-absorbing dielectric random medium; $\langle c^2 \rangle$ denotes the average-medium value of the square of the speed of light. Eq. (3.115) demonstrates that, apart from the topological factor $\langle c^2 \rangle$, the DOS *per momentum interval* does not depend on disorder.
For a volume L^3 we find explicitly that

$$\hat{g}(L) = \frac{2}{\pi^2}\, \ell(L)\, L\, p^2\, \langle c^2 \rangle , \tag{3.116}$$

so that indeed group and transport velocity are absent. The absence of these velocities in the prediction of the location of the mobility edge is in agreement with the self-consistent theory of Vollhardt and Wölfe [60], which has, at least in three dimensions, a stationary ($\omega = 0$) formulation. Their final result can be expressed in terms of a *correlation length* ξ. The transport mean free path ℓ, the length scale in the diffusion coefficient via $D = v_E\ell/3$, is given by $\ell = \ell_s^2/\xi$, with ℓ_s the scattering mean free path. In the absence of absorption,

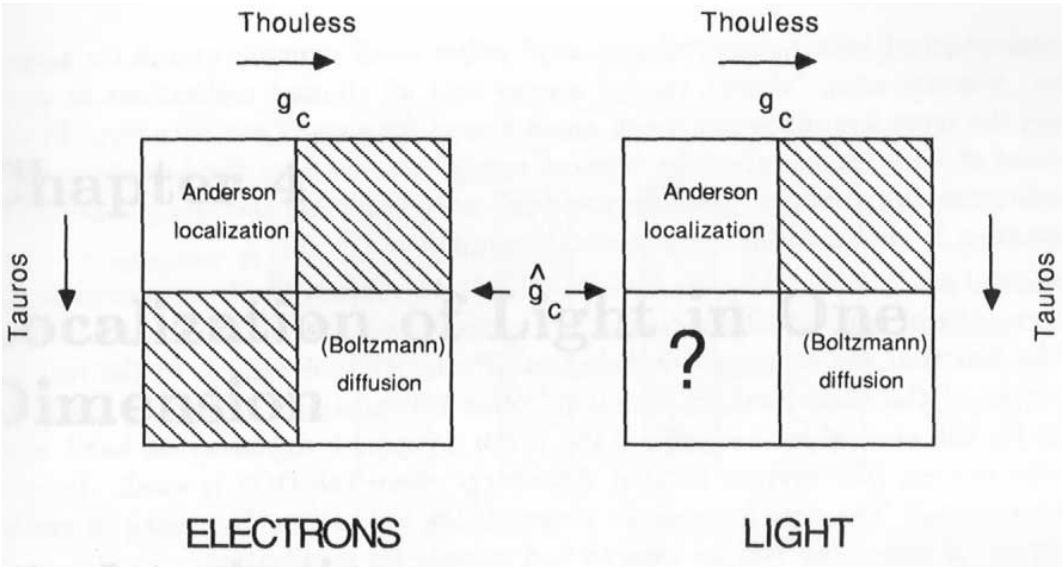

Figure 3.16: *The Thouless criterion (horizontal) and the "Tauros" criterion (vertical). Shaded areas are "forbidden". The figure on the left applies to electrons and both criteria are the same, the right figure is for classical waves, assuming that* $\delta^1 > 0$.

$1/\xi = 1/\xi_0 + 1/L$, where ξ_0 is the correlation length of the infinite system, $\xi_0 = \ell_c^2/(\ell_s - \ell_c)$. The mobility edge is reached once the system is completely correlated, $\xi = L$, so that $\ell = \ell_c^2/L$. Again this is a comparison of length scales. The Tauros criterion becomes

$$\hat{g}_c = \frac{2}{\pi^2}\,(p\ell_c)^2\langle c^2\rangle \approx 1\,. \tag{3.117}$$

This is in agreement with Ref. [99]. The outcome in Eq. (3.46) for isotropic point scatterers suggests that $\hat{g}_c = 0.191$. In a random medium containing perfect metallic scatterers with packing fraction f the topological factor in Eq. (3.115) lowers the DOS by a factor $1 - f$ so that localization is predicted to become easier. The Ioffe-Regel criterion is then shifted upwards, according to $p\ell_c \sim 1/\sqrt{1-f}$.

For classical waves the original Thouless criterion is proportional to the transport velocity v_E. If we let $p = E/v_p$ in the Tauros criterion we conclude that

$$g = \frac{\hat{g}}{1 + n\delta^1(E) + \cdots}\,. \tag{3.118}$$

Near resonances is $g \ll \hat{g}$. What happens if $g < g_c$ and $\hat{g} > g_c$? According to the Tauros criterion we do not expect Anderson localization. Since g compares *time scales*, the Thouless criterion may somehow be relevant in a *dynamic measurement*, possibly giving rise to interesting new phenomena. In Fig. 3.16 the most important results in this section have been summarized.

Chapter 4

Localization of Light in One Dimension

4.1 Introduction

In this chapter we discuss localization of light in random dielectric multilayers. These are three-dimensional dielectric media in which the disorder has been imposed in one direction only. Two dimensions obey translational symmetry, along which the transport of energy is purely *ballistic*.

In general, the statement is that there will be no (diffusive) transport along the direction of disorder, so that a random walk picture is completely destroyed by interference. If the dielectric multilayer has a finite extent in the direction of disorder, this transport is expected to be exponentially small. These results are consistent with the scaling theory of localization [80] which predicts all states to be exponentially localized in one dimension for an arbitrary degree of disorder.

In one dimension, on the other hand, much more can be said. Techniques first developed by Furstenberg [81] have been used to treat localization in one dimension in a mathematically rigorous way [139] [140] without any reference to perturbation theory. Unfortunately, this elegant approach can only be extended to quasi one-dimensional systems [141], and does not work in two or more dimensions.

The physical quantity that determines exponential decay of the wave function, is the (upper) *Lyapunov exponent*. Given a set of random matrices $\{\mathbf{M}_i(\varpi)\}$ for a realization ϖ of the random system, the Lyapunov exponent is defined as

$$\gamma \equiv \lim_{N\to\infty} \frac{1}{N} \log || \, \mathbf{M}_1(\varpi) \cdot \mathbf{M}_2(\varpi) \cdots \mathbf{M}_N(\varpi) \, || \, . \tag{4.1}$$

For ergodic stochastic processes [142] the Lyapunov exponent is, for "almost any" energy [143], a positive quantity that is "almost surely" independent of ϖ. The conclusion is that "almost all" states are exponentially localized for "almost any" realization ϖ.

The mathematical terminology "almost any" refers to all energies except for a set of (Lesbesque) measure zero; "almost surely" means that all allowed realizations ϖ of the system have the same Lyapunov exponent, again except for a set of measure zero. From a physical point of view the terminology "almost surely" implies that the Lyapunov exponent is a self-averaging quantity. Because you don't need ensemble-averaging, localization in one dimension is very suitable for numerical simulation.

A very useful result is the Thouless formula [144] [145], relating the Lyapunov exponent to the density of states (DOS) by means of a dispersion relation. This formula finds its origin in the fact that the Lyapunov exponent and the DOS correspond to the real and imaginary part of the same analytic function. This fundamental dispersion relation is responsible for the anomalous behavior [146] of the Lyapunov exponent on band edges of the parent system (the system without disorder), where the DOS is small. In more dimensions, a simple Thouless formula no longer holds but, as we have seen in section 3.5, the density of states can still be used to find criteria for localization.

To model one-dimensional localization of *electrons*, most workers treat the Anderson (Tight-binding) model with "diagonal" disorder. The basic concept, however, involves the use of random transfer matrices. These matrices show up in the description of light propagation in random layers as well. The theory of random matrices [81], when applied to this situation, predicts that a large stack of dielectric layers, with randomized thickness and/or index of refraction will act as a perfect mirror. The presence of disorder-induced localized states in a (semi-infinite) multilayer forces incoming waves to be reflected back totally.

Recently, the study of quasi-periodic stacks, within the context of both electron [147] [148] and light transmission [149] [150] [151], has become very popular. It has been realized that these deterministic structures can also give rise to localized states and as such, form an important regime between order and disorder.

We shall investigate the influence of periodicity of the parent system on the Lyapunov exponent. If the system is periodic, the energy spectrum has a band structure, which means that only certain energies (bands) have propagating solutions. Other energy regions (gaps) are not allowed. This so-called *Bloch theorem* is well known in solid state physics because it explains why metals are good conductors. Since "periodicity" and "interference" are the basic concepts, the Bloch theorem must also apply for light in periodic dielectric structures.

By subjecting (one-dimensional) periodic systems to small disorder, we do not expect that the Bloch picture is changed dramatically. On the other hand, the nature of the eigenstates in the bands changes. According to statements made earlier, there is no mobility edge in one dimension and all states in the bands are "localized", rather than "extended". Concerning electron propagation, this implies that one-dimensional metals do not exist, despite Bloch's theorem. If a dielectric multilayer is imposed with small disorder, the transmission of light will decrease exponentially with size. Because this decrease is determined by the Lyapunov exponent, the latter is a very important quantity.

We anticipate that localization is most pronounced near band edges (small DOS) of the

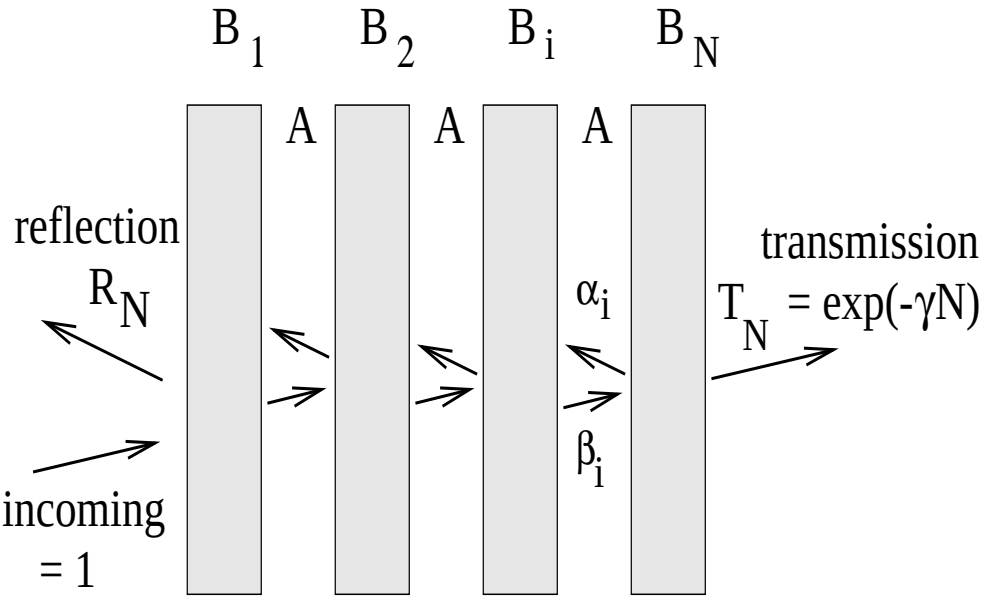

Figure 4.1: *The one-dimensional dielectric multilayer. A denotes a vacuum layer, the B_i denote dielectric layers with random dielectric constant.*

underlying crystal, and weak near the band center (large DOS) of the underlying crystal. In this chapter we investigate the influence of the band structure of the parent system on the Lyapunov exponent. The system, shown in Fig. 4.1, is of the form $AB_1AB_2AB_3...$ where the indices of refraction of the B_i's will be given random distributions, with average B_0 and standard deviation σ.

Near band edges of the parent system the Lyapunov exponent of the Anderson model [146] is known to behave non-analytically as a function of deviation: $\gamma \sim \sigma^{2/3}$. We studied this behavior for a random dielectric multilayer. It turns out that the Anderson model with diagonal disorder (which is for many reasons a simplified model in solid state physics) mimics localization properties of our random multilayer (an existing physical system) very well.

In the center of the band very interesting things happen. These effects occur in the Anderson model too, but for light they can be more pronounced. Very large dips in the Lyapunov exponent are discovered near special energies in the band center. These energies will be referred to as *Fabry-Perot* resonances. They occur if the average index of refraction of the B-layers is *rational*. The very sensitive behavior of the Lyapunov exponent near these energies can be used to construct sharp filters.

Both near band edges and in the band center, our numerical simulations show universal behavior of the Lyapunov exponent. Excellent agreement is found with theory developed by Derrida and Gardner [146], Kappus and Wegner [152] and Lambert [153] when applied to our case.

4.2 Random Dielectric Multilayers

We consider the propagation of electromagnetic waves in a stack of homogeneous dielectric layers, and confine ourselves to the case of normal incidence of linearly polarized light. We define the state vector $\mathbf{F} \equiv (\, m(x)E_z, B_y \,)$, with E_z and B_y the components of the electric and magnetic fields along the z-axis and y-axis. The x-axis is located normal to the slab, in the direction of propagation (Fig. 4.1); $\varepsilon = m^2$ is the dielectric constant. As was pointed out in chapter 1, Maxwell's equations imply the dynamics

$$\partial_t \mathbf{F} = -i \begin{pmatrix} 0 & m^{-1}(x)\, p \\ p\, m^{-1}(x) & 0 \end{pmatrix} \cdot \mathbf{F} \,. \tag{4.2}$$

Here is $p \equiv -i\partial/\partial x$, $m(x) \equiv \varepsilon^{1/2}(x)$ is the index of refraction and $c_0 = 1$. If we insert modes $\exp(-iEt)$ the solution of Eq. (4.2) in the j^{th} layer is

$$\mathbf{F}_j(x) = \alpha_j \begin{pmatrix} 1 \\ -1 \end{pmatrix} \mathrm{e}^{-ik_j(x-x_j)} + \beta_j \begin{pmatrix} 1 \\ 1 \end{pmatrix} \mathrm{e}^{ik_j(x-x_j)} \,, \tag{4.3}$$

with $k_j \equiv Em_j$. The continuity of E_z and B_y on the interface of two layers fixes the transfer matrix according to

$$\begin{pmatrix} \alpha_{j+1} \\ \beta_{j+1} \end{pmatrix} = \mathbf{M}(j \to j+1) \cdot \begin{pmatrix} \alpha_j \\ \beta_j \end{pmatrix} ,$$

$$\begin{aligned} \mathbf{M}(j \to j+1)_{11} &= \mathbf{M}(j \to j+1)^*_{22} = \frac{m_j + m_{j+1}}{2m_j}\, \mathrm{e}^{-ik_{j+1}(x_{j+1}-x_j)} \,, \\ \mathbf{M}(j \to j+1)_{12} &= \mathbf{M}(j \to j+1)^*_{21} = \frac{m_{j+1} - m_j}{2m_j}\, \mathrm{e}^{-ik_{j+1}(x_{j+1}-x_j)} \,. \end{aligned} \tag{4.4}$$

The layers with even j are taken identical and fixed, and are for simplicity referred to as vacuum. The index n counts the vacuum layers only. The wave function at "site" n determines the electromagnetic field in the n^{th} vacuum layer; m_n is the reciprocal speed of light in between the n^{th} and $(n+1)^{\text{th}}$ vacuum layer. The transfer matrix mapping one vacuum layer onto the next one is

$$\mathbf{M}(n \to n+1) = \begin{pmatrix} a_n & iq_n \\ -iq_n & a_n^* \end{pmatrix} , \tag{4.5}$$

where a_n and q_n are given by

$$a_n = \mathrm{e}^{-iy} \left[\cos y m_n - i\, \frac{m_n^2 + 1}{2m_n}\, \sin y m_n \right] \quad ; \quad q_n = \mathrm{e}^{-iy}\, \frac{1 - m_n^2}{2m_n} \sin y m_n \,.$$

All layers are supposed to have the same width d; $y \equiv Ed$ is a dimensionless energy parameter. The exponent in q_n can be eliminated by a (n-independent) unitary transformation. The matrix $\mathbf{M}(n \to n+1)$ has determinant 1. If all non-vacuum layers would

have the same value for m_n a superlattice structure [154] is present. The "photon" band structure for this superlattice is determined by the criterion that both eigenvalues have unit norm. This in turn implies $|\mathrm{Re}\, a| \leq 1$.
In the periodic case it is possible to write down the equation,

$$\begin{pmatrix} \alpha_{n+1} \\ \beta_{n+1} \end{pmatrix} + \begin{pmatrix} \alpha_{n-1} \\ \beta_{n-1} \end{pmatrix} = 2\,\mathrm{Re}\, a_n \begin{pmatrix} \alpha_n \\ \beta_n \end{pmatrix}, \tag{4.6}$$

which bears a strong resemblance to the Anderson model with diagonal disorder V_n (interpreted as the random potential at site n),

$$\psi_{n+1} + \psi_{n-1} = (E + V_n)\ \psi_n\,. \tag{4.7}$$

When we introduce disorder in the index of refraction,

$$m_n \equiv m_0 + \delta_n\,, \qquad \langle \delta_n \rangle = 0\ \ , \ \ \left\langle \delta_n^2 \right\rangle = \sigma^2\,, \tag{4.8}$$

the correspondence between the Anderson model and our problem is lost. The reason is that variation of the index of refraction gives rise to "off-diagonal" disorder (disorder that appears in the off-diagonal part of the transfer matrix) too.

We do not randomize the width of the layers [155]. The δ_n's are supposed to be mutually independent, identically distributed stochastic variables with zero mean and deviation $\sigma < m_0$. That guarantees the stochastic process to be ergodic [142], and all statements made in the introduction of this chapter apply. Consequently, the Lyapunov exponent can be calculated numerically on the computer by generating only *one* realization $\varpi = \{m_n\}$, and then evaluating the product in Eq. (4.1). Many authors used the stationarity of the underlying probability measure, to find the behavior of both the Lyapunov exponent and the DOS in the Anderson model, often in the limit of weak disorder. We investigated the validity of these predictions in our model.

In the next sections we study the Lyapunov exponent in two special energy regimes. First we investigate the band edges of the parent system, next we deal with "Fabry-Perot" energies, which are energies in the bans center.

4.2.1 The Band Edges

Many predictions exist about the anomalous behavior of the Lyapunov exponent on a band edge [156] [157] [158]. A very elegant renormalization treatment was given by Bouchaud and Daoud [159] resulting in $\gamma \sim \sigma^{2/3}$ at the band edges. A straightforward application of their method to our random matrix (4.5) yields, in the limit $\sigma, \Delta \to 0$,

$$\gamma(\Delta, \sigma) = \sigma^{2/3} F_b\left(\frac{\Delta}{\sigma^{4/3}}\right), \tag{4.9}$$

with F_b a general positive-definite scaling function. Here $\Delta \equiv y - y_{\mathrm{edge}}$. On the band side of the edge we expect on physical grounds the anomalous behavior to disappear and to go

over into $\gamma \sim \sigma^2$. Hence $F_b(\eta) \sim 1/\eta$. On the gap side the Lyapunov exponent approaches the logarithm of the largest eigenvalue of the transfer matrix, which implies $F_b(\eta) \sim \sqrt{\eta}$. However, this does not fix $F_b(\eta)$ completely. Using the degenerate perturbation theory of Kappus and Wegner [152], Derrida and Gardner [146] calculated the function $F_b(\eta)$ for the Anderson model,

$$F_b(\eta) = \frac{1}{2} \frac{\int_0^\infty dt\ t^{1/2}\, \mathrm{e}^{-t^3/6+2\eta t}}{\int_0^\infty dt\, t^{-1/2}\, \mathrm{e}^{-t^3/6+2\eta t}}\,. \tag{4.10}$$

We compare our model with the Anderson model, with energy E and diagonal disorder V_n. Identifying as in Eq. (4.6),

$$E + V_n = 2\,\mathrm{Re}\, a(y, m_n) = 2\,\mathrm{Re}\, a(y, m_0) + 2\,\frac{\partial \mathrm{Re}\, a}{\partial m}(y, m_0)\,\delta_n\,, \tag{4.11}$$

we will prove that, within the scaling assumption of Derrida and Gardner, Eq. (4.10) is valid for our model as well.

Proof.
We show that the random matrices

$$\mathbf{M}_1 = \begin{pmatrix} a_n & iq_n \\ -iq_n & a_n^* \end{pmatrix} \text{ and } \mathbf{M}_2 = \begin{pmatrix} 2\,\mathrm{Re}\, a_n & -1 \\ 1 & 0 \end{pmatrix}$$

have the same Lyapunov exponent near the band edge, in the scaling limit of Derrida and Gardner [146]. $\mathbf{M}_2$ is in "Anderson" form if the identification Eq. (4.11) is made. The change of base $\mathbf{U}_n$, mapping $\mathbf{M}_1$ onto $\mathbf{M}_2$,

$$\mathbf{U}_n \cdot \mathbf{M}_2 \cdot \mathbf{U}_n^{-1} = \mathbf{M}_1\,,$$

is given by

$$\mathbf{U}_n = \begin{pmatrix} s_n & s_n z_n \\ -1/2 s_n z_n & 1/2 s_n \end{pmatrix}\,,$$

where $s_n = \sqrt{2iq_n/(a_n z_n + 1)}$, $z_n = i\,\mathrm{Im}\, a_n + \sqrt{1 - (\mathrm{Im}\, a_n)^2}$. If we denote the wave function corresponding to the transfer matrix $\mathbf{M}_2$ by the vector $(\tilde{\alpha}_n,\, \tilde{\beta}_n\,)$ and $R_n \equiv \tilde{\alpha}_n/\tilde{\beta}_n$, we find, after some algebra, that

$$\frac{\alpha_{n+1}}{\alpha_n} = a_n + \left(a_n + z_n^{-1}\right) \frac{R_n - z_n}{R_n + z_n}\,. \tag{4.12}$$

Notice that $\langle \log |\alpha_{n+1}/\alpha_n| \rangle$, respectively, $\langle \log |R_n| \rangle$ equals the Lyapunov exponent of $\mathbf{M}_1$, respectively, $\mathbf{M}_2$. Next, a scaling expansion must be employed for a_n, z_n and R_n. Following Ref. [146] we take $y - y_{edge} \sim \lambda^{4/3}$, $m_n - m_0 \sim \lambda$, and $R_n = \pm 1 + \lambda^{2/3} r$, with λ small. To lowest order in λ it is easily inferred that only the scaling of R_n matters in Eq. (4.12). Consequently, $\log |\alpha_{n+1}/\alpha_n| = \lambda^{2/3} K\, r$. From Eq. (4.12) it follows that $K = 1$ whenever

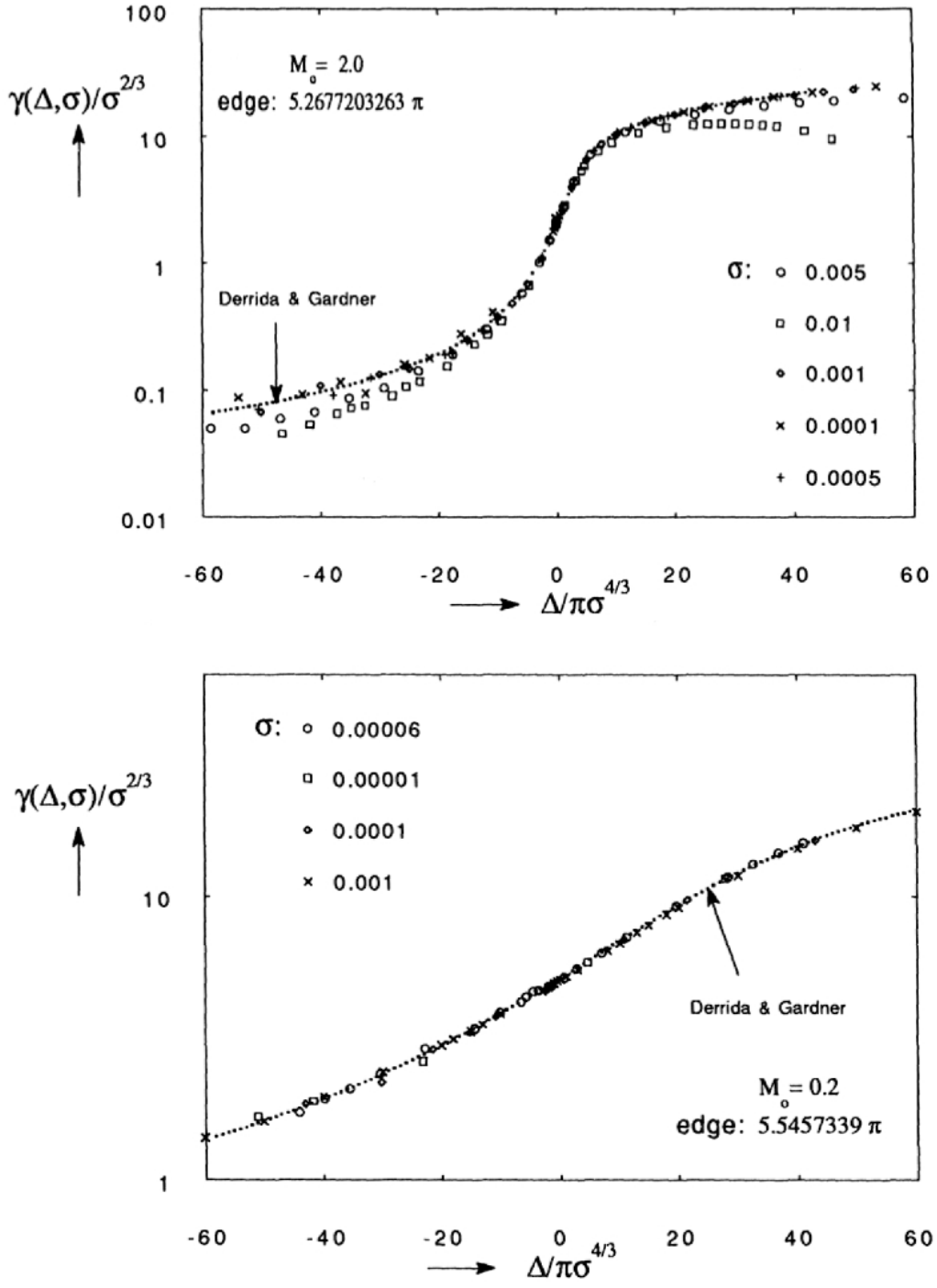

Figure 4.2: *Numerical simulation of the Lyapunov exponent near a band edge, using* $N = 5 \cdot 10^5$ *layers, and a Gaussian distribution with deviation* σ*. The dotted line is the theory for the Anderson model translated to our model.*

$|q_{edge}| < 1$, so that $|z_n| = 1$. The Lyapunov exponent of both matrices is determined by the average of the stochastic variable r, and gives, as shown in Ref. [146], Eq. (4.20). □

Figs. (4.2) compare the scaling prediction for the Lyapunov exponent to numerical simulations, performed on a VAX 3100 workstation. The distribution of the δ's was taken to be Gaussian, and *every* data point was generated independently from all the others. Because the deviation σ of the index of refraction is assumed to be orders of magnitude smaller than the average m_0, the unphysical situation that $m < 0$ is extremely unlikely.

Not only do we confirm the scaling behavior predicted by Eq. (4.9), the analytic solution for F_b is confirmed as well. The agreement between the scaling result and the simulations is good over three decades in disorder and is even better than expected beforehand. We conclude that the scaling theory of the Anderson model provides an accurate description of the Lyapunov exponent near the edges of a band in our model.

4.2.2 The Band Center; Fabry-Perot Resonances

In the previous section we did not put constraints on the average index of refraction m_0 of the B-layers. In this section we let m_0 be rational. In that case the band structure of the parent system itself becomes periodic in energy. Special energies E exist, to which we shall refer as Fabry-Perot energies, for which a multiple of the wavelength $2\pi/m_nE$ fits exactly in both the vacuum layer and the average of the random layer. Such an energy is located in the band center of the parent system and $\mathrm{Re}\, a(m_0) = \pm 1$. Using again the procedure of Bouchaud and Daoud [159] it is easily established that the scaling limit of small σ and Δ takes the form

$$\gamma(\Delta, \sigma) = \sigma^2 F_a\left(\frac{\Delta}{\sigma^2}\right) . \tag{4.13}$$

Now, $\Delta \equiv y - n\pi$. We have taken $m_0 = m/n$, with m and n integers. The scaling function $F_a(\eta)$ will be calculated using the degenerate perturbation theory of Kappus and Wegner. Since the transfer matrix has determinant 1 we have a conservation law,

$$|\alpha_n|^2 - |\beta_n|^2 = \text{constant} . \tag{4.14}$$

For a semi-infinite system it is easily seen that this constant is zero, so that we can take $\alpha_n/\beta_n = i\,\mathrm{e}^{i\phi_n}$. Eq. (4.5) results in

$$\mathrm{e}^{i\phi_{n+1}} = \frac{\mathrm{e}^{i(\theta_n+\phi_n)} + S_n}{\mathrm{e}^{-i\theta_n} + S_n \mathrm{e}^{i\phi_n}} , \tag{4.15}$$

where we defined $S_n \equiv q_n/|a_n|$ and $\mathrm{e}^{i\theta_n} \equiv a_n/|a_n|$. With $\mu_j \equiv \langle \mathrm{e}^{ij\phi} \rangle$ and $a_{kl} \equiv \langle S^k \mathrm{e}^{il\theta} \rangle$ it follows [153] that

$$\sum_{j=1}^{\infty} W_{lj}\, \mu_j = a_{ll} ,$$

$$W_{lj} = \delta_{lj} - \sum_{k \geq l-j}^{l} (-1)^{j+k-l} \frac{l\,(l+k-1)!}{(l-k)!\,k!\,(j+k-l)!} a_{2k+j-l,l+j}\ , \tag{4.16}$$

(the paper of Lambert [153] contains an erroneous factor $l!$ instead of l in the numerator of Eq. (4.16)). We search for a scaling solution of the form (4.13). To this end we write $y_j = n\pi + \lambda^2 s_j$ and $m_j = m/n + \lambda t_j$, with λ small. The variables a_j and q_j in Eq. (4.5) can be expanded as follows;

$$a_j = (-1)^{m+n}\left[1 - iA\lambda - iB\lambda^2 - C\lambda^2\right]\ ,\ \ q_j = (-1)^m\left[D\lambda + E\lambda^2\right]\ ,$$

with

$$\begin{aligned}
A &= \pi\,(m^2+n^2)\,t_j/2m \\
B &= (m^2+3n^2)\,s_j/2n^2 + \pi\,(m^2-n^2)\,t_j^2 n/2m^2 \\
C &= n^2\pi^2 t_j^2/2 \\
D &= \pi\,(m^2-n^2)\,t_j/2m \\
E &= (m^2-n^2)\,s_j/2m^2 + \pi\,(m^2+n^2)\,t_j^2 n/2m^2\,.
\end{aligned}$$

We find to order λ^2,

$$\begin{aligned}
a_{0k} &= (-1)^{k(m+n)}\left[1 - \left(\frac{1}{2}k^2\langle A^2\rangle + ik\langle B\rangle\right)\lambda^2\right]\ , \\
a_{1k} &= (-1)^{m+k(n+m)}\left(\langle E\rangle - ik\langle AD\rangle\right)\lambda^2\ \ ,\ \ a_{2k} = (-1)^{k(n+m)}\langle D^2\rangle\lambda^2\,.
\end{aligned} \tag{4.17}$$

All other a_{lk} are higher order in λ and must be ignored. The matrix elements W_{lk}, again to order λ^2, can now be obtained from

$$W_{l,l} = 1 - a_{0,2l} + l^2 a_{2,2l}\ ,\ W_{l,l\pm1} = \pm l\,a_{1,2l\pm1}\ ,\ W_{l,l\pm2} = -\frac{1}{2}l(l\pm1)a_{2,2l\pm2}\,. \tag{4.18}$$

These elements are all seen to be proportional to λ^2 so that we write $W_{lk} \equiv Q_{lk}\lambda^2$; the other elements are zero to order λ^2. Furthermore $a_{11} \equiv v_1\lambda^2$, $a_{22} \equiv v_2\lambda^2$, and $v_i = 0$ for $i \geq 3$. The moments $(\mu_1, \mu_2, ...) \equiv \boldsymbol{\mu}$ are seen to follow from the equation,

$$\mathbf{Q}\cdot\boldsymbol{\mu} = \mathbf{v}\,. \tag{4.19}$$

Since $1 \geq |\mu_j| \to 0$ as $j \to \infty$ it can be solved accurately, choosing a sufficiently large dimensionality M for the matrix $\mathbf{Q}$. We find, with $\eta = s/t^2$,

$$F_a(\eta) = \frac{1}{2\sigma^2}\left\langle \log\left|a + q\,e^{-i\phi}\right|^2\right\rangle = \frac{D^2}{2t^2} + \mathrm{Re}\left[\frac{E}{t^2}\mu_1 - \frac{AD}{t^2}i\mu_1 - \frac{D^2}{2t^2}\mu_2\right] + \mathcal{O}(\lambda)\,. \tag{4.20}$$

Figs. (4.3) display the result of numerical simulations for the Lyapunov exponent, for different degrees of disorder, as well as a calculation based upon Eqs. (4.17) - (4.20). The remarkable dip in the Lyapunov exponent is known as an *anomaly*, and turns out to be slightly redshifted with respect to the Fabry-Perot energy $n\pi$. The enormous anomaly in

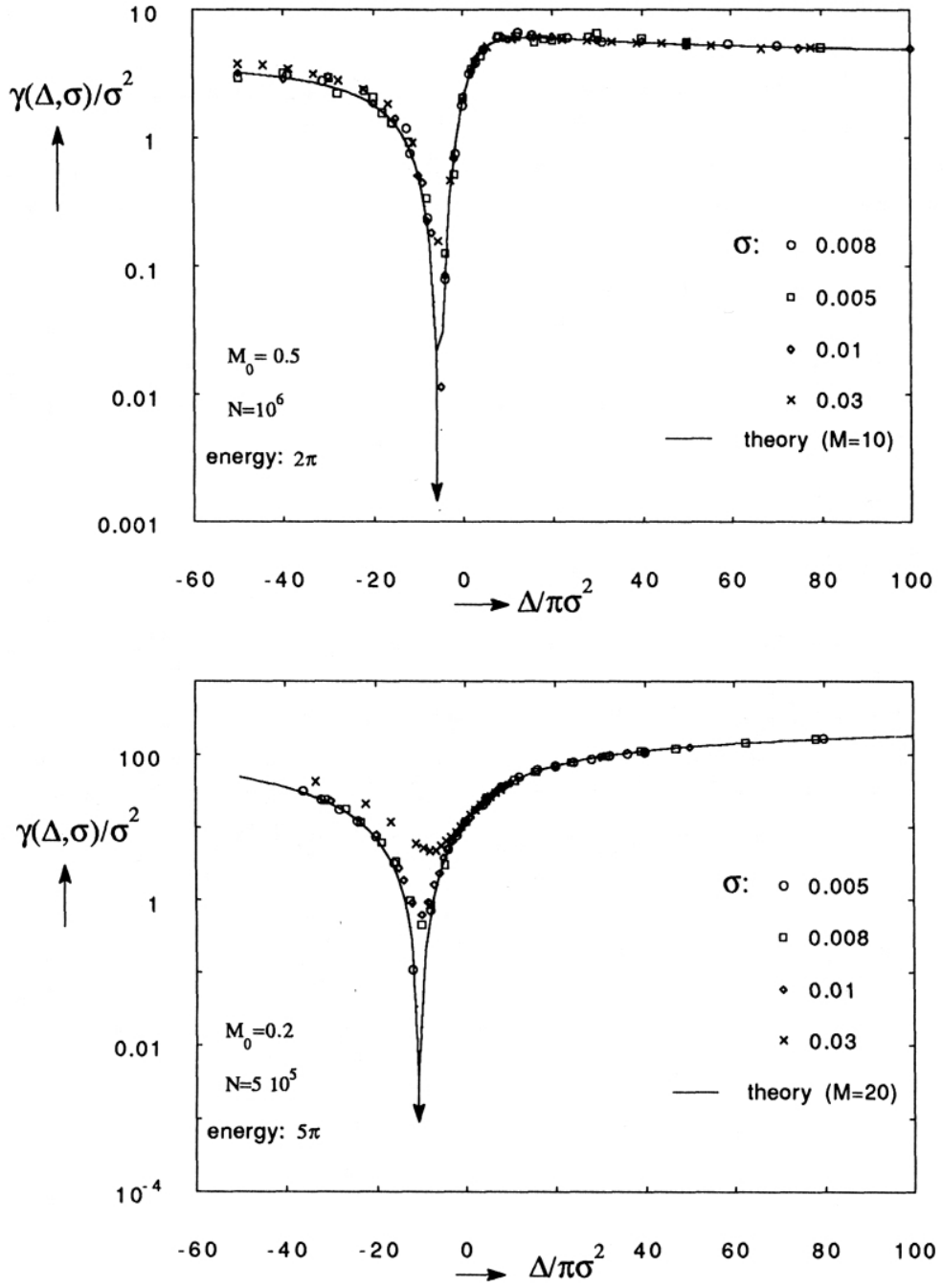

Figure 4.3: *Numerical simulation of the Lyapunov exponent near two special Fabry-Perot energies, using a Gaussian distribution. The bold line is the scaling theory of this section, calculated by the diagonalization of an $M \times M$ matrix.*

the band center is one of the most beautiful manifestations of Thouless criterion (section 3.5).

¿From the simulations we infer that the dip disappears for large deviations and hence the scaling result becomes inaccurate. Because the theory still involves the diagonalization of a matrix of infinite dimensionality, it is not clear whether the scaling result vanishes rigorously in the center of the anomaly. This anomaly may have an important application [160]. Near a Fabry-Perot energy we expect a very large random multilayer to act ("almost surely") as a narrow bandpass filter.

The scaling theory demonstrates the irrelevance of the nature of the probability distribution, provided the scaling hypothesis is satisfied (the deviation σ must exist and be "sufficiently" small). This is certainly true for a binary distribution of the kind $m/n \pm \sigma$, both with probability 1/2. Numerical results for a stack generated according to such a distribution are presented in Fig. 4.4. The simulation is found to coincide nicely with the scaling solution.

4.2.3 Binary Distribution.

The one-dimensional Anderson model with diagonal binary disorder was studied extensively by Nieuwenhuizen and Luck [161] among others. A singular power-law behavior of the density of states was predicted, as well as the existence of extremely narrow and pronounced dips in the Lyapunov exponent. These dips were referred to as "islands" in order to distinguish them from anomalies which are not specific for binary distributions. Very recently, Crisanti [162] investigated a binary optical multilayer and found zero Lyapunov exponents on special Fabry-Perot energies, for any disorder.

The theory of section 4.2.2 is valid for a general dielectric multilayer, not only one satisfying some scaling hypothesis. We can therefore apply it to a binary distribution as well. We consider again the sequence $AB_1AB_2...$ and assume that $B_i = A$ $(m = 1)$ with probability $1 - p$ and $B_i = B_0$ $(m = m(B))$ with probability p. Furthermore a and q are the parameters defined in Eq. (4.5) corresponding to $m(B)$. With the notation of section 4.2.2 it is easily shown that

$$a_{kl} = \delta_{0k}(1-p)\,\mathrm{e}^{-2liy} + p\left(\frac{q}{|a|}\right)^k \left(\frac{a}{|a|}\right)^l . \tag{4.21}$$

The phase-shifts μ_i can be found using Eq. (4.16). The Lyapunov exponent is then calculated from

$$\gamma = \left\langle \log\left|\frac{\alpha_{n+1}}{\alpha_n}\right|\right\rangle = \mathrm{Re}\left\langle \log\left(a + q\,\mathrm{e}^{-i\phi}\right)\right\rangle = p\,\log\,|a| - \sum_{j=1}^{\infty}\frac{(-1)^j}{j}\mathrm{Re}\,(a_{jj}\mu_j)\ . \tag{4.22}$$

Fig. 4.5 shows a comparison of the simplest version of the theory $(M = 2)$ with a numerical simulation on $5\cdot10^5$ layers. On the vertical axis we plotted $\gamma(p)/p(1-p)$, knowing that the denominator is proportional to the variance of the binary distribution. We found perfect

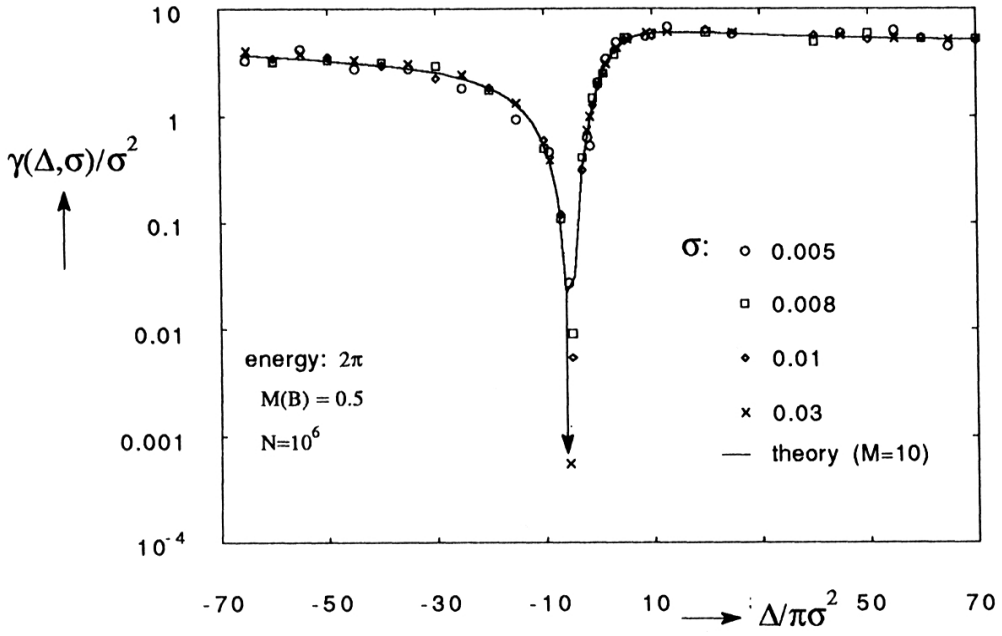

Figure 4.4: *As in Fig. 4.3 but now using a binary distribution of the kind* $m_n = 0.5 \pm \sigma$, *both with probability* $1/2$.

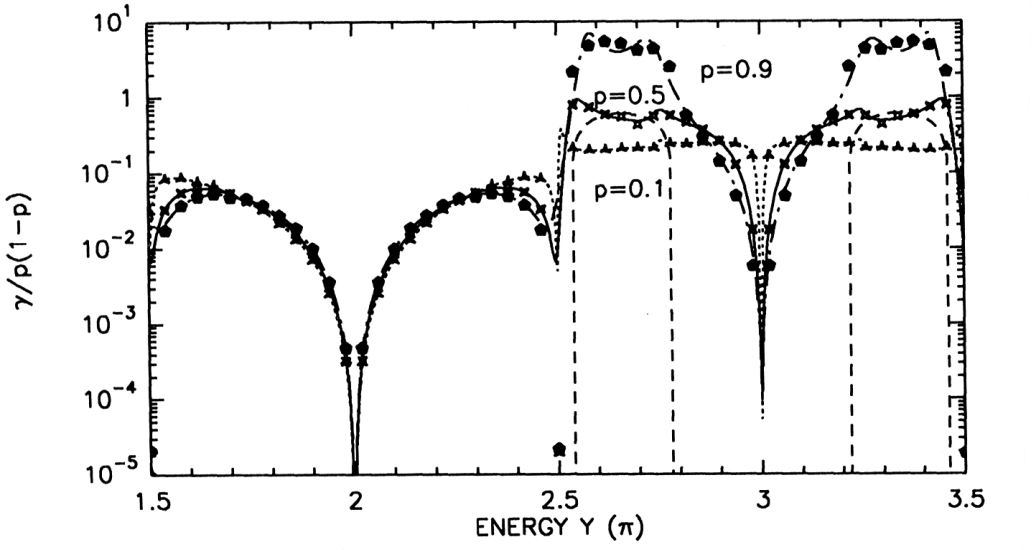

Figure 4.5: *The Lyapunov exponent for a multilayer with binary distribution. The data points are simulations on* $5 \cdot 10^5$ *layers. The lines present the theory* ($M = 2$). *The dashed line is the exponent for* $p = 1$.

agreement with theory for $M = 10$, but the outcome for $M = 2$ is surprisingly satisfactory (and is analytically available). In addition, we plotted the Lyapunov exponent for the periodic system $B_0AB_0AB_0...$ ($p = 1$). For energies in the spectrum of this system, we observe that $\gamma \sim \sigma^2$ and anomalous behavior is absent. We did not find evidence for the presence of islands, but this may well be due to insufficient energy resolution. Because the binary distribution is attractive from an experimental point of view, these random multilayers may find important applications in X-ray optics [163].

4.2.4 Poisson Distribution

We discuss briefly another kind of disorder. In this approach we let the *number* of vacuum layers be the stochastic variable, rather than the index of refraction. Together with the binary distribution such a disorder might be relevant for experimental purposes [160]. The transfer matrix for mapping the wave function in the n^{th} non-vacuum layer onto the $(n+1)^{\text{th}}$ non-vacuum layer, with a number of j_n vacuum layers in between, can be found. We calculated the transfer matrices for arbitrary angle of incidence, for both polarization channels. They can again be represented by formula (4.5). With m the index of refraction of the non-vacuum layers,

$$\begin{aligned} a^S(j_n) &= \mathrm{e}^{-imys'}\left[\cos(j_n \cdot ys) - i\,\frac{m^2s'^2 + s^2}{2mss'}\,\sin(j_n \cdot ys)\right], \\ q^S(j_n) &= \frac{m^2s'^2 - s^2}{2mss'}\,\sin(j_n \cdot ys)\,\mathrm{e}^{-imys'}, \end{aligned} \tag{4.23}$$

for s-polarization and

$$\begin{aligned} a^P(j_n) &= \mathrm{e}^{-imys'}\left[\cos(j_n \cdot ys) - i\,\frac{m^2s^2 + s'^2}{2mss'}\,\sin(j_n \cdot ys)\right], \\ q^P(j_n) &= \frac{s'^2 - m^2s^2}{2mss'}\,\sin(j_n \cdot ys)\,\mathrm{e}^{-imys'}, \end{aligned} \tag{4.24}$$

for p-polarization. We have defined $s \equiv \sin\theta$ and $s' \equiv \sin\theta'$, θ and θ' being the angle of the transmitted wave with respect to the surface of the vacuum and non-vacuum layers, respectively. According to Snell's law,

$$m\cos\theta' = \cos\theta\,. \tag{4.25}$$

We adopt a Poisson distribution for the number of layers,

$$P(j) = \mathrm{e}^{-\lambda}\,\frac{\lambda^{j-1}}{(j-1)!}\,, \tag{4.26}$$

with an average $\langle j\rangle = \lambda$. It is understood that all j_n are mutually independent. The Lyapunov exponent can be calculated using Eq. (4.16). To this end we notice that the

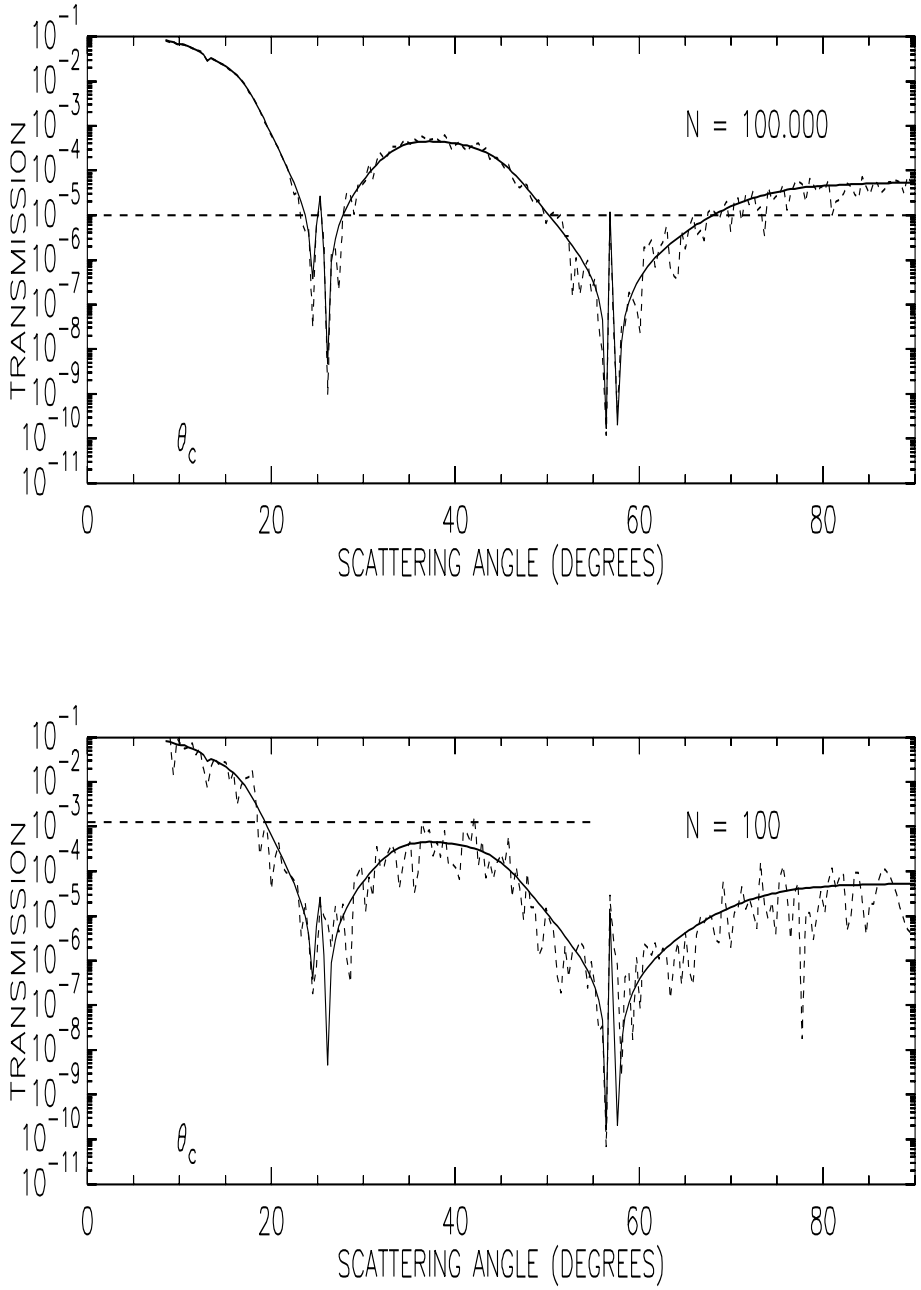

Figure 4.6: *The Lyapunov exponent for the s-channel. We adopted a Poisson distribution with* $\lambda = 1$. *All dielectric units have a width of* 1.2 *wavelengths;* $m = 0.99$. *The critical angle of the homogeneous system is indicated. The horizontal line satisfies* $\gamma N = 1$. *If* $\gamma N > 1$, *the stack is a good reflector. Bold: theory* ($M = 10$).

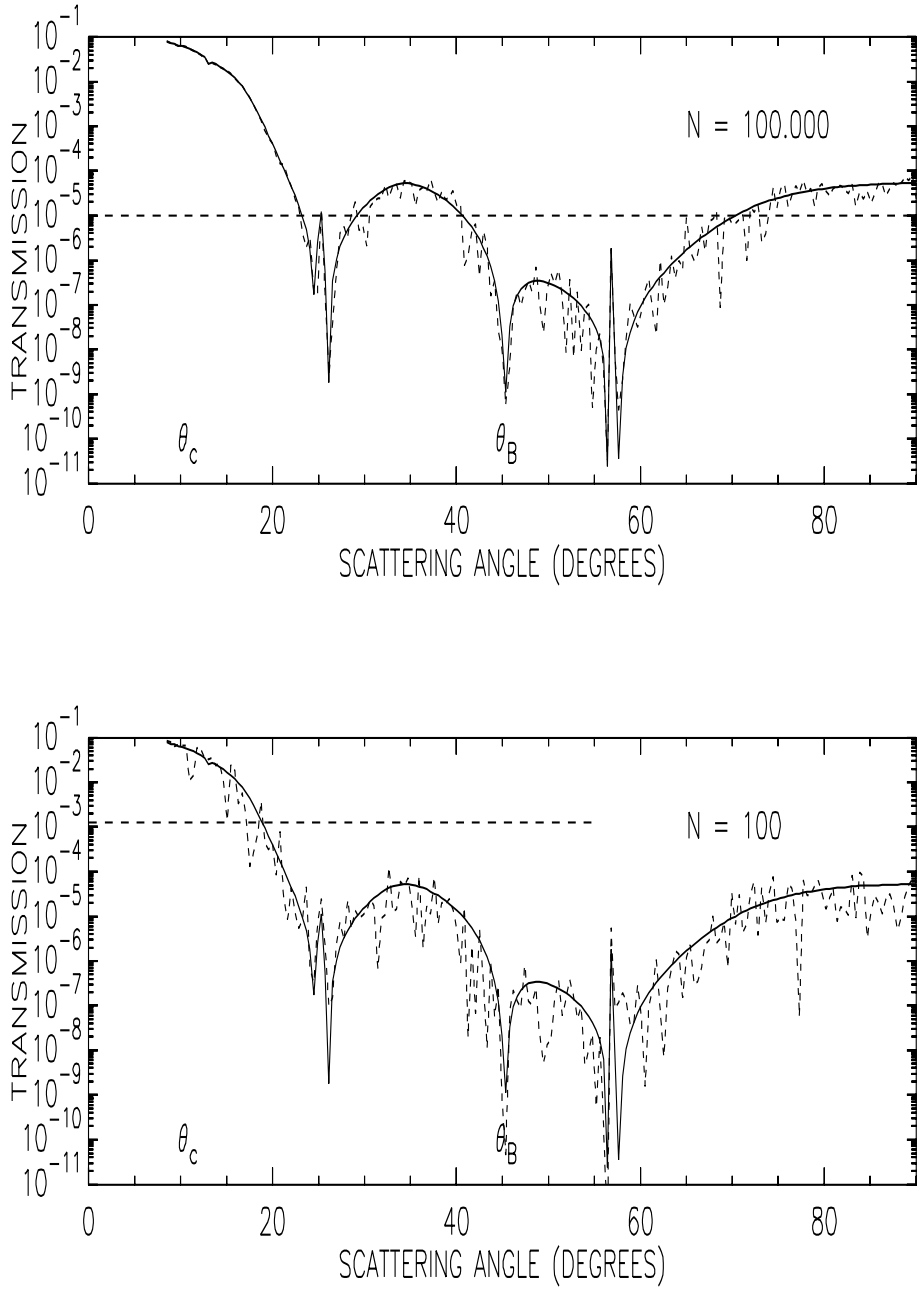

Figure 4.7: *As in the former figure but now for the p-channel. The Brewster angle is indicated by* θ_B.

coefficients a_{kl} are given by

$$a_{kl} = \left\langle \left(\frac{a}{|a|}\right)^l \left(\frac{q}{|a|}\right)^k \right\rangle = \mathrm{e}^{-\lambda} \sum_{j=1}^{\infty} \frac{\lambda^{j-1}}{(j-1)!} \, \frac{a(j)^l q(j)^k}{|a(j)|^{k+l}} \, . \tag{4.27}$$

The formula (4.16) can now easily be solved numerically for the average phase shifts μ_l, as all infinite summations converge rapidly. The Lyapunov exponent becomes

$$\gamma = \mathrm{Re} \left\langle \log\left(a^* + q\mathrm{e}^{i\phi}\right) \right\rangle = \langle \log|a| \rangle - \sum_{l=1}^{\infty} \frac{(-1)^l}{l} \mathrm{Re} \left(a^*_{l,-l} \, \mu_l\right) \, . \tag{4.28}$$

In Figs. (4.6) and (4.7) we have plotted some of the results, choosing an average of $\lambda = 1$ vacuum layer.

In view of a recent interest from the thin-film department at our institute in these Poisson multilayers, we have given special attention to angles near the critical angle of the non-vacuum layers, ($s' = 0$ or $\cos\theta = m$), and near the Brewster angle ($ms = s'$ or equivalently $\tan\theta = 1/m$) of the p-channel. In the last case one anticipates a vanishing reflection, and the density of states is large. This makes the Lyapunov exponent very small, indicating that localization is feeble. Near the critical angle the density of states is small and localization becomes very pronounced. These random stacks may enhance the effective critical angle considerably. One might even speculate about the existence of *Lifshitz tails* [142] [164] in the density of states beyond the critical angle. The density of states (per site or per layer) can be calculated straightforwardly from the imaginary part of Eq. (4.28). The bottom figures show what remains of the Lyapunov exponent for a *finite* stack of 100 units, generated randomly.

Appendices

A. Dwell Time in Quantum Mechanics

In this appendix we derive an expression for the dwell time in the case of ordinary potential scattering. Starting with the Schrödinger wave equation with a yet complex potential,

$$i\partial_t\psi(\mathbf{r},t) = -\boldsymbol{\nabla}^2\psi(\mathbf{r},t) + V(\mathbf{r})\psi(\mathbf{r},t)\,, \tag{A.1}$$

we obtain the well known *equation of continuity*,

$$\partial_t\frac{1}{2}|\psi(\mathbf{r},t)|^2 + \boldsymbol{\nabla}\cdot\mathbf{J} = \operatorname{Im}V(\mathbf{r})|\psi(\mathbf{r},t)|^2\,, \tag{A.2}$$

with $\mathbf{J} = \operatorname{Im}\psi^*\boldsymbol{\nabla}\psi$. Finally, we take the limit of vanishing imaginary part. We define the linear functional,

$$\Phi[g] = \int_{-\infty}^{\infty} dt \int d\mathbf{r}\, g(\mathbf{r})\,|\psi(\mathbf{r},t)|^2\,, \tag{A.3}$$

where $g(\mathbf{r})$ is real-valued and has compact support. If $\operatorname{Im}V(\mathbf{r}) = V_i\, g(\mathbf{r})$ we get

$$\Phi[g] = \lim_{V_i\to 0}\frac{1}{V_i}\int_{-\infty}^{\infty} dt \int d\mathbf{S}\cdot\mathbf{J}(\mathbf{r},t)\,. \tag{A.4}$$

By Gauss' Theorem, the surface integral can be performed on *any* closed surface surrounding the support of g. We shall work it out in three dimensions. The asymptotic (outgoing) solution of the Schrödinger equation is, in terms of the scattering amplitude $f_{\mathbf{k}}(\theta) = t_{\mathbf{k}\,k\hat{\mathbf{r}}}(k^+)$,

$$\psi(\mathbf{r},t) = \sum_{\mathbf{k}}\psi_0(\mathbf{k})\left[\mathrm{e}^{i\mathbf{k}\cdot\mathbf{r}} - f_{\mathbf{k}}(\theta)\frac{\mathrm{e}^{ikr}}{4\pi r}\right]\mathrm{e}^{-ik^2t}\,,$$

with θ fixing the direction of $\mathbf{r}$. It follows, for $r\to\infty$, that

$$\int_{-\infty}^{\infty} dt\,\hat{\mathbf{r}}\cdot\mathbf{J}(\mathbf{r},t) = \pi\mathrm{Re}\sum_{\mathbf{k}\mathbf{k}'}\delta(k-k')\psi_0(\mathbf{k})^*\psi_0(\mathbf{k}')\Big[\mathrm{e}^{i(\mathbf{k}'-\mathbf{k})\cdot\mathbf{r}}\,(\hat{\mathbf{r}}\cdot\hat{\mathbf{k}}')$$
$$-\,\mathrm{e}^{-i\mathbf{k}\cdot\mathbf{r}}\frac{\mathrm{e}^{ikr}}{4\pi r}f_{\mathbf{k}'}(\theta) - \mathrm{e}^{i\mathbf{k}'\cdot\mathbf{r}}\frac{\mathrm{e}^{-ikr}}{4\pi r}f_{\mathbf{k}}(\theta)^*(\hat{\mathbf{r}}\cdot\hat{\mathbf{k}}') + \frac{f_{\mathbf{k}}(\theta)^*f_{\mathbf{k}'}(\theta)}{(4\pi r)^2} + \mathcal{O}\left(\frac{1}{r^3}\right)\Big]\,.$$

Making use of the formal identity that

$$\lim_{r\to\infty} r\,\mathrm{e}^{\pm ikr}\int_{-1}^{1} dc\,F(c)\,\mathrm{e}^{\mp ikrc} = \frac{\pm i}{k}F(1)\,,$$

where $c=\cos\theta$, we obtain, finally

$$\Phi[g] = \pi\lim_{V_i\downarrow 0}\frac{1}{V_i}\mathrm{Re}\sum_{\mathbf{k}\mathbf{k}'}\psi_0(\mathbf{k})^*\psi_0(\mathbf{k}')\,\delta(k-k')\left[-\frac{i}{2k}\left(f_{\mathbf{k}'}(\hat{\mathbf{k}})-f^*_{\mathbf{k}}(\hat{\mathbf{k}}')\right)+\int d\hat{\mathbf{r}}\,\frac{f^*_{\mathbf{k}}(\hat{\mathbf{r}})\,f_{\mathbf{k}'}(\hat{\mathbf{r}})}{(4\pi)^2}\right].$$

This is further simplified by concentrating $\psi_0(\mathbf{k})$ in the element $dkd\Omega$, while retaining its normalization. Upon introduction of the *functional derivative* [165],

$$\delta^{\xi}_V H[V] = \lim_{\Delta\downarrow 0}\frac{H[V(\mathbf{r})+\Delta\xi(\mathbf{r})]-H[V(\mathbf{r})]}{\Delta}\,, \tag{A.5}$$

where $\xi(\mathbf{r})$ can be complex-valued, we arrive at

$$\frac{d\Phi[g]}{d\Omega} = \frac{1}{2}\left(\frac{k}{2\pi}\right)^2\delta^{ig}_V\left[\frac{1}{k}\,\mathrm{Im}\,f_{\mathbf{k}}(\hat{\mathbf{k}})+\int d\hat{\mathbf{r}}\,\frac{d\sigma}{d\Omega}(\hat{\mathbf{k}}\to\hat{\mathbf{r}})\right]. \tag{A.6}$$

Here $|f_{\mathbf{k}}(\hat{\mathbf{r}})|^2/(4\pi)^2 \equiv d\sigma/d\Omega$, is the differential cross-section in the direction $\hat{\mathbf{r}}$. Eq. (A.6) can be recognized as a derivative of the absorption cross-section with respect to the imaginary part of the potential, similar to Eq. (1.87). Using the fact that $f_{\mathbf{k}}$ depends functionally on $V(\mathbf{r})$, whereas $f^*_{\mathbf{k}}$ depends on its complex conjugate, this can also be written as

$$\frac{d\Phi[g]}{d\Omega} = -\frac{1}{2}\left(\frac{k}{2\pi}\right)^2\left[-\frac{1}{k}\,\delta^g_V\mathrm{Re}\,f_{\mathbf{k}}(\hat{\mathbf{k}})+2\int d\hat{\mathbf{r}}\,\frac{d\sigma}{d\Omega}(\hat{\mathbf{k}}\to\hat{\mathbf{r}})\delta^g_V\phi(\hat{\mathbf{r}})\right]. \tag{A.7}$$

Here $\phi(\hat{\mathbf{r}})$ is the complex phase of the T-matrix in the direction $\hat{\mathbf{r}}$. Alternatively, Eq. (A.7) can be obtained from Eq. (A.6) by application of the Cauchy-Riemann equations. In one dimension there is no solid angle degeneracy and the result reads

$$\Phi[g] = -\frac{1}{2}\delta^{ig}_V\left[1-|R(k)|^2-|T(k)|^2\right] = -|R(k)|^2\delta^g_V\phi_R-|T(k)|^2\delta^g_V\phi_T\,. \tag{A.8}$$

$R(k)$ and $T(k)$ represent the complex reflection and transmission coefficient ; ϕ_R and ϕ_T are their phase-shifts.

We discuss two relevant choices for g. First, we can take $g(\mathbf{r})$ equivalent to the *characteristic function* of the potential barrier $\chi_B(\mathbf{r})$. Then

$$\Phi[\chi_B] = \int_{-\infty}^{\infty} dt\int_B d\mathbf{r}\,|\psi(\mathbf{r},t)|^2 = \tau_B, \tag{A.9}$$

where τ_B is the dwell time analogous to Eq. (1.74). We conclude that the dwell time can be formulated in terms of a functional derivative with respect to the potential in the direction

of its characteristic function. This conclusion is in complete agreement with Ref. [166]. Another very interesting option is obtained by choosing g such that $V(\mathbf{r}) = V_0 g(\mathbf{r})$. In that case the functional derivative δ_V^g reduces to an ordinary derivative d/dV_0. Going to the plane wave limit of $\Phi[V]$ in three dimensions, yields, in combination with Eq. (A.7),

$$\langle \psi_{\mathbf{k}}^+ \,|\, g \,|\, \psi_{\mathbf{k}}^+ \rangle = \frac{d}{d\,(\mathrm{Im} V_0)} \left[\mathrm{Im}\, f_{\mathbf{k}}(\hat{\mathbf{k}}) + k \int d\hat{\mathbf{r}}\, \frac{d\sigma}{d\Omega}(\hat{\mathbf{k}} \to \hat{\mathbf{r}}) \right] = -k\, \frac{d\sigma_{\mathrm{abs}}}{d(\mathrm{Im}\, V_0)}$$
$$= \frac{d\,\mathrm{Re}\, f_{\mathbf{k}}(\hat{\mathbf{k}})}{d\, V_0} - 2k \int d\Omega\, \frac{d\sigma}{d\Omega}\, \frac{d\phi(\Omega)}{d\, V_0}\,. \qquad (A.10)$$

Only for a rectangular potential is g constant in the potential region and the integral of $|\psi_{\mathbf{k}}^+|^2$ over this region equals the derivative of the phase-shift with respect to the potential [167] [168].

B. Spectral Function for Scalar Waves

This appendix deals with a useful sum rule valid for the spectral function, defined in terms of the averaged amplitude Green's function in Eq. (3.23). The mass-operator $\Sigma(z)$ is defined according to

$$G(z) = \frac{1}{z^2 - p^2 - \Sigma(z)} = \left\langle \frac{1}{z^2 \varepsilon - p^2} \right\rangle . \qquad (B.1)$$

ε is the dielectric constant of the random medium, $<>$ denotes ensemble-averaging in the thermodynamic limit, and z is a complex energy. By letting $z \to \infty$ it follows that

$$\lim_{z\to\infty} \left[1 - \frac{\Sigma(z)}{z^2} \right] = \langle \varepsilon^{-1} \rangle^{-1} . \qquad (B.2)$$

This is still an operator identity but can easily be formulated for the matrix element $\Sigma(z,p)$, using the diagonality in momentum space. For a vacuum filled with dielectric scatterers with packing fraction f and speed of light c_{sc} we then obtain for the right-hand side of Eq. (B.2): $\langle c^2 \rangle = (1-f) + f c_{\mathrm{sc}}^2$. It can be inferred from Eq. (B.1) that the matrix element $G(z,p)$ must be analytic in both sheets $\mathrm{Im}\, z >< 0$, since p and ε are real-valued. The scalar wave equation has *two* physical sheets, separated by a branch cut (the spectrum) located along the whole real axis. A consequence is the following sum rule,

$$\int_{-\infty}^{\infty} \frac{dE}{2\pi}\, S(E,p) = \langle c^2 \rangle . \qquad (B.3)$$

Proof.
First we write $S(E,p) = iE\,[G(E^+,p) - G(E^-,p)]$, with $E^\pm \equiv E \pm i0$. Since $G(E^\pm,p)$ asymptotically decays as $\langle c^2 \rangle / E^2$ both terms cannot be handled separately. If we subtract

the asymptotical limit of Eq. (B.2) from both terms, with

$$f(z) \equiv \frac{z}{z^2 - p^2 - \Sigma(z,p)} - \frac{\langle c^2 \rangle}{z}\,,$$

we arrive at

$$\int_{-\infty}^{\infty} \frac{dE}{2\pi i} \left[f(E^-) - f(E^+) \right] = \int_{\Gamma^-} \frac{dz}{2\pi i}\, f(z) - \int_{\Gamma^+} \frac{dz}{2\pi i}\, f(z) - \oint_{z=0} \frac{dz}{2\pi i}\, f(z)\,.$$

$\Gamma^{\pm}$ denotes a very large closed half circle in the upper and lower sheet, respectively. Because $f(z)$ is analytic in both sheets, the first two integrals vanish. The third Cauchy integral is easily shown to be equal to $-\langle c^2 \rangle$. □

C. Conventions & Notation

I. Units:
$c_0 = 1/\sqrt{\varepsilon_0} = 1$ in Maxwell's equations.
$\hbar/2m_e = 1$ in Schrödinger's Equation.

II. Conventions of Laplace and Fourier transformation:

Fourier	$f(\mathbf{r}) = \sum_{\mathbf{p}} \mathrm{e}^{-i\mathbf{p}\cdot\mathbf{r}}\, f(\mathbf{p})$	$f(\mathbf{p}) = \int d\mathbf{r}\, \mathrm{e}^{i\mathbf{p}\cdot\mathbf{r}}\, f(\mathbf{r})$
Laplace	$f(t) = \int_0^{\infty} dt\, f(t)\, \mathrm{e}^{izt}$	$f(t) = \int_{\Gamma} \frac{dz}{2\pi}\, f(z)\, \mathrm{e}^{-izt}$

III. List of used symbols (in alphabetic order):

NOTATION	EXPLANATION	INTRODUCTION
a	albedo = scattering/extinction	1.88
D	diffusion constant	3.2
E	(internal) frequency or energy	1.20
f	packing fraction	3.84
$\|\underline{\mathbf{F}}\rangle$	six-dimensional vectorfield in $\mathcal{K}$	chapter 1
$\|\mathbf{f}\rangle$	three-dimensional vectorfield: $\|\mathbf{f}\rangle \otimes \|\mathbf{f}\rangle \in \mathcal{K}$	chapter 1
$g(L)$	Thouless/Tauros parameter	3.110

NOTATION	EXPLANATION	INTRODUCTION
$\mathbf{k}$, $\mathbf{p}$	(internal) momentum	chapter 1
$\hat{\mathbf{k}}$	normalized vector $\mathbf{k}/\lvert\mathbf{k}\rvert$	1.20
$\underline{\underline{\mathbf{K}}}_{(0)}$	(free) time evolution for Maxwell's equations	1.8, 1.13
m	(complex) index of refraction	1.18
$N(E)$	density of states per unit volume	3.24
N	number of scatterers or layers	1.50
n	number density of scatterers	2.6
$\mathbf{q}$	external momentum, $-i\mathbf{q} \leftrightarrow \boldsymbol{\nabla})_{\text{macroscopic}}$	3.15
r_0	size of Mie sphere	1.71
s	dimensionless isotropic T-matrix $E\,t/4\pi$	2.29
$S(E,p)$	spectral function	3.23
$U_{\mathbf{pp}'}(\omega\,\mathbf{q}\lvert E)$	Irreducible Vertex	2.11
v_p	phase velocity	3.28
v_g	group velocity	3.73
v_E	transport, energy velocity	3.65
$W(\cdots)$	(average) energy density	1.10
x	size parameter for Mie sphere	1.58
z	complex frequency or energy	1.15
z_0	extrapolation length	2.47
$\gamma(\mu,\mu')$	bistatic coefficient	2.1
$\gamma(E)$	Ioffe-Regel parameter (chapter 3)	3.37

NOTATION	EXPLANATION	INTRODUCTION
$\gamma(E)$	Lyapunov exponent (chapter 4)	4.1
$\delta(E)$	dynamic vertex correction	3.65
$\varepsilon(\mathbf{r})$	dielectric constant	1.4
η	disorder parameter	2.28
$\mathcal{K}$	Hilbert space for electromagnetic field	1.12
ℓ_s	scattering mean free path	2.9
ℓ_e	extinction mean free path	2.9
$\ell\,(\ell^B)$	(Boltzmann) transport mean free path	3.3
ℓ_a	absorption mean free path	2.9
$\mu_{i,s}$	$\cos\theta_{\text{in,scattered}}$	2.1
$\mu(\mathbf{r})$	magnetic permeability	1.4
ν	number of scatterers per optical volume $\eta\,\lvert s\rvert^3$	2.62
$\underline{\underline{\mathbf{\Pi}}}_{(0)}$	transverse projections in $\mathcal{K}_{(0)}$	1.14
$\sum_{\mathbf{p}}$	$\int d\mathbf{p}\,(2\pi)^{-3}$	1.63
$\sum_{j\hat{\mathbf{k}}E}$	$\sum_{j=\pm1}\int_{4\pi} d\hat{\mathbf{k}}\int_{-\infty}^{+\infty} dE\,(2\pi)^{-3}$	1.22
$\Sigma(z,\mathbf{p})$	self-energy or Mass-operator	2.3
$\sigma(\mathbf{r})$	electric conductivity	1.4
σ	standard deviation	4.9
τ	optical depth	2.21
ω	external frequency, $-i\omega \leftrightarrow \partial_t)_{\text{macroscopic}}$	3.12
$\underline{\underline{\mathbf{\Omega}}}_{\pm}$	Møller wave operators	1.25

Bibliography

[1] S.R. de Groot, *The Maxwell Equations*, eds. J. de Boer and G.E. Uhlenbeck (North-Holland, 1969).

[2] J.D. Jackson, *Classical Electrodynamics* (John Wiley & Sons New York, 1975).

[3] H. Feshbach, A Unified Theory of Nuclear Reactions, *Ann. Phys.*, **19**, 287 (1962).

[4] H.C. van de Hulst, *Light Scattering from Small Particles* (Dover, New York, 1981).

[5] R.D. Richtmeier, *Principles of Advanced Mathematical Physics* Vol. 1 (Springer-Verlag New York, 1978).

[6] M. Reed and B. Simon, *Methods of Modern Mathematical Physics*, Vol. III *Scattering Theory* (Academic Press New York, 1979).

[7] M. Reed and B. Simon, The Scattering of Classical Waves from Inhomogeneous Media, *Math. Z.* **155**, 163 (1977).

[8] J.R. Schulenberger and C.H. Wilcox, Completeness of the Wave Operators for Perturbations of Uniformly Propagative Systems, *J. Funct. An.* **7**, 447 (1971).

[9] R.G. Newton, *Scattering Theory of Waves and Particles* (McGraw-Hill Company, New York, 1966).

[10] C.J. Joachain, *Quantum Collision Theory* (North-Holland Publishing Company, 1975).

[11] C.F. Bohren and D.R. Huffman, *Absorption and Scattering of Light by Small Particles* (John Wiley & Sons, New York, 1983).

[12] P.C. Waterman, Symmetry, Unitarity, and Geometry in Electromagnetic Scattering, *Phys. Rev. D* **3**, 825 (1971).

[13] R. Peierls, *Surprises in Theoretical Physics* (Princeton University Press, Princeton, 1979) section 6.1.

[14] J.P. Antoine, F. Gesztesy and J. Shabani, Exactly Solvable Models of Sphere Interactions in Quantum Mechanics, *J. Phys. A.* **20**, 3687 (1987).

[15] S. Albeverio, F. Gesztesy, R. Høegh-Krohn and H. Holden, *Solvable Models in Quantum Mechanics* (Springer-Verlag, New York, 1988).

[16] A. Grossmann, R. Høegh-Krohn and M. Mebkhout, A Class of Explicitly Soluble, Local, Many-center Hamiltonians for One-particle Quantum Mechanics in Two and Three Dimensions, *J. Math. Phys.* **21**, 2379 (1980).

[17] A. Grossmann and T.T. Wu, Fermi Pseudopotential in Higher Dimensions, *J. Math. Phys.* **25**, 1742 (1984).

[18] T.T. Wu, Fermi Pseudo Potentials and Resonances in Arrays, in: *Resonances-Models and Phenomena* eds. S. Albeverio, L.S. Ferreira and L. Streit (Springer-Verlag, Berlin 1984).

[19] D.K. Freeman, The Pseudodipole as a Limit of Resonant Cylindrical Dipole, *J. Math. Phys.* **32**, 1961 (1991).

[20] E.P. Wigner, Lower Limit for the Energy Derivative of the Scattering Phase Shift, *Phys. Rev.* **98**, 145 (1955).

[21] Th.M. Nieuwenhuizen, submitted to *Phys. Lett. A* (1992).

[22] H.J. Dorren and A. Tip, Maxwell's Equations for Non-smooth Media: Fractal-shaped and Pointlike Objects, *J. Math. Phys.* **32**, 3060 (1991).

[23] R. Loudon, *The Quantum Theory of Light* (Clarendon, Oxford, 1973) first edition.

[24] J.F. van Diejen, *Point Interactions in Pontryagin Spaces*, Master's thesis, AMOLF Amsterdam (1989).

[25] J.F. van Diejen and A. Tip, Scattering from Generalized Point Interactions Using Self-adjoint Extensions in Pontryagin Spaces, *J. Math. Phys.* **32**, 630 (1991).

[26] H.J. Dorren, *A Point Interaction Model for Light*, Master's thesis, AMOLF Amsterdam (1991).

[27] A. Bott and W. Zdunkowski, Electromagnetic Energy within Dielectric Spheres, *J. Opt. Soc. Am. A* **4**, 1361 (1987).

[28] J.A. Stratton, *Electromagnetic Theory* (McGraw-Hill Company, New York, 1941).

[29] G.J. Rosasco and H.S. Bennett, Internal Field Structure: Implications for Optical Absorption and Scattering by Microscopic Particles, *J. Opt. Am. Soc.* **68**, 1242 (1978), & *Selected Papers on Light Scattering*, Spie Milestone Series Vol. 951, ed. M. Kerker (Spie, Washington, 1988), page 290.

[30] A. Ishimaru, *Wave Propagation in Random Media*, Vols. 1 & 2 (Academic New York, 1978).

[31] K.M. Watson, Multiple Scattering of Electromagnetic Waves in an Underdense Plasma, *J. Math. Phys.* **10**, 688 (1969).

[32] D.A. de Wolf, Electromagnetic Reflection from an Extended Turbulent Medium: Cumulative Forward-Scatter Single-Backscatter Approximation, *IEEE Transactions on Antennas and Propagation* Vol. AP-19, page 254 (1971).

[33] Yu.N. Barabanenkov, Wave Corrections to the Transfer Equation for Backscattering, *Isz. Vyssh. Uch. Zav.-Radiofiz.* **16**, 88 (1973).

[34] S. Chandrasekhar, *Radiative Transfer*, (Dover, New York, 1960).

[35] H.C. van de Hulst, *Multiple Light Scattering* Vols. 1 & 2 (Academic, New York, 1980).

[36] E. Akkermans, P.E. Wolf and R. Maynard, Coherent Backscattering of Light by Disordered Media: Analysis of the Peak Line Shape, *Phys. Rev. Lett.* **56**, 1471 (1986).

[37] M. Kaveh, M. Rosenbluh, I. Edrei and I. Freund, Weak Localization and Light Scattering from Disordered Solids, *Phys. Rev. Lett.* **57**, 2049 (1986).

[38] M.P. van Albada and A. Lagendijk, Observation of Weak Localization of Light in Random Media, *Phys. Rev. Lett.* **55**, 2692 (1985).

[39] M.B. van der Mark, M.P. van Albada and A. Lagendijk, Light Scattering in Strongly Scattering Media: Multiple Scattering and Weak Localization, *Phys. Rev. B* **37**, 3575 (1988).

[40] M.B. van der Mark, *Propagation of Light in Disordered Media: A Search for Anderson Localization*, Ph.D. thesis, University of Amsterdam (1990).

[41] E.E. Gorodnichev, S.L. Dudarev and D.B. Rogozkin, Coherent Wave Backscattering by Random Media: Exact Solution of the Albedo Problem *Phys. Lett. A* **144**, 48 (1990).

[42] F.C. MacKintosh and S. John, Coherent Backscattering in the Presence of Time-reversed-noninvariant and Parity-nonconserving Media, *Phys. Rev. B* **37**, 1884 (1988).

[43] M.J. Stephen and G. Cwilich, Rayleigh Scattering and Weak Localization: Effects of Polarization, *Phys. Rev. B* **34**, 7564 (1986).

[44] M.P. van Albada, M.B. van der Mark and A. Lagendijk, Polarization Effects in Weak Localization of Light, *J. Phys. D Appl. Phys.* **21**, S28 (1988).

[45] M.P. van Albada and A. Lagendijk, Vector Character of Light in Weak Localization: Spatial Anisotropy in Coherent Backscattering from a Random Medium, *Phys. Rev. B* **36**, 2353 (1987).

[46] I. Freund, M. Rosenbluh, R. Berkovits and M. Kaveh, Coherent Backscattering of Light in a Quasi-two-dimensional System, *Phys. Rev. Lett.* **61**, 1214 (1988).

[47] A. Lagendijk, Terrestrial Redshifts from a Diffuse Light Source, *Phys. Lett. A* **147**, 389 (1990).

[48] E. Wolf, Invariance of the Spectrum of Light on Propagation, *Phys. Rev. Lett.* **56**, 1370 (1986).

[49] A.A. Maradudin *et al.* , Enhanced Backscattering and Transmission of Light from Random Surfaces on Semi-infinite Substrates and Thin Films, *Waves in Random Media* **3**, S129 (1991).

[50] K. Muinonen, *Light Scattering by Inhomogeneous Media: Backward Enhancement and Reversal of Linear Polarization*, Ph.D. thesis, University of Helsinki (1990).

[51] R. Vreeker, M.P. van Albada, R. Sprik and A. Lagendijk, Femtosecond Time-Resolved Measurements of Weak Localization of Light, *Phys. Lett. A* **132**, 51 (1988).

[52] K.M. Yoo and R.R. Alfano, Time Resolved Depolarization of Multiple Backscattered Light from Random Media, *Phys. Lett. A* **142**, 531 (1989).

[53] F.C. MacKintosh and S. John, Diffusion-Wave Spectroscopy and Multiple Scattering of Light in Correlated Random Media, *Phys. Rev. B* **40**, 2383 (1989).

[54] D.J. Pine, D.A. Weitz, J.X. Zhu and E. Herbolzheimer, Diffusing-wave Spectroscopy: Dynamic Light Scattering in the Multiple Scattering Limit, *J. Phys. France* **18**, 2101 (1990).

[55] D.J. Durian, D.A. Weitz and D.J. Pine, Scaling Behavior in Shaving Cream, *Phys. Rev. A* **44**, R7902 (1991).

[56] Y. Pomeau and P. Resibois, Time Dependent Correlation Functions and Mode-Mode Coupling Theories, *Phys. Rep.* **19**, 63 (1975).

[57] J.X. Zhu, D.J. Durian, J. Müller, D.A. Weitz and D.J. Pine, Scaling of Transient Hydrodynamic Interactions in Concentrated Suspensions, *Phys. Rev. Lett.* **68**, 2559 (1992).

[58] D. Wiersma, *Beyond Linear Light Scattering*, Master's thesis, AMOLF Amsterdam (1991).

[59] W. Götze, A Theory for the Conductivity of a Fermion Gas Moving in a Strong Three-dimensional Random Potential, *J. Phys. C* **12**, 1279 (1979).

[60] D. Vollhardt and P. Wölfe, Diagrammatic, Self-consistent Treatment of the Anderson Localization Problem in $d \leq 2$ Dimensions, *Phys. Rev. B* **22**, 4666 (1980).

[61] P.W. Anderson, Absence of Diffusion in Certain Random Lattices, *Phys. Rev.* **109**, 1492 (1958).

[62] U. Frisch, *Probabilistic Methods in Applied Mathematics*, Vol. I ed. A.T. Bharucha-Reid (Academic New York, 1968).

[63] H.C. van de Hulst, Diffuse Reflection from a Spherical Interstellar Dust Cloud, in: *Evolution of Interstellar Dust and Related Topics* eds. A. Bonneti, J.M. Greenberg and S. Aiello, (North-Holland, Amsterdam, 1989).

[64] U. Fano, Pressure Broadening as a Prototype of Relaxation, *Phys. Rev.* **131**, 259 (1963).

[65] A. Tip, Random Time Evolution and Direct Integrals: Constants of the Motion and the Mass Operator, submitted to *J. Math. Phys.* (1992).

[66] N.E. Cusack, *The Physics of Structurely Disordered Matter: an Introduction*, (IOP Publishing Ltd, 1987).

[67] D. Forster, Hydrodynamic Fluctuations, Broken Symmetry, and Correlation Functions, *Frontiers in Physics* (ed. D. Pines, 1975).

[68] P.A. Lee, Universal Conductance Fluctuations in Disordered Metals, *Physica A* **140**, 169 (1986).

[69] G.D. Mahan, *Many-Particle Physics* (Plenum, New York, 1981).

[70] R. Maynard, E. Akkermans and P.E. Wolf, Coherent Backscattering and Weak Localization Phenomena in Optics and in Metals: Analogies and Differences, in: *Chance and Matter (Les Houches, 1986)* session 46, eds. J. Souletie, J. Vannimenus and R. Stora, (North-Holland, Amsterdam, 1986).

[71] H.C. van de Hulst and R. Stark, Accurate Eigenvalues and Exact Extrapolation Lengths in Radiative Transfer, *Astron. Astrophys.* **235**, 511 (1990).

[72] D. Schmeltzer and M. Kaveh, Backscattering of Electromagnetic Waves in Random Dielectric Media, *J. Phys. C: Solid State Phys.* **20**, L175 (1987).

[73] I.S. Gradsteyn and I.M. Ryzhik, *Table of Integrals, Series and Products* (Academic, New York, 1980).

[74] J. Rammer, Quantum Transport Theory of Electrons in Solids: A Single-particle Approach, *Rev. Mod. Phys.* **63**, (1991).

[75] M. Kaveh, Localization of Photons in Disordered Systems, *Phil. Mag. B* **56**, 693 (1987).

[76] A.F. Ioffe and A.R. Regel, Non-Crystalline, Amorphous, and Liquid Electronic Semiconductors, *Progress in Semiconductors* **4**, 237 (1960).

[77] B. Souillard, Waves and Electrons in Inhomogeneous Media, in: *Chance and Matter (Les Houches, 1986)* session 46, eds. J. Souletie, J. Vannimenus and R. Stora, (North-Holland, Amsterdam, 1986).

[78] T.V. Ramakrishnan, Electron Localization, in: *Chance and Matter (Les Houches, 1986)* session 46, eds. J. Souletie, J. Vannimenus and R. Stora (North-Holland, Amsterdam, 1986).

[79] P. Wölfe and D. Vollhardt, Self-Consistent Theory of Localization, in: *Anderson Localization* eds. Y. Nagaoka and H. Fukuyama, (Springer-Verlag, Berlin, 1982).

[80] E. Abrahams, P.W. Anderson, D.C. Licciardello and T.V. Ramakrishnan, Scaling Theory of Localization: Absence of Quantum Diffusion in Two Dimensions, *Phys. Rev. Lett.* **42**, 673 (1979).

[81] H. Furstenberg, Noncommuting Random Matrices, *Trans. Am. Math. Soc.* **108**, 377 (1963).

[82] M. Ya. Azbel, Quantum Particle in a Random Potential: Implications of an Exact Solution, *Phys. Rev. Lett.* **67**, 1787 (1991).

[83] D.J. Thouless, Electrons in Disordered Systems and the Theory of Localization, *Phys. Rep.* **13**, 93 (1974).

[84] D. Vollhardt, Normal ^{3}He: An Almost Localized Fermi Liquid, *Rev. Mod. Phys.* **56**, 99 (1984).

[85] P.W. Anderson, The Question of Classical Localization: A Theory of White Paint, *Phil. Mag. B* **52**, 505 (1985).

[86] A.Z. Genack, Fluctuations, Correlations and Average Transport of Electromagnetic Radiation in Random Media, in: *Scattering and Localization of Classical Waves in Random Media* (ed. P. Sheng, World Scientific, Singapore, 1990).

[87] M.P. van Albada, B.A. van Tiggelen, A. Lagendijk and A. Tip, Speed of Propagation of Classical Waves in Strongly Scattering Media, *Phys. Rev. Lett.* **66**, 3132 (1991).

[88] J.M. Drake, and A.Z. Genack, Observation of Nonclassical Optical Diffusion, *Phys. Rev. Lett.* **63**, 259 (1989).

[89] D. Sornette and B. Souillard, Strong Localization of Waves by Internal Resonances, *Europhys. Lett.* **7**, 269 (1988).

[90] C.A. Condat and T.R. Kirkpatrick, Resonant Scattering and Localization of Acoustic Waves, *Phys. Rev. B* **36**, 6782 (1987).

[91] P. Sheng and Z.Q. Zhang, Scalar-Wave Localization in a Two-component Composite, *Phys. Rev. Lett.* **57**, 1879 (1986).

[92] E.N. Economou, C.M. Soukoulis and A.D. Zdetsis, Localized States in Disordered Systems as Bound States in Potential Wells, *Phys. Rev. B* **30**, 1686 (1984).

[93] Th.M. Nieuwenhuizen and G.V. Shlyapninkov, Light Propagation in Media with Resonant Atoms at Random Positions, in preparation (1992).

[94] G. Grimvall, The Electron-Phonon Interaction in Normal Metals, *Physica Scripta* **14**, 63 (1976).

[95] E. Yablonovitch and T.J. Gmitter, Photonic Band Structure: The FCC Case, *Phys. Rev. Lett.* **63**, 1950 (1989).

[96] S. John, The Localization of Light and Other Classical Waves in Random Media, *Comm. Cond. Mat. Phys.* **4**, 193 (1988).

[97] S. John, Strong Localization of Photons in Certain Disordered Dielectric Superlattices, *Phys. Rev. Lett.* **58**, 2486 (1987).

[98] J. Qi, and T. Rui-bao, Self-consistent Treatment for Strong Localization of Light in Disordered Dielectric Superlattices, *Phys. Rev. B* **43**, 6136 (1991).

[99] N. Garcia and A.Z. Genack, Anomalous Photon Diffusion at the Threshold of the Anderson Localization Transition, *Phys. Rev. Lett.* **66**, 1850 (1991).

[100] I.S. Graham, L. Piché and M. Grant, Experimental Evidence for Localization of Acoustic Waves in Three Dimensions, *Phys. Rev. Lett.* **64**, 3135 (1991).

[101] N.F. Mott, Metal-Insulator Transitions, *Physics Today*, november 1978, 42.

[102] G.A. Thomas and M.A. Paalanen, Recent Developments in the Metal-Insulator Transition, in: *Localization, Interaction, and Transport Phenomena* eds. B. Kramer, G. Bergmann and Y. Bruynseraede, (Springer-Verlag, Berlin, 1985).

[103] M. Kaveh and N.F. Mott, The Metal-Insulator Transition in Disordered 3D Systems: a New View, *J. Phys.C: Condens. Matter* **15**, L697 (1982).

[104] for an overview see: *The Quantum Hall Effect*, eds. R.E. Prange and S.M. Girvin (Springer-Verlag, New York, 1987).

[105] H.P. Wei, D.C. Tsui, and A.M.M. Pruisken, Metal-Insulator Transition in the Integer Quantum Hall Effect, in: *Localization and Confinement of Electrons in Semiconductors* eds. F. Kuchar, H. Heinrich and G. Bauer, (Springer-Verlag, Berlin, 1990).

[106] T.R. Kirkpatrick, Localization of Acoustic Waves, *Phys. Rev. B* **31**, 5746 (1985).

[107] Z.Q. Zhang and P. Sheng, Wave Diffusion and Localization in Random Composites, in: *Scattering and Localization of Classical Waves in Random Media* (ed. P. Sheng, World Scientific, Singapore, 1990).

[108] E.N. Economou, *Green's Functions in Quantum Physics* (Springer-Verlag, Berlin, 1979).

[109] A.J. McKane and M. Stone, Localization as an Alternative to Goldstone's Theorem, *Ann. of Phys.* **131**, 36 (1981).

[110] L. Tsang and A. Ishimaru, Theory of Backscattering Enhancement of Random Discrete Isotropic Scatterers Based on the Summation of all Ladder and Cyclical Terms, *J. Opt. Soc. Am. A* **2**, 1331 (1985).

[111] A.D. Zdetsis, C.M. Soukoulis, E.N. Economou and G.S. Grest, Localization in Two- and Three-Dimensional Systems away from the Band Center, *Phys. Rev. B* **32**, 7811 (1985).

[112] V.N. Bringi, T.A. Seliga, V.K. Varadan and V.V. Varadan, Bulk Propagation Characteristics of Discrete Random Media, in: *Multiple Scattering and Waves in Random Media* eds. P.L. Chow, W.E. Kohler and G.C. Papanicolaou, (North-Holland Publishing Company, 1981).

[113] S. Ström, On the Integral Equations for Electromagnetic Scattering, *Am. J. Phys.* **43**, 1060 (1975).

[114] A. Lagendijk, R. Vreeker and P. de Vries, Influence of Internal Reflection on Diffusive Transport in Strongly Scattering Media, *Phys. Lett. A* **136**, 81 (1989).

[115] J.X. Zhu, D.J. Pine and D.A. Weitz, Internal Reflection of Diffusive Light in Random Media, *Phys. Rev. A* **44**, 3948 (1991).

[116] I. Freund, Surface Reflections and Boundary Conditions for Diffusive Photon Transport, *Phys. Rev. A* **45**, 8854 (1992).

[117] A.L.J. Burgmans and J.P. Woerdman, Selective Reflection from Sodium Vapour at Low Densities, *J. Phys. France* **37**, 677 (1974).

[118] J.P. Woerdman and M.H.F. Schuurmans, Spectral Narrowing of Selective Reflection from Sodium Vapour, *Opt. Comm.* **14**, 248 (1975).

[119] J. Fröhlich and Th. Spencer, Absence of Diffusion in the Anderson Tight Binding Model for Large Disorder or Low Energy, *Comm. Math. Phys.* **88**, 151 (1983).

[120] J.F. de Boer, M.P. van Albada and A. Lagendijk, Intensity and Field Correlations in Multiple Scattered Light, *Physica B*, **175**, 17 (1991); *Phys. Rev. B* **45**, 658 (1992).

[121] L. Brillouin, *Wave Propagation and Group Velocity* (Academic, New York, 1960) page 98-124 (as stated in Ref. [122] the speed obtained here contains a minor error).

[122] R. Loudon, The Propagation of Electromagnetic Energy Through an Absorbing Dielectric, *J. Phys. A* **3**, 233 (1970).

[123] P.M. Morse, and H. Feshbach, *Methods of Theoretical Physics*, (McGraw-Hill book company, 1953) page 304.

[124] D. Lenstra and W. van Haeringen, Playing with Electrons and Photons in Rings, in: *Analogies in Optics and Micro Electronics* eds. W. van Haeringen, and D. Lenstra, (Kluwer Academic, 1990), see also: *Huygens' Principle 1690-1990, Theory and Applications*, (eds. H. Blok, H.A. Ferweda and H.K. Kuiken, Elsevier Science Publishers BV, 1992).

[125] F. Liu, K.M. Yoo, and R.R. Alfano, Speed of the Coherent Component of Femtosecond Laser Pulses Propagating Through Random Scattering Media, *Opt. Lett.* **16**, 351 (1991).

[126] S. Engelsberg and J.R. Schrieffer, Coupled Electron-Phonon System, *Phys. Rev.* **131**, 993 (1963).

[127] L.D. Landau, The Theory of a Fermi Liquid, *Sov. Phys. JETP* **3**, 920 (1957).

[128] S. Grossmann, On Transport Theory in Real Gases, *Nuovo Cim.* **37**, 698 (1965).

[129] B.J. Baumgartl, Application of Landau's Transport Equation to Moderately Dense Gases, *Phys. Rev.* **168**, 200 (1968).

[130] Yu.N. Barabanenkov and V.D. Ozrin, *Phys. Lett. A* **154**, 38 (1991).

[131] E.P. Wigner, Resonance Reactions, *Phys. Rev.* **70**, 606 (1946).

[132] G.F. Weir, M.A. Howson, B.L. Gallagher and G.J. Morgan, Hybridization in Amorphous Metals, *Phil. Mag. B* **47**, 163 (1983).

[133] M.P. van Albada, private communication, with thanks (1990).

[134] J.M. Jauch, K.B. Sinha and B.N. Misra, Time-Delay in Scattering Processes, *Helv. Phys. Acta* **45**, 398 (1972).

[135] Ph.A. Martin, On the Time-Delay of Simple Scattering Systems, *Comm. Math. Phys.* **4**, 221 (1976).

[136] S. Hikami, Anderson Localization in a Nonlinear-σ-model Representation, *Phys. Rev. B* **24**, 2671 (1981).

[137] The name "Tauros criterion" came into being at the localization workshop on Crete (1992).

[138] R. Berkovits and M. Kaveh, Propagation of Waves Through a Slab Near the Anderson Transition: a Local Scaling Approach, *J. Phys. C : Condensed Matter* **2**, 307 (1990).

[139] F. Delyon, H. Kunz, and B. Souillard, One-dimensional Wave Equations in Disordered Media, *J. Phys. A.* **16**, 25 (1983).

[140] for a recent review see: R. Carmona and J. Lacroix, *Spectral Theory of Random Schrödinger Operators* (Birkhäuser Boston, 1990).

[141] A. MacKinnon, Localization in One-Dimensional and Quasi-One-Dimensional Systems, in: *Anderson Localization* (eds. Y. Nagaoka and H. Fukuyama, Springer-Verlag, Berlin, 1982).

[142] W. Kirsch, in: *Schrödinger Operators* (eds. H. Holden and A. Jensen, Springer Verlag, 1988), page 264-370.

[143] B. Simon, Kotani Theory for One Dimensional Stochastic Jacobi Matrices, *Comm. Math. Phys.* **89**, 227 (1983).

[144] D.J. Thouless, A Relation Between the Density of States and Range of Localization for One Dimensional Random Systems, *J. Phys. C: Solid State Phys.* **5**, 77 (1972).

[145] Th.M. Nieuwenhuizen, Exact Electronic Spectra and Inverse Localization Lengths in One Dimensional Random Systems, *Physica* **120A**, 468 (1983).

[146] B. Derrida and E. Gardner, Lyapunov Exponent of the One Dimensional Anderson Model: Weak Disorder Expansion, *J. Phys. France* **45**, 1283 (1984).

[147] Y. Avishai, and D. Berend, Transmission Through a One-dimensional Fibonacci Sequence of δ-function Potentials, *Phys. Rev. B* **41**, 5492 (1990).

[148] M. Kohmoto, L.P. Kadanoff, and C. Tang, Localization Problem in One Dimension: Mapping and Escape, *Phys. Rev. Lett.* **50**, 1870 (1983).

[149] T. Megademini, Principles and Possibilities of Interferential Multilayer Mirrors of Nonintegral Dimensionality, *Phys. Rev. B* **41**, 4693 (1990).

[150] E. Gu, G.V. Marr and M.A. Player, Optimization of Reflectivity of Periodic and Quasiperiodic Multilayer Films at Soft X-ray Wavelengths, *Opt. Comm.* **77**, 99 (1990)

[151] M. Kohmoto, B. Sutherland, and K. Iguchi, Localization in Optics: Quasiperiodic Media, *Phys. Rev. Lett.* **58**, 2436 (1987).

[152] M. Kappus and F. Wegner, Anomaly in the Band Center of the One-Dimensional Anderson Model, *Z. Phys. B* **45**, 15 (1981).

[153] C.J. Lambert, Anomalies in the Transport Properties of a Disordered Solid, *Phys. Rev. B* **29**, 1091 (1984).

[154] X.I. Saldana, G. Gonzalez de la Cruz, Electromagnetic Surface Waves in Semi-infinite Superlattices, *J. Opt. Soc. Am. A* **8**, 36 (1991).

[155] K.M. Yoo and R.R. Alfano, Photon Localization in a Disordered Multilayered System, *Phys. Rev. B* **39**, 5806 (1989).

[156] G. Paladin and A. Vulpiani, Scaling Law and Generalized Lyapunov Exponents of the One Dimensional Anderson Model, *Phys. Rev. B* **35**, 2015 (1987).

[157] G. Parisi and A. Vulpiani, Scaling Law for the Maximum Lyapunov Characteristic Exponent of Infinite Product of Random Matrices, *J. Phys. A* **19**, L425 (1986).

[158] R. Lima and S. Ruffo, Scaling Laws for Lyapunov Exponents: Models and Measurements, *J. Stat. Phys.* **52**, 259 (1988).

[159] E. Bouchaud and M. Daoud, Reflection of Light by a Random Layered System, *J. Phys. France* **47**, 1467 (1986).

[160] J. Verhoeven, private communication, with thanks (1991).

[161] Th.M. Nieuwenhuizen and J.M. Luck, Singular Behavior of the Density of States and the Lyapunov Coefficient in Binary Random Harmonic Chains, *J. Stat. Phys.* **41**, 745 (1985).

[162] A. Crisanti, Resonances in Random Binary Optical Media, *J. Phys. A* **23**, 5235 (1990).

[163] M.P. Bruijn, *Deposition and Characterization of Multilayer X-ray Reflection Coatings*, Ph.D. Thesis, Vrije Universiteit van Amsterdam (1986).

[164] J.M. Luck and Th.M. Nieuwenhuizen, Lifshitz Tails and Long-Time Decay in Random Systems with Arbitrary Disorder, *J. Stat. Phys.* **52**, 1 (1988).

[165] E. Hille and R.S. Phillips, Functional Analysis and Semi-Groups, *Am. Math. Soc. Colloquium Publications* Vol. XXXI (1957) page 110.

[166] Ph. Martin and M. Sassoli de Bianchi, On the Theory of the Larmor Clock and Time Delay, *J. Phys. A* **25**, 3627 (1992).

[167] M. Büttiker, Larmor Precession and the Traversal Time for Tunneling, *Phys. Rev. B* **27**, 6178 (1983).

[168] C.R. Leavens and G.C. Aers, Extension to Arbitrary Barriers of the Landauer-Büttiker Characteristic Barrier Interaction Times, *Solid State Comm.* **63**, 1101 (1987).

DANKWOORD

Dit proefschrift is tot stand gekomen in samenwerking met een aantal mensen die ik hiervoor wil bedanken.

Allereerst mijn promotor Ad Lagendijk. De vele (soms rommelige) discussies die ik met jou gevoerd heb zijn naar bijna evenveel leuke resultaten toe geconvergeerd. Jouw aanhoudende grote belangstelling voor alles wat niet triviaal is, bezorgde mij weliswaar slapeloze nachten, maar is een voortdurende leidraad geweest voor het onderzoek.

Mijn kamergenoot en co-promotor Adriaan Tip bedank ik voor de wiskundige stoomcursus tijdens mijn verblijf op het AMOLF. Jouw complete kennis van verstrooiingstheorie is zowel voor mijn onderzoek als voor mijn algemene ontwikkeling een verrijking geweest.

Een wetenschappelijke discussie met Theo Nieuwenhuizen levert altijd nieuwe gezichtspunten op. Zijn intensieve betrokkenheid bij zowel mijn onderzoek als de totstandkoming van mijn proefschrift heb ik zeer gewaardeerd.

Het gezonde verstand van Meint van Albada is voor mij vele malen aanleiding geweest mijn berekeningen te herzien. Met groot respect heb ik één maal moeten constateren dat een rigoureuze berekening van mij in drie cijfers na de komma samenviel met wat heuristisch kladwerk van Meint op de achterkant van een schrift.

Met Martin van der Mark heb ik vele discussies gehad, en zijn proefschrift was een uitstekende opstap voor mij. Diederik Wiersma heeft zijn Mie-programma ooit eens snel aangepast voor mijn doeleinden en is toen een essentiële schakel geweest in mijn onderzoek. Frans Vitalis heeft mij niet alleen zo nu en dan een lekkere sigaar toegeschoven, hij heeft ook zijn contacten aangewend om mij snel wegwijs te maken op de supercomputer. Dankzij de hulp van Tina Weeding zijn de grootste taalblunders uit mijn proefschrift verdwenen.

Een deel van mijn berekeningen in hoofdstuk 4 is geïnspireerd door een samenwerking met Jan Verhoeven van de "dunne-lagen afdeling" van ons lab. Ik hoop dat sommige ideeën die uit ons gezamenlijk brainstormen naar voren kwamen, inderdaad experimenteel uitvoerbaar blijken te zijn.

Ondanks het feit dat ik één van de weinige theoretici was op het AMOLF, zijn de afgelopen jaren voor mij zeer wel besteed geweest. Een experimentele omgeving werkt zeer inspirerend. Een struikelpartij over zonnecellen heeft mij meerdere malen weer met beide benen op de grond gebracht. Wel ben ik verbaasd over het feit dat sommige promovendi op het AMOLF zo intens aan hun apparaat aan het sleutelen zijn, dat de diagonalisatie van een twee-bij-twee matrix al gauw doorgaat voor "de formele theorie".

Tenslotte bedank ik mijn vriendin Lucienne. Lieve Lucienne, zonder jou had ik waarschijnlijk veel meer tijd gehad voor mijn proefschrift, maar had het lang niet zoveel waarde voor mij gehad.

Même quand le doute est trop fort, faut pas glisser, tenir encore (Patrick Bruel, 1990).

MULTIPLE SCATTERING AND LOCALIZATION OF LIGHT

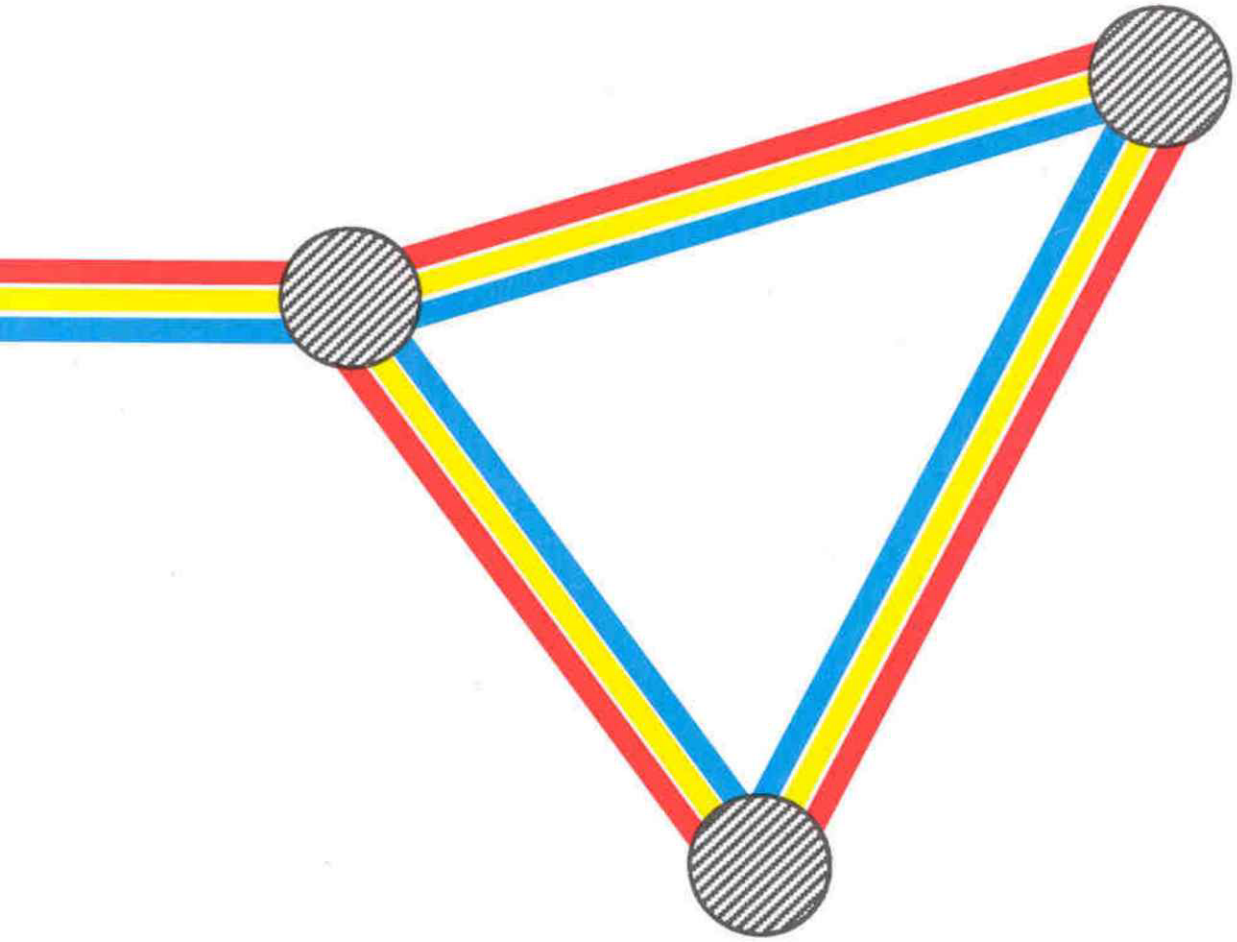

BART A.
VAN TIGGELEN